



# The formation, modification and characterisation of monolithic ion exchangers for separation science

Eoin Gillespie, B.Sc.

Student No.: 51047795

Under the supervision of Prof. Brett Paull

A thesis submitted to Dublin City University for consideration  
for the degree of:  
Doctor of Philosophy

Dublin City University  
School of Chemical Sciences

January 2009

I hereby certify that this material, which I now submit for assessment on the programme of study leading to the award of *Doctor of Philosophy* is entirely my own work, that I have exercised reasonable care to ensure that the work is original, and does not to the best of my knowledge breach any law of copyright, and has not been taken from the work of others save and to the extent that such work has been cited and acknowledged within the text of my work.

Signed: \_\_\_\_\_

(Candidate) ID No.: \_\_\_\_\_ Date: \_\_\_\_\_

# Table of Contents

<b>Declaration</b>	2
<b>Abstract</b>	11
<b>List of abbreviations</b>	12
<b>List of figures</b>	15
<b>List of tables</b>	34
<b>List of publications</b>	36
<b>List of poster presentations</b>	37
<b>List of oral presentations</b>	40
<b>List of awards</b>	40
<b>Acknowledgments</b>	41
<b>Chapter 1: Literature survey</b>	42
<b>1.1 Liquid chromatography.</b>	43
<b>1.2 Stationary phases.</b>	43
<i>1.2.1 Particulate stationary phases.</i>	43
<i>1.2.2 Monolithic stationary phases.</i>	47
<i>1.2.2.1 Origins.</i>	47
<i>1.2.2.2 Production of silica and polymeric monoliths.</i>	48
<i>1.2.2.4 Advantages of monoliths over particulate.</i>	50
<i>1.2.2.3 Advantages and disadvantages of silica and polymeric monoliths.</i>	52
<b>1.3. Modification of stationary phase chemistries.</b>	54
<i>1.3.1 Surfactant coating.</i>	54
<i>1.3.2 Chemical modification.</i>	56
<i>1.3.3 Photografting methods.</i>	59

<b>1.4 Characterisation of modified stationary phases.</b>	63
1.4.1 <i>Scanning electron microscopy - Energy dispersive X-ray spectroscopy (SEM-EDX).</i>	64
1.4.2 <i>Chromatographic performance.</i>	66
1.4.3 <i>Fluorescence.</i>	69
<b>1.5 Capillary chromatography.</b>	70
1.5.1 <i>Applications of capillary IC.</i>	72
<b>1.6 Detection in capillary liquid chromatography.</b>	86
1.6.1 <i>UV.</i>	86
1.6.2 <i>Fluorescence.</i>	87
1.6.3 <i>Amperometric.</i>	88
1.6.4 <i>Conductivity.</i>	88
1.6.5 <i>Capacitively coupled contactless conductivity detection.</i>	88
<b>1.7 Capacitively coupled contactless conductivity detection.</b>	89
1.7.1 <i>Origins.</i>	89
1.7.2 <i>Operation principles.</i>	89
1.7.2.1 <i>Capacitance.</i>	89
1.7.2.2 <i>Capacitance in C<sup>4</sup>D.</i>	91
1.7.2.3 <i>Operational characteristics of C<sup>4</sup>D.</i>	94
1.7.2.4 <i>Cell geometries, Electrode length &amp; detection gap.</i>	98
1.7.3 <i>Applications of C<sup>4</sup>D.</i>	100
1.7.3.1 <i>Capillary electrophoresis</i>	100
1.7.3.2 <i>Capillary electrochromatography</i>	103
1.7.3.3 <i>Liquid chromatography</i>	105
1.7.3.4 <i>Ion chromatography</i>	108
<b>1.8 Conclusions.</b>	112
<b>1.9 References.</b>	114

<b>Chapter 2: A comparison of capacitively coupled contactless conductivity detection on monolithic capillary columns and open fused silica capillaries</b>	119
<b>2.1 Introduction.</b>	120
<i>2.1.1 Ion exchange via surfactant coating of reversed-phase columns.</i>	120
<i>2.1.2 Capillary chromatography.</i>	121
<b>2.2 Experimental.</b>	122
<i>2.2.1 Instrumentation.</i>	122
<i>2.2.2 Reagents.</i>	124
<i>2.2.3 Sample preparation.</i>	124
<b>2.3 Results and discussion.</b>	124
<i>2.3.1 Separation of inorganic anions on a capillary monolithic column.</i>	124
<i>2.3.2 Eluent variation and detector signal.</i>	126
<i>2.3.3 On-column detection for separation of inorganic anions.</i>	133
<b>2.4 Conclusions.</b>	136
<b>2.5 References.</b>	138
<b>Chapter 3: Use of contactless conductivity detection for characterisation of capillary column surfactant coatings and subsequent ion chromatographic determination of cations and amino acids.</b>	139
<b>3.1 Introduction.</b>	140
<i>3.1.1 On-column detection for the evaluation of coating.</i>	140
<b>3.2 Experimental.</b>	142
<i>3.2.1 Instrumentation.</i>	142
<i>3.2.2 Reagents.</i>	142

3.2.3 Column coating and washing procedures.	143
3.2.3.1 Coating and washing procedure for Column #1.	144
3.2.3.2 Coating and washing procedure for Column # 2.	145
3.2.3.3 Coating and washing procedure for Column # 3.	146
3.2.4 Stationary phase gradients.	146
3.2.5 Counter-ion study.	146
3.2.6 Separation of inorganic cations and amino acids.	147
3.2.7 Sample treatment.	147
<b>3.3 Results and discussion</b>	147
3.3.1 Preliminary use of $C^4D$ for stationary phase characterisation.	148
3.3.2 Detailed investigation into the use of $C^4D$ in stationary phase characterisation (Column # 2).	152
3.3.3 Coating and washing of Column # 3.	157
3.3.4 Comparison of Column # 1, Column # 2 and Column # 3.	159
3.3.5 Controlled coating modification – stationary phase gradients.	162
3.3.6 Counter ion study.	165
3.3.7 Analysis of cations.	169
3.3.8 Analysis of drinking water.	172
3.3.9 Separation of selected amino acids.	173
<b>3.4 Conclusions.</b>	175
<b>3.5 References.</b>	178

<b>Chapter 4: Characterisation of photografted polymeric monolithic ion exchangers using capacitively coupled contactless conductivity detection</b>	179
<b>4.1 Introduction.</b>	180
<b>4.2 Experimental.</b>	182
4.2.1 Instrumentation.	182
4.2.2 Reagents.	183
4.2.3 Vinylisation of fused silica capillaries for monolith production.	183
4.2.4 Preparation of methacrylate monolithic capillary columns.	184
4.2.5 Photografting of porous methacrylate monoliths with 2-acrylamido-2-methyl-1-propanesulfonic acid (AMPS).	184
4.2.6 Verification of the presence of charged groups on functionalised monoliths using $C^4D$ .	187
4.2.7 In-house photografting holder.	187
4.2.8 Washing of photografted monoliths.	189
<b>4.3 Results and discussion.</b>	190
4.3.1 Washing of photografted monoliths.	190
4.3.2 Spatial location and accuracy of photografting procedure.	194
4.3.3 Comparison of Monolith # 1 and Monolith # 2 using $C^4D$ response.	195
4.3.4 Calibration of photografted zone (Monolith # 3 and 4).	196
<b>4.4 Conclusion.</b>	201
<b>4.5 References.</b>	202

<b>Chapter 5: Accurate non-invasive determination of <math>pK_a</math> of immobilised functional groups on polymeric monoliths using capacitively coupled contactless conductivity detection</b>	202
<b>5.1 Introduction.</b>	203
<b>5.2 Experimental</b>	207
5.2.1 Instrumentation.	207
5.2.2 Reagents.	207
5.2.3 Fabrication of methacrylate monoliths.	208
5.2.4 Photografting of polyethylene glycol methacrylate.	208
5.2.5 Photografting of vinyl azlactone.	209
5.2.6 Immobilisation of <i>m</i> -aminophenylboronic acid via azlactone chemistry.	209
5.2.7 Immobilisation of ADA and IDA via azlactone chemistry.	209
5.2.8 Immobilisation of ethanolamine via azlactone chemistry.	209
5.2.9 Verification of immobilised zones.	210
5.2.10 Titration of free <i>m</i> -aminophenylboronic acid.	210
5.2.11 On-column titration of immobilised APBA.	210
5.2.12 On-column titration of immobilised IDA, ADA and ethanolamine.	211
5.2.13 On-column titration of ADA in the presence of metals.	211
<b>5.3 Results and discussion.</b>	211
5.3.1 Immobilisation of APBA via VAL.	211
5.3.2 On-column titration of APBA.	213
5.3.3 Immobilisation of ADA via VAL.	218
5.3.4 On-column titration of ADA.	219
5.3.5 Immobilisation of IDA via VAL.	223
5.3.6 On-column titration of IDA.	224

5.3.7 <i>On-column titration of ethanolamine.</i>	226
5.3.8 <i>Investigation of VAL-ADA complexation with metals using C<sup>4</sup>D.</i>	229
<b>5.4 Conclusion.</b>	232
<b>5.5 References.</b>	233
<b>Chapter 6: Development of a contactless conductivity detector cell for 1.6 mm O.D. (1/16<sup>th</sup> inch) HPLC tubing micro-bore columns with on-column detection.</b>	235
<b>6.1. Introduction.</b>	236
<b>6.2. Experimental.</b>	237
6.2.1 <i>Instrumentation.</i>	237
6.2.1.1 <i>Chromatographic instrumentation.</i>	237
6.2.1.2 <i>Preparation of packed capillary columns.</i>	237
6.2.1.3 <i>Contactless conductivity 1.59 mm (1/16") detector cell.</i>	239
6.2.1.4 <i>Comparative studies.</i>	241
6.2.2 <i>Reagents.</i>	242
6.2.3 <i>Noise calculation.</i>	242
<b>6.3. Results and discussion.</b>	243
6.3.1 <i>Detector design and optimisation: Bode plots.</i>	243
6.3.2 <i>Detector optimisation: response, signal to noise and peak shape.</i>	246
6.3.3 <i>Performance evaluation compared with commercial C<sup>4</sup>D detector.</i>	248
6.3.4 <i>Intra-run detector movement.</i>	252
6.3.5 <i>Evaluating the homogeneity of stationary phase packing.</i>	254
<b>6.4. Conclusion.</b>	257

<b>6.5 References.</b>	258
<b>Chapter 7: Final conclusions and summation</b>	260

**Abstract:**

Studies into the formation, surface modification, and physical characterisation of silica and polymer-based monolithic phases for separation science are presented. The application of capacitively contactless conductivity detection ( $C^4D$ ) to capillary ion chromatography and the characterisation of the above modified capillary stationary phases have been investigated. The non-contact character of  $C^4D$  allows the placement of the detector directly onto the separation column. The characterisation of the behaviour of  $C^4D$  with variations in eluents and detection position (both on- and off- column) has been shown. The detection of anions and cations using surfactant coated capillary monolithic columns shows  $C^4D$  to both a sensitive detector on-column and also the removal of extra-column band broadening due to off-column detector placement. The characterisation of novel stationary phases has generally relied upon the use of destructive or indirect methods to date (i.e. SEM or chromatographic performance); however, the use of  $C^4D$  allows for the characterisation in both a spatial and a temporal manner. The coating of surfactant onto reversed-phase monolithic stationary phases is characterised in detail, with  $C^4D$  permitting the visualisation of the removal of excess surfactant. The modification of such modified stationary phases by organic solvent to create stationary phase gradients has also been shown. Investigations into the physio-chemical properties of stationary phases using  $C^4D$  is documented with a counter ion study. The application of  $C^4D$  to the characterisation of photografted polymeric capillary monoliths is shown, with the ability to spatially locate such photografted zones. The relationship of  $C^4D$  response with regard to the amount of energy used to initiate the photograft lends this technique as an aid in the optimisation of photografting methods. The application of  $C^4D$  to columns of larger diameters showed an equivalent performance to that of a commercial capillary  $C^4D$  cell. The ability to scale up  $C^4D$  will open new avenues for this detection technique in the characterisation of columns in a variety of dimensions other than capillary scale.

## List of abbreviations

A	Eddy diffusion term of van Deemter equation
A.C.	Alternating current
ADA	N-(2-acetamido)iminodiacetic acid
AMPS	2-acrylamido-2-methyl-1-propanesulfonic acid
APBA	<i>m</i> -aminophenylboronic acid
B	Axial diffusion term of van Deemter equation
BDDE	1,4-butanedioldiglycidyl ether
BSA	Bovine serum albumin
BuMA	Butyl methacrylate
C	Mass transfer term of van Deemter equation
CPC	Cetylpyridium chloride
CEC	Capillary electrochromatography
C4D	Capacitively coupled contactless conductivity detection
CE	Capillary electrophoresis
CTAB	Cetyltrimethylammonium bromide
CHAPS	3-[(3-Cholamidopropyl)dimethylammonio]-1-propanesulfonate
CHAPSO	3 - [( 3-cholamidopropy1)dimethylammoniol-2-hydroxy-1-propanesulfonate
DDAB	Didodecyldimethylammonium bromide
DMAEA-Q	2-(triethylammonium) ethyl methacrylate chloride
DMAPAA-Q	N-[3-(dimethylamino) propyl] acrylamide methyl chloride-quaternary salt
DMA	Dimethylamine
D.C.	Direct current
DOSS	Diocylsulfosuccinate
DDMAU	<i>N</i> -dodecyl- <i>N,N</i> -(dimethylammonio)undecanoate
DI	De-ionised
EOF	Electroosmotic flow
EDMA	Ethylene dimethacrylate

EDTA	Ethylenediaminetetraacetic acid
EDX	Energy dispersive X-ray spectroscopy
FIA	Flow injection analysis
FSC	Fused silica capillary
FWHM	Full width half maximum
GMA	Glycidyl methacrylate
GFP	Green fluorescent protein
HETP	Height equivalent to theoretical plate
IDA	Iminodiacetic acid
IC	Ion chromatography
k	Retention factor
LOD	Limit of detection
LOQ	Limit of quantitation
MAS	3-methacryloxypropyltriethoxysilane
META	[2-(methacryloyloxy) ethyl] trimethylammonium chloride
N	Theoretical plate
NFS	Nano-flow sensor
NSAID	Non-steroidal anti-inflammatory drug
OT	Open tubular
Op-amp	Operational amplifier
PBMA	poly(butadiene-maleic acid)
PEEK	Polyether ether ketone
PEGMA	Poly(ethylene glycol) methacrylate
PEI	Polyethylenimine
RP	Reversed phase
SEM	Scanning electron microscopy
SDS	Sodium dodecylsulphate
SAX	Strong anion exchanger
u	Linear velocity
UV	Ultraviolet light
VAL	2-vinyl-4,4-dimethylazlactone

$V_{(p-p)}$

Voltage peak-to-peak

### List of figures:

Figure 1.1: Knox plot (reduced plate height vs. reduced linear velocity) showing the effect of reducing particle diameter on plate height [1].

Figure 1.2: Schematic depicting two paths possible from point A to point B within a packed column.

Figure 1.3: Contributions of A, B and C terms in the van Deemter plot.

Figure 1.5: Schematic for the preparation of rigid macroporous polymer monoliths [15].

Figure 1.6: Plots of plate height values for uracil against linear velocity of mobile phase: conventional size columns; Mightysil (■) and Chromolith (○) [16].

Figure 1.7: SEM images of a silica monolith showing (a) the macro-pores or through-pores and (b) the meso-porous structure of the silica skeleton [17].

Figure 1.8: SEM of methacrylate monolith showing micro-globules [18].

Figure 1.9: (a) Structure of a typical surfactant (SDS), (b) interaction of SDS with a reversed-phase stationary phase creating an ion exchange phase.

Figure 1.10: Comparison of column capacity and selectivity for Mn, Cd, Zn, and Pb on IDA silica monolith and IDA silica gel columns; Eluent = 0.2 M KCl (pH 2.0). Detection = Post-column reaction with PAR [39].

Figure 1.11: Chemical conversion of epoxy groups by means of various reagents. I. Amination; II. alkylation; III. sulfonation; IV. hydrolysis; V. carboxymethylation; VI. modification with *p*-hydroxyphenylboronic acid [14].

Figure 1.12: Depiction of photografting technique for the formation of one discrete zone of AMPS onto a polymer monolith.

Figure 1.13: Schematic representation of the growing polymer chains during photografting with increasing irradiation time from (a) to (c) [42].

Figure 1.14: Reaction of VAL, once photografted onto the surface of a monolith, with an amine containing compound creating a covalent linkage the monolith surface.

Figure 1.15: Fluorescence microscope image of porous poly (butyl methacrylate-co-ethylene dimethacrylate) monolith in a 50  $\mu\text{m}$  capillary photografted through a mask with poly (4, 4-dimethyl-2-vinylazlactone) chains for 1 (a) and 3 minutes (b) and subsequently reacted with Rhodamine 6G [42].

Figure 1.16: Consecutive patterning of multiple GFP patches on a polymer monolith in a 100  $\mu\text{m}$  capillary. The top image shows the location of GFP simultaneously immobilised in multiple patches; each GFP patch is  $\sim 750 \mu\text{m}$  in length. The lower image shows the fluorescence from GFP patches after a second round of GFP immobilisation on the same monolith. The plot shows profiles of the GFP fluorescence along the length of the capillary for the above images; the fluorescence intensity at each point in the column was determined by averaging the fluorescence intensity across the cross section of the monolith. In the images above, the diameter of the monolith has been increased over the actual aspect ratio to more clearly show the patch positions [43].

Figure 1.17: Calculated UV dose profiles along the relative length of the monolith using the moving shutter (A) and neutral density filter (B). Conditions: actual length 8.5 cm; UV light intensity  $15 \text{ mW cm}^{-2}$ , irradiation time 0– 60 s (A); irradiation time 600 s, UV intensity  $0.2\text{--}0.006 \text{ mW cm}^{-2}$  (B) [47].

Figure 1.18: Comparison of theoretical gradient and actual gradient for photografting of AMPS onto the surface of a polymeric monolith capillary column through a neutral density filter [47].

Figure 1.19: Radial sulfur profile of a monolith uniformly grafted with 2-acrylamido-2-methyl-1-propanesulfonic acid for 60 s determined by EDX [47].

Figure 1.20: Exponential fits for retention loss under various coating conditions. Conditions: 100 × 4.6 mm RP-18e Chromolith column coated until breakthrough. Anion separations using 10.0 mM 4-hydroxybenzoic acid eluent (pH 4.6) at 2 mL min<sup>-1</sup>, 4 mL min<sup>-1</sup> flushing, 0.05 mM analyte ions, 20 µL injection, non-suppressed conductivity detection. Temperature 30 °C unless otherwise stated [48].

Figure 1.21: Stability of monolithic silica capillary columns modified with dilauryldimethylammonium ion or cetyltrimethylammonium ion. Columns, monolithic silica capillary columns (200 × 0.1 mm i.d.) modified with a dilauryldimethylammonium ion (A) or a cetyltrimethylammonium ion (B); eluent, aqueous solution of 50 mM sodium chloride (pH 5.8); flow-rate, 2.1 µL min<sup>-1</sup>; analyte ion, nitrate [49].

Figure 1.22: Effect of grafting time on electroosmotic mobility (□) and column efficiency (■). Column, 34 cm (8.5 cm effective length) × 100 µm i.d., porous monolith grafted with AMPS using neutral density filter. Mobile phase, 80:20 acetonitrile: 10 mM phosphate buffer, pH 2.5; voltage -25 kV; injection -5 kV for 5 s; UV detection at 254 nm; EOF marker thiourea 200 µg mL<sup>-1</sup> [47].

Figure 1.23: Indirect photometric detection of six inorganic cations. Column, Develosil 30-5, 50 mm × 0.35 mm i.d.; eluent, 2.0mM BETMAC in 30% (v/v) acetonitrile (pH 6.5); flow rate, 4.2 µL min<sup>-1</sup>; analytes, 1 = lithium, 2= sodium, 3= ammonium, 4= potassium, 5= rubidium and 6= caesium; sample size, 0.2 µL; wavelength of UV detection, 208 nm [54].

Figure 1.24: Background subtracted gradient chromatogram on a 50 cm x 180  $\mu\text{m}$  i.d. packed capillary column (Dionex AS-11). Linear gradient from 2 mM NaOH to 38 mM NaOH from 5 to 17 minutes was used. Peak identities: 1, acetate; 2, formate; 3, methanesulfonate; 4, monochloroacetate; 5, bromate; 6, chloride; 7, nitrite; 8, trifluoroacetate; 9, dichloroacetate; 10, bromide; 11, nitrate; 12, chlorate; 13, sulfate; 14, phthalate; 15, chromate. All ions were 50 mM except dichloroacetate which was 60 mM. [55]

Figure 1.25: Separation of inorganic anions on packed capillary column. Separation column, TSKgel IC-Anion-PWXL (100mm x 0.32mm i.d.); packed capillary suppressors, TSKgel SCX (30mm x 0.32mm i.d.); mobile phase, 1.75 mM  $\text{NaHCO}_3$  /1.5 mM  $\text{Na}_2\text{CO}_3$ ; flow rate, 4.2  $\mu\text{L min}^{-1}$ ; detection, contactless conductivity; analytes, 1 = fluoride, 2 = chloride, 3 = nitrite, 4 = bromide, 5 = nitrate, 6 = sulfate; concentration of analyte anions, 0.05 mM each; injection volume, 0.2  $\mu\text{L}$  [56].

Figure 1.26: Chromatographic separation of inorganic anions using a hybrid silica monolith. 200H-DMAEA-Q column: column size, 200  $\mu\text{m}$  i.d. x 300 mm; mobile phase, 0.5 M NaCl; detection,  $\lambda = 210$  nm; temperature, ambient; pressure, 3.5 MPa. Analytes: 1,  $\text{S}_2\text{O}_3^-$ ; 2,  $\text{NO}_2^-$ ; 3,  $\text{Br}^-$ ; 4,  $\text{NO}_3^-$ ; 5,  $\text{I}^-$  [64].

Figure 1.27: Micro-IC separation of anions mixture composed of (1) thiourea; (2) iodate; (3) bromate; (4) nitrate; (5) bromide; (6) iodide; (7) thiocyanate. The sample solution (2 mg  $\text{mL}^{-1}$  of each component, 4  $\mu\text{L}$ ) was injected in a split flow and injection mode with a pump flow rate of 0.40  $\text{mL min}^{-1}$ . Column: 100H-MOP-DMAPAA-Q, 33 cm length; mobile phase: 50 mM sodium phosphate (pH 6.6), linear velocity:  $u=1.4$   $\text{mm s}^{-1}$ ,  $\lambda=210$  nm [65].

Figure 1.28: Separation of authentic mixture of five anions and bromide in a seawater sample on a monolithic silica capillary column modified with

cetyltrimethylammonium ion. Column: 400 mm x 0.1 mm i.d. Eluent: 500 mM sodium chloride containing 0.1 mM CTAC. Flow rate: 5.6  $\mu\text{L min}^{-1}$ . Injection volume: 20 nL. Samples: 0.5 mM each for the upper trace; seawater for the lower trace. Wavelength of UV detection: 210 nm.

Figure 1.29: Separations of common cations on a sulfonated GMA monolith at different flow rates of (A) 3, (B), (C) 9, (D) 12, and (E) 15  $\mu\text{L min}^{-1}$ . Sample, 2 mM each of  $\text{Na}^+$ ,  $\text{K}^+$ ,  $\text{Mg}^{2+}$ , and  $\text{Ca}^{2+}$ ; cation exchange capacity, 80  $\mu\text{equiv mL}^{-1}$  [67].

Figure 1.30: SEM image of original BuMA-co-EDMA-co-AMPS monolith (A) and its latex-coated counterpart (B) [68].

Figure 1.31: Separation of a mixture of carbohydrates by anion-exchange chromatography using an optimised latex-coated polymeric monolithic capillary column. Conditions: column size 10 cm x 250  $\mu\text{m}$  i.d., pore size 0.97  $\mu\text{m}$ . Flow rate 13  $\mu\text{L min}^{-1}$  mobile phase aqueous ammonium hydroxide 64 mM (pH 12.8). Peaks: d(+)galactose (1), d(+)glucose (2), d(+)xylose (3), d(+)mannose (4), maltose (5), d(-)fructose (6), sucrose (7). Injection volume 100 nL; sample concentration 1  $\text{mg mL}^{-1}$  [68].

Figure 1.32: Effect of increasing concentration of hydroxide in the eluent on the observed separation using suppressed conductivity detection. Conditions: eluent, as marked; column; 250  $\mu\text{m}$  i.d. x 30 cm, 3.5  $\mu\text{m}$  pore size coated with AS18; flow rate, 12.5  $\mu\text{L min}^{-1}$ ; sample loop, 50  $\mu\text{m}$  x 5.0 cm; regenerant, 5 mM  $\text{H}_2\text{SO}_4$  flowing at 0.5  $\text{mL min}^{-1}$ ; analytes, 50  $\mu\text{M}$ . Peaks: 1, iodate; 2, bromate; 3, nitrite; 4, bromide; 5, nitrate [69].

Figure 1.33: Separation of a 7 anion mixture\* using: (A) a 24.1 cm 250 mm AS18-coated GMA-co-EDMA monolith that was sulfonated using method (i). Eluent: 10 mM  $\text{NaClO}_4$ , flow-rate 3.6  $\text{mL min}^{-1}$ , detector: Agilent. (B) A 34.8 cm x 250 mm AS18-coated GMA-co-EDMA monolith that was sulfonated using method (ii).

Eluent: 10 mM NaClO<sub>4</sub>, flow rate 3.0 mL min<sup>-1</sup>, detector: Agilent. (C) A 14.3 cm 250 mm AS 18 coated GMA-co-EDMA monolith that was sulfonated using method (iii). Eluent: 10 mM NaClO<sub>4</sub>, flow-rate 3.2 mL min<sup>-1</sup>, detector: Agilent. \* Analytes: 1 = IO<sub>3</sub><sup>-</sup>, 2 = BrO<sub>3</sub><sup>-</sup>, 3 = NO<sub>2</sub><sup>-</sup>, 4 = Br<sup>-</sup>, 5 = NO<sub>3</sub><sup>-</sup>, 6 = I<sup>-</sup>, 7 = benzenesulfonate, each 0.14 mM [70].

Figure 1.34: Speed separation of five anions on a monolithic anion-exchange capillary column with methacrylate matrix aminated with the mixture of PEI and DMA, pH = 4.25, eluent potassium phthalate, column length 465 mm, pressure 13 bar [71].

Figure 1.35: Representation of enhancement of fluorescence signal in the presence of stationary phase [75].

Figure 1.36: Diagram of a capacitor in a D.C. circuit.

Figure 1.37: Diagram of a capacitor in an A.C. circuit.

Figure 1.38: Equivalent Circuit diagram of the C<sup>4</sup>D showing the inclusion of the op-amp.

Figure 1.39: Schematic of an actual C<sup>4</sup>D arrangement excitation electrode (A), pick-up electrode (B), shield (C), eluent flow path (D) and direction of flow (E).

Figure 1.40: Sketch of the cell model that describes the basic behaviour of the C<sup>4</sup>D [80].

Figure 1.41: C<sup>4</sup>D set-up commonly used in microchips.

Figure 1.42: Frequency plots (Bode plots) for a model cell (—), and for a real cell (-•-) [79].

Figure 1.43: Bode plots measured for a real C<sup>4</sup>D cell with OPA 655 and OPA 606 [80].

Figure 1.44: Effect of the excitation frequency on the appearance of the electro – pherograms [80].

Figure 1.45: Bode plots showing the effect of different electrode lengths on C<sup>4</sup>D behaviour [80].

Figure 1.46: Effect of electrode length on capacitance of cell [80].

Figure 1.47: Bode plots showing the effect of changing detection gap distance [80].

Figure 1.48: Separation of a standard mixture of inorganic cations comparing UV and conductivity detection. Conditions: fused-silica capillary,  $L = 60$  cm,  $L_1 = 40$  cm to conductivity detector,  $L_2 = 52.5$  cm to UV detector (214 nm),  $U = +20$  kV,  $I = 3.0$   $\mu$ A, and  $T = 23$  °C; electrolyte, 10 mM lactic acid, 8 mM 4-methylbenzylamine, and 15 % methanol, pH 4.9; injection, 30 s; sample concentration, 0.1 mM [78].

Figure 1.49: Determination of cations and anions in a red wine sample with a PEEK capillary of 60 cm. The sample was diluted 1:20 with buffer. (A) (1) K<sup>+</sup>, (2) Ca<sup>2+</sup> and (3) Na<sup>+</sup>. (B) (1) Cl<sup>-</sup>, (2) SO<sub>4</sub><sup>2-</sup>, (3) tartrate, (4) succinate, (5) acetate and (6) lactate. Buffer: 10 mM MES/His, 1 mM 18-crown-6 (pH 6.0). Injection: electrokinetic (non-stacking conditions), 5 s at +5 V for cations and at -5 kV for anions. Separation: +25 kV for cations and -25 kV for anions [85].

Figure 1.50: OT-CEC-C<sup>4</sup>D determination of five alkali cations. CEC conditions as in separation column, four layers of PBMA, BGE solution, 100 mM acetic acid [87].

Figure 1.51: Determination of five NSAIDs standards using HPLC with C<sup>4</sup>D and UV detection. HPLC conditions: column, Nucleosil 120-5 C<sub>18</sub>; flow rate, 1.0 mL min<sup>-1</sup>; mobile phase composition, 65% acetonitrile, 0.17 mM acetic acid and 0.25 mM sodium acetate. Concentration of analytes, 250 μM. Peak description: (1) salicylic acid, (2) acetylsalicylic acid, (3) diclofenac, (4) mefenamic acid and (5) ibuprofen. UV detection at 220 nm [88].

Figure 1.52: Determination of underivatized amino acids using HPLC with C<sup>4</sup>D detection. (#1) raw data, (#2) after normalisation using the Peaks software package [89].

Figure 1.53: HPLC–C<sup>4</sup>D determination of proteins separated on the monolithic capillary column. Mobile phase A, 0.004% TFA in 10% acetonitrile; mobile phase B, 0.006% TFA in 52% acetonitrile. Gradient program, 0–100% B in 12 minutes, flow rate, 1.65 μL min<sup>-1</sup>. (a) C<sup>4</sup>D parameters: excitation voltage, 360 V<sub>pp</sub>; excitation frequency, 130 kHz. (b) UV detection at 214 nm. Analyte concentrations: trypsin, 20 μg mL<sup>-1</sup>; other proteins 10 μg mL<sup>-1</sup>. The baselines were normalised using the Peaks software package [74].

Figure 1.54: (A) Determination of three inorganic anions in the non-suppressed conductivity mode: (a) C<sup>4</sup>D (150 kHz and 50 V<sub>p-p</sub>), (b) commercial conductivity detector. Eluent: 2.5 mM phthalic acid adjusted to pH 4.25 with Tris, flow rate = 1.5 mL min<sup>-1</sup>. Anion concentrations: fluoride, chloride 10 mg L<sup>-1</sup> and nitrate 20 mg L<sup>-1</sup>. (B) Determination of inorganic anions in tap water in the non-suppressed conductivity mode: (a) C<sup>4</sup>D (150 kHz and 50 V<sub>p-p</sub>), (b) commercial conductivity detector. IC conditions as in (A) [82].

Figure 1.55: OT-IC-C<sup>4</sup>D determination of inorganic cations in separation columns with various numbers of PBMA layers. Eluent, 1 mM tartaric acid; flow rate, 1.5 μL min<sup>-1</sup>; injection volume, 200 nL; 120/106 cm total/effective length; 75/375 μm I.D./O.D.; analyte concentration, 10–40 μM in DI water. SP: System peak [87].

Figure 1.56: Separation of inorganic anions using latex coated suppressed ion exchange chromatography. Eluent: 5.0 mM KOH, flow: 12.5  $\mu\text{L min}^{-1}$ . Peaks: 1, iodate; 2, bromate; 3, nitrite; 4, bromide; 5, nitrate [69].

Figure 2.1: Structure of *N*-dodecyl-*N,N*-(dimethylammonio)undecanoate (DDMAU).

Figure 2.2: Schematic of flow system used to deliver  $\mu\text{L}$  flow rates to capillary monolith. (a) Conventional pump, (b) T-piece connector, (c) waste line, (d) injector (10 nL), and (e) column.

Figure 2.3: Overlaid chromatograms of mixed anion standards ranging from 10 to 100  $\text{mg L}^{-1}$  (100 pg to 1 ng injected mass) obtained using the DDMAU modified monolithic silica capillary column with a 0.5 mM phthalate eluent (pH 4.0) and on-column  $\text{C}^4\text{D}$  detection. Detector position: 13 cm from column inlet. Flow rate = 1.0  $\mu\text{L min}^{-1}$ . Injection volume = 10 nL. Peak ID: 1= iodate, 2= nitrite, 3= bromide, 4= nitrate, \* = system peak.

Figure 2.4: Linearity of inorganic anion separation on the DDMAU coated capillary monolith.  $\triangle$  = bromide,  $\square$  = nitrite,  $\diamond$  = iodate,  $\circ$  = sulphate,  $*$  = iodide,  $\times$  = nitrate. Conditions as per Figure 2.3.

Figure 2.5:  $\text{C}^4\text{D}$  response across a silica reversed-phase monolithic column with acetate eluents of 1 to 20 mM (pH 4).

Figure 2.6:  $\text{C}^4\text{D}$  response across a silica reversed-phase monolithic column with acetate eluents of 1 to 50 mM (pH 4).

Figure 2.7: Schematic of the  $\text{C}^4\text{D}$  cell placed (a) directly on-column, (b) on open fused silica capillary and (c) on open fused silica capillary 'detector cell'. (i)

reversed-phase monolith, (ii) C<sup>4</sup>D cell, (iii) open fused silica capillary and (iv) zero dead volume union.

Figure 2.8: Peak areas of unretained chloride peaks recorded for the unmodified monolithic capillary column (□), a 100 μm i.d. open capillary (◇) and a section of 100 μm i.d. open capillary coupled to the end of the unmodified monolithic capillary column (△).

Figure 2.9: Sketch depicting the virtual electrode in a C<sup>4</sup>D cell. A = cross sectional area below electrode, l = distance separating the electrodes [19].

Figure 2.10: C<sup>4</sup>D response across a DDMAU modified reversed-phase monolithic column (◇) and a 100 μm i.d. fused silica capillary 'detector cell' (□) with KCl eluents (1 -50 mM).

Figure 2.11: C<sup>4</sup>D response across a DDMAU modified reversed-phase monolithic column (□) and a 100 μm i.d. fused silica capillary 'detector cell' (◇) with phthalate eluents (0 -0.5 mM, pH 4.0).

Figure 2.12: Separation of four anions on the modified monolithic silica capillary column recorded (a) directly on the monolithic capillary using C<sup>4</sup>D at ~13 cm column length, and (b) on an end-coupled 100 μm i.d. open capillary at ~16 cm column length<sup>a</sup>. <sup>a</sup> Distance includes the length of open fused silica capillary, 1= iodate, 2= nitrate, 3= bromide, 4= nitrite, \* = system peak. All other conditions as Figure 2.3.

Figure 2.13: Comparison of unretained injection peaks recorded with the monolithic capillary column (1;  $t_0 = 0.72$  min) and with the coupled monolithic and open capillary columns (2;  $t_0 = 1.03$  min). All other conditions as per Figure 2.3.

Figure 3.1: Structure of sodium dioctyl sulfosuccinate (DOSS).

Figure 3.2: C<sup>4</sup>D cell placed directly on-column with a ruler as a guide to allow reproducible movement along the length of the column.

Figure 3.3: Chromatographic system used for separations (a), column coating/washing (b) and column set up used in coating/washing (c). A = back pressure regulator on waste line, B = T-piece connector as flow splitter, C = movable detector cell, D = capillary column, E = zero dead volume microtight union, F = range of positions available to measurement with C<sup>4</sup>D, G = effective column length, H = detector cell lead, NFS = nanoflow sensor. Note: (c) is not to scale.

Figure 3.4: Breakthrough curves for a coating solution of 1 mM DOSS used to modify Column # 1, first coating from the capillary INLET to the OUTLET, followed by a second coating in the reverse direction.

Figure 3.5: Detector response across an unmodified Column # 1 compared with responses across the same column modified once from INLET to the OUTLET, and a second time in the reverse direction. First coating inlet to outlet (—◇—), second coating outlet to inlet (—□—) and unmodified (—\*—).

Figure 3.6: Detector responses recorded across Column # 1 following increasing periods of washing with deionised water (A–I show responses for subsequent 30 min intervals, J–M show stable response after washing for ~18 h). Note that curve A is the same as second coating outlet to inlet (—□—) in Figure 3.6.

Figure 3.7: Breakthrough curves for Column # 2 for forward and reverse coating with 1 mM DOSS solution at 1  $\mu\text{L min}^{-1}$ .

Figure 3.8: C<sup>4</sup>D response along the length of capillary Column #2 for the Unmodified monolith (→✖←), coating from inlet to outlet (→◇←), and coating from outlet to inlet (←□←).

Figure 3.9: 3D representation of the concentration of charged groups, and their spatial distribution, along the length of Column # 2 as a function of equilibration time.

Figure 3.10: Comparison of Column # 3 under two separate coatings in one direction only. Unmodified Column # 3 prior to 1<sup>st</sup> coating (→✖←), Column # 3 after 1<sup>st</sup> coating (←□←), unmodified Column # 3 prior to 2<sup>nd</sup> coating (←△←), Column # 3 after 2<sup>nd</sup> coating (←◇←) ( $n=3$ ).

Figure 3.11: Comparison of Column # 1; unmodified (←△←) and coated (←◇←) and Column # 2; unmodified (→✖←) and coated (←□←) ( $n=3$ ).

Figure 3.12: Comparison of Column # 1; unmodified (←△←) and coated (←◇←) and Column # 3 (1<sup>st</sup> coating); unmodified (→✖←) and coated (←□←).

Figure 3.13: Comparison of Column # 2; unmodified (←◇←) and coated (←◇←) and Column # 3; unmodified (←□←) and coated (←✖←) ( $n=3$ ).

Figure 3.14: Effect upon coating distribution due to inclusion of increasing amount of methanol in DI washing solution passed through the Column # 3 at 1  $\mu\text{L min}^{-1}$  for 30 minutes. A= unmodified monolith, B = modified monolith following equilibration with water, C-E = following 10% methanol wash, F = 20 % methanol wash, G = 30 % methanol wash, H = 40 % methanol wash, I = 50 % methanol wash.

Figure 3.15: Expanded view of the effect of washing with 40 % methanol for 30 minutes. Column # 3.

Figure 3.16: Response along column length for counter ion variation ( $n=3$ ). Column # 3.

Figure 3.17: Logarithmic relationship between coating response and counter ion equivalent ionic conductance for Column # 3.

Figure 3.18: Separation of (1) magnesium ( $5 \text{ mg L}^{-1}$ ), (2) calcium ( $10 \text{ mg L}^{-1}$ ), (3) strontium ( $20 \text{ mg L}^{-1}$ ) and (4) barium ( $40 \text{ mg L}^{-1}$ ) on Column #2. Eluent:  $0.5 \text{ mM}$  ethylenediamine (pH 4.5), flow rate:  $1 \text{ } \mu\text{L min}^{-1}$ , injection volume:  $10 \text{ nL}$ . Detection: Indirect  $\text{C}^4\text{D}$ . Column # 2.

Figure 3.19: Chromatograms of real sample analysis, 1 = Blank, 2 = Standards, 3 = Bottled water sample #1 (1/2 dilution), 4 = Tap water (1/10 dilution) and 5 = Bottled water sample #2 (1/10 dilution). Conditions as in Figure 3.18.

Figure 3.20: Separation of twelve amino acids on the DOSS coated capillary column (Column #2) (1= Asparagine, 2= Glycine, 3= Proline, 4= Glutamine, 5= Alanine, 6 =unknown, 7 =Valine, 8= Methionine, 9= Isolucine, 10 = Leucine, 11= Lysine, 12= Histidine, 13= Phenylalanine,  $100 \text{ mg L}^{-1}$  each,  $10 \text{ nL}$  injection). Eluent:  $10 \text{ mM}$  nitric acid (pH 3.0), flow rate:  $1 \text{ } \mu\text{L min}^{-1}$ , injection volume:  $10 \text{ nL}$ . Detection: Indirect  $\text{C}^4\text{D}$ .

Figure 4.1: Structure of AMPS.

Figure 4.2: Set-up used for photgrafting of AMPS onto monolith surface, (a) monolith, (b) PEEK sleeves as masks, (c) cardboard covers, (d) area to be photografted (*ca.*  $10 \text{ mm}$ ), (e) light source, (f) light blocked from initiating photografting, (g) light permitted to initiate photografting.

Figure 4.3: Wave-guide effect of FSC. Showing (a) perpendicular light, (b) high angle light, (c) high angle light undergoing total internal reflection and propagating

along monolith, inducing photografting beyond mask, (d) PEEK sleeves, (e) capillary wall.

Figure 4.4: Schematic of in-house built photografting holder. (a) “Chimney” to allow only perpendicular and low angle light to enter, (b) UV lamp, (c) monolith to be photografted, (d) area to be photografted, (e) perpendicular UV light and (f) high angle UV light being blocked.

Figure 4.5: C<sup>4</sup>D scan of Monolith # 1 showing the presence of three photografted zones of AMPS. (a) Zone 1, (b) Zone 2, (c) Zone 3, (i) starting position of Zone 3, (ii) excess AMPS washing from Zone 3, (iii) final reading of Zone 3 ( $n=3$ ).

Figure 4.6: Expanded view of Figure 4.5, (c) Zone 3, (i) starting position of Zone 3, (ii) excess AMPS washing from Zone 3, (iii) final reading of Zone 3 ( $n=3$ ).

Figure 4.7: Effect of short methanol wash on Zone 1 of Monolith # 1, showing a *ca.* 10% decrease in signal from before short methanol wash (—⊗—) and after short methanol wash (—▲—),  $n=3$ .

Figure 4.8: 3D-plot of washing of Monolith # 2. (a) Zone 1, (b) Zone 2, (c) Zone 3, (d) washing of excess AMPS in frontal chromatographic nature.

Figure 4.9: C<sup>4</sup>D profile showing the spatial tolerances obtained during photografting ( $n=3$ ). Monolith # 1.

Figure 4.10: Comparison of Monolith # 1 (i) & # 2 (ii) after wash cycles, (a) zone 1 ( $\text{J cm}^{-2}$ ), (b) zone 2 ( $3 \text{ J cm}^{-2}$ ) and (c) zone 3 ( $5 \text{ J cm}^{-2}$ ). Each scan is an average of triplicate reading (errors bars equal to standard deviation).

Figure 4.11: Monolith # 3, showing five zones of photografted AMPS. (a) Zone 1 ( $1 \text{ J cm}^{-2}$ ), (b) Zone 2 ( $2 \text{ J cm}^{-2}$ ), (c) Zone 3 ( $3 \text{ J cm}^{-2}$ ), (d) Zone 4 ( $4 \text{ J cm}^{-2}$ ) and (e) Zone 5 ( $7 \text{ J cm}^{-2}$ ).

Figure 4.12: Monolith # 4, showing one zone of photografted AMPS ( $n=3$ ). (a) Zone 1 ( $0.25 \text{ J cm}^{-2}$ ), (b) Zone 2 ( $0.5 \text{ J cm}^{-2}$ ) and (c) Zone 3 ( $1 \text{ J cm}^{-2}$ ).

Figure 4.13: Comparison of Zone 1 (receiving  $1 \text{ J cm}^{-2}$  of UV energy) for Monolith # 3 ( $\text{---}\square\text{---}$ ) and Monolith # 4 ( $\text{---}\square\text{---}$ ) ( $n=3$ ).

Figure 4.14: Effect on UV energy used to photograft on ( $\text{---}\diamond\text{---}$ ) zone height and ( $\text{---}\square\text{---}$ ) area of zone.

Figure 5.1: Schematic representation of (a) the reaction of azlactone and *m*-aminophenylboronic and (b) the transition of planar boronic acid to a tetrahedral boronic acid anion under high pH conditions.

Figure 5.2: (a) Contributions of  $\text{C}^4\text{D}$  signal of a photografted zone at two pH values, (b) contributions to  $\text{C}^4\text{D}$  signal of a photografted zones and (c) background subtracted signal for a photografted zone at two pH values.

Figure 5.3: Uncorrected  $\text{C}^4\text{D}$  scan of two VAL-APBA modified zones on a monolithic capillary column with pH 10.2 buffer.

Figure 5.4:  $\text{C}^4\text{D}$  scan of VAL-APBA modified zones on a monolithic capillary column at ( $\text{---}\ast\text{---}$ ) pH 4.0, ( $\text{---}\times\text{---}$ ) pH 6.1, ( $\text{---}\triangle\text{---}$ ) pH 6.8 and ( $\text{---}\square\text{---}$ ) pH 10.2 (normalised to first reading of each column).

Figure 5.5: Baseline response of unmodified monolithic capillary column for each buffer used in on-column titration of VAL-APBA.

Figure 5.6: Comparison of on-column titration of a polymer monolith capillary column modified with two zones of VAL-ADA over pH a range of 4 to 10 with titration of APBA in solution. Zone 1 () and Zone 2 () and free APBA in solution ()

Figure 5.7: 1<sup>st</sup> derivative analysis of two zones of VAL-APBA on modified monolithic capillary columns (1) Zone 1 & (2) Zone 2 on column and (3) titration of APBA in solution.

Figure 5.8: 1<sup>st</sup> derivative analysis of four zones of VAL-APBA on modified monolithic capillary columns, ( $n=4$ , two columns each with two zones) with an average  $pK_a$  of  $6.45 \pm 0.06$ , (a) Column #1 and (b) Column # 2.

Figure 5.9: Uncorrected C<sup>4</sup>D scan of VAL-ADA modified zones on a monolith capillary column with pH 10.2 buffer.

Figure 5.10: On-column titration of a polymer monolith capillary column modified with two zones of VAL-ADA over a pH range of 3 to 10.

Figure 5.11: 1<sup>st</sup> derivative of on-column titration of a polymer monolith capillary column modified with two zones of VAL-ADA over a pH range of 3 to 10.

Figure 5.12: Structure of VAL-ADA.

Figure 5.13: C<sup>4</sup>D scan of VAL-IDA modified zones on a monolith capillary column with pH 10.2 buffer.

Figure 5.14: Structure of IDA linked to monolith surface via azlactone (note the amide group).

Figure 5.15: On-column titration of a polymer monolith capillary column modified with two zones of VAL-IDA over a pH range of 3 to 10.

Figure 5.16: 1<sup>st</sup> derivative of on-column titration of a polymer monolith capillary column modified with two zones of VAL-IDA over a pH range of 3 to 10.

Figure 5.17: Ethanolamine linked to the monolith surface via VAL.

Figure 5.18: Comparison of the on-column titrations of VAL zones reacted with (a) APBA (—▲—), (b) ADA (—◇—) and (c) IDA (—□—) and then blocked with ethanolamine, with the on-column titration of VAL zones reacted with ethanolamine only (—◇—).

Figure 5.19: Effect of the inclusion of copper on the on-column titration of VAL-ADA over pH 3 to 9. Zone 1 titration (—◇—), Zone 2 titration (—▲—), Zone 1 titration with copper (—△—) and Zone 2 titration with copper (—□—).

Figure 5.20: Comparison of the response for VAL-ADA modified monolithic capillary monolith with a series of metals, at pH 9, compared to the known formation constant of these metals with N-(hydroxymethyl)-iminodiacetic acid.

Figure 6.1: Set-up used to pack PEEK columns. (a) Packing solvent, (b) HPLC pump, (c) pressure gauge, (d) high pressure packing bomb, (e) vial with phase, (f) column, (g) union with frit, (h) waste line, (i) waste packing solvent.

Figure 6.2: Schematic of dual C<sup>4</sup>D set-up. 1 = Union with frit, 2 = 1.59 mm o.d. (1/16<sup>th</sup>) packed PEEK column (381 μm i.d.), 3 = C<sup>4</sup>D cell under investigation (suitable for 1.59 mm (1/16<sup>th</sup>) PEEK tubing), 4 = commercial C<sup>4</sup>D cell, 5 = 360 μm o.d. 100 μm i.d. fused silica capillary, 6 = Movement of the test C<sup>4</sup>D cell along the column length.

Figure 6.3: Layout of C<sup>4</sup>D detector cell for use with 1.59 mm o.d. (1/16<sup>th</sup>) PEEK tubing; (a): cell input (excitation) lead, (b): copper excitation electrode, (c): Faraday shield. (d): copper signal pick-up electrode, (e): feedback resistor, (f): signal output lead, (g): Teflon sleeve, (h): column, (i): cell power leads.

Figure 6.4: Pictures of signal generation, pick-up and processing., a= in-put from function generator to rectifier unit, b = in-put signal from rectifier unit to cell, c = out-put signal from cell to rectifier unit, d = signal out from rectifier to eDAQ.

Figure 6.5 (a) Bode plots with column and mobile phase positioned within the cell. *Column*: 190 mm × 380 μm i.d. PEEK column packed with Dionex OmniPac 8.5 μm PAX-100 anion exchange resin. *Mobile phase*: 0.5 mM sodium benzoate containing 2% methanol. *Flow rate*: 20 μL min<sup>-1</sup>. (b) Bode plots illustrating stray capacitance with dry empty PEEK tubing (1.59 mm × 380 μm) positioned within the cell. *Legend*: 4.7 MΩ (—▲—), 3.3 MΩ (—■—) and 1.0 MΩ (—◆—).

Figure 6.6: Effect of input frequency upon (a) peak height and (b) signal to noise ratio for three different resistors. Conditions as in Figure 6.5. Other conditions: *Injection volume*: 1 μL, *Sample*: 10 mg L<sup>-1</sup> nitrite. *Noise calculation*: noise was measured from 2.5 minutes to 4.5 minutes in each blank chromatogram. *Legend*: 4.7 MΩ (—▲—), 3.3 MΩ (—■—) and 1.0 MΩ (—◆—).

Figure 6.7 Chromatogram of 10 mg L<sup>-1</sup> nitrite at (a): 200 kHz (b): 1000 kHz and (c): 10 KHz showing the effect of frequency on peak height and shape. Conditions as in Figure 6.6.

Figure 6.8: Comparison of chromatograms obtained with (a) 1.59 mm C<sup>4</sup>D on-column detector and (b) off-column commercial detector for 20 mg L<sup>-1</sup> nitrite (1) and 10 mg L<sup>-1</sup> nitrate (2). Eluent: 2.5 mM sodium benzoate (2% methanol), flow rate: 20 μL min<sup>-1</sup>, injection volume: 10 μL min<sup>-1</sup>.

Figure 6.9: Separation of nitrite, nitrate and sulfate at (a)  $L_{\text{eff}}$  230 mm, (b)  $L_{\text{eff}}$  60 mm, and (c) initial  $L_{\text{eff}}$  230 mm with detector moved to 60 mm after 4 minutes. *Column*: 250 mm  $\times$  380  $\mu\text{m}$  i.d. PRP-X100 phase. Eluent: 1 mM phthalate eluent (pH 4.0) containing 2% methanol. Flow: 20  $\mu\text{L min}^{-1}$ , injection volume: 10  $\mu\text{L}$ . Peaks: (1) 10  $\text{mg L}^{-1}$  nitrite, (2) 10  $\text{mg L}^{-1}$  nitrate, (3) 20  $\text{mg L}^{-1}$  sulfate.

Figure 6.10: Evaluating the homogeneity of the stationary phase packing of a 1.59 mm o.d. column using contactless conductivity. Each point along both horizontal lines represents a location on the column at which the cell (measured from the exact position of the electrodes within the die-cast metal casing) was placed and an output voltage reading was recorded.

**List of tables:**

Table 1.1: Comparison of limits of detection obtained for C<sup>4</sup>D and UV detection for the determination of inorganic anions in CEC [86].

Table 1.2: LODs obtained for C<sup>4</sup>D and UV detection for NSAIDs [88].

Table 1.3: Comparison of LODs for non-suppressed and suppressed IC separations using C<sup>4</sup>D and commercial conductivity detector [82].

Table 2.1: Linearity data for injection of KCl with 100 µm i.d. FSC, silica monolith and silica monolith with 100 µm i.d. fused silica capillary.

Table 3.1: Selectivity of the DOSS coated column (Column #2) for selected alkali metals, alkaline earth metals and transition metals with an ethylenediamine eluent.

Table 3.2: Analytical performance data for separation of cations. Note: 0.25 mg L<sup>-1</sup> standard for strontium and barium was omitted since these levels are below their respective LOD's. Column # 2.

Table 3.3: Concentration of calcium and magnesium determined for three samples.

Table 3.4: Efficiency data for amino acid separation.

Table 4.1: The number of zones and the respective energy used to photograph each zone.

Table 4.2: Wash cycle of photografted monoliths.

Table 5.1: Buffers used for on-column titration of APBA.

Table 6.1: Comparison of the analytical performance criteria for the 1.59 mm C<sup>4</sup>D and commercial C<sup>4</sup>D.

## List of publications:

1) Evaluation of capillary ion exchange stationary phase coating distribution and stability using radial capillary column contactless conductivity detection

*Eoin Gillespie, Miroslav Macka, Damian Connolly and Brett Paull, Analyst, 2006, 131, 886.*

Times cited: 12

*Note: Obtained front cover of Analyst*

2) Capillary ion chromatography of inorganic anions on octadecyl silica monolith modified with an amphoteric surfactant

*Colmán Ó Ríordáin, Eoin Gillespie, Damian Connolly, Pavel N. Nesterenko and Brett Paull, Journal of Chromatography A, 2007, 1142, 185.*

Times cited: 8

3) Use of contactless conductivity detection for non-invasive characterisation of monolithic stationary-phase coating for application in ion chromatography

*Eoin Gillespie, Damian Connolly, Miroslav Macka, Pavel N. Nesterenko and Brett Paull, Analyst, 2007, 132, 1238.*

Times cited: 2

*Note: Obtained front cover of Analyst and listed as HOT PAPER on RSC website.*

4) Development of a contactless conductivity detector cell for 1.6 mm O.D. (1/16th inch) HPLC Tubing and Micro-Bore Columns with On-Column Detection

*Eoin Gillespie, Damian Connolly, Miroslav Macka, Peter C. Hauser and Brett Paull, Analyst, 2008, 133, 1104 DOI: 10.1039/b803038c*

Times cited: 0

5) Accurate non-invasive determination of  $pK_a$  of surface functionalised ion exchange monoliths using capacitively coupled contactless conductivity detection

*Eoin Gillespie, Damian Connolly, Pavel N. Nesterenko and Brett Paull*

**Analyst**, 2008, 133, 874. DOI: 10.1039/b803349h

Times Cited: 0

**List of poster presentations:**

1) Capillary ion chromatography using monolithic columns and across column detection using contactless conductivity detection

*Colmain O'Riordain, Eoin Gillespie, Damien Connolly, Pavel. N. Nesterenko and Brett Paull, 4th Biennial Conference on Analytical Sciences in Ireland, DIT, Dublin, 11-12 April 2006.*

2) Capillary ion chromatography using monolithic columns and across column detection using contactless conductivity detection

*Colmain O'Riordain, Eoin Gillespie, Damien Connolly, Pavel. N. Nesterenko and Brett Paull, Analytical Research Forum, University College Cork, Cork, 13-14 July 2006.*

3) Evaluation of capillary ion exchange stationary phase coating stability and distribution using capacitively coupled contactless conductivity detection.

*Eoin Gillespie, Miroslav Macka, Damian Connolly and Brett Paull, International Ion Chromatography Symposium (IICS), Pittsburgh, PA, USA, 24-27 September 2006. NOTE: Short-listed for student poster prize*

4) Use of contactless conductivity detection for the characterisation of stationary phase chemistry in surface modified monolithic capillary columns; application to ion chromatographic determination of inorganic cations and amino acids.

*Eoin Gillespie, Miroslav Macka, Damian Connolly and Brett Paull, 31<sup>st</sup> International Symposium on High Performance Liquid Phase Separations and Related Techniques (HPLC 2007), Ghent, Belgium, 17-21 June 2007.*

5) New Possibilities for capillary ion chromatography of inorganic and small organic ions using silica based ion exchangers with on-column contactless conductivity detection.

*Damian Connolly, Eoin Gillespie, Miroslav Macka, Damian Connolly and Brett Paull, 31<sup>st</sup> International Symposium on High Performance Liquid Phase Separations and Related Techniques (HPLC 2007), Ghent, Belgium, 17-21 June 2007.*

*Note: Short-listed for 25 top posters at conference (out of approx. 800 posters).*

6) Use of contactless conductivity detection for the characterisation of stationary phase chemistry in surface modified monolithic capillary columns; application to ion chromatographic determination of inorganic cations and amino acids.

*Eoin Gillespie, Miroslav Macka, Damian Connolly and Brett Paull. Analytical Research Forum, University of Strathclyde, Glasgow, 16-18 July 2007.*

7) Advances in evaluation of capillary polymer monolith surface chemistry using photografting methods and contactless conductivity detection.

*D. Connolly, E. Gillespie, Z. Walsh, V. O'Shea and B. Paull, 12<sup>th</sup> Symposium on the Interface of Regulatory & Analytical Sciences for Biotechnology Health Products (WCBP 2008), Washington DC, USA, 28<sup>th</sup>-\*30<sup>th</sup> January 2008.*

8) Use of contactless conductivity detection for the characterisation of stationary phase chemistry in surface modified monolithic capillary columns.

*Eoin Gillespie, Damian Connolly, Miroslav Macka, and Brett Paull, 5<sup>th</sup> Biennial Conference of Analytical Sciences in Ireland, Waterford Institute of Technology, 7th May, 2008*

9) A novel contactless conductivity detector for 1/16th" PEEK tubing and packed micro-columns.

*Eoin Gillespie, Damian Connolly, Miroslav Macka, Peter Hauser and Brett Paull, 5<sup>th</sup> Biennial Conference of Analytical Sciences in Ireland, Waterford Institute of Technology, 7th May, 2008*

10) Use of contactless conductivity detection for the characterisation of stationary phase chemistry in surface modified monolithic capillary columns.

*Eoin Gillespie, Damian Connolly, Miroslav Macka, and Brett Paull, Analytical Research Forum, University of Hull, 21<sup>st</sup> – 23<sup>rd</sup> July 2008.*

11) A novel contactless conductivity detector for 1/16th" PEEK tubing and packed micro-columns.

*Eoin Gillespie, Damian Connolly, Miroslav Macka, Peter Hauser and Brett Paull, Analytical Research Forum, University of Hull, 21<sup>st</sup> – 23<sup>rd</sup> July 2008.*

12) A novel contactless conductivity detector for 1/16th" PEEK tubing and packed micro-columns.

*Eoin Gillespie, Damian Connolly, Miroslav Macka, Peter Hauser and Brett Paull, , International Ion Chromatography Symposium, 21<sup>st</sup>-24<sup>th</sup> Septmeber 2008, Red Lion Hotel on the River, Portland, Oregon, USA.*

13) Use of contactless conductivity detection for the characterisation of stationary phase chemistry in surface modified monolithic capillary columns.

*Eoin Gillespie, Damian Connolly, Miroslav Macka, and Brett Paull, , International Ion Chromatography Symposium, 21<sup>st</sup>-24<sup>th</sup> Septmeber 2008, Red Lion Hotel on the River, Portland, Oregon, USA.*

**List of oral presentations:**

1) Use of contactless conductivity detection for the characterization of stationary phase chemistry on surface modified monolithic capillary columns

*Eoin Gillespie, Damian Connolly, Miroslav Macka, Brett Paull.*

*The 32nd International Symposium on Capillary Chromatography (ISCC), 27<sup>th</sup>-30<sup>th</sup> May 2008, Congress Centre, Riva del Garda, Italy.*

NOTE: Key note lecture

2) Use of Contactless Conductivity for the Characterization of Capillary Monolithic Columns Covalently Modified with Ionic Species

*Eoin Gillespie, Damian Connolly, Miroslav Macka, Pavel N.Nesterenko, Brett Paull, International Ion Chromatography Symposium, 21<sup>st</sup>-24<sup>th</sup> Septmeber 2008, Red Lion Hotel on the River, Portland, Oregon, USA.*

**List of awards:**

Outstanding Graduate Researcher Award 2008, presented by the Faculty Research Committee of DCU.

Royal Society of Chemistry overseas conference travel grant – 2008

CASSS conference busrary-2008

I would like to thank Prof. Brett Paull, firstly for the opportunity to undertake this PhD and also for all the guidance and advice over the duration of this PhD. Many thanks also go to Dr. Mirek Macka, Prof. Pavel Nesterenko and Prof. Peter Hauser for all their advice.

A great deal of gratitude goes to all the other excellent people who I've had the privilege of working with over the last few years, especially to Dr. Damian Connolly and Dr. Leon Barron. My thanks also go to all the technical staff and postgraduates of the School of Chemical Sciences, for the many questions answered and craic had during demonstrating.

I would like to thank my family, my parents John and Christina and my sister Lisa, for all the support both financial and emotional, without which I would not have completed this PhD.

Special thanks go to Ms. Aisleen Haughey, who kept me sane during the more difficult times. Without your constant support and commitment to getting to me this point, I would have fallen long ago.

A small thanks goes to the late great Douglas Adams, who when I needed escape from the science of earth, transported me to Heart of Gold or the planet Krikket in 30 minute adventures.

Undoubtedly I have forgotten to mention some people, who very much deserve to be, but alas I always forget someone, to you too I extend my thanks.

---

## **Chapter 1: Literature survey**

---

## 1.1 Liquid chromatography.

Liquid chromatography is an analytical technique that results in the separation of chemical species depending on their interaction with and within two discrete phases, a flowing mobile phase (a liquid) and a stationary phase (a solid). The relative affinity of the analytes for the two phases results in their separation. Since the discovery of chromatography in 1903 by Mickhal Tswett, the growth in the variety of chromatographic modes and techniques has been dramatic. Dependant on the mode of separation, analytes of every class can be separated (i.e. polar, non-polar, ionic, low and high molecular weight). The driving force behind the development of chromatographic techniques able to separate these different classes of molecules, in an ever more efficient and timely fashion, has been the advancement in stationary phases, both in the creation of new chemistries but also in new formats.

## 1.2 Stationary phases.

### *1.2.1 Particulate stationary phases.*

The stationary phase component of a chromatographic system can often be considered the most important part. The selectivity and efficiency of the stationary phase results in the chromatographic performance of the column. Stationary phases to date have largely been based upon particulate resins. In these columns spherical particles of silica or polymeric beads, generally in the range of 3 to 10  $\mu\text{m}$  diameter, are tightly packed within a cylindrical housing of 1 to 6 mm internal diameter (i.d.) [1]. In the last fifty years the size of the particles has continuously decreased. In the 1950s particle sizes were around 100  $\mu\text{m}$  and dropped to ca. 3  $\mu\text{m}$  in 2000, giving efficiencies of  $\sim 1,300$  and  $\sim 160,000 \text{ N m}^{-1}$ , respectively. The theoretical advantage of moving to smaller diameter particles has been known for more than 30 years [1]. The Knox plot (Figure 1.1) of reduced plate height vs.

reduced linear velocity for different diameter particles shows a reduction in plate height for small particles and thus higher efficiency.

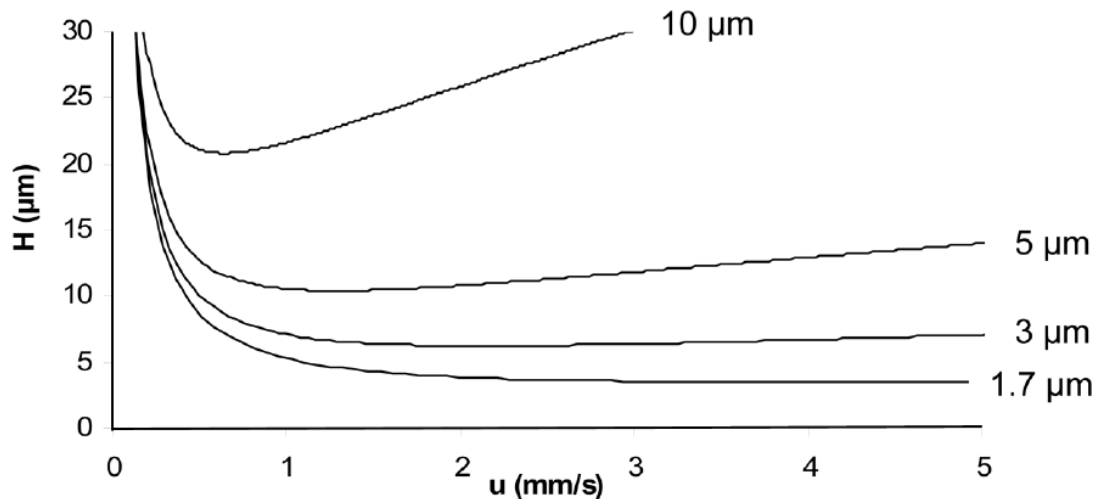


Figure 1.1: Knox plot (reduced plate height vs. reduced linear velocity) showing the effect of reducing particle diameter on plate height [1].

The main advantage of reducing particulate size is the much lower contribution of the  $C$  term to the van Deemter plot. The van Deemter equation (Equation 1.1 below) describes the contributions to the height equivalent to theoretical plate (HETP) of a column:

$$HETP = A + \frac{B}{u} + Cu \quad \text{Equation 1.1}$$

where  $A$  = Eddy diffusion,  $B$  = axial diffusion,  $C$  = mass transfer and  $u$  = linear velocity of the mobile phase.

A) Eddy diffusion: As analytes move along the column in the mobile phase they are presented with multiple paths to the same point. The interconnected networks of interparticulate voids, in packed columns, and through-pores, in monoliths, present a multitude of possible paths through the column. As some molecules will

move on a more direct path than the majority of molecules, they will appear to advance along the column in a shorter time. Conversely some molecules will move on a more circuitous path than the majority of molecules they will appear to advance along the column for a longer time. This results in a distribution of molecules around a central mass [2]. Figure 1.2 depicts two possible paths for a single molecule from point A to B.

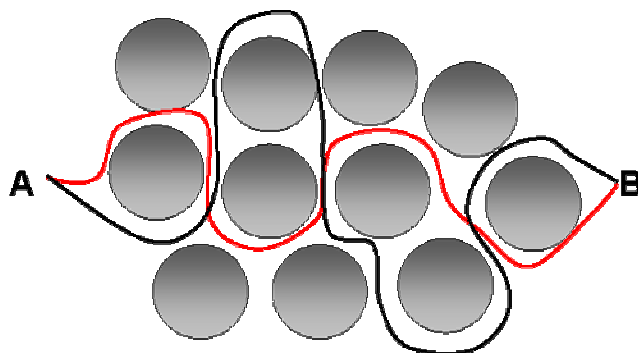


Figure 1.2: Schematic depicting two paths possible from point A to point B within a packed column.

B) Longitudinal diffusion: As the sample is introduced into the column it will undergo diffusion symmetrically around its centre of mass. As the analytes in a chromatographic column are within a flowing system the contribution of longitudinal diffusion is small [2].

C) Mass transfer: As an analyte passes along the column it will partition into the stationary phase and reside there for a period of time, and then partition back into the mobile phase. During the partitioning into the stationary phase the analyte will not be advancing along the column and will therefore be retarded compared to the centre of mass of the analyte. The time spent in the stationary phase will determine the extent to which the analyte is “held back” compared to the centre of mass. If the time spent is short (i.e. fast transfer kinetics) the difference between the centre of mass and the analyte in the stationary phase will be low, whereas if

the time spent in the stationary phase is long (i.e. slow transfer kinetics) the difference will be larger [2].

The contributions of these three parameters to the efficiency (as height equivalent to theoretical plate (HETP) vs. linear velocity) of a column are shown graphically in Figure 1.3.

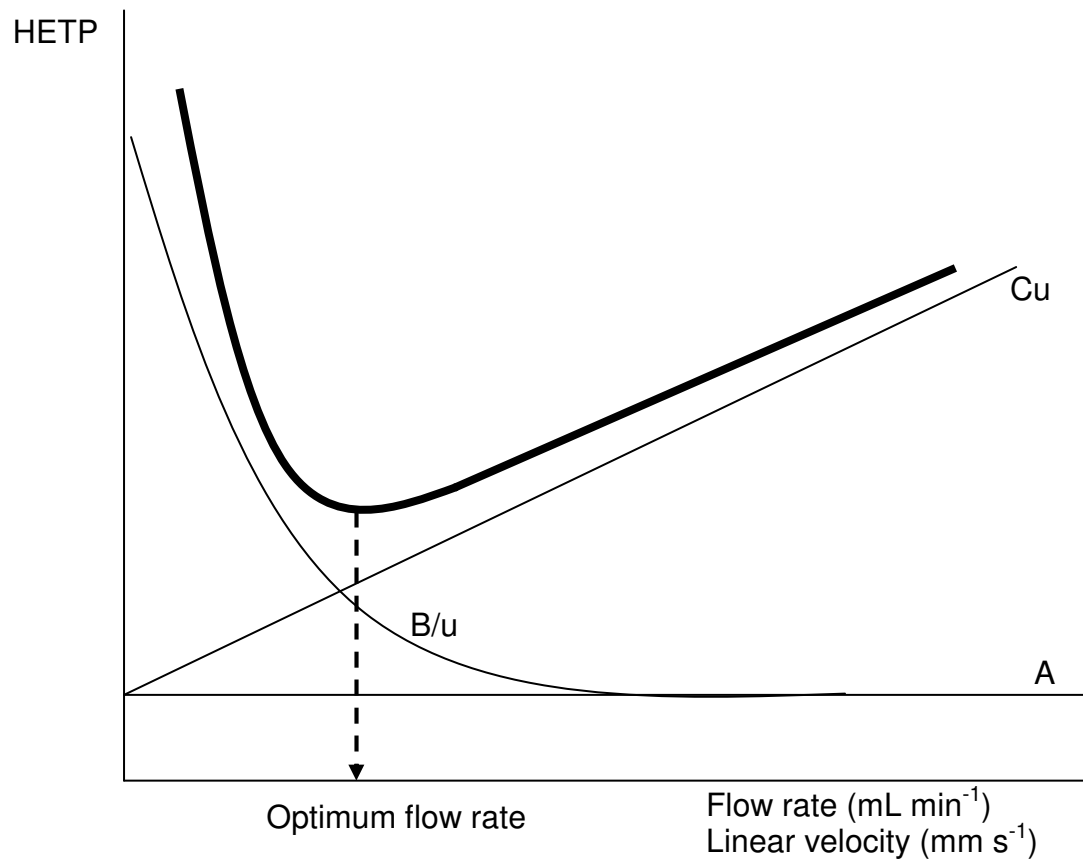


Figure 1.3: Contributions of A, B and C terms in the van Deemter plot.

The faster mass transport (low  $C$ -term of the van Deemter equation) associated with these particles also allows for the use of higher flow rates without a sacrifice in efficiency [1]. However, one drawback of using smaller and smaller particles in these columns is the increasing back pressure generated. The increase in pressure is directly proportional to the cube of the particle diameter used; for

example the pressure generated by a 1.7  $\mu\text{m}$  compared to a 5  $\mu\text{m}$  particle column of the same length under optimal flow conditions, will be 27 times higher [1]. A result of this increase in back pressure is the requirement for more specialised pumps capable of pumping up to the required pressures.

Another way to exploit a relatively low  $C$ -term, but without a dramatic increase in back pressure is the use of “monolithic” stationary phases.

### *1.2.2 Monolithic stationary phases.*

The term *monolith* comes from Greek for “one stone” or in this case “one piece”. A monolithic stationary phase, rather than being made up of small individual pieces (i.e. spherical particles), is constructed of one large porous piece through which the mobile phase flows [3]. A monolith can be viewed as if the inter-particulate void of a packed column was replaced with stationary phase and the particles removed [3]. The result is a single piece of material that has a porous nature with multiple, tortuous paths through it.

#### *1.2.2.1 Origins.*

The concept of monolithic stationary phases were proposed as far back as the 1960's [3]. However, for the sake of brevity, in this Chapter, monoliths will be defined as *rigid* macro-porous stationary phases, manufactured from either silica or polymer. In 1992, Svec *et al.* published the first paper on the production of rigid macro-porous polymeric monoliths for chromatography [4]. Until this point other attempts to produce monolithic stationary phases were not rigid and suffered from compression and/or swelling [4]. *Rigid* monoliths have a permanent pore structure, persisting even when dry [5]. The introduction of polymeric monoliths was followed in 1996 by the first publications of silica-based rigid monoliths [6, 7]. In recent years the production of monoliths based on carbon [8] and zirconia [9] have received interest, taking advantage of their different chemistries.

### *1.2.2.2 Production of silica and polymeric monoliths.*

The production of silica based monolithic rods is based on sol-gel chemistry. In sol-gel chemistry, hydrolysis and polycondensation reactions of alkoxysilanes lead to the formation of an insoluble silica mass, which precipitates (i.e. phase separation) [3, 10, 11]. The reaction mixture contains a silica source (e.g. tetramethoxysilane) and an inert compound (e.g. polyethylene glycol) [3, 10, 11]. The hydrolysis and polycondensation reactions of the alkoxysilanes can lead to the formation of particulates or a monolith depending on the experimental conditions. The silica solid shrinks after the phase separation (i.e. the precipitation of the silica) has taken place. One method of producing silica monoliths is the mould method. The silica monolith mixture is placed into a cylindrical mould, sealed and placed into a water bath. When silica monoliths are produced using a mould, the shrinkage must be taken into account. For a column of 4.6 mm i.d. a mould of 6 mm i.d. must be used [12]. However, when silica monoliths are produced within fused silica capillaries, which has been activated with sodium hydroxide, the monolith is chemically bonded to the surface and shrinkage is not observed. Once the silica gel is produced it is then aged under alkaline conditions to produce its meso-porous structure [3, 13]. Figure 1.4 is a schematic of the preparation of silica monoliths [13].

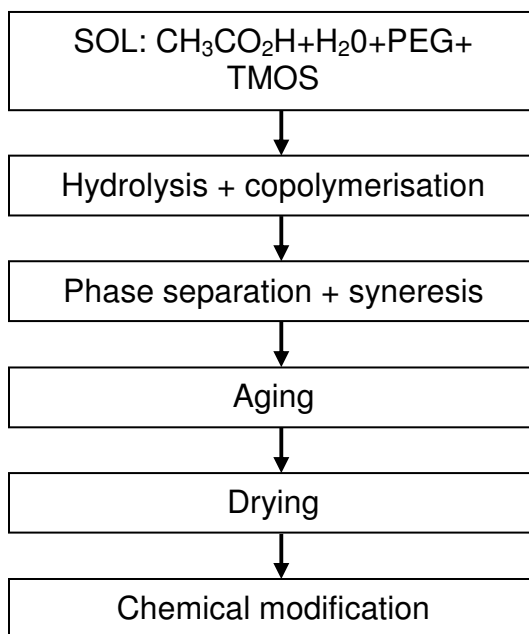


Figure 1.4: Schematic representation of the synthetic steps for the preparation of silica-based HPLC monoliths [13].

The production of polymeric monoliths has been based on several organic polymers including polystyrene, methacrylate and acrylamide [3]. The synthesis of polymeric monoliths follows a simple reaction scheme. The required components in the synthesis are: monomers (which form the monolith), a free radical initiator (to start the polymerisation) and a porogen system (one or more solvents). The polymerisation starts with the decomposition of the initiator, forming a free radical, which results in the initiation of the polymerisation. As the polymer chain length grows their solubility in the porogen system decreases. These chains then precipitate from the porogen system as nuclei (i.e. phase separation). The un-polymerised monomers are a better solvent for the nuclei than the porogen system, leading to the nuclei becoming swollen with the monomers, resulting in polymerisation occurring within the nuclei. The nuclei continue to grow as the polymerisation progresses, forming micro-globules, to a point where they crosslink between one another. This then forms the final structure of the monolith, where the macro-pores of the monolith are occupied by the porogen system [14]. Figure

1.5 depicts the preparation of a polymeric monolith using a mould and heat to initiate the polymerisation (i.e. thermopolymerisation).

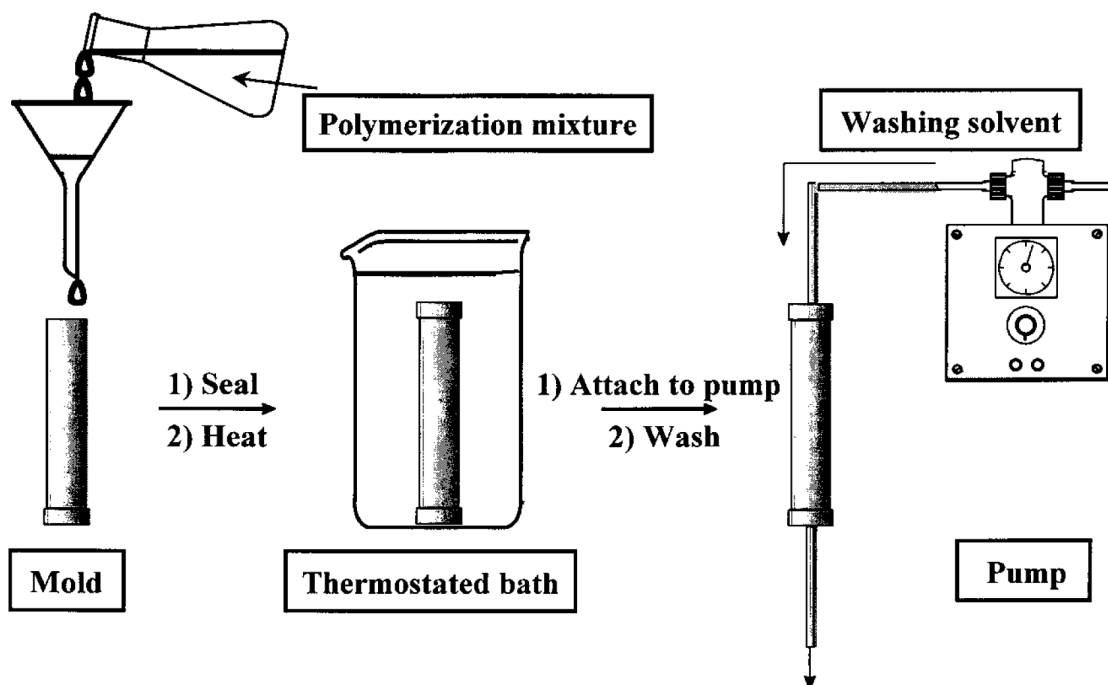


Figure 1.5: Schematic for the preparation of rigid macroporous polymer monoliths [15].

#### 1.2.2.4 Advantages of monoliths over particulate.

When van Deemter plots of particulate and monolithic columns are compared one major difference is apparent, the contribution of the  $C$  term. The  $C$  term contribution in monolithic columns is much lower than that of particulate columns. This is due to higher mass transfer kinetics, i.e. faster partitioning of analytes between the mobile and stationary phase reported to be a result of convection-based diffusion processes [13-16]. Figure 1.6 compares the van Deemter plot for uracil on a particulate and monolithic column. It is evident that the monolithic column affords the use of higher flow rates without a severe loss in efficiency.

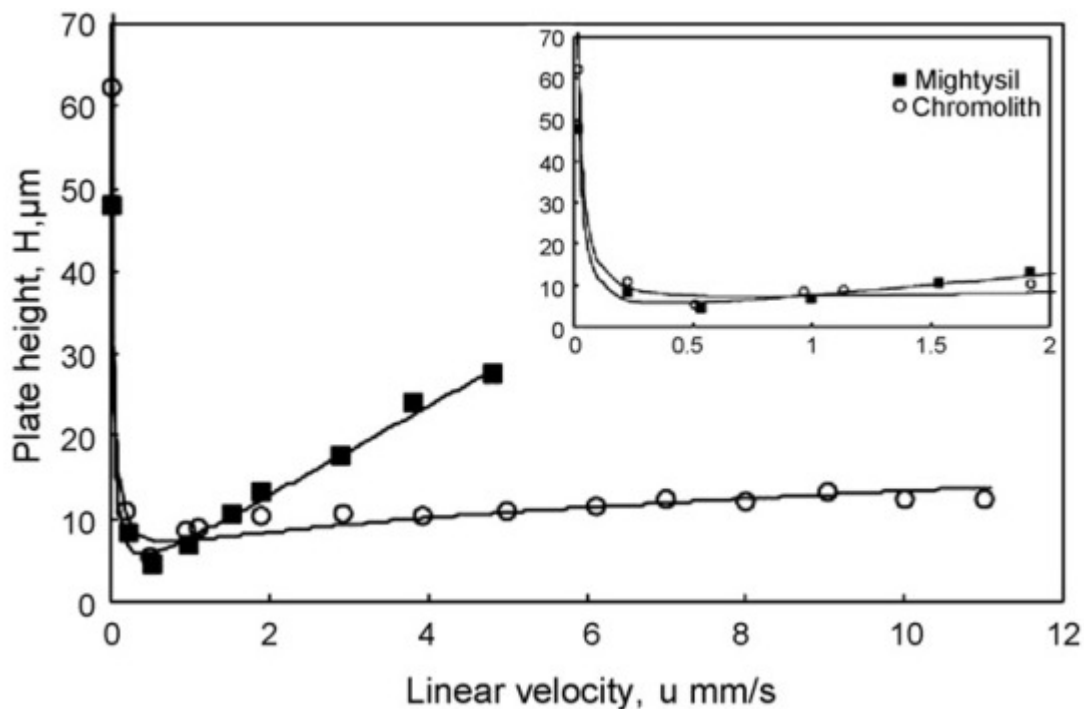


Figure 1.6: Plots of plate height values for uracil against linear velocity of mobile phase: conventional size columns; Mightysil (■) and Chromolith (○) [16].

As mentioned above, the improved mass transfer kinetics of monolithic stationary phases can be attributed to convective rather than diffusive mass transfer. This is due to the fact that the mobile phase is forced to flow through the pores of the monolith whereas in a particle column the majority of the mobile phase flows between the particles [5].

Another advantage of monolithic columns over particulate phases is the lower back pressures due to their higher permeability. Comparing the porosity of a particulate (40-60 %, dependant on packing) and monolithic column (>80%), it is clear that the monolithic column has a higher porosity. This higher porosity results in a lower resistance to flow through the bed of the monolith; meaning that much higher flow rates can be used with a smaller increase in back pressure [10].

Other advantages of monolithic over particulate stationary phases include: no requirement for frits to retain the phase; they can be produced in several formats (e.g. disks, capillary, microfluidic devices); and ease of modification.

### *1.2.2.3 Advantages and disadvantages of silica and polymeric monoliths.*

The main difference between silica and polymeric monoliths is in their pore structures. Silica monoliths have a *bimodal* pore structure. Bimodal means that there are two main types of pores present in these columns [17]. Firstly there are the macro-pores (or through-pores) which allow for the passage of mobile phase through the stationary phase. These pores generally range from 1 to 10  $\mu\text{m}$  in diameter. On the surface of these through-pores are the meso-pores, with diameters of 2 to 400 nm [17]. The meso-pores on the surface of the macro-pores result in silica monoliths having a large surface area (up to  $300 \text{ m}^2 \text{ g}^{-1}$ ). This high surface area allows for greater interaction of small molecules as they are able to diffuse in and out of the pores rapidly. This bimodal pore structure results in silica monoliths being applicable to the separation of small molecules. Figure 1.7 shows the bimodal pore structure of a silica monolith. The meso-porous structure of silica monoliths has a major disadvantage, due to the diffusion rates of macro-molecules being lower than small molecules. As a result macro-molecules (e.g. proteins) become “trapped” within the mesopores leading to very low efficiency separations on silica monoliths, due to band broadening. However, the use of the correct meso-porous structure can allow the efficient separation of proteins [13].

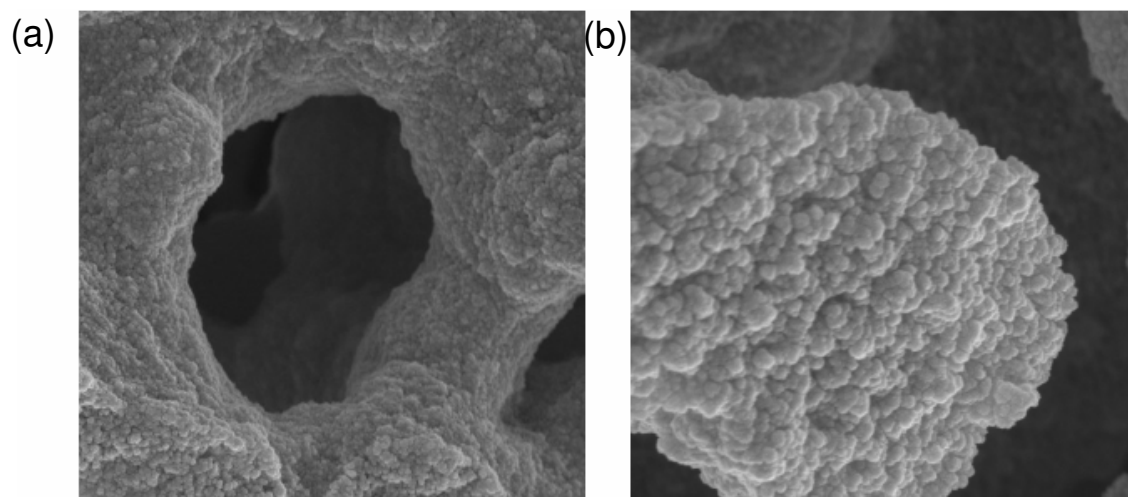


Figure 1.7: SEM images of a silica monolith showing (a) the macro-pores or through-pores and (b) the meso-porous structure of the silica skeleton [17].

Polymeric monoliths lack the bimodal pore structure of silica monoliths, with only a macro-porous structure [3]. Figure 1.8 depicts a methacrylate monolith showing the micro-globules [18]. This leads to a much lower surface area than silica, and are therefore not suitable to the separation of small molecules. However, the lack of a meso-porous structure allows for the efficient separation of macromolecules (e.g. proteins) due to the lack of pore diffusion [3].

Another difference in the properties of silica and polymeric monoliths is their pH stability. Silica monoliths are only stable from pH 2 to 8, due to solubility of silica under alkaline conditions, whereas polymeric monoliths are stable over the entire pH range. The use of polymeric monoliths also allows the exploitation of a large variety of chemistries. The chemistry of polymeric monoliths can be tailored from the start to produce the required selectivity by the correct choice of monomers.

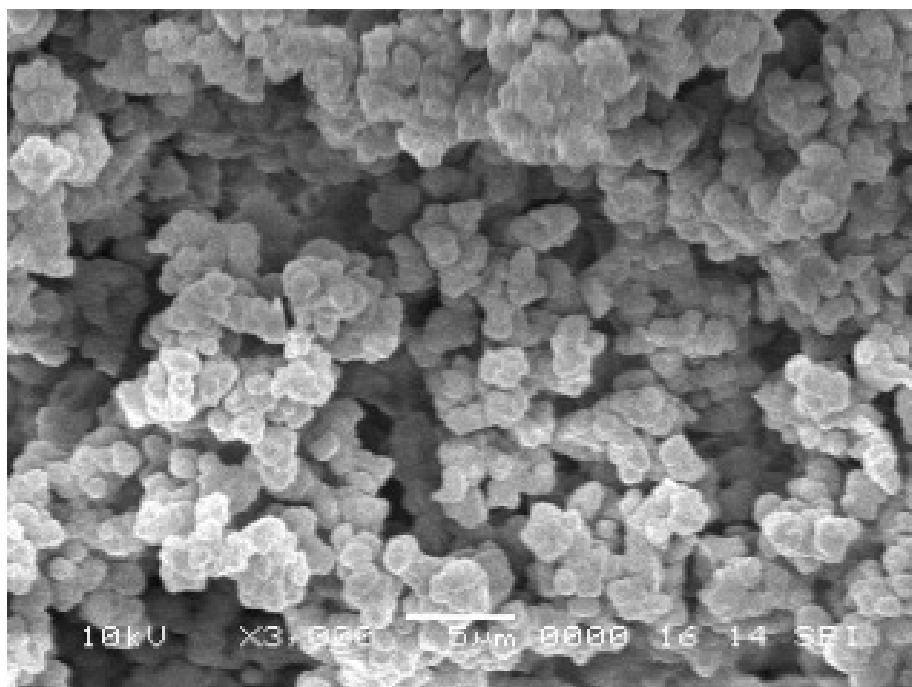


Figure 1.8: SEM of methacrylate monolith showing micro-globules [18].

### **1.3. Modification of stationary phase chemistries.**

The modification of stationary phase chemistries is generally carried out to change the selectivity of the phase. This may be to take advantage of certain characteristics of one stationary phase and apply them to different mode of chromatography.

#### *1.3.1 Surfactant coating.*

Surfactants are molecules that possess both hydrophobic and hydrophilic characteristics. In the modification of stationary phases ionic surfactants have been used to render reversed-phase columns suitable for ion exchange. The hydrophobic nature of ionic surfactants is generally due to alkyl chain (e.g.  $C_{18}H_{17}$ ) and the hydrophilic nature due to an ionic group (e.g.  $SO_3^-$ ). An example of a surfactant is sodium dodecylsulfate (SDS), the structure of which is given below in Figure 1.9 (a). As the hydrophobic tail of the surfactant will interact with a

hydrophobic environment, surfactants can be coated onto the surface of reversed-phase columns (e.g. C<sub>18</sub>). This coating will result in the hydrophilic head of the surfactant being presented to the mobile phase as shown in Figure 1.9 (b). This process results in a reversed-phase column being modified to become an ion exchange column.

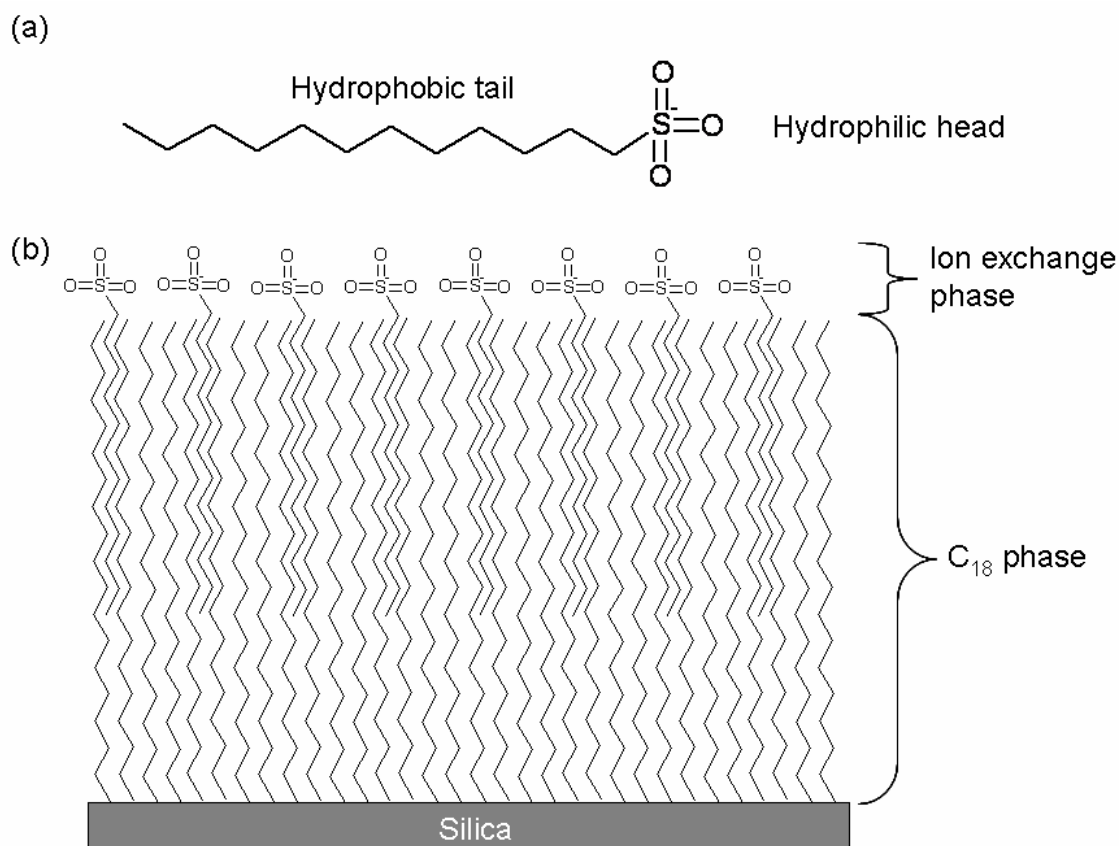


Figure 1.9: (a) structure of a typical surfactant (SDS), (b) interaction of SDS with a reversed-phase stationary phase creating an ion exchange phase.

This modification technique has been exploited for the analysis of inorganic ions on both particulate and monolithic reversed-phase columns [19-33] 19-34]. Surfactant coating of reversed-phase monolithic columns allowed the higher flow rates and higher efficiencies of these stationary phases to be applied to IC. This modification method is however not permanent. As it is based on hydrophobic

interactions, the coating can be removed by washing with organic solvents, or may even leach in an aqueous eluent, leading to changes in retention time.

The coating of surfactants onto reversed-phase columns has been carried out by a number of groups using anionic [19-26], cationic [27-35] and zwitterionic surfactants [36-38].

### *1.3.2 Chemical modification.*

For permanent modification of stationary phase chemistry the formation of chemical bonds is required. The modification is generally carried out on-column in a flowing system. Sugrue *et al.* modified the surface of both particle and silica-based monolithic columns with iminodiacetic acid (IDA) [39]. Before modification, the silica had to be activated by pumping DI water through the column at 60 °C for 4 hr. The modification was performed by pumping a solution of  $\gamma$ -glycidoxypropyltrimethoxysilane and IDA for 6 hr at 70 °C. The column was then washed with 0.01 M nitric acid for 1 hr before being equilibrated with the eluent. The modification was facilitated by the reaction of the epoxy group with the nitrogen of the IDA molecule, and the reaction of the silane group with the bare silica of the column. The columns were then suitable for the analysis of transition metal cations. The monolithic column was found to yield faster more efficient separations when using high ionic strength eluents compared to the particle based column (Figure 1.10) [39].

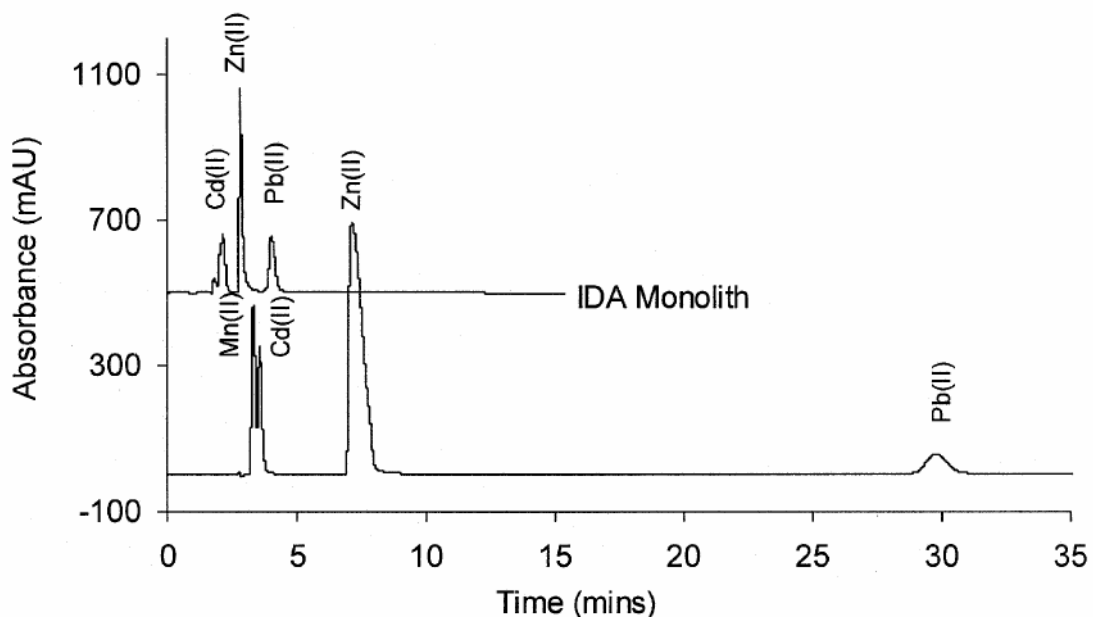


Figure 1.10: Comparison of column capacity and selectivity for Mn, Cd, Zn, and Pb on IDA silica monolith and IDA silica gel columns; Eluent = 0.2 M KCl (pH 2.0). Detection = Post-column reaction with PAR [39].

Using the same functionalisation methodology Sugrue *et al.* functionalised a silica monolith with lysine for the separation of both anions and cations on one stationary phase. This was possible as lysine once bonded to the silica monolith will act as a zwitterionic stationary phase [40].

The use of epoxy group reactivity to functionalise stationary phases has been used widely in conjunction with glycidyl methacrylate (GMA) based monoliths. Figure 1.11 depicts a selection of functionalities created using epoxy groups on the surface of GMA monoliths [14].

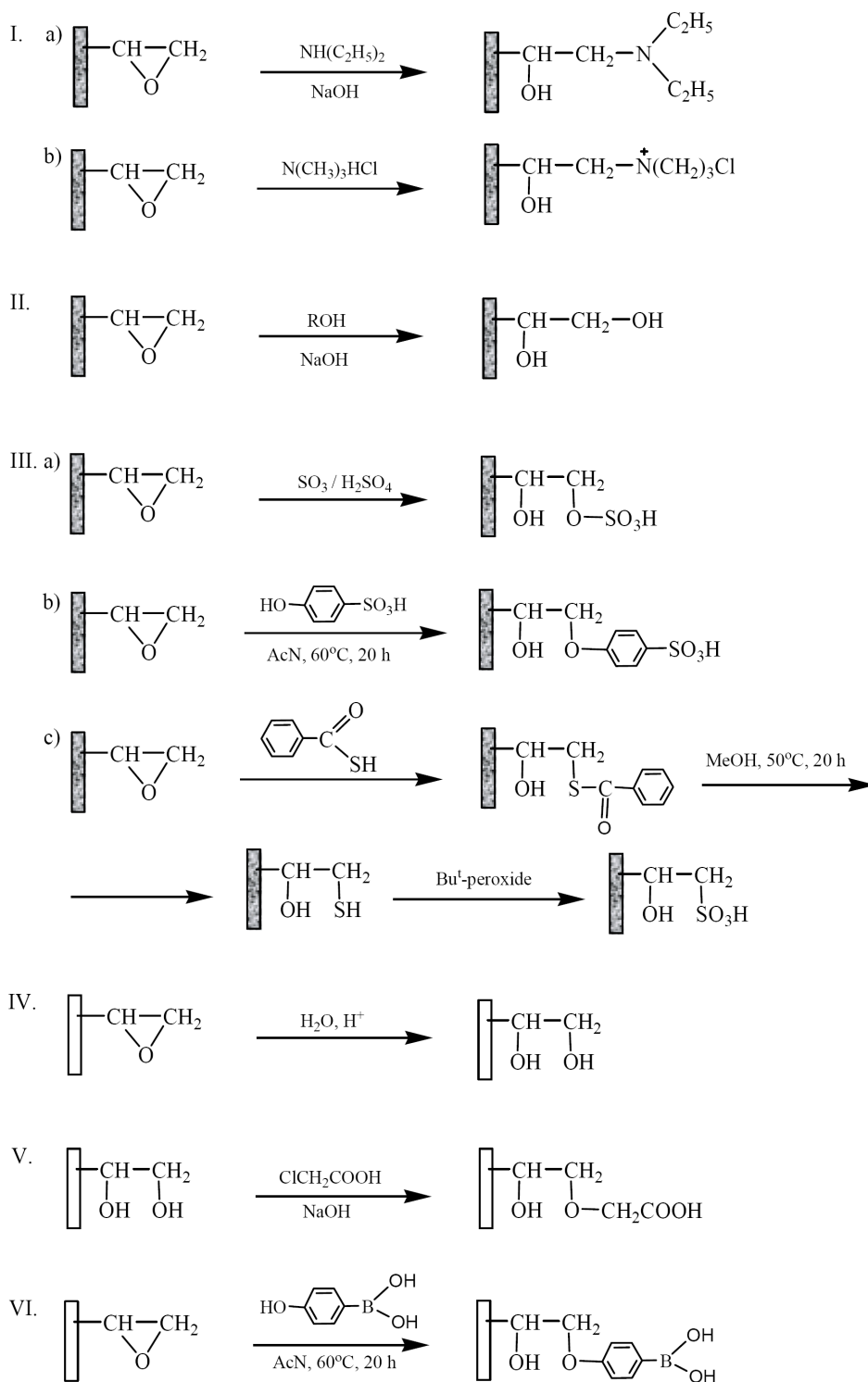


Figure 1.11: Chemical conversion of epoxy groups by means of various reagents. I. Amination; II. alkylation; III. sulfonation; IV. hydrolysis; V. carboxymethylation; VI. modification with *p*-hydroxyphenylboronic acid [14].

### 1.3.3 Photografting methods.

Generally the modification of a stationary phase occurs along the entire length of the column, as the reactions are carried out on-column in a flowing system, with no way of controlling the distribution of functional groups. However, as the interest in monolithic capillary columns formed within fused silica capillary has grown in the last decade, another avenue for modification has appeared. If the capillary used for the production of the monoliths are coated with UV transparent Teflon as opposed the more common non-UV transparent polyimide, photoinitiated reactions can be used. The advantage of using photoinitiated reactions is that not only the entire length, but also discrete zones of the column, can be modified [41, 42]. Photografting involves the production of a base monolith, into which a solution containing the functionality required, a free radical initiator and solvent system are pumped. If only specific regions of the column are to be functionalised, masks are used to restrict the parts of the column exposed to UV light. Figure 1.12 depicts the process involved in photografting one discrete of 2-acrylamido-2-propanesulfonic acid (AMPS) zone of a polymer monolith.

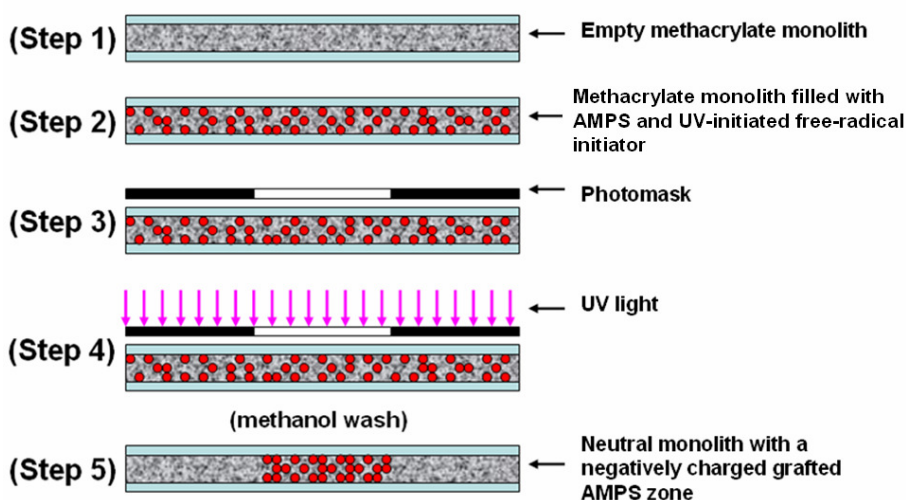


Figure 1.12: Depiction of photografting technique for the formation of one discrete zone of AMPS onto a polymer monolith.

In 2003 Rohr *et al.* reported the photografting of chains AMPS and 4, 4,-dimethyl-2-vinylazlactone (VAL) onto the surface of a butylmethacrylate /ethylene dimethacrylate monolith [42]. AMPS is a vinyl anionic monomer resulting in a negative charge being imparted onto the surface of the monolith. The grafting of the AMPS onto the surface of the monolith results in the formation of dendritic like arrays. These structures are due to abstractable hydrogens on the monolith surface and the monomer itself, and with increasing irradiation time the chains will grow away from the surface of the monolith giving a high density of functional groups and thus a higher capacity. Figure 1.13 depicts the arrays obtained in the photografting of AMPS with increasing irradiation time [42].

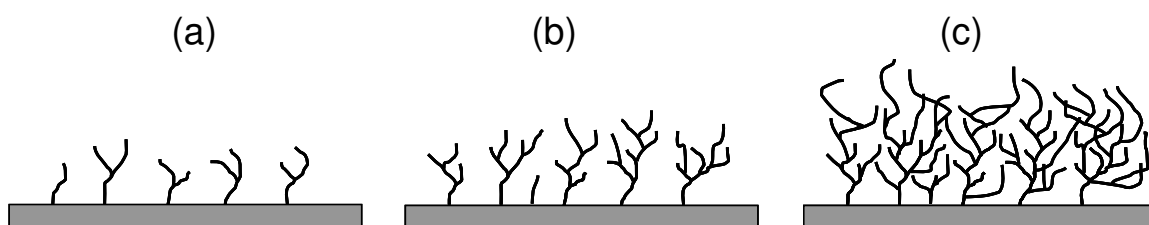


Figure 1.13: Schematic representation of the growing polymer chains during photografting with increasing irradiation time from (a) to (c) [42].

VAL is a reactive monomer that once photografted onto the surface of the monolith will react with amine containing compound to covalently link them to the surface. Figure 1.14 shows the reaction of VAL on the surface of a monolith with amine containing compound (Rhodamine 6G).

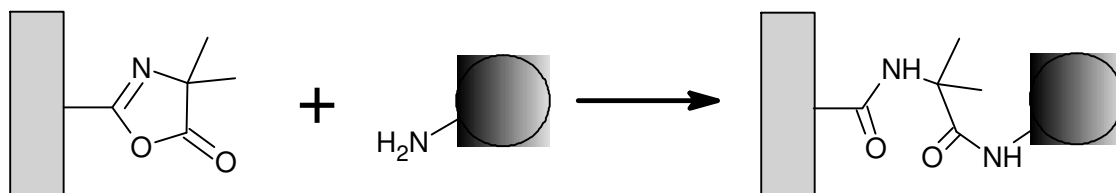


Figure 1.14: Reaction of VAL, once photografted onto the surface of a monolith, with an amine containing compound creating a covalent linkage the monolith surface.

Rohr *et al.* exploited this fact to covalently link Rhodamine 6G to the surface of the monolith allowing for fluorescence imaging of the zones, showing the ability to create discrete zones of functionality along the length of the monolith. Figure 1.15 shows the immobilisation of Rhodamine 6G into three discrete zones along a monolith, and visualised by fluorescence microscopy.

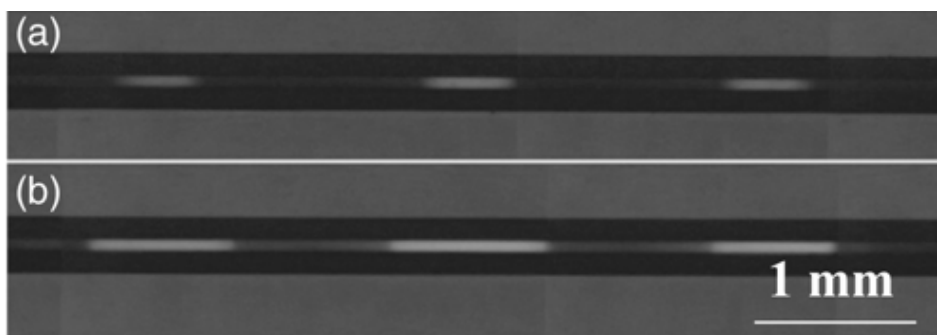


Figure 1.15: Fluorescence microscope image of porous poly (butyl methacrylate-co-ethylene dimethacrylate) monolith in a 50  $\mu\text{m}$  capillary photografted through a mask with poly (4, 4-dimethyl-2-vinylazlactone) chains for 1 (a) and 3 minutes (b) and subsequently reacted with Rhodamine 6G [42].

Logan *et al.* exploited photografting to place discrete zones of green fluorescent (GFP) protein onto the surface of a polymer monolith via VAL. GFP zones were photografted in two separate steps, showing that this method could be used to place a second set of zones onto the surface without damage or further reaction of the first set. The fluorescence signal of the first set of GFP zones did not change as result of the immobilisation of the second set of GFP zones. Figure 1.16 shows the fluorescence profile of the monolith with two separate rounds of photografting of VAL and the subsequent immobilisation of GFP [43].

The major advantage of photografting is the ability to control the amount of functional groups on the surface of the monolith. To achieve the same using co-polymerisation of the starting monolith mixture would require re-optimisation of each monomer solution. Another advantage of photografting is the ability to

photograft monomers that would otherwise form non-homogeneous monomer mixtures allowing for the creation of otherwise impossible stationary phase chemistries [44,45]. Photografting also ensures the functional groups are presented at the surface of the monolith, where as in co-polymerisation a large amount of functional groups are hidden within the monolith itself [46].

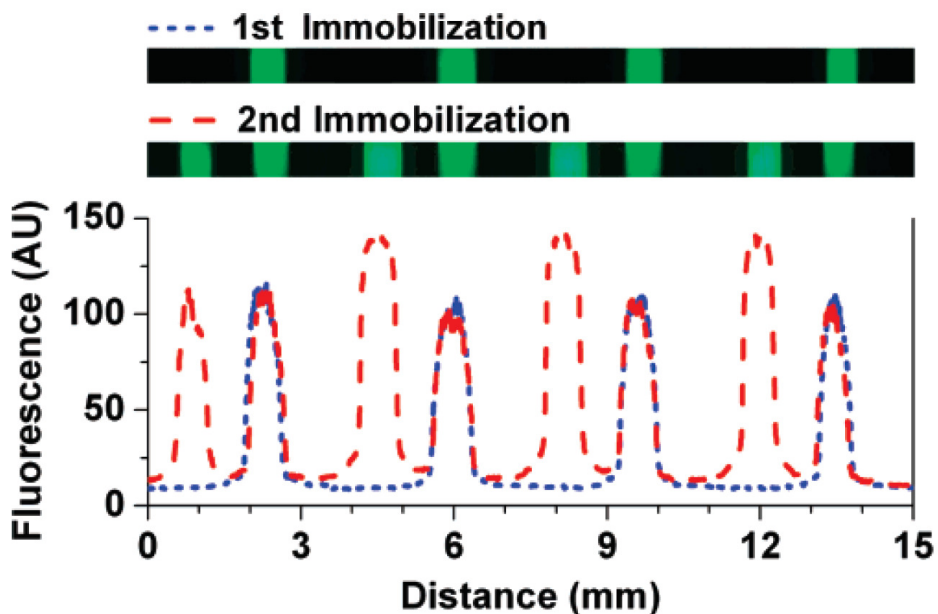


Figure 1.16: Consecutive patterning of multiple GFP patches on a polymer monolith in a 100  $\mu\text{m}$  capillary. The top image shows the location of GFP simultaneously immobilised in multiple patches; each GFP patch is  $\sim 750 \mu\text{m}$  in length. The lower image shows the fluorescence from GFP patches after a second round of GFP immobilisation on the same monolith. The plot shows profiles of the GFP fluorescence along the length of the capillary for the above images; the fluorescence intensity at each point in the column was determined by averaging the fluorescence intensity across the cross section of the monolith. In the images above, the diameter of the monolith has been increased over the actual aspect ratio to more clearly show the patch positions [43].

The ability to control the amount of functional groups being put down on the surface of the monolith and also their placement leads to possibility of varying the capacity along the length of the column (i.e. the creation of stationary phase

gradients). Pucci *et al.* reported the used of two methods for the creation of such gradients (1) changing the relative exposure time along the length of the columns using a moving shutter, (2) varying the intensity of light incident along the length of the column by a neutral density filter. Figure 1.17 shows the calculated gradients using the two methods [47].

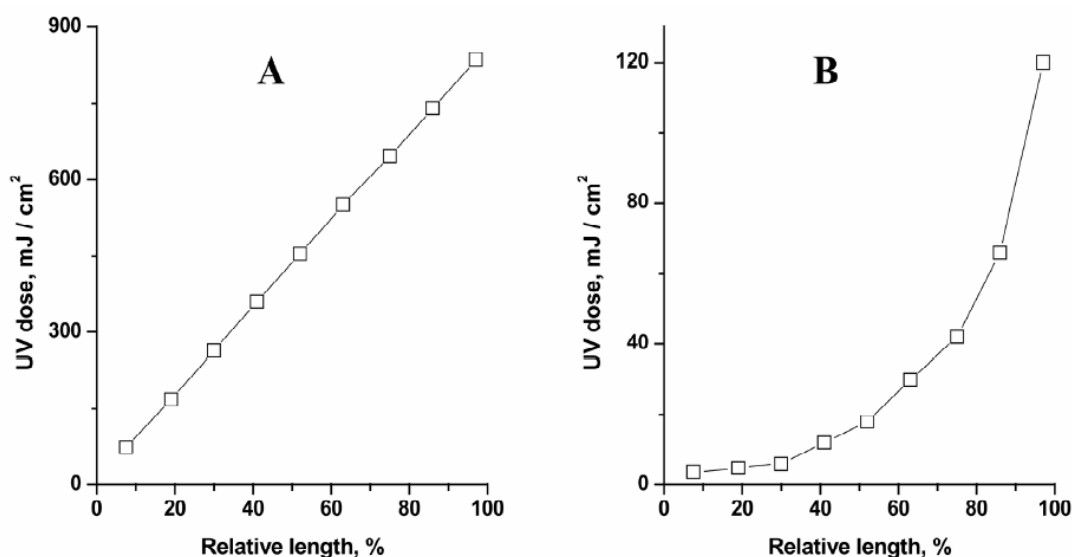


Figure 1.17: Calculated UV dose profiles along the relative length of the monolith using the moving shutter (A) and neutral density filter (B). Conditions: actual length 8.5 cm; UV light intensity 15 mW cm<sup>-2</sup>, irradiation time 0 - 60 s (A); irradiation time 600 s, UV intensity 0.2–0.006 mW cm<sup>-2</sup> (B) [47].

#### 1.4 Characterisation of modified stationary phases.

The production of novel stationary phases, especially those in capillary formats has resulted in the need for more detailed characterisation of these phases. Evaluation of chromatographic performance (e.g. retention time) is the most common and simple method, giving only an overall picture of the column modification. However, analysis at the morphological and chemical levels generally requires destructive methods (e.g. SEM-EDX).

#### 1.4.1 Scanning electron microscopy - Energy dispersive X-ray spectroscopy (SEM-EDX).

One valuable method for the analysis of stationary phase modifications is scanning electron microscopy (SEM), coupled with energy dispersive X-ray spectroscopy (EDX). SEM allows the analyst to view the stationary phase at the micrometer down to the nanometre level depending on the instrumentation used. The ability to look at the fine detail of the physical structure of monolithic materials, allows for investigation of pore size and morphology. Being able to view a material at this level when coupled with EDX allows for the probing of the chemical composition at known points within the stationary phase. EDX is an analysis technique based on the known energy transitions of elements, allowing for individual elements to be identified and quantitated. Sugrue *et al.* used EDX to investigate the longitudinal distribution of IDA on modified silica columns (see Section 1.3.2) [39]. EDX was firstly used to probe for nitrogen on sections of the de-packed particle columns and the monolith once cut into sections. The analysis for nitrogen was found to be inconclusive; however, another approach was used where copper was loaded onto the IDA groups. Analysis using EDX when probing for copper gave results showing a non-homogenous distribution of copper, and therefore IDA, along the length of the column. These results were further corroborated by using atomic absorption spectroscopy for copper chelated by IDA and then released from the sections of the column. The results of both techniques showed a 30 to 40% drop in IDA density from the column inlet to outlet. The reason for the non-homogeneous distribution of the IDA was attributed to the reactions occurring during the on-column modification. The competing reaction of IDA and diol-containing silanes resulted in two competing species in the modification of the silica. These two competing species would interact with the bare silica and undergo separation. The IDA-silane is more polar and would therefore be retained more than the diol-silane before reaction with the silanols of the silica. This results in the inlet of the column reacting with the IDA-silane and the outlet of the column reacting with the diol-silanes. The IDA-silane would move

along the column in a frontal chromatographic manner. As some of the epoxy groups had already reacted with the diol-silane the available sites for IDA-silane to bond to the surface had been reduced. This results in non-homogeneous distribution of IDA along the column length.

SEM-EDX has also been used for the characterisation of monolithic capillary columns. Due to the small nature of the samples available for analysis with these columns, SEM-EDX is a useful tool. Pucci *et al.* utilised SEM-EDX to characterise photografted gradients along the length of a capillary column using two methods (see Section 1.3.3) [47]. The capillary columns were cut into sections and probed for sulphur (the column was modified with AMPS, a sulphur containing monomer). The relative amount of sulphur allowed the author to compare the actual gradient to that which was predicted. The results showed a good correlation in the actual gradient to that calculated. Figure 1.18 depicts the results obtained compared to the theoretical gradient based on photografting through a neutral density filter.

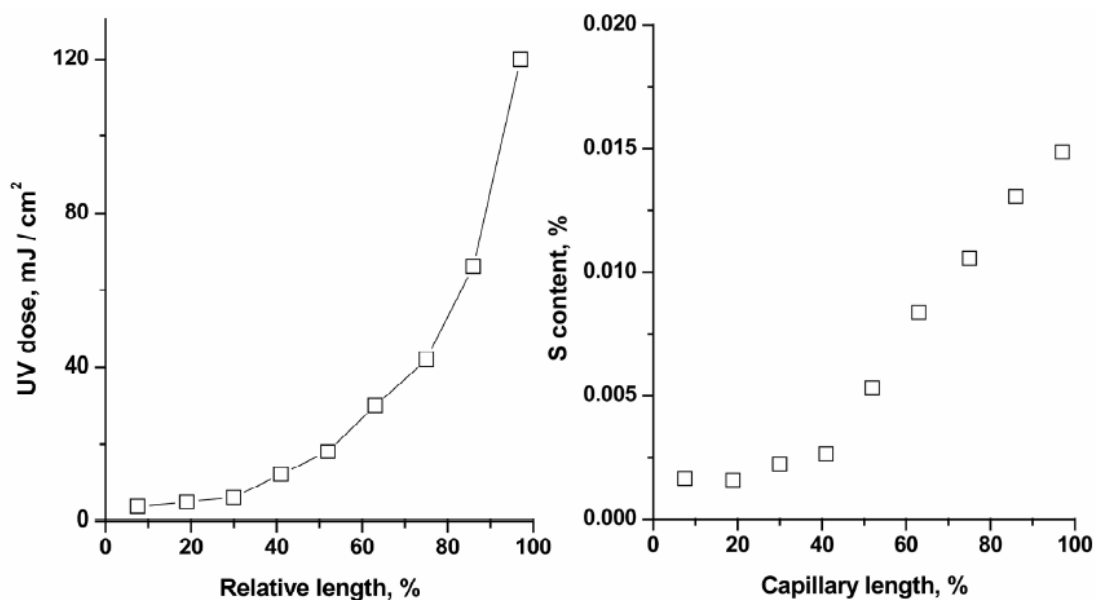


Figure 1.18: Comparison of theoretical gradient and actual gradient for photografting of AMPS onto the surface of a polymeric monolith capillary column through a neutral density filter [47].

Pucci *et al.* also used SEM-EDX to probe the radial distribution of AMPS within the columns produced. Figure 1.19 shows one of the sections probed (radially) for the presence of sulphur, thus showing the homogeneity across the monolithic bed [47].

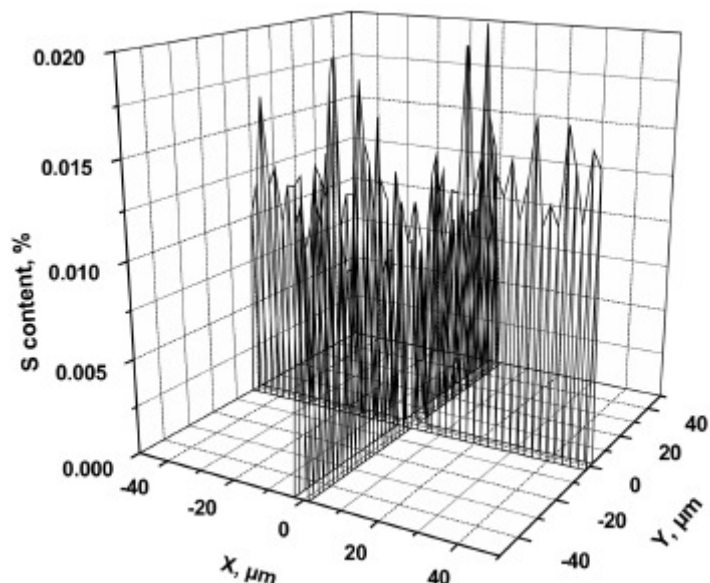


Figure 1.19: Radial sulfur profile of a monolith uniformly grafted with 2-acrylamido-2-methyl-1-propanesulfonic acid for 60 s determined by EDX [47].

The use of SEM-EDX is a valuable tool for the characterisation of modified stationary phases; however it suffers from one major drawback. The sample preparation for the analysis requires the destruction of the column under investigation.

#### *1.4.2 Chromatographic performance.*

The simplest method for investigating the effect of modifying stationary phase chemistry is the monitoring of changes in the chromatographic performance of the column. If the stationary phase chemistry is changed, and therefore its selectivity, a change in the separation behaviour will be observed. In the method described in Section 1.3.1, the coating of surfactants onto the surface of a reversed-phase

column changes its selectivity from reversed-phase to ion exchange. The coating of these surfactants requires an extensive wash step to remove any weakly or non-specifically bound surfactant from the surface of the column. The bleeding off of this excess surfactant will change the capacity of the column and therefore the retention time of the analytes. In a recent publication the effect of coating procedures on the retention of inorganic ions was investigated. Glenn *at al.*, using a variety of coating conditions, such as organic solvent content of the coating solution, systematically monitored the retention of sulphate (as capacity factor) during the wash cycle of the column [48]. The authors found that as the wash cycle progressed the retention of sulphate decreased until it reached a stable level. Figure 1.20 shows the effect of the excess surfactant washing from the column on the capacity factor over time for a variety of coating conditions.

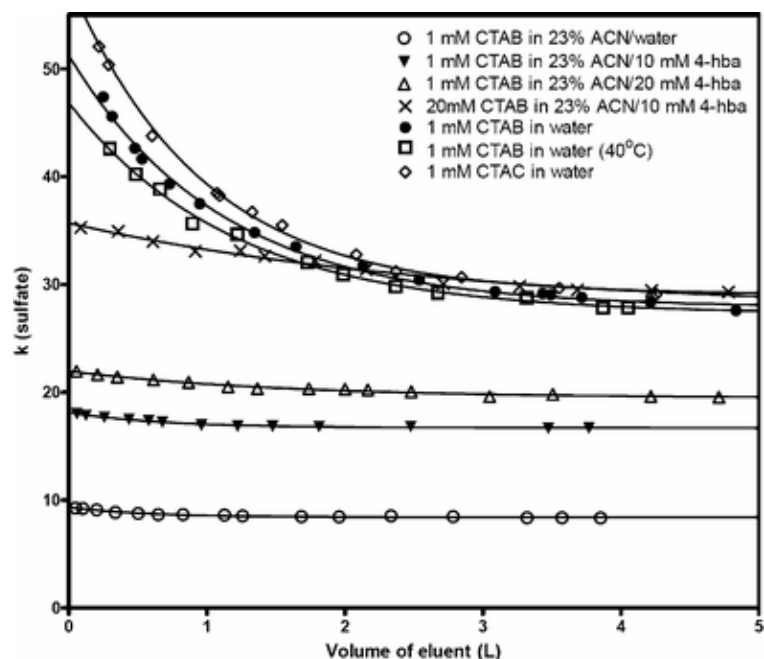


Figure 1.20: Exponential fits for retention loss under various coating conditions. Conditions:  $100 \times 4.6$  mm RP-18e Chromolith column coated until breakthrough. Anion separations using 10.0 mM 4-hydroxybenzoic acid eluent (pH 4.6) at  $2 \text{ mL min}^{-1}$ ,  $4 \text{ mL min}^{-1}$  flushing, 0.05 mM analyte ions, 20  $\mu\text{L}$  injection, non-suppressed conductivity detection. Temperature 30 °C unless otherwise stated [48].

Suzuki *et al.* compared the coating stability of two different surfactants onto bare silica monolithic capillary columns [49]. The change in retention factor of the two columns over a 10 hr period showed the stability of a cetyltrimethylammonium chloride (CPC) column was much less than a dilauryldimethylammonium bromide (DDAB). Figure 1.21 shows the change in the retention fraction for the two columns. The increased stability of the DDAB column was, according to the authors, due to the use of eluents of high salt concentration causing a “salting out” effect. However, DDAB is a much more hydrophobic surfactant than CPC due the presence of two alkyl chains which may explain it higher stability.

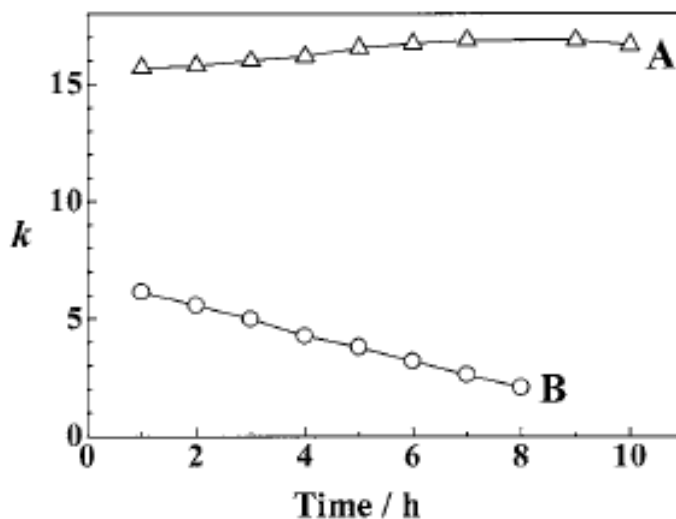


Figure 1.21: Stability of monolithic silica capillary columns modified with dilauryldimethylammonium ion or cetyltrimethylammonium ion. Columns, monolithic silica capillary columns (200 × 0.1 mm i.d.) modified with a dilauryldimethylammonium ion (A) or a cetyltrimethylammonium ion (B); eluent, aqueous solution of 50 mM sodium chloride (pH 5.8); flow-rate, 2.1  $\mu\text{L min}^{-1}$ ; analyte ion, nitrate [49].

The production of capillary monolith columns with modified stationary phases is becoming more popular in the field in CEC. The modification of these stationary phases is carried out to control the electroosmotic flow (EOF) and/or the selectivity of the column. A popular method for evaluating these modifications is the monitoring of the EOF using a marker. Pucci *at al.* in the creation of stationary

phase gradients on capillary monolith columns investigated the effect of the grafting time on the EOF of the monolith [47]. The EOF was found to increase in a linear fashion (Figure 1.22). However, the efficiency of the EOF marker was found to increase until 600 s then decreased across the grafting time.

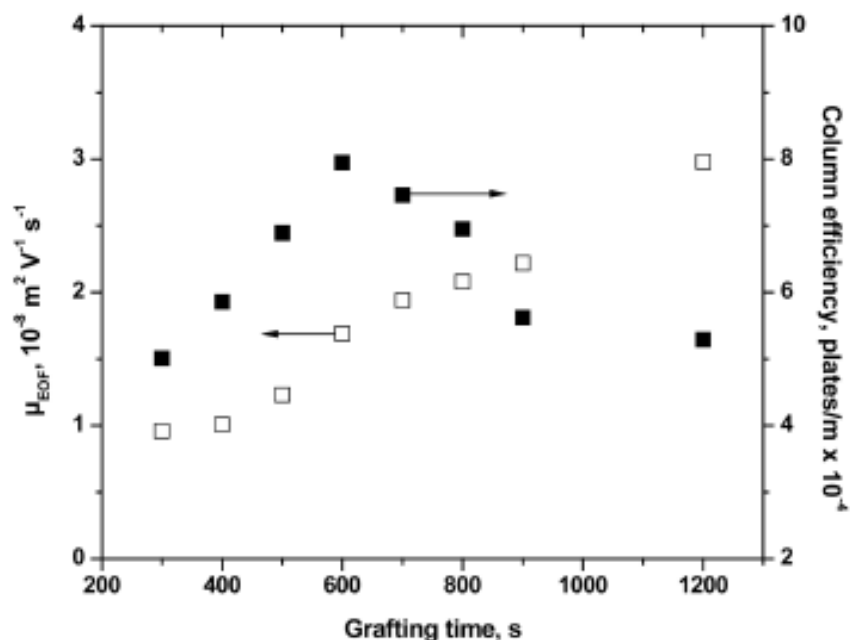


Figure 1.22: Effect of grafting time on electroosmotic mobility (□) and column efficiency (■). Column, 34 cm (8.5 cm effective length)  $\times$  100  $\mu\text{m}$  i.d., porous monolith grafted with AMPS using neutral density filter. Mobile phase, 80:20 acetonitrile: 10 mM phosphate buffer, pH 2.5; voltage  $-25$  kV; injection  $-5$  kV for 5 s; UV detection at 254 nm; EOF marker thiourea 200  $\mu\text{g mL}^{-1}$  [47].

However, the monitoring of chromatographic performance, albeit a non-destructive method, gives an overall picture of the column. It does not allow for investigations into the longitudinal distribution of functional groups along the column length.

### 1.4.3 Fluorescence.

The use of UV transparent fused silica capillary for the production of monoliths also allows for use of fluorescence to characterise the stationary phase [42,43]. By

introducing a fluorophore into the column the interactions of these molecules can be investigated. As previously mentioned Rohr *et al.* utilised fluorescence microscopy to visualise both the presence and effectiveness of the immobilisation of Rhodamine 6G via VAL chemistry (Figure 1.15 Section 1.3.3) [42]. The non-contact and non-destructive nature of fluorescence detection for the characterisation of stationary phase modification is an advantage over the use of SEM-EDX and the ability to probe along the length of the column is an advantage over using chromatographic performance. However, the major drawbacks of this technique are (1) the requirement of UV transparent fused silica capillary and (2) it is only applicable to fluorescent compounds.

### **1.5 Capillary chromatography.**

To date the majority of liquid chromatography has been performed on columns of diameters ranging from 1 to 4.6 mm; however, in the last decade the use of capillary scale (e.g. 100 to 500  $\mu\text{m}$  i.d.) [50] has received increasing interest. The use of capillary scale columns has several advantages, namely a reduction in the (a) amount of mobile phase consumed, (b) waste generated, (c) sample volume required and (d) on-column dilution of the sample (and hence the detection limits are improved) [50].

The reduction in the mobile phase volume required is proportional to the square of the column radius. As an example a reduction in column diameter from 4.6 mm to 0.32 mm results in a 200 fold decrease in the amount of mobile phase required (and thus a 200 fold decrease in the waste generated) [50]. This allows for the use of more exotic and expensive mobile phases, as well a reduction in running costs using conventional mobile phases.

The reduction in the column size also results in the reduction in the amount of stationary phase required, allowing the creation of exotic stationary phases with limited amount of reagents. Another advantage of using capillary scale columns is

their inherent compatibility with mass spectrometric detection. The use of capillary scale columns removes the need for flow splitting prior to introduction into mass spectrometers and thus all the sample can be used in detection which in turn increases the mass detection limits [50].

However, the reduction in column i.d., flow rates and sample volume also poses some disadvantages. The reduction in flow rates and sample volume leads to need for specialised chromatographic instrumentation. Dead volume in the system (e.g. injector, tubing and connectors) can have drastic effects on the efficiency of the separation due to extra column band broadening [50]. The reduction in these parameters also requires modification of detection systems, for example the use of specialist UV detector cells with low flow through cells of 3 nL (Dionex UVD-3000 [51]), compared to 14  $\mu$ L (Agilent 1200 [52]) for standard UV detection.

The on-column dilution of a sample decreases proportionally to the square of the column radius (Eq. 1.2); therefore a reduction in column diameter from 4.6 mm to 320  $\mu$ m can result in a 200 fold increase in peak height and mass sensitivity. However, the advantages of this are only possible when the volume injected onto the column is the same for both columns. Equation 1.2 relates the on-column dilution to the column dimensions and the volume of sample injected [50].

$$D = \frac{\epsilon\pi r^2(1+k)\sqrt{2\pi LH}}{V_{inj}} \quad (\text{Eq 1.2})$$

where:

D= Dilution factor

$\epsilon$  = column porosity

k = capacity factor

L= column length

H = plate height

$V_{inj}$  = volume of sample injected

r = radius

The effect of using such low flow rates in capillary liquid chromatography puts considerable focus on the tubing used to connect the chromatographic column to the injector and detector. If the sweep volume of the tubing is large compared to the flow rate of the system the band(s) of analytes will undergo dispersion within the tubing. This results in band broadening that is not associated with the separation (i.e. the column). The length of the tubing used should be as short as possible to retain the resolution as much as possible, any source of dead volume (e.g. unions) should be removed unless absolutely necessary [50].

### *1.5.1 Applications of capillary IC.*

For the sake of brevity, the application of capillary ion chromatography (Cap-IC) to the separation of small inorganic ions and selected examples of organic ions will be discussed here (e.g. organic acids and carbohydrates).

The application of capillary scale separations to the field of ion chromatography (IC) has grown in popularity in the last 25 years. The first papers on capillary ion chromatography, published in 1983, involved the use of columns of 190  $\mu\text{m}$  i.d. packed with standard ion exchange phase (10  $\mu\text{m}$  diameter), used in connection with Nafion perfluorosulphonate hollow fibre suppressors. With a column of 0.19 x 470 mm Rokushika *et al.* was able to separate seven inorganic anions in 15 minutes using UV detection. In 1996 Munaf *et al.* using columns of 350  $\mu\text{m}$  i.d. packed with porous reversed-phase particles performed a separation of six inorganic monovalent cations using benzyltrimethyl-ammonium chloride in aqueous acetonitrile as the mobile phase, using indirect UV detection [54]. Figure 1.23 is an example of the separations obtained with these capillary columns.

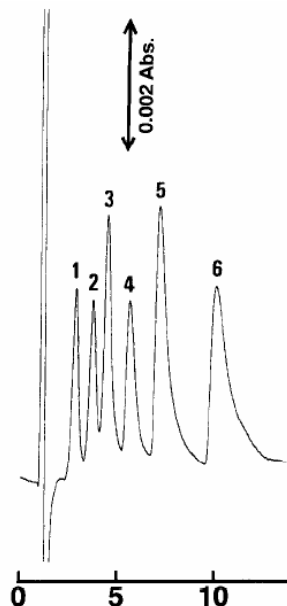


Figure 1.23: Indirect photometric detection of six inorganic cations. Column, Develosil 30-5, 50 mm x 0.35 mm i.d.; eluent, 2.0mM BETMAC in 30% (v/v) acetonitrile (pH 6.5); flow rate, 4.2  $\mu\text{L min}^{-1}$ ; analytes, 1 = lithium, 2= sodium, 3= ammonium, 4= potassium, 5= rubidium and 6= caesium; sample size, 0.2  $\mu\text{L}$ ; wavelength of UV detection, 208 nm [54].

The advantages of capillary scale separations, namely low solvent consumption and increased mass detection, lead to the development of a field portable IC system. Using a 50 cm x 190  $\mu\text{m}$  i.d column with suppression the system was found to have detection limits in the sub to low ppb range and mass detection limits > 100 than conventional IC systems. In the analysis using a gradient program with suppressed conductivity detection the separation of 15 anions was possible in less than 30 minutes (See Figure 1.24) [55].

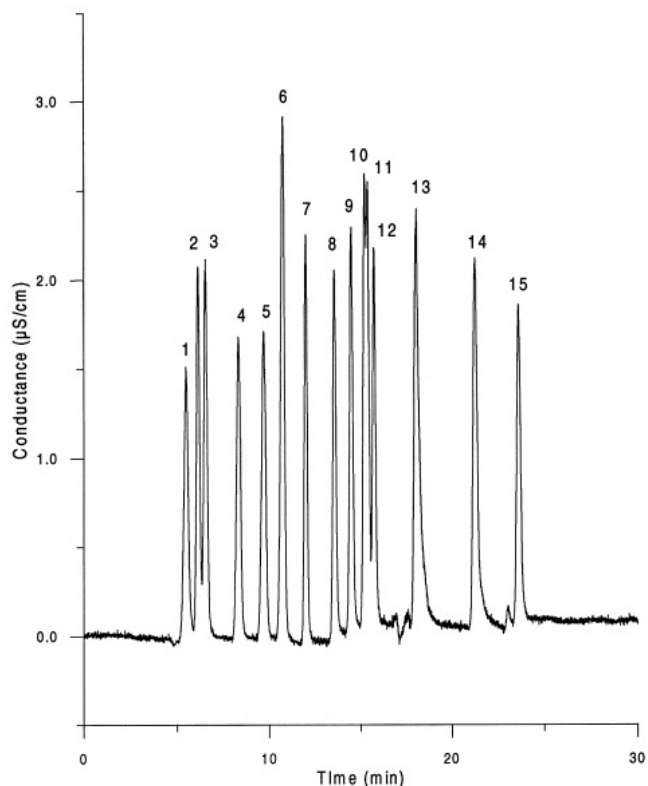


Figure 1.24: Background subtracted gradient chromatogram on a 50 cm x 180  $\mu\text{m}$  i.d. packed capillary column (Dionex AS-11). Linear gradient from 2 mM NaOH to 38 mM NaOH from 5 to 17 minutes was used. Peak identities: 1, acetate; 2, formate; 3, methanesulfonate; 4, monochloroacetate; 5, bromate; 6, chloride; 7, nitrite; 8, trifluoroacetate; 9, dichloroacetate; 10, bromide; 11, nitrate; 12, chlorate; 13, sulfate; 14, phthalate; 15, chromate. All ions were 50 mM except dichloroacetate which was 60 mM. [55]

Sedyohutomo *at al.* reported the use of a particulate packed ion exchange capillary column (320  $\mu\text{m}$  i.d.) with the use of a packed capillary suppressor (320  $\mu\text{m}$  i.d.) for the separation of inorganic anions [56]. The suppressor was packed with a strong cation exchange phase and operated in a cycling mode via two six port switching valves allowing the regeneration of one suppressor as the other was in use. The isocratic separation of six common inorganic anions was obtained in *ca.* 20 minutes at a flow rate of 4.5  $\mu\text{L min}^{-1}$ . LODs for the six anions ranged from 10 to 100 ppb using the suppressor (See Figure 1.25).

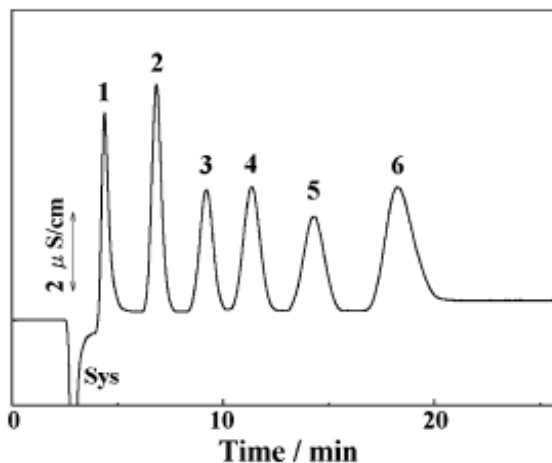


Figure 1.25: Separation of inorganic anions on packed capillary column. Separation column, TSKgel IC-Anion-PWXL (100mm x 0.32mm i.d.); packed capillary suppressors, TSKgel SCX (30mm x 0.32mm i.d.); mobile phase, 1.75 mM NaHCO<sub>3</sub> /1.5 mM Na<sub>2</sub>CO<sub>3</sub>; flow rate, 4.2 μL min<sup>-1</sup>; detection, contactless conductivity; analytes, 1 = fluoride, 2 = chloride, 3 = nitrite, 4 = bromide, 5 = nitrate, 6 = sulfate; concentration of analyte anions, 0.05 mM each; injection volume, 0.2 μL [56].

The Takeuchi laboratory has reported the coating of reversed-phase columns of 0.32 mm i.d. with proteins (bovine serum albumin, BSA) to render them suitable for ion exchange of inorganic anions [57]. The modification of other stationary phases (i.e. ion exchangers) has been carried out with polysaccharides (chondroitin sulfate, dextran sulfate and heparin [58-60]) for the separation of inorganic ions, with the modifications resulting in a change in selectivity.

Commercial Cap-IC systems for use the analysis of small inorganic ions has been the topic of several presentations at the International Ion Chromatography Symposium (IICS) documenting the work undertaken by Dionex cooperation. However no commercial products have are as yet on the market [61, 62].

The use of capillary scale columns packed with standard IC phases was a logical progression in the separation of ions, as is the movement to monolithic stationary

phases for the same applications. As discussed previously monoliths can be separated into two types, silica and polymeric. However, the application of polymeric monoliths to the analysis of small molecules has been hampered due to their poor efficiencies compared to that of silica-based monoliths. Silica-based monoliths having a bimodal pore structure (i.e. macro- and meso-pores) which results in a higher surface area and is more suited to separation of small molecules [17]. Conversely, polymeric monoliths have a macro-porous structure with lower surface area (due to the lack of meso-pores) and are suited to the separation of macromolecules (e.g. proteins) [3]. In a review published by Svec, this problem was mentioned as a misconception and does not mean that polymeric monoliths cannot be used for small molecules, merely that the optimisation of monoliths for these applications will be very much the focus of future research into polymeric monoliths [63].

One method for creating a silica-based monolith for the separation of inorganic ions involves the covalent modification of a base silica monolith with polymeric stationary phases, so called hybrid monoliths. In 2007, Ikegami *et al.* reported the production of strong/weak anion and cation exchange monoliths [64]. The production of these monoliths involved the synthesis of a base silica monolith which was then reacted with 3-methacryloxypropyltriethoxysilane (MAS) to allow the anchoring of the polymeric stationary phase to the surface of the silica monolith (e.g. 2-(triethylammonium) ethyl methacrylate chloride (DMAEA-Q) for SAX). Depending on the polymer coated onto the monolith a variety of ion exchange stationary phases were produced, allowing for the separation of three inorganic anions in less than 10 minutes. Figure 1.26 is an example of the separations possible using a strong anion exchange (SAX) hybrid silica monolith. The bonding of these polymeric functionalities onto the surface of the monolith allows for the high surface area, due to the meso-pores, to be used for the analysis of small inorganic anions, while taking advantage of the variety of functionalities available through organic chemistry.

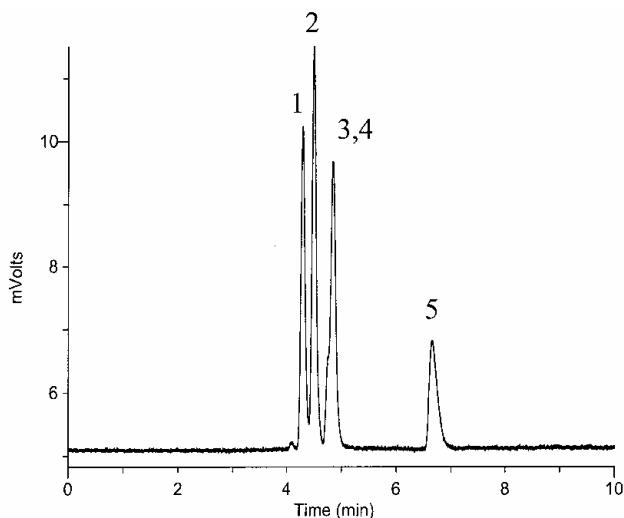


Figure 1.26: Chromatographic separation of inorganic anions using a hybrid silica monolith. 200H-DMAEA-Q column: column size, 200  $\mu\text{m}$  i.d. x 300 mm; mobile phase, 0.5 M NaCl; detection,  $\lambda = 210$  nm; temperature, ambient; pressure, 3.5 MPa. Analytes: 1,  $\text{S}_2\text{O}_3^-$ ; 2,  $\text{NO}_2^-$ ; 3,  $\text{Br}^-$ ; 4,  $\text{NO}_3^-$ ; 5,  $\text{I}^-$  [64].

Jaafar *et al.* also employed hybrid monoliths with the on-column copolymerisation of N-[3-(dimethylamino) propyl] acrylamide methyl chloride-quaternary salt (DMPAA-Q) with 3-methacryloxypropyl moieties anchored to the surface of a silica monolith [65]. The resulting monolith was a SAX stationary phase, allowing for the separation of seven inorganic anions in less than 20 minutes (Figure 1.27). The plate height calculated for the column was found to equivalent to a 10  $\mu\text{m}$  diameter particle column.

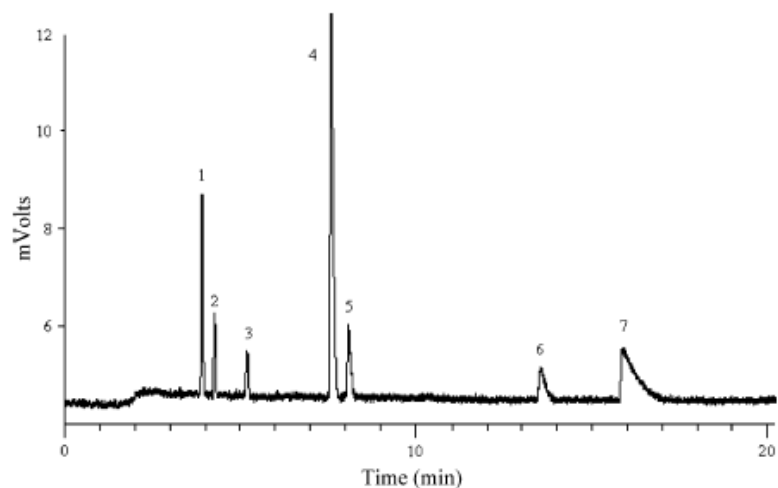


Figure 1.27: Micro-IC separation of anions mixture composed of (1) thiourea; (2) iodate; (3) bromate; (4) nitrate; (5) bromide; (6) iodide; (7) thiocyanate. The sample solution ( $2 \text{ mg mL}^{-1}$  of each component,  $4 \text{ }\mu\text{L}$ ) was injected in a split flow and injection mode with a pump flow rate of  $0.40 \text{ mL min}^{-1}$ . Column: 100H-MOP-DMAPAA-Q, 33 cm length; mobile phase: 50 mM sodium phosphate (pH 6.6), linear velocity:  $u=1.4 \text{ mm s}^{-1}$ ,  $\lambda=210 \text{ nm}$  [65].

Another method for creating ion exchange silica monoliths is the use of surfactants. Suzuki *et al.* applied this principle to a  $100 \text{ }\mu\text{m}$  i.d. bare silica monolith for the determination of bromide in sea water [66]. The surfactant used in this case was cetyltrimethylammonium ion chloride (CPC). The coating of the column was due to the formation of a bilayer of the surfactant on the surface of the monolith. The cationic head of the surfactant is electrostatically retained on the silica monolith, and a second layer of surfactant was then coated by hydrophobic interaction of the surfactant tail. This ultimately results in the formation of an ion exchange phase with the cationic head of the surfactant presented to the mobile phase. To ensure the stability of the surfactant coating, and therefore the reproducibility of the column, the surfactant had to be included in the eluent used. The separation of five anions was possible using this system and was successfully applied to the determination of bromide in sea water samples (Figure 1.28).

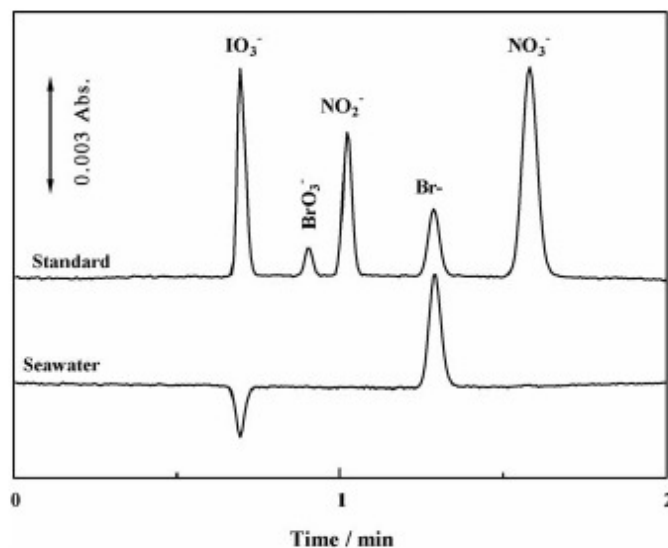


Figure 1.28: Separation of authentic mixture of five anions and bromide in a seawater sample on a monolithic silica capillary column modified with cetyltrimethylammonium ion. Column: 400 mm x 0.1 mm i.d. Eluent: 500 mM sodium chloride containing 0.1 mM CTAC. Flow rate: 5.6  $\mu\text{L min}^{-1}$ . Injection volume: 20 nL. Samples: 0.5 mM each for the upper trace; seawater for the lower trace. Wavelength of UV detection: 210 nm.

Similar work by Suzuki *et al.* using DDAB coated onto bare silica monolithic columns using the above method resulted in retention factors *ca.* twice that of the CPC coated column [49]. The stability of the coating was also found to be greater than the CPC coated column, with little change over a 10 hr period (see Section 1.3.1).

The use of polymeric monoliths has a growing interest in the field of IC, the main reason being the pH stability of these monoliths. However, the production of polymeric monoliths which are capable of separating small molecules is only an emerging area of research. As discussed previously, the lack of a meso-porous structure and thus low surface areas limits their application in this field. Publications dealing with the application of polymeric monoliths in IC have utilised several methods of overcoming these difficulties.

Ueki *et al.* modified a glycidyl methacrylate/ethylene dimethacrylate monolith (250  $\mu\text{m}$  i.d.) to create a strong cation exchange phase [67]. Using the reaction of sodium sulfite and the epoxy groups of the glycidyl methacrylate, sulfonate groups were formed on the surface of the monolith. It was found that by controlling the pH, time and temperature of the sulfonation reaction the capacity of the monolith could be controlled (capacities of 90 and 300  $\mu\text{eq mL}^{-1}$  were produced using pH 7 and 11, respectively). The separation of inorganic cations using a 150  $\mu\text{eq mL}^{-1}$  column was found to have efficiencies of 20,000  $\text{N m}^{-1}$ . As the monolith had a hydrophilic nature it was subjected to injections of proteins (e.g. bovine serum albumin) and the proteins were found to elute at nearly the void volume. This showed the monolith to be protein resistant and was then applied to the direct analysis of inorganic cations in human saliva. Figure 1.29 depicts the separations obtained using a 80  $\mu\text{equiv mL}^{-1}$  column at different flow rates.

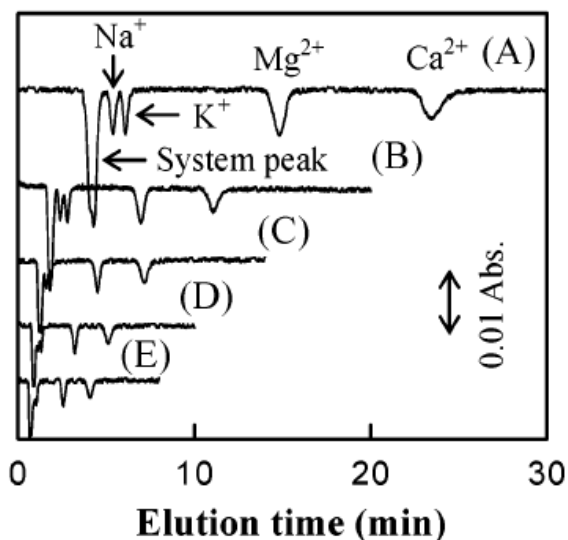


Figure 1.29: Separations of common cations on a sulfonated GMA monolith at different flow rates of (A) 3, (B), (C) 9, (D) 12, and (E) 15  $\mu\text{L min}^{-1}$ . Sample, 2 mM each of Na<sup>+</sup>, K<sup>+</sup>, Mg<sup>2+</sup>, and Ca<sup>2+</sup>; cation exchange capacity, 80  $\mu\text{equiv mL}^{-1}$  [67].

In 2004, Hilder *et al.* reported the production of an anionic monolith (250  $\mu\text{m}$  i.d.) by the co-polymerisation of AMPS with butyl methacrylate/ethylene dimethacrylate which allowed the electrostatic coating of the monolith with aminated latex

nanoparticles (60 nm diameter) [68]. The coating of these latex nanoparticles was found to increase the surface area of the polymeric monolith from 35.2 to 47.3 m<sup>2</sup> g<sup>-1</sup>, with associated increase of back pressure of 2.6 to 5.7 MPa at 5 μL min<sup>-1</sup>. Figure 1.30 shows SEM images of uncoated and coated monoliths, with the latex nano-particles clearly evident in Figure 1.30 (B). The principle of coating the stationary phase with latex nanoparticles is one that has been used in commercial particle packed columns, where it affords a short path of diffusion, and thus allows for more efficient separations.

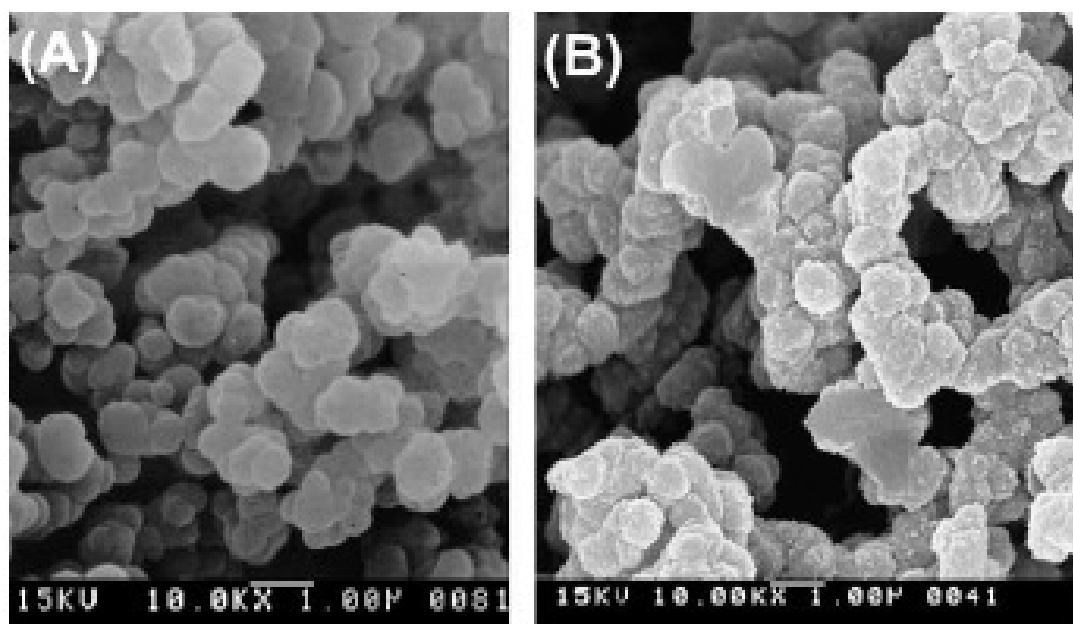


Figure 1.30: SEM image of original BuMA-co-EDMA-co-AMPS monolith (A) and its latex-coated counterpart (B) [68].

The, now cation exchange, monolith was applied to the separation of saccharides, with resolution of seven analytes in less than 10 minutes, Figure 1.31.

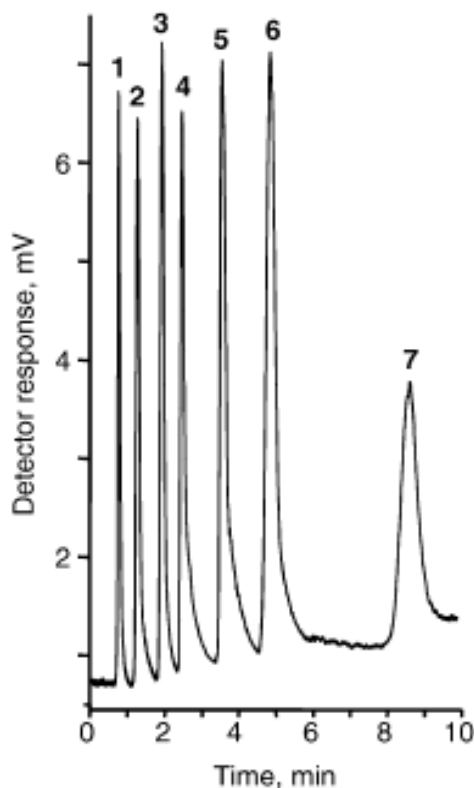


Figure 1.31: Separation of a mixture of carbohydrates by anion-exchange chromatography using an optimised latex-coated polymeric monolithic capillary column. Conditions: column size 10 cm x 250  $\mu\text{m}$  i.d., pore size 0.97  $\mu\text{m}$ . Flow rate 13  $\mu\text{L min}^{-1}$  mobile phase aqueous ammonium hydroxide 64 mM (pH 12.8). Peaks: d(+)-galactose (1), d(+)-glucose (2), d(+)-xylose (3), d(+)-mannose (4), maltose (5), d(-)-fructose (6), sucrose (7). Injection volume 100 nL; sample concentration 1  $\text{mg mL}^{-1}$  [68].

Zakaria *et al.* applied the same methodology to the separation of inorganic anions [69]. The separations were performed in suppressed IC mode with a micro-column suppressor. The coating of the latex particles (this time Dionex AS-18 phase) resulted in the separation five inorganic anions in less than 10 minutes Figure 1.32 shows the separations obtained and the effect of increasing the concentration of the potassium hydroxide (KOH) eluent.

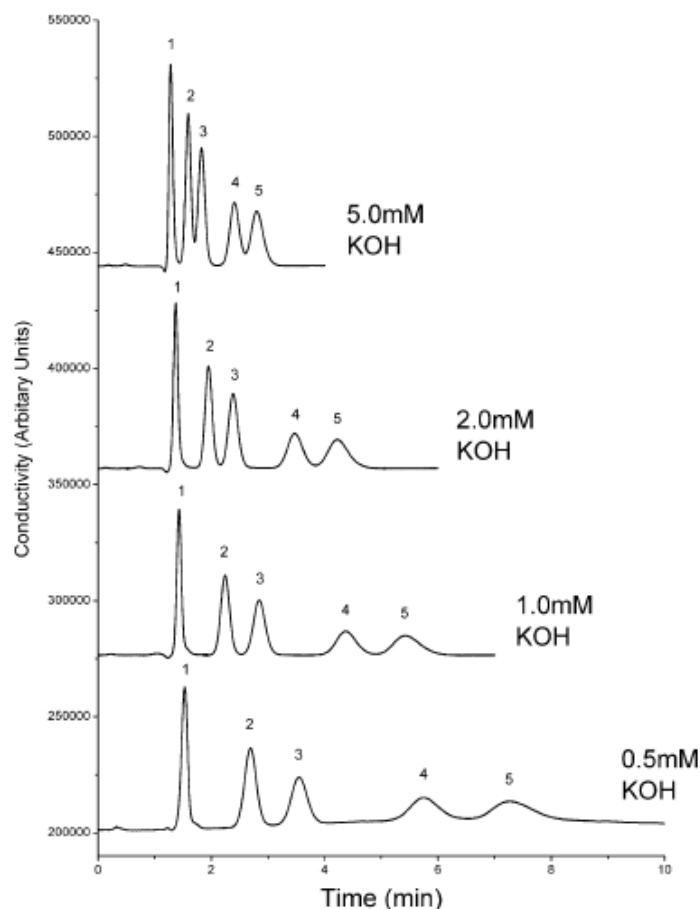


Figure 1.32: Effect of increasing concentration of hydroxide in the eluent on the observed separation using suppressed conductivity detection. Conditions: eluent, as marked; column; 250  $\mu\text{m}$  i.d. x 30 cm, 3.5  $\mu\text{m}$  pore size coated with AS18; flow rate, 12.5  $\mu\text{L min}^{-1}$ ; sample loop, 50  $\mu\text{m}$  x 5.0 cm; regenerant, 5 mM  $\text{H}_2\text{SO}_4$  flowing at 0.5 mL  $\text{min}^{-1}$ ; analytes, 50  $\mu\text{M}$ . Peaks: 1, iodate; 2, bromate; 3, nitrite; 4, bromide; 5, nitrate [69].

Hutchinson *et al.* (2005) similarly applied the use of polymeric monoliths coated with latex nano-particles [70]. In this study different methods of increasing the ion exchange capacity were investigated. The surface modification of both polystyrene and methacrylate-based monoliths were varied to increase the amount of latex nano-particles electrostatically bound to the surface of the monoliths via three methods. Figure 1.33 shows the effect of the three different methods on the chromatographic performance of the monoliths. From this study it

is clear that the method of modification of the monolith surface chemistry is an important parameter in the production of efficient capillary polymeric monoliths for IC.

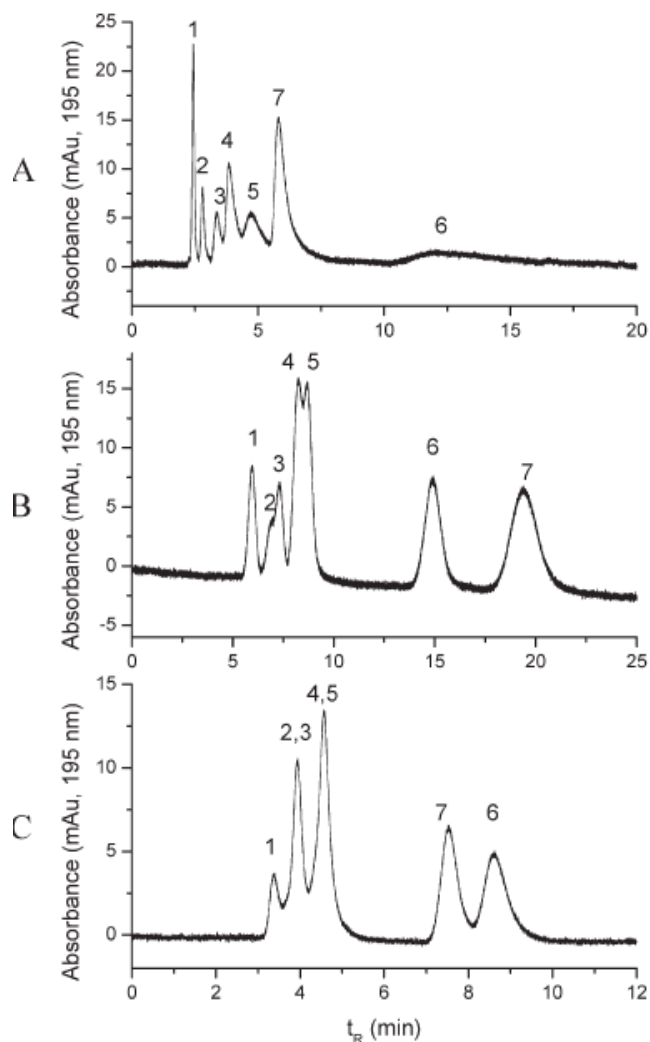


Figure 1.33: Separation of a 7 anion mixture\* using: (A) a 24.1 cm 250 mm AS18-coated GMA-co-EDMA monolith that was sulfonated using method (i). Eluent: 10 mM NaClO<sub>4</sub>, flow-rate 3.6 mL min<sup>-1</sup>, detector: Agilent. (B) A 34.8 cm x 250 mm AS18-coated GMA-co-EDMA monolith that was sulfonated using method (ii). Eluent: 10 mM NaClO<sub>4</sub>, flow rate 3.0 mL min<sup>-1</sup>, detector: Agilent. (C) A 14.3 cm 250 mm AS 18 coated GMA-co-EDMA monolith that was sulfonated using method (iii). Eluent: 10 mM NaClO<sub>4</sub>, flow-rate 3.2 mL min<sup>-1</sup>, detector: Agilent. \* Analytes: 1 = IO<sub>3</sub><sup>-</sup>, 2 = BrO<sub>3</sub><sup>-</sup>, 3 = NO<sub>2</sub><sup>-</sup>, 4 = Br<sup>-</sup>, 5 = NO<sub>3</sub><sup>-</sup>, 6 = I<sup>-</sup>, 7 = benzenesulfonate, each 0.14 mM [70].

In 2008 Katyanyeva *et al.* reported the use of ethylene glycol dimethacrylate (EDMA)/ glycidyl methacrylate (GMA) monoliths for the separation of small inorganic anions [71]. The production of the monoliths was very much different to normal methods. The polymerisation time of the monolith produced was 1-2 hr (by thermo-polymerisation), compared to *ca.* 20 hr for most other publications [67]. Svec *et al.* studied the effect of polymerisation time on the pore size distribution and surface area of poly (glycidymethacrylate-co-ethylene dimethacrylate) monoliths, varying the time from 1 to 30 hr, keeping all other parameters constant [72]. The pore volume was found to decrease as the polymerisation time increased, with 3.759 and 1.101 mL g<sup>-1</sup>, for 1 hr and 30 hr respectively. The surface area also followed the same trend with a decrease of 217.5 to 66.0 m<sup>2</sup> g<sup>-1</sup>, for 1 hr and 30 hr respectively. The short polymerisation time utilised by Katyanyeva *et al.* resulted in the creation of large diameter through pores, and hence a larger surface area suitable for the separation of small molecules. Once the base monolith of required characteristics was produced it was then functionalised with either dimethylamine (DMA) or polyethylenimine (PEI) or a mixture of both at room temperature for 12 hr. The functional groups were finally quarternised using methyl iodide. The optimum separation was obtained using a 1:1 ratio of DMA to PEI. Figure 1.34 shows the optimum chromatogram using this polymeric monolithic capillary column for the separation of five anions in less than 10 minutes.

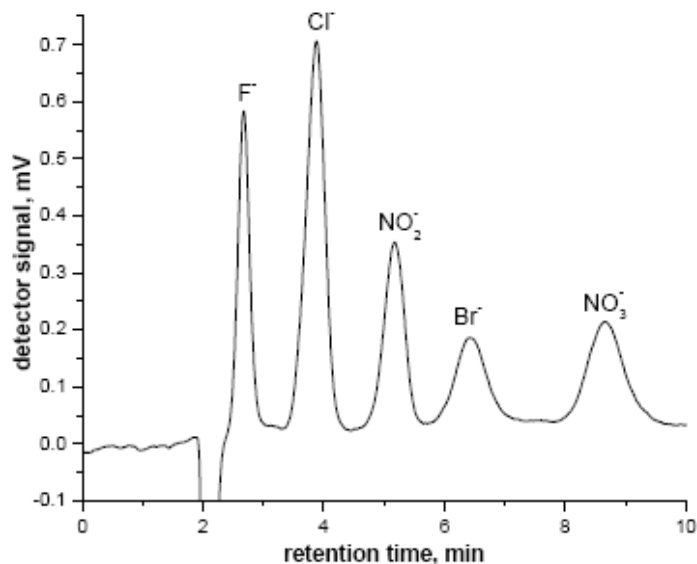


Figure 1.34: Speed separation of five anions on a monolithic anion-exchange capillary column with methacrylate matrix aminated with the mixture of PEI and DMA, pH = 4.25, eluent potassium phthalate, column length 465 mm, pressure 13 bar [71].

## 1.6 Detection in capillary liquid chromatography.

The detection of separated analytes in capillary LC can be achieved via the same methods as in conventional liquid chromatography; however, there are technical obstacles to be overcome. The coupling of detectors to capillary columns (whether of packed or monolithic stationary phases) requires miniaturisation. The low flow rates associated with capillary liquid chromatography result in the requirement of removing any possible sources of extra column band broadening [73, 74].

### 1.6.1 UV.

Conventional UV detector flow cells have volumes of  $\sim 10 \mu\text{L}$ . If such cells were coupled to capillary columns with flow rates of  $1\text{--}10 \mu\text{L min}^{-1}$  it would take 60 – 600 seconds to sweep the volume of the cell, and the band broadening experienced by an analyte peak would reduce the efficiency of the separation drastically. Dionex

Corp. have released a commercial UV detector for use with capillary separations, with flow cells of 45 nL and 3 nL, depending on the flow rate used (i.e. nano or micro flow rates [51]). The miniaturisation of UV detectors requires relatively long optical paths to ensure sensitivity can be achieved [73].

### 1.6.2 Fluorescence.

Fluorescence detection for capillary liquid columns is often performed on-column, i.e. detection occurs on the stationary phase [75]. Enhancement of the fluorescence signal can occur on the stationary phase resulting in improved LODs. Figure 1.35 depicts the type of signal enhancement possible. However, the changing environment the fluorescent analyte experience can affect its fluorescence characteristics [73].

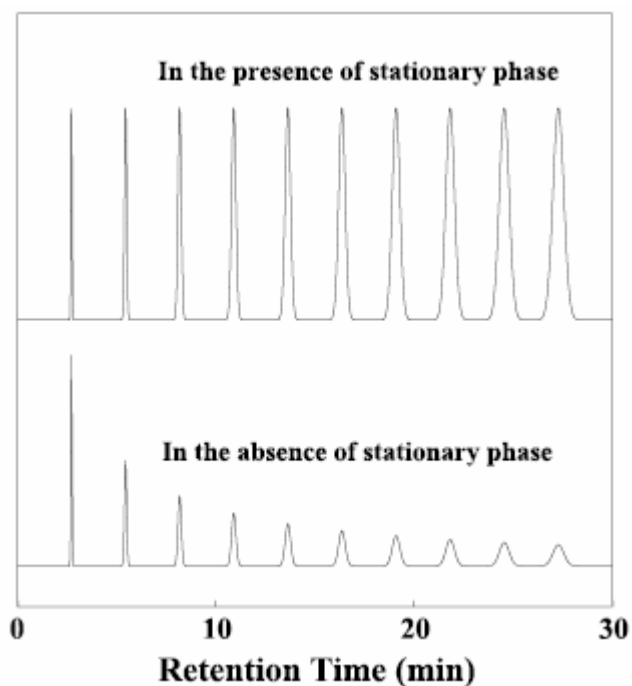


Figure 1.35: Representation of enhancement of fluorescence signal in the presence of stationary phase [75].

### *1.6.3 Amperometric.*

The use of amperometric detection in capillary LC has the advantage that it is amenable to miniaturisation without loss in sensitivity [73]. The ability to selectively detect electroactive species makes amperometric detection popular for the detection of compounds such as cystine. One disadvantage of amperometric detection in capillary liquid chromatography is the miniaturisation and placement of the electrodes to achieve sensitive detection often requires modification of the capillary.

### *1.6.4 Conductivity.*

Conductivity like amperometric detection has the advantage that it is amenable to miniaturisation. The application of conductivity detection to capillary electrophoresis shows the advantages and disadvantages, the ability to miniaturise the electrode but also the need to modify the capillary to allow placement of the electrodes within the capillary [76]. As with all conductivity detection techniques based on a galvanic cell, contact with the sample is required.

### *1.6.5 Capacitively coupled contactless conductivity detection.*

An emerging detection technique used in both capillary electrophoresis and capillary liquid chromatography is the *capacitively coupled contactless conductivity detector (C<sup>4</sup>D)*. In the next Section the operation principles and applications of this detector will be discussed in detail.

## 1.7 Capacitively coupled contactless conductivity detection.

### 1.7.1 Origins.

In 1998 two groups published work on new detection mode for use with CE [77, 78]. This detection technique relied on the use of coupled capacitance to detect within fused silica capillary. The main advantage of the technique was that C<sup>4</sup>D was a non-contact method, requiring no modification of the separation capillary, such as burning a detection window through the polyimide coating as in UV detection. [77-79]. The early C<sup>4</sup>D setups were made by either painting on conducting silver varnish onto the outside of a capillary or by cutting needle cannulas [79] to the correct size through which the capillary was passed. Such setups were originally used for the detection of inorganic ions in CE separations [78, 79].

### 1.7.2 Operation principles.

The name given to this new technique denotes its principle of operation, *capacitively coupled contactless conductivity detection*, i.e. it relies on capacitance which is coupled between two electrodes and operates in a non-contact manner.

#### 1.7.2.1 Capacitance.

When two conductors are separated by an insulator (or a vacuum, also known as a dielectric) they form a capacitor. In a parallel plate capacitor, depicted in Figure 1.36, where the plates are connected to a direct current (D.C.) power source, and the switch is closed, electrons from the upper plate (P1) are attracted to the positive terminal and flow in that direction, to keep the current constant throughout the circuit electrons flow from the negative terminal of the power source to the lower plate (P2). The result of this flow of electrons is the creation of a net positive charge on P1 and a net negative charge on P2. Eventually the voltage between

P1 and P2 will rise to that of the power source, when the capacitor is fully charged the current drops to zero. When the switch is opened this voltage is maintained, until it is required for use. Therefore capacitors in a D.C. circuit are suited to storing energy.

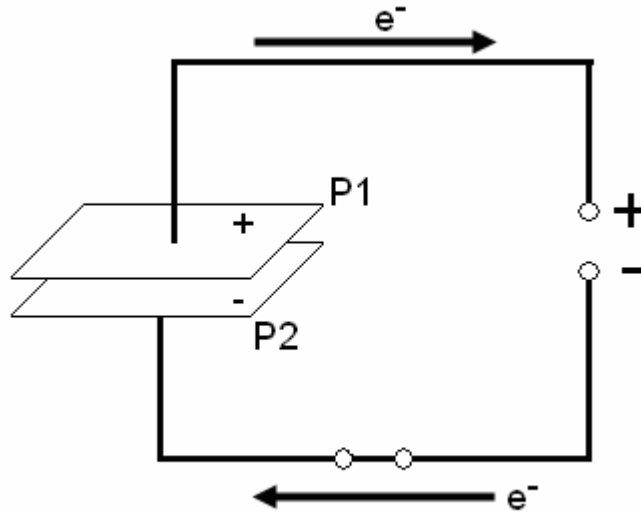


Figure 1.36: Diagram of a capacitor in a D.C. circuit.

However, when a capacitor is placed into an alternating current (A.C.) circuit (Figure 1.37) the voltage is constantly changing and the capacitor is constantly charging and discharging. The constant ebbing and flowing of electrons in the wire leading the capacitor results in an alternating current flowing in the circuit as if the capacitor had been replaced by a resistor. However, no electrons are flowing through the insulator between the plates and the plates of the capacitor are constantly charging at one polarity and then charging to the opposite polarity.

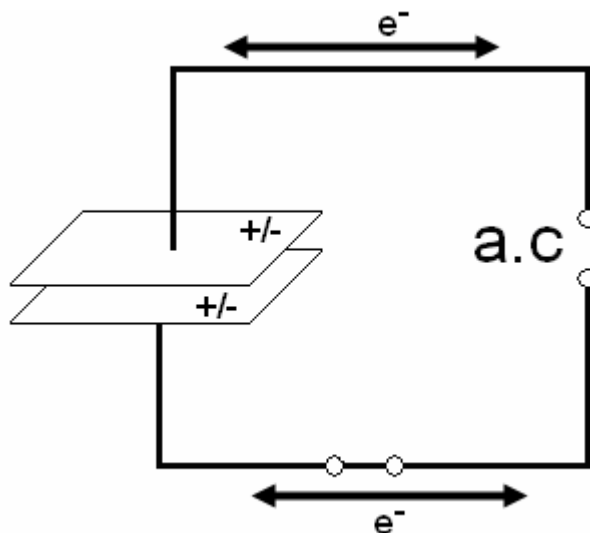


Figure 1.37: Diagram of a capacitor in an A.C. circuit.

This then results in the fact that capacitors do not allow the passage of D.C. but do allow the passage of A.C.

#### 1.7.2.2 Capacitance in $C^4D$ .

In a  $C^4D$  circuit there are two capacitors in series separated by a resistor. Figure 1.38 shows a simplified circuit diagram of this. The capacitors in a  $C^4D$  cell are not of two metallic plates, one plate is a metallic cylinder, and the other is the fluid at the internal surface of the capillary tubing (e.g. fused silica capillary) [80]. The resistor between the two capacitors is the fluid inside the tubing between the two capacitors. To the excitation electrode an A.C. of fixed frequency is applied, this ring electrode forms a capacitor with the fluid under it, the current then passes through the detection gap (ca. 2 mm) to the second ring electrode which acts as the pick-up electrode. As the analyte enters the detection gap it causes a reduction in resistance, therefore an increase in conductivity. If the peak to peak voltage of the applied A.C. is kept constant then using Ohm's Law:

$$V = IR$$

Eq. 1.3

Where:

$V$  = Voltage

$I$  = Current

$R$  = Resistance

A decrease in the resistance of the solution leads to an increase in the current flowing through the detection gap. The pick-up electrode is connected to an operational amplifier (op-amp) which converts current to voltage. As here the resistor is fixed then, using Equation 1.3, and increase in the current (due to an increase in conductivity) will result in an increase in output voltage. As a result of this  $C^4D$  outputs are reported in volts (generally mV) as opposed to siemens. Figure 1.38 is a circuit diagram of the  $C^4D$  showing the inclusion of the op-amp.

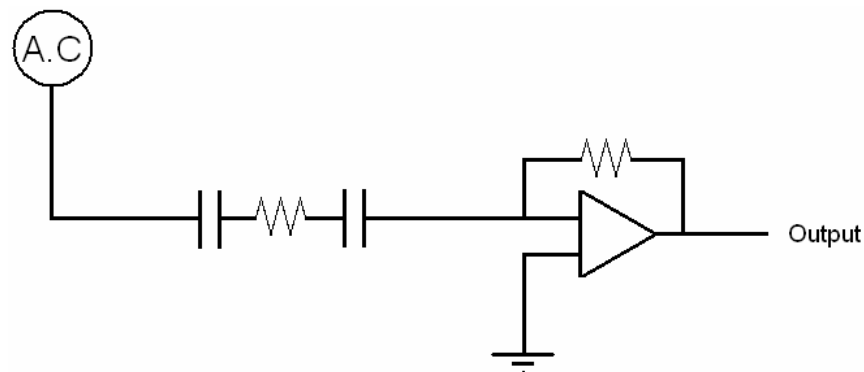


Figure 1.38: Equivalent Circuit diagram of the  $C^4D$  showing the inclusion of the op-amp.

The two ring electrodes need to be isolated from one another to prevent stray capacitance between them, which would be detrimental to the signal-to-noise ratio of the detector. This shielding is achieved by placement of a copper sheet between the electrode, through which the tubing itself passes. Figure 1.39 shows the simplified general set-up of a  $C^4D$ .

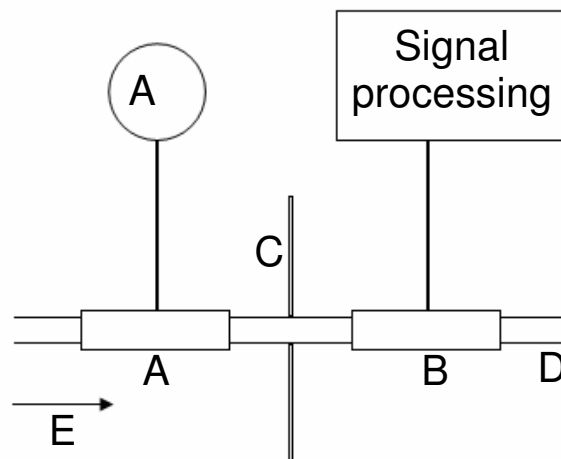


Figure 1.39: Schematic of an actual C<sup>4</sup>D arrangement excitation electrode (A), pick-up electrode (B), shield (C), eluent flow path (D) and direction of flow (E).

The ring electrodes can be viewed in the same way a classical conductivity cells operate, with the cross-sectional area of the tubing below the ring electrodes (Figure A) as the area of a galvanic cell electrode and the detection gap (Figure I) as that of the separation of two galvanic cell electrodes. In this way the C<sup>4</sup>D can be seen to have “virtual electrodes” (see Figure 1.40) [80].

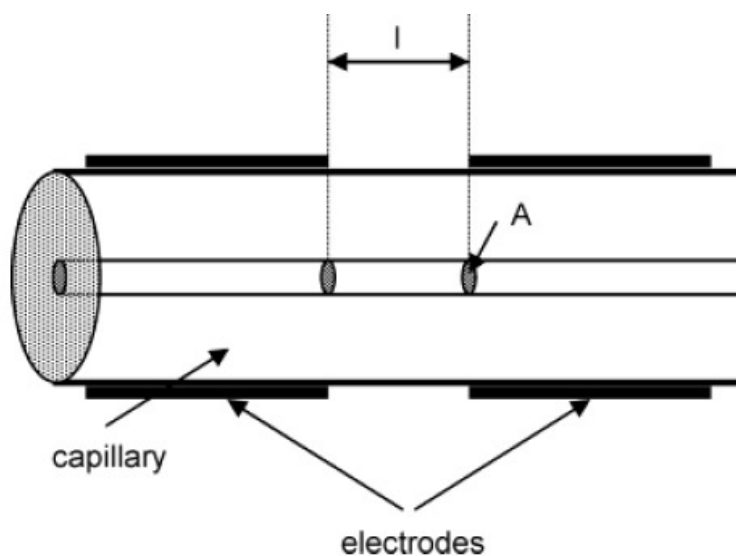


Figure 1.40: Sketch of the cell model that describes the basic behaviour of the C<sup>4</sup>D [80].

In  $C^4D$  for use with microchip system the electrodes are planar and placed under the separation channel, a typical set-up is shown in Figure 1.41. Although the electrodes are planar in nature the same fundamental operational characteristics apply [81].

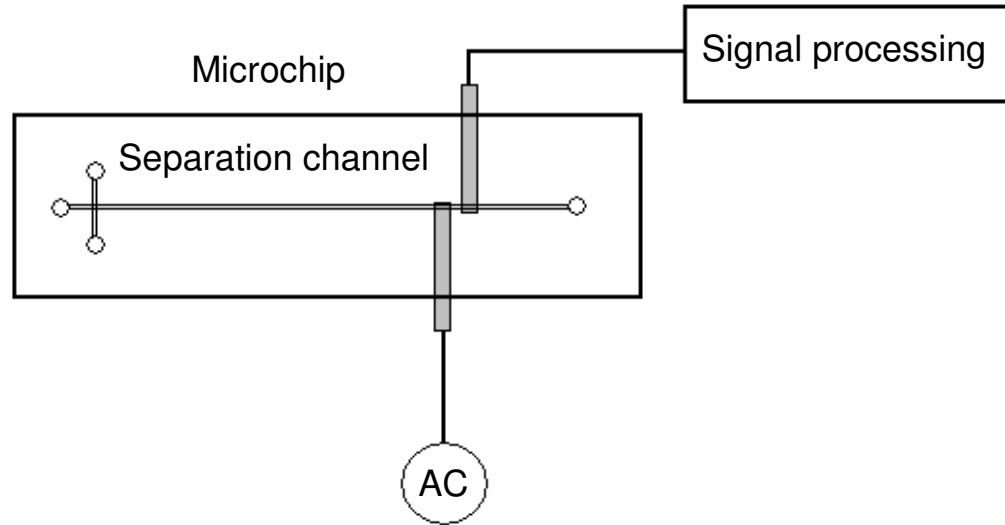


Figure 1.41:  $C^4D$  set-up commonly used in microchips.

### 1.7.2.3 Operational characteristics of $C^4D$ .

As  $C^4D$  relies on capacitance it is highly frequency dependant and it is important to consider the behaviour of the  $C^4D$  signal with regard to A.C. inputs.

As previously mentioned the capacitor allows the passage of current through the cell and behaves as if there was a resistor in its place; however, this is not absolutely correct. When a capacitor is placed in an A.C. circuit the following phenomena must be considered.

When a capacitor in a D.C. circuit is fully charge the current drops to zero, as in an A.C. circuit the capacitor is constantly charging and discharging the current is constantly rising and falling in the circuit. This relationship leads to the fact that in a A.C. circuit containing one capacitor the current leads the voltage by  $90^\circ$  (i.e.

$\pi/2$ ). However, in a C<sup>4</sup>D cell there are two capacitors in series and the current will lead the voltage by 180° ( $\pi$ ). Therefore, in C<sup>4</sup>D the current will reach its maximum when the voltage reaches its minimum. As previously stated the signal at the op-amp on the pick-up electrode side of the cell converts the current to voltage, as a result of this the output voltage will be 180° ( $\pi$ ) out of phase with the input voltage.

The output voltage can be described by Ohm's Law where [82]:

$$V_{out} = -iR_f \quad (\text{Eq.1.4})$$

where:

$V_{out}$  = output voltage in V.

$i$  = cell current in A

$R_f$  = Reference resistor of op-amp in  $\Omega$

Note: the minus sign for the current will revert the phase of the output voltage back to that of the input voltage.

In the optimisation of a C<sup>4</sup>D a plot of output voltage against the input frequency is used, which is referred to as a Bode plot. This graph is constructed simply by scanning through a range of input frequencies and collecting the voltage of the op-amp of the cell (before it is rectified). From such plots it can be seen that the output voltage increases with the input frequency until a certain frequency after which the output voltage levels off (i.e. a plateau). C<sup>4</sup>D cells are operated in this plateau region (Figure 1.42). The frequency at which the plateau occurs is dependant on the resistance (i.e. the conductivity) of the solution in the detection gap and also by the capacitance of the cell.

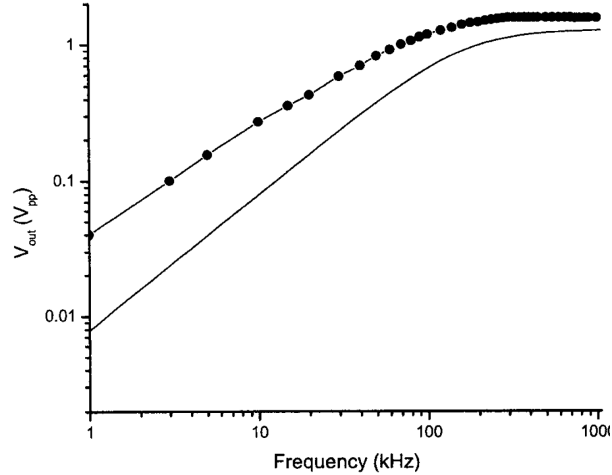


Figure 1.42: Frequency plots (Bode plots) for a model cell (—), and for a real cell (-•-) [79].

It is important to note that the op-amp used in a C<sup>4</sup>D should be a unity gain stable op-amp to prevent the op-amp itself dominating the frequency dependence of the output. Using other op-amps results in a peak in the Bode plot where the plateau is expected using a unity gain stable op-amp. Figure 1.43 shows the comparison of two op-amps, OPA 655 is a unity gain stable op-amp whereas OPA 606 is not. The domination of OPA 606 in the Bode plot at higher frequencies (> 100 kHz) is clearly evident.

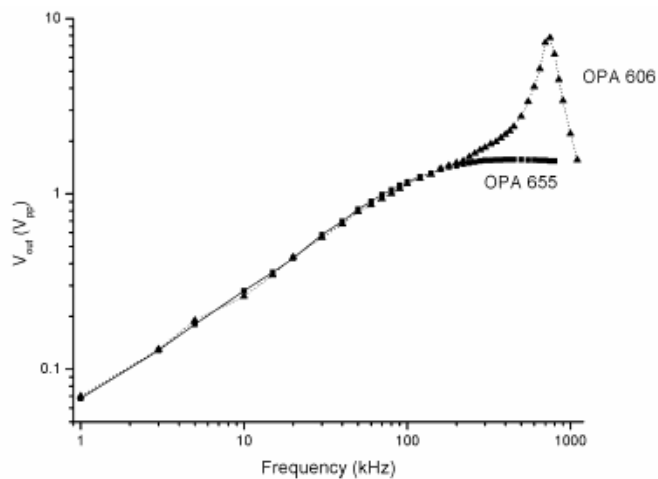


Figure 1.43: Bode plots measured for a real C<sup>4</sup>D cell with OPA 655 and OPA 606 [80].

Kuban *et al.* using a  $C^4D$  cell with 4 mm electrodes separated by a 2 mm detection gap monitored the effect of operating frequency on the electropherograms for the separation of inorganic cations. The frequencies chosen were 10, 30, 100, 250, 400 and 800 kHz. It was found that frequencies from 10 to 100 kHz, taken from the region before Bode plot plateau, gave non-optimal behaviour with regard to peak height/area also exhibiting peak overshoot (i.e. disturbance at the front and/or tail of the peak). For the frequencies in the plateau region of the Bode plot the peak height/area and signal to noise ratio were optimal with no evidence of peak overshoot (Figure 1.44).

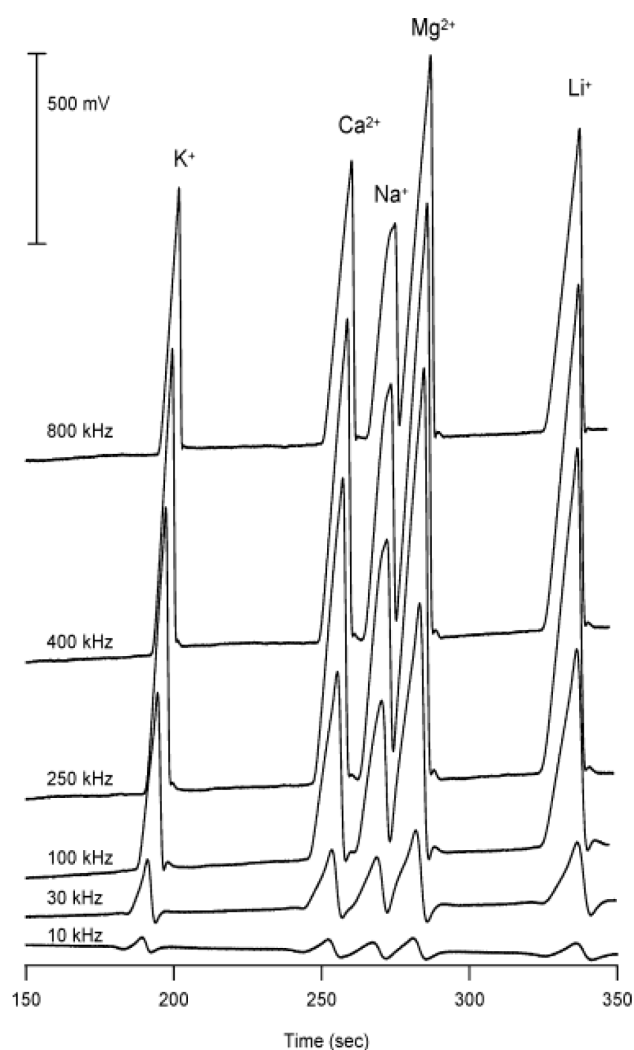


Figure 1.44: Effect of the excitation frequency on the appearance of the electro – pherograms [80].

#### 1.7.2.4 Cell geometries, electrode length & detection gap.

The optimisation and characterisation of C<sup>4</sup>D has been carried out by different groups over the last decade, however the parameters have been investigated in near isolation from each other. Kuban *et al.* was the first author to investigate all the parameters with one cell [80]. Therefore, in the discussion of these parameters this important paper will be the main source.

In a C<sup>4</sup>D cell two main parameters in the electrode geometry can be changed in the design, the distance between the electrodes and the electrode length. Kuban *et al.* investigated the effect of differing length of electrodes, with electrode lengths of 2, 4, 6 and 8 mm separated by a 2 mm detection gap. Constructing Bode plots for each of these electrode lengths showed little difference in the operating frequency of the cell (Figure 1.45). Only minor differences were observed at lower frequencies. The results indicate that there is no difference in the ohmic resistance of the cell with regard to electrode length and that the capacitance of the cell increases with longer electrode lengths as in Figure 1.46 (as would be expected from the theory of capacitors).

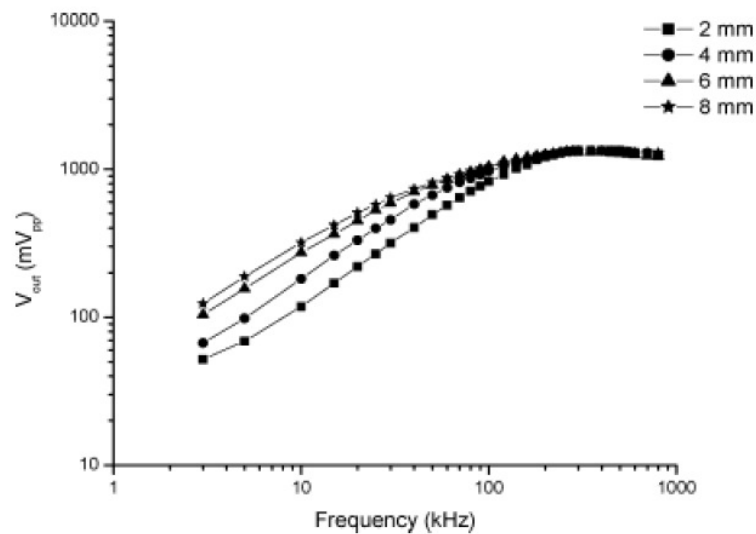


Figure 1.45: Bode plots showing the effect of different electrode lengths on C<sup>4</sup>D behaviour [80].

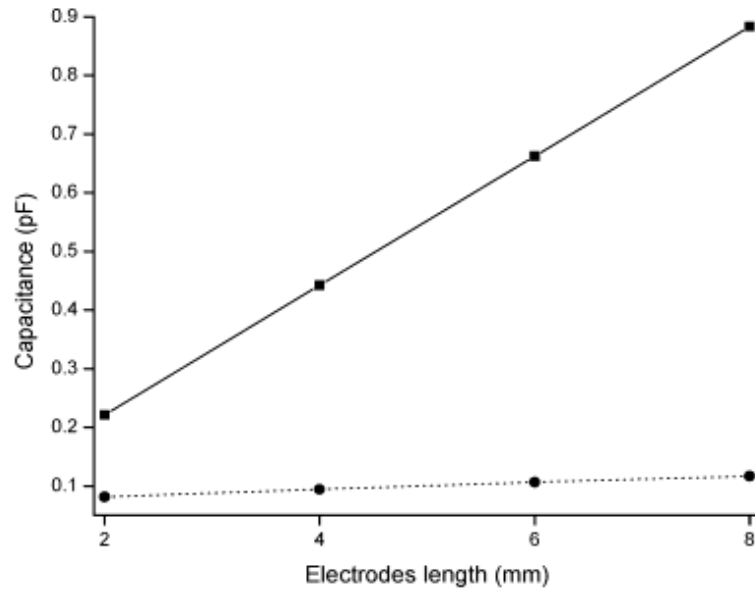


Figure 1.46: Effect of electrode length on capacitance of cell [80].

Kuban *et al.* also examined the effect of changing the length of the detection gap (1, 2, 3, 4 and 5 mm). From the resultant Bode plots (Figure 1.47) it was found that by increasing the detection gap the plateau level (in V) is lower with longer detection gaps, as was expected. However, the plateau region was found to be shortened at longer detection gaps and this deviation from the expected results could not be explained.

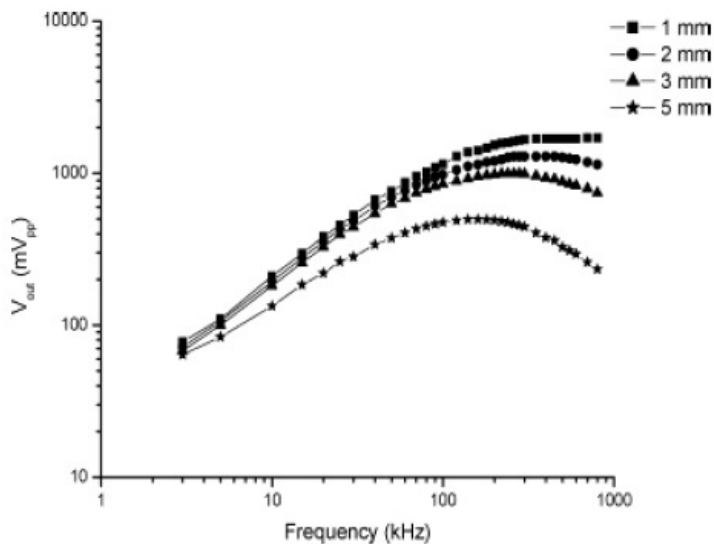


Figure 1.47: Bode plots showing the effect of changing detection gap distance [80].

As the detection gap is increased the cell resistance is expected to increase in a linear fashion. The experimental data followed this trend, although the cell resistance was much higher than predicted, and to account for this the “virtual electrodes” of the cell must include a small portion of the capillary volume under the electrodes.

### 1.7.3 Applications of $C^4D$ .

#### 1.7.3.1 Capillary electrophoresis

The application of  $C^4D$  to capillary electrophoresis (CE) has had a growing interest since the publications in 1998 by Zemmann and do Logo [77, 78]. Indeed  $C^4D$  was introduced on these papers solely for use in CE. The first publications centred on the analysis of inorganic ions. In Zemmann *et al.* the separation of inorganic anions (e.g.  $Br^-$ ,  $F^-$  and  $NO_3^-$ ) and cations (e.g.  $Li^+$ ,  $Na^+$  and  $Mg^{2+}$ ) was performed and the operation of  $C^4D$  was found to be acceptable [78]. When the peak heights of simultaneous UV detection and  $C^4D$  (here called CCCD) were compared the UV signal required a five fold multiplication to achieve the same response as  $C^4D$

(Figure 1.48). LODs for the C<sup>4</sup>D were found to be 200 ppb for sodium and chloride, with a linear range over three orders of magnitude. The electrodes in this cell were of cut needle cannulas.

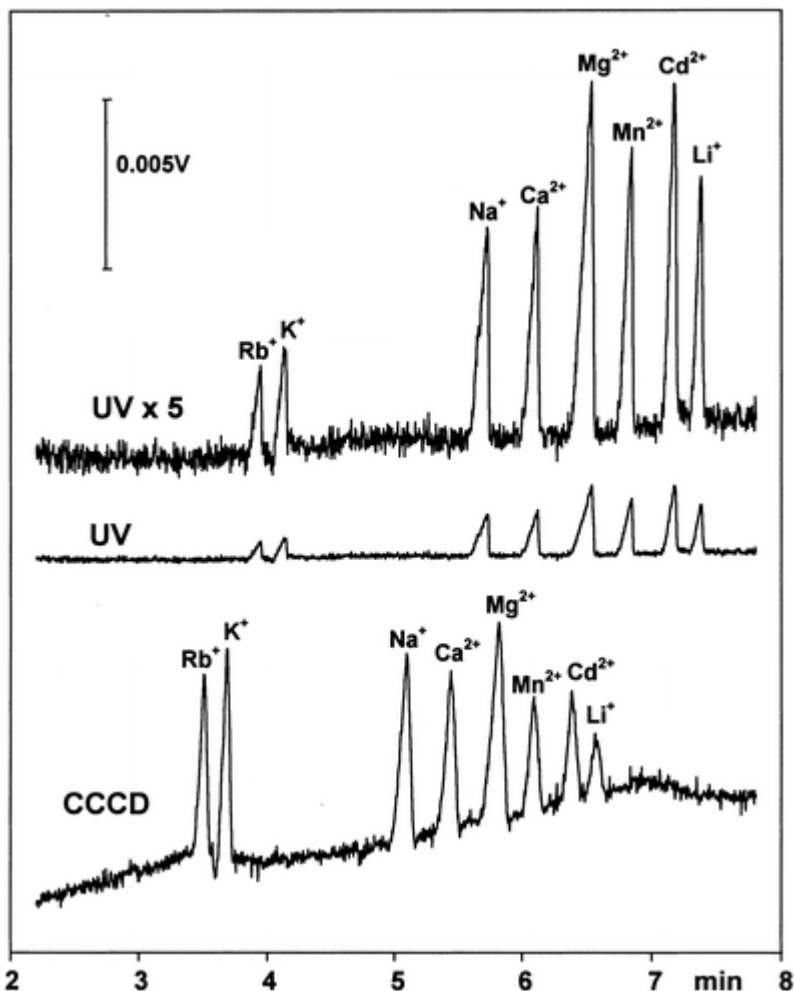


Figure 1.48: Separation of a standard mixture of inorganic cations comparing UV and conductivity detection. Conditions: fused-silica capillary,  $L = 60$  cm,  $L_1 = 40$  cm to conductivity detector,  $L_2 = 52.5$  cm to UV detector (214 nm),  $U = +20$  kV,  $I = 3.0$   $\mu$ A, and  $T = 23$  °C; electrolyte, 10 mM lactic acid, 8 mM 4-methylbenzylamine, and 15 % methanol, pH 4.9; injection, 30 s; sample concentration, 0.1 mM [78].

In the same year da Silva and da Logo *et al.* reported the use of a C<sup>4</sup>D cell based on silver paint electrodes for the indirect detection of organic cations (e.g. organic amines). Da Silva and da Logo were also the first CE-C<sup>4</sup>D paper to report the

effect of the input frequency on the signal to noise ratio of the detector, showing the frequency dependence of C<sup>4</sup>D. From these simple beginnings C<sup>4</sup>D in CE has been applied to a variety of electrophoretic separations with analytes ranging from vitamins [83] to herbicides [84].

The application of C<sup>4</sup>D in CE is not limited to use with fused silica capillaries. Tanyanyiwa *et al.* applied the use of C<sup>4</sup>D to CE in polyether ether ketone (PEEK) capillaries [85]. The use of PEEK capillary tubing in CE offers a substrate that has very low EOF due to a lack of surface charges, and therefore no need for an EOF modifier in the background electrolyte. However, the major drawback of using PEEK is finding a suitable detection technique as PEEK has very poor optical transparency at short wavelengths. Tanyanyiwa *et al.* used to their advantage the non-contact nature of C<sup>4</sup>D to overcome this roadblock in the use of PEEK in CE. Figure 1.49 shows an example of the separations obtained with PEEK capillaries for the separation of inorganic anions and cations.

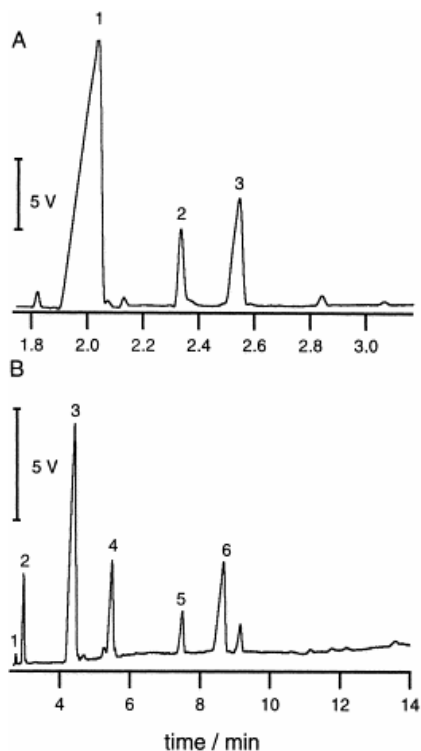


Figure 1.49: Determination of cations and anions in a red wine sample with a PEEK capillary of 60 cm. The sample was diluted 1:20 with buffer. (A) (1)  $K^+$ , (2)  $Ca^{2+}$  and (3)  $Na^+$ . (B) (1)  $Cl^-$ , (2)  $SO_4^{2-}$ , (3) tartrate, (4) succinate, (5) acetate and (6) lactate. Buffer: 10 mM MES/His, 1 mM 18-crown-6 (pH 6.0). Injection: electrokinetic (non-stacking conditions), 5 s at +5 V for cations and at -5 kV for anions. Separation: +25 kV for cations and -25 kV for anions [85].

### 1.7.3.2 Capillary electrochromatography.

The application of  $C^4D$  to use in capillary electrochromatography (CEC) was investigated by Hilder *et al.* The separation of inorganic anions was performed with both  $C^4D$  and UV detection. The LODs obtained for the  $C^4D$  were found to be lower than those obtained with UV detection (Table 1.1) The added advantage of using  $C^4D$  with an UV absorbing eluent (such as *p*-toluene-sulfonic acid) is that higher concentrations can be used allowing for better control of the separation [86].

Table 1.1: Comparison of limits of detection obtained for C<sup>4</sup>D and UV detection for the determination of inorganic anions in CEC [86].

Analyte	LOD (ppb)	
	UV	C <sup>4</sup> D
Chloride	11	5
Nitrate	92	14
Phosphate	95	31

Another application of C<sup>4</sup>D in CEC carried out by Kuban *et al.* involved the creation of multiple layers of poly(butadiene-maleic acid) copolymer (PBMA) onto the internal surface of fused silica capillary (i.e. open tubular CEC) [87]. The creation of this cation exchange phase on the surface on the capillary was used for the separation of inorganic cations (e.g. Li<sup>+</sup>, Ca<sup>2+</sup>, Figure 1.50). C<sup>4</sup>D was used as the detection method and the LODs obtained compare well with both CE and CEC with pre-concentration.

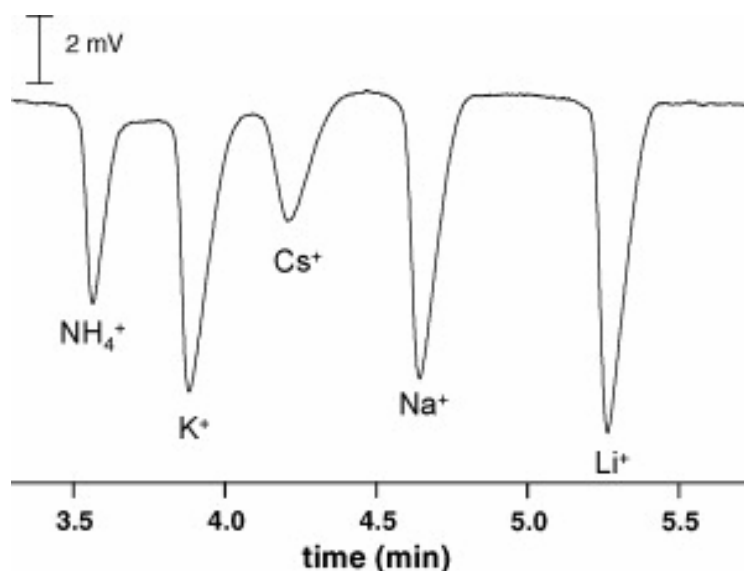


Figure 1.50: OT-CEC-C<sup>4</sup>D determination of five alkali cations. CEC conditions as in separation column, four layers of PBMA, BGE solution, 100 mM acetic acid [87].

### 1.7.3.3 Liquid Chromatography.

From the introduction of  $C^4D$  into CE in 1998 it was nearly 10 years before it was applied as detector in liquid chromatography (LC). In 2006 Kuban *et al.* introduced the concept of using  $C^4D$  as a detector in LC for the determination of non-UV absorbing analytes [88]. The placement of the  $C^4D$  cell on a piece of fused silica capillary post column was employed and was used for the detection of non-steroidal anti-inflammatory drugs (NSAIDs, Figure 1.51), beta-blockers and underivatised amino acids. All separations were performed under isocratic conditions using mobile phases of organic solvents (acetonitrile, methanol) with acetic acid and trifluoroacetic acid to ensure the correct ionisation state of the analytes. The LODs for all separations were found to be comparable (indeed sometimes exceeding) the UV detection LODs for the same separations, Table 1.2 lists the LODs obtained.

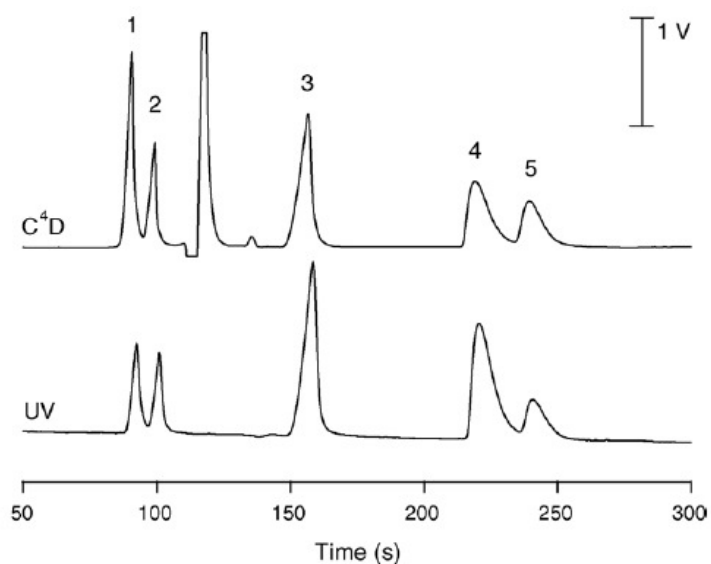


Figure 1.51: Determination of five NSAIDs standards using HPLC with  $C^4D$  and UV detection. HPLC conditions: column, Nucleosil 120-5  $C_{18}$ ; flow rate,  $1.0 \text{ mL min}^{-1}$ ; mobile phase composition, 65% acetonitrile,  $0.17 \text{ mM}$  acetic acid and  $0.25 \text{ mM}$  sodium acetate. Concentration of analytes,  $250 \text{ }\mu\text{M}$ . Peak description: (1) salicylic acid, (2) acetylsalicylic acid, (3) diclofenac, (4) mefenamic acid and (5) ibuprofen. UV detection at  $220 \text{ nm}$  [88].

Table 1.2: LODs obtained for C<sup>4</sup>D and UV detection for NSAIDs [88].

Analyte	LOD ( $\mu M$ )	
	C <sup>4</sup> D	UV
Salicyclic acid	0.15	1.0
Acetyl-salicyclic acid	0.20	1.0
Diclofenac	0.15	0.5
Mefanamic acid	0.40	1.0
Ibuprofen	0.40	2.0

Following on from this work Kuban *et al.* applied C<sup>4</sup>D to detection of underivatised amino acids and small peptides using reversed-phase gradient separations on standard bore columns with the C<sup>4</sup>D attached via fused silica capillary [89]. In the application of C<sup>4</sup>D to gradient separations it was important to balance the conductivity of the two mobile phases (i.e. to have near *isoconductive* mobile phases). This was to limit the amount of baseline disturbance caused by the transfer between mobile phases. However, even with the control of the two mobile phase conductivities computational treatment of the resultant chromatograms was required to yield suitable results. In Figure 1.52 the separation of underivatised amino acids is shown. The mobile phases used were 0.15% acetic acid in DI water and 0.9 % acetic acid in 30% methanol. The raw chromatogram exhibits large baseline disturbance due to the gradient program; however the use of computational treatment yielded a suitable chromatogram for quantitative analysis.

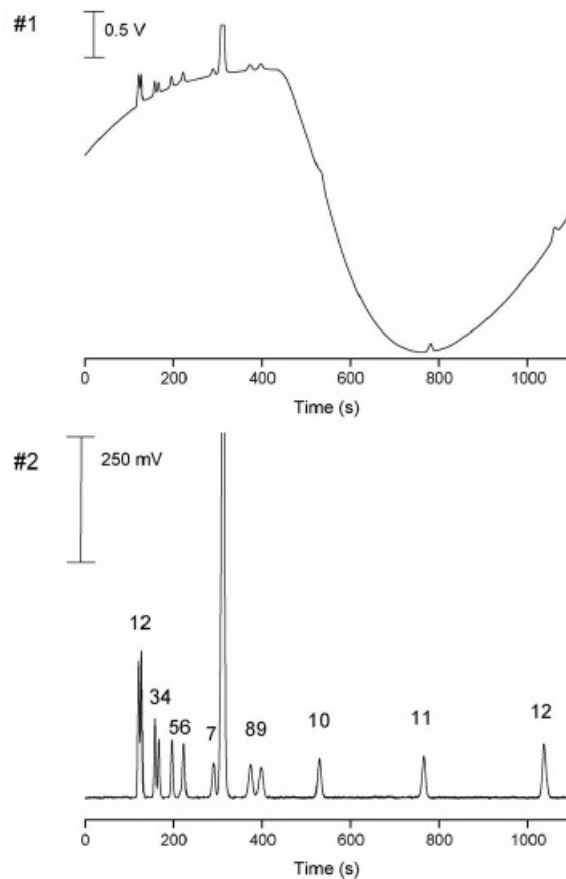


Figure 1.52: Determination of underivatised amino acids using HPLC with C<sup>4</sup>D detection. (#1) raw data, (#2) after normalisation using the Peaks software package [89].

Further work by Kuban *et al.* applied the same principle to the separation of peptides and proteins using monolithic capillary columns (200  $\mu\text{m}$  i.d.) with simultaneous UV detection [74]. For the analysis of intact proteins (e.g. Cytochrome C and trypsin) the LODs obtained were found to be lower for C<sup>4</sup>D in all cases. Figure 1.53 shows the resultant chromatograms using C<sup>4</sup>D and UV detection.

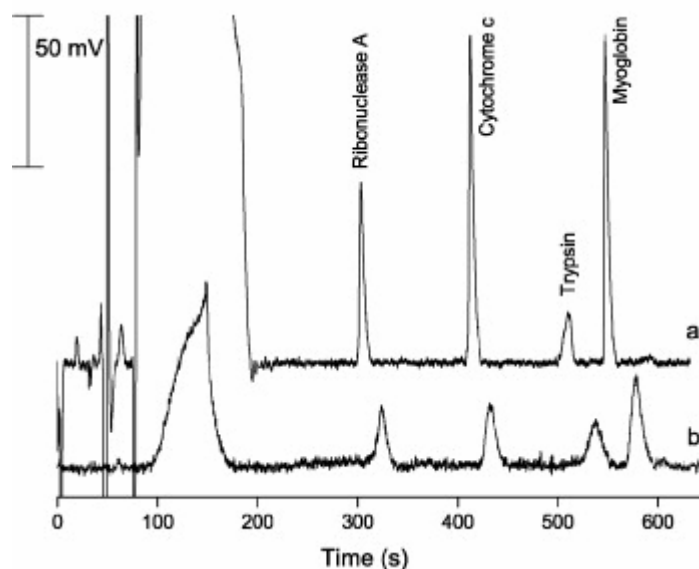


Figure 1.53: HPLC–C<sup>4</sup>D determination of proteins separated on the monolithic capillary column. Mobile phase A, 0.004% TFA in 10% acetonitrile; mobile phase B, 0.006% TFA in 52% acetonitrile. Gradient program, 0–100% B in 12 minutes, flow rate, 1.65  $\mu\text{l min}^{-1}$ . (a) C<sup>4</sup>D parameters: excitation voltage, 360 V<sub>pp</sub>; excitation frequency, 130 kHz. (b) UV detection at 214 nm. Analyte concentrations: trypsin, 20  $\mu\text{g ml}^{-1}$ ; other proteins 10  $\mu\text{g ml}^{-1}$ . The baselines were normalised using the Peaks software package [74].

#### 1.7.3.4 Ion chromatography

The use of C<sup>4</sup>D in the determination of inorganic ions in CE leads to the possible application of C<sup>4</sup>D in IC separations. Kuban *et al.* investigated the relevance of C<sup>4</sup>D to IC separations (suppressed and non-suppressed modes) by placing a C<sup>4</sup>D cell on fused silica capillary after the separation column or suppressor [82]. The performance of the detector was compared to that of a commercial conductivity detector (Figure 1.54). In both IC modes the C<sup>4</sup>D was found to perform in a comparable way, or actually superior, to that of the commercial conductivity detector. Table 1.3 details the LODs obtained for inorganic anions in non-suppressed and suppressed IC using C<sup>4</sup>D and a commercial conductivity detector.

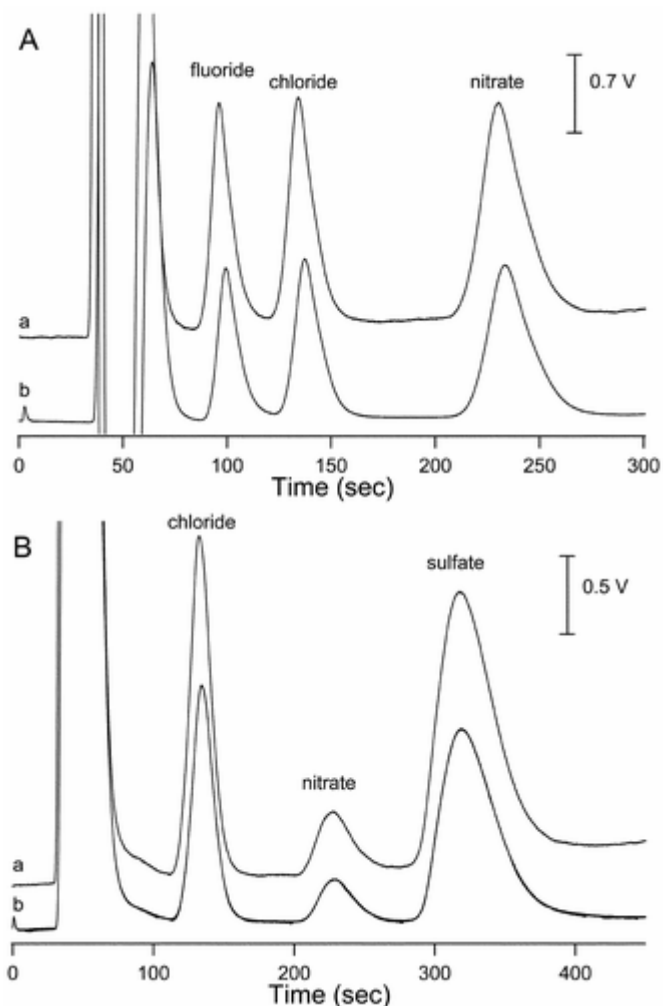


Figure 1.54: (A) Determination of three inorganic anions in the non-suppressed conductivity mode: (a) C<sup>4</sup>D (150 kHz and 50 V<sub>p-p</sub>), (b) commercial conductivity detector. Eluent: 2.5 mM phthalic acid adjusted to pH 4.25 with Tris, flow rate = 1.5 mL min<sup>-1</sup>. Anion concentrations: fluoride, chloride 10 mg L<sup>-1</sup> and nitrate 20 mg L<sup>-1</sup>. (B) Determination of inorganic anions in tap water in the non-suppressed conductivity mode: (a) C<sup>4</sup>D (150 kHz and 50 V<sub>p-p</sub>), (b) commercial conductivity detector. IC conditions as in (A) [82].

Table 1.3: Comparison of LODs for non-suppressed and suppressed IC separations using C<sup>4</sup>D and commercial conductivity detector [82].

Non-suppressed	LOD ( $\mu\text{g mL}^{-1}$ )	
	C <sup>4</sup> D	UV
Lithium	2.9	3.4
Sodium	7	7.2
Potassium	22.2	23.2
Fluoride	160	150
chloride	110	110
Nitrate	250	260
Suppressed		
Fluoride	1.5	1.5
chloride	2	2
Nitrate	5	5
Sulfate	4	4

C<sup>4</sup>D has also been utilised in the separation of inorganic cations using open tubular IC (i.e. OT-IC-C<sup>4</sup>D). Separation was performed on poly(butadiene-maleic acid) copolymer (PBMA) coated fused silica capillary with a tartaric acid eluent and indirect detection as method for evaluating the coating procedure prior to use in OT-CEC-C<sup>4</sup>D. Using a similar methodology for creation of OT-IC phases, Kuban *et al.* placed layers of a copolymer of methylamine (MA) and 1,4-butanedioldiglycidyl ether (BDDE) onto the inner wall of fused silica capillary. Using this stationary phase the separation of inorganic anions was possible and C<sup>4</sup>D was used as the detection method (Figure 1.55).

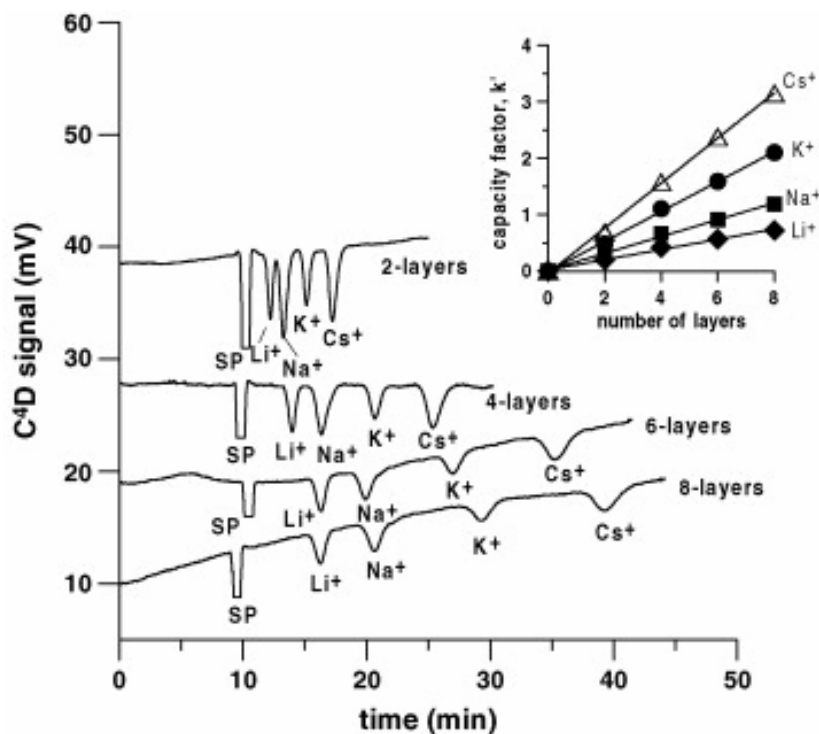


Figure 1.55: OT-IC-C<sup>4</sup>D determination of inorganic cations in separation columns with various numbers of PBMA layers. Eluent, 1 mM tartaric acid; flow rate, 1.5  $\mu\text{L min}^{-1}$ ; injection volume, 200 nL; 120/106 cm total/effective length; 75/375  $\mu\text{m}$  I.D./O.D.; analyte concentration, 10–40  $\mu\text{M}$  in DI water. SP: System peak [87].

Zakaria *et al.* applied C<sup>4</sup>D as the detection mode in latex-coated polymeric monolithic ion-exchange (see Section 1.5.1). The C<sup>4</sup>D cell in this instance was placed off-column using open fused silica capillary. Figure 1.56 show an example of the separations obtained using the latex-coated monolithic stationary phase under suppressed IC conditions using C<sup>4</sup>D [69].

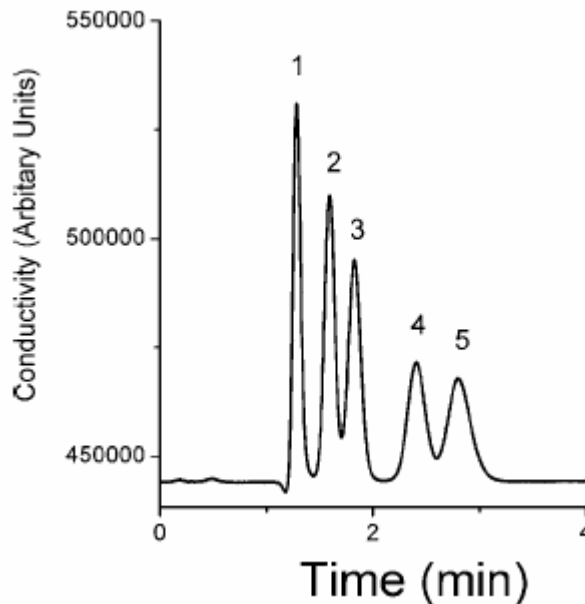


Figure 1.56: Separation of inorganic anions using latex coated suppressed ion exchange chromatography. Eluent: 5.0 mM KOH, flow: 12.5  $\mu\text{L min}^{-1}$ . Peaks: 1, iodate; 2, bromate; 3, nitrite; 4, bromide; 5, nitrate [69].

## 1.8 Conclusions.

The progression of stationary phase chemistries and formats has been a continuous and important section of research in chromatography. The ability to produce novel stationary phases allows for more selective separations, and the development of new formats (i.e. monolithic and capillary scale column) allows for potentially faster and more efficient separations. However, these new stationary phases require more and more detailed characterisation. The use of destructive methods such as SEM-EDX allow for detailed characterisation; however, the destruction of the column produced may not be advantageous. Indirect methods such as monitoring the chromatographic performance of the column allows only an over all view of the stationary phase, and fluorescent methods are restricted in the functionalities available for analysis. The emergence of contactless conductivity detection in the late 1990's offers a novel detection technique for use with capillary scale columns. Since its first publication, where C<sup>4</sup>D was proposed

as a detector for CE it has grown in popularity and has been applied to reversed-phase, both isocratic and gradient, and IC separations. The non-contact, non-destructive and non-invasive operation of this detector opens up the possibility for its use not only as a detector in Cap-IC but also its application to stationary phase characterisation of capillary monolithic stationary phases.

## 1.9 References.

- [1] D.T.-T. Nguyen, D. Guillarme, S. Rudaz, J.L. Veuthey, *J. Sep. Sci.*, 2006, **29**, 1836.
- [2] H. Small, *Ion Chromatography*, Plenum Publishing Corp., New York, USA.
- [3] G. Guichon, *J. Chromatogr. A.*, 2007, **1168**, 101.
- [4] F. Svec, J.M.J. Frechet, *Anal. Chem.*, 1992, **64**, 820.
- [5] F. Svec, *J. Sep. Sci.*, 2004, **27**, 747.
- [6] S.M. Fields, *Anal. Chem.*, 1996, **68**, 2709.
- [7] H. Minakuchi, K. Nakanishi, N. Soga, N. Ishizuka, N. Tanaka, *Anal. Chem.*, 1996, **68**, 3498.
- [8] S.D. Chambers, C.A. Lucy, *J. Chromatogr. A.*, 2007, **1176**, 178.
- [9] J. Randon, S. Huguet, A. Piram, G. Puy, C. Demesmay, J.L. Rocca, *J. Chromatogr. A.*, 2006, **1109**, 19.
- [10] K.K. Unger, R. Skudas, M.M. Schulte, *J. Chromatogr. A.*, 2008, **1184**, 393.
- [11] E. Wu, L. Hu, F. Wang, M. Ye, H. Zou, *J. Chromatogr. A.*, 2008, **1184**, 369.
- [12] O. Nunez, K. Nakanishi, N. Tanaka, *J. Chromatogr. A.*, 2008, **1191**, 231.
- [13] L. Rieux, H. Niederlander, E. Verpoote, R. Bischoff, *J. Sep. Sci.*, 2005, **28**, 1628.
- [14] E. G. Vlakh, T. B. Tennikova, *J. Sep. Sci.*, 2007, **30**, 2801.
- [15] E.C. Peters, F. Svec, J.M.J. Frechet, *Adv. Mater.*, 1999, **11**, 1109.
- [16] H. Kobayashi, D. Tokuda, J. Ilchimar, T. Ikegami, K. Miyabe, N. Tanaka, *J. Chromatogr. A.*, 2006, **1109**, 2.
- [17] K. Caberra, *J. Sep. Sci.*, 2004, **27**, 843.
- [18] J. Urban, P. Jandera, *J. Sep. Sci.*, 2008, **31**, 2521.
- [19] S. Pelletier, C.A. Lucy, *J. Chromatogr. A.*, 2006, **1125**, 189.
- [20] D. Connolly, D. Victory, B. Paull, *J. Sep. Sci.*, 2004, **27**, 912.
- [21] D. Victory, P.N. Nesterenko, B. Paull, *Analyst.*, 2004, **129**, 700.
- [22] K. Ito, Y. Takayama, N. Makabe, R. Mitsui, T. Hirokawa, *J. Chromatogr. A.*, 2005, **1083**, 63.
- [23] S. Pelletier, C.A. Lucy, *J. Chromatogr. A.*, 2006, **1118**, 12.
- [24] J. Li, Y. Zhu, Y.Y. Guo, *J. Chromatogr. A.*, 2006, **1118**, 46.

- [25] Q. Xu, M. Mori, K. Tanaka, M. Ikedo, W. Hu, P.R. Haddad, *J. Chromatogr. A.*, 2004, **1041**, 95.
- [26] P. Hatsis, C.A. Lucy, *Analyst*, 2002, **127**, 451.
- [27] Z. Yana, P.R. Haddad, J.S. Fritz, *J. Chromatogr. A.*, 2003, **985**, 359.
- [28] J.S. Fritz, Z. Yanb, P.R. Haddad, *J. Chromatogr. A.*, 2003, **997**, 21.
- [29] D. Connolly, B. Paull, *J. Chromatogr. A.*, 2002, **953**, 299.
- [30] Q. Xu, M. Mori, K. Tanaka, M. Ikedo, W. Hu, *J. Chromatogr. A.*, 2004, **1026**, 191
- [31] Q. Xu, K. Tanaka, M. Mori, M.I. Helaleh, W. Hu, K. Hasebe, H. Toada, *J. Chromatogr. A.*, 2003, **997**, 183.
- [32] L. Barron, M, P.N. Nesternko, D. Diamond, M. O'Toole, K.T. Lau, B. Paull, *Analytica Chimica Acta*, 2006, **577**, 32.
- [33] D. Connolly, D. Victory, B. Paull, *J. Sep. Sci.*, 2004, **27**, 912.
- [34] Q. Xu, K. Tanaka, M. Mori, M.I. Helaleh, H. Toada, W. Hu, K. Hasebe, *Chromatographia*, 2003, **57**, 19.
- [35] P. Hatsis, C.A. Lucy, *Anal. Chem.*, 2003, **75**, 995.
- [36] B. Paull, C. O'Riordain, P.N. Nesterenko, *Chem. Commun.*, 2005, **215**.
- [37] C. O'Riordain, P.N. Nesterenko, B. Paull, *J. Chromatogr. A* 2005, **1070**, 71.
- [38] C. O'Riordain, L. Barron, E. Nesterenko, P.N. Nesterenko, B. Paull, *J. Chromatogr. A.*, 2006, **1109**, 111.
- [39] E. Sugrue, P.N. Nesterenko, B. Paull, *J. Sep Sci.*, 2004, **27**, 921.
- [40] E. Sugrue, P.N. Nesterenko, B. Paull, *J. Chromatogr. A.*, 2005, **1075**, 167.
- [41] C. Viklund, A. Nordstrom, K. Irgum, *Macromolecules*, 2001, **34**, 4361.
- [42] T. Rohr, E.F. Hilder, J.J. Donovan, F. Svec, J.M.J. Frechet, *Macromolecules*, 2003, **36**, 1677.
- [43] T.C. Logan, D.J. Clark, T.B. Stackowiak, F. Svec, J.M.J. Frechet, *Anal. Chem.*, 2007, **79**, 6592.
- [44] N.W. Smith, Z. Jiang, *J. Chromatogr. A.*, 2008, **1184**, 416.
- [45] S. Eeltink, E.F. Hilder, L. Geiser, F. Svec, J.M.J. Frechet, G.P. Rozing, P.J. Shoemakers, W.T. Kok, *J. Sep. Sci.*, 2007, **30**, 407.
- [46] R. Wu, L.Hu, F. Wang, M. Ye, H. Zou, *J. Chromatogr. A.*, 2008, **1184**, 369.

- [47] V. Pucci, M.A. Raggi, F. Svec, J.M.J Frechet, J. Sep. Sci., 2004, **27**, 779.
- [48] K.M. Glenn, C.A. Lucy, Analyst, 2008, **133**, 1581.
- [49] A. Suzuki, L.W. Lim, T. Takeuchi, Anal. Sci., 2007, **23**, 1081.
- [50] Y. Saito, K. Jinno, T. Greibrokk, J. Sep. Sci., 2004, **27**, 1379.
- [51] [http://www.dionex.com/en-us/webdocs/62080\\_DS\\_UltiMate3000VWD\\_26Aug08\\_LPN1947\\_02.pdf](http://www.dionex.com/en-us/webdocs/62080_DS_UltiMate3000VWD_26Aug08_LPN1947_02.pdf) (27-11-2008, 18:13).
- [52] <http://www.chem.agilent.com/Library/datasheets/Public/5989-4342EN.pdf> (27-11-2008, 18:15)
- [53] S. Rokushika, Z.Y. Qiu, Z.L. Sun, H. Hatano, J. Chromatogr., 1983, **280**, 69.
- [54] E. Munaf, R. Zein, T. Takeuchi, T. Miwa, Analytica Chemica Acta, 1996, **334**, 39.
- [55] C.B. Boring, P.K. Dasgupta, A. Sjorgen, J. Chromatogr. A., 1998, **804**, 45.
- [56] A. Sedyohutomo, L.W. Lim, T. Takeuchi, J. Chromatogr. A., 2008, **1203**, 239.
- [57] R. Zein, E. Munaf, T. Takeuchi, T. Miwa, Analytica Chemica Acta, 1996, **335**, 261.
- [58] T. Takeuchi, Safni, T. Miwa, J. Chromatogr. A., 1997, **789**, 201.
- [59] Sanfi, T. Takeuchi, T. Miwa, J. Chromatogr. B., 2001, **735**, 409.
- [60] T. Takeuchi, Safni, T. Miwa, Y. Hasimoto, H. Moriyama, Analisis, 1998, **26**, 61.
- [61] International Ion Chromatography Symposium (IICS) 2006, Y. Liu, V. Barreto, C. Pohl, Lecture 13, book of abstracts pg. 31.
- [62] International Ion Chromatography Symposium (IICS) 2008, Y. Liu, V. Barreto, C. Pohl, book of abstracts pg. 29.
- [63] F. Svec, C.G. Huber, Anal. Chem., 2006, **78**, 2101.
- [64] T. Ikegami, J. Ichimaru, W. Kajiwara, N. Nagasawa, K. Hosaga, N. Tanaka, Anal. Sci., 2007, **23**, 109.
- [65] J. Jaafar, Y. Watanabe, T. Ikegami, K. Migamoto, N. Takana, Anal. Bionanal. Chem., 2008, **391**, 2551.
- [66] A. Suzuki, L.W. Lim, T. Hiroi, T. Takeuchi, Talanta, 2006. **70**, 190.

- [67] Y. Ueki, T. Umemura, J. Li, T. Odake, K. Tsunoda, *Anal. Chem.*, 2004, **76**, 7007.
- [68] E.F. Hilder, F. Svec, J.M.J. Frechet, *J. Chromatogr. A.*, 2004, **1053**, 101.
- [69] P. Zakaria, J.P. Hutchinson, N. Avdalovic, Y. Liu, P.R. Haddad, *Anal. Chem.*, 2005, **77**, 417.
- [70] J.P. Hutchinson, E.F. Hilder, R.A. Shellie, J.A. Smith, P.R. Haddad, *Analyst*, 2006, **131**, 215.
- [71] A. Y. Katyaneyeva, E.N. Vitorova, A.A. Korolev, A.A. Kurganov, *J. Sep. Sci.*, 2007, **30**, 2836.
- [72] F. Svec, J.M.J Frechet, *Chem. Mater.*, 1995, **7**, 707.
- [73] J.P.C Vissers, *J. Chromatogr. A.*, 1999, **856**, 117.
- [74] P. Kuban, P.C. Hauser, *J. Chromatogr. A.*, 2007, **1176**, 185.
- [75] T. Takeuci, *Chromatography*, 2005, **26**, 7.
- [76] P.K. Dasgupta, L. Bao, *Anal. Chem.*, 1993, **65**, 1103.
- [77] J.A. Fracassi da Silva, C.L. do Logo, *Anal. Chem*, 1998, **70**, 4339.
- [78] A.J. Zemann, E. Schnell, D. Volgger, G.K. Bonn, *Anal. Chem*, 1998, **70**, 563.
- [79] P. Kuban, P.C. Hauser, *Electroanalysis*, 2004, **16**, 2009.
- [80] P. Kuban, P.C. Hauser, *Electrophoresis*, 2004, **25**, 3387.
- [81] P. Kuban, P.C. Hauser, *Analytica Chimica Acta*, 2008, **607**, 15.
- [82] P. Kuban, M.A. Muri, P.C. Hauser, *Analyst*, 2004, **129**, 82.
- [83] W.S. Law, P. Kuban, J.H. Zhao, S.F.Y. Li, P.C. Hauser, *Electrophoresis*, 2005, **26**, 4648.
- [84] Y. Xu, W.L. Wang, S.F.Y. Li, *Electrophoresis*, 2007, **28**, 1530.
- [85] J. Tanyanyiwa, S. Leuthardt, P.C. Hauser, *J. Chromatogr. A.*, 2002, **978**, 205.
- [86] E.F. Hilder, A.J. Zemann, M. Macka, P.R. Haddad, *Electrophoresis*, 2001, **22**, 1273.
- [87] P.Kuban, P. Kuban, V. Kuban, P.C. Hauser, P. Bocek, *J. Chromatogr. A.*, 2008, **1196**. 377.

- [88] P. Kuban, E.M. Abad-Villar, P.C. Hauser, J. Chromatogr. A., 2006, **1107**, 159.
- [89] P. Kuban, P.C. Hauser, J. Chromatogr. A., 2006, **1128**, 97.

---

**Chapter 2: A comparison of capacitively coupled contactless conductivity detection on monolithic capillary columns and open fused silica capillaries**

---

"Freedom is the freedom to say that two plus two make four. If that is granted, all else follows."

-George Orwell, 1984

## 2.1 Introduction.

There has been growing interest in capillary chromatography in the separation science community over the last 20 years, and as the ability to produce capillary scale columns and instrumentation has improved [1], new detection modes are being applied to this class of separations.

### *2.1.1 Ion exchange via surfactant coating of reversed-phase columns.*

The ability to modify reversed-phase columns (both particulate and monolithic) to render them suitable for ion exchange chromatography has been exploited since the early 1980's [2]. The main reason for coating a reversed-phase column with a surfactant for ion exchange is to take advantage of the high efficiency of these columns, the different formats these columns are available in, and the different selectivity of these surfactants. Since then, a variety of surfactants have been used for such analysis, which can be separated into two main groups: ionic surfactants and zwitterionic surfactants. Ionic surfactants possess only a positive or a negative charge, whereas zwitterionic surfactants possess both positive and negative charges. The two different classes allow for different selectivities to be exploited in the separation of ions. Within the group of ionic surfactants used for analysis of inorganic ions there are sodium dioctylsulfosuccinate (DOSS) [3], didodecyldimethylammonium bromide (DDAB) [3,4], cetyltrimethylammonium bromide (CTAB) [5-7], tetradecyl-trimethylammonium (TTA) [8], myristyltrimethylammonium [9], lithium dodecylsulphate [10] and cetylpyridium chloride (CPC) [11]. The zwitterionic surfactants used for separation of inorganic anions are CHAPS [12], CHAPSO [12], 3-(*N,N*-dimethylmyristylammonio)-propanesulfonate (Zwittergent 3-14) [12,13], *N*-dodecyl-*N,N*-(dimethylammonio)undecanoate (DDMAU) [14], *N*-dodecylphosphocholine [15] and a number of (*N*-dodecyl-*N,N*-dimethylammonio)alconates [16]. To date, all of these modifications have been carried out on 4.6 mm i.d. columns.

### *2.1.2 Capillary chromatography.*

The use of capillary scale columns has increased in the last 20 years, due to the advantage of a reduction in sample volumes and mobile phase consumption (and therefore waste generation) and higher mass sensitivity due to reduced dilution on-column [17]. However, the commercial availability of monolithic ion-exchange columns is non-existent (at the time of this work), so to take advantage of monolithic stationary phases for the separation of inorganic anions at both the capillary scale and conventional scale, surfactant coating methods have been used. However, using a capillary monolithic column creates obstacles for sensitive analysis. As the flow rates used can be in the range from 100 nL min<sup>-1</sup> to 10 μL min<sup>-1</sup>, dead volume in any part of system can cause delays and, particularly post column, extra-column band broadening [17]. Also, in reducing the cross sectional area of the column the injection volume must also be reduced to avoid overloading of the column, as must the volume of the detector cell to allow for sensitive detection. Capacitively coupled contactless conductivity detection (C<sup>4</sup>D) is a detector that can address two of these issues (see Chapter 1). As C<sup>4</sup>D is a detection technique designed to be placed on the outside of the capillary column, no connectors are needed, thus eliminating band broadening. Also conductivity detection is a technique amenable to miniaturisation, without loss in sensitivity.

In this Chapter the application of C<sup>4</sup>D to capillary ion chromatography using silica-based monolithic capillary column coated with the zwitterionic surfactant DDMAU (Figure 2.1) was investigated. In addition, both modes of operation (i.e. on-column and off-column) are compared and contrasted with a view to evaluating the main advantages of C<sup>4</sup>D.

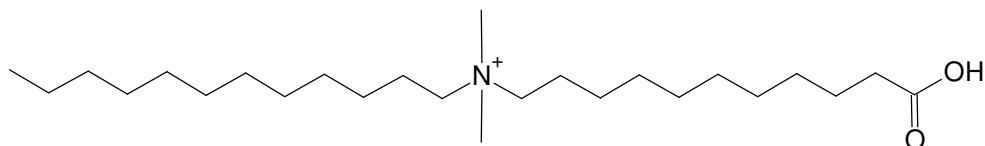


Figure 2.1: Structure of *N*-dodecyl-*N,N*-(dimethylammonio)undecanoate (DDMAU).

## 2.2 Experimental.

### 2.2.1 Instrumentation.

The pump used for eluent delivery was an Applied Biosystems 400 Solvent Delivery System (Foster City, CA, U.S.A.). Eluent flow through the capillary column was controlled by a custom built adjustable flow splitter based upon a T-piece connector with variable back pressure applied to the waste line (Figure 2.2). By placing a T-piece connector in the flow path with a back pressure coil on the waste side the flow from the pump (i.e. the master flow) is split down by a set ratio. A detailed explanation of flow splitting for capillary LC is given by Takeuchi *et al.* [18]. By increasing the back pressure on the waste side the flow through the column is increased. Flow rates were calculated by recording the weight of water delivered through the monolith for a fixed time using a Sartorius ED124S balance. Samples were injected using a Rheodyne MX Module Nano Injector (Alltech Associates, Applied Science Ltd., Lancashire, U.K.), with a fixed injection volume of 10 nL, into which the capillary column itself was connected directly (therefore reducing band broadening). The capillary column used for this section of work was an Onyx monolithic reversed-phase C<sub>18</sub> column (150 mm × 0.1 mm i.d., 0.365 mm O.D.) (Phenomenex, Cheshire, U.K.). Fused silica capillary (FSC) was purchased from Composite Metal Services (ShIPLEY, UK) In a manner similar to that described previously [15,20], the capillary column was semi-permanently coated with the zwitterionic anion exchanger, *N*-dodecyl-*N,N*-(dimethylammonio)undecanoate (DDMAU) (Calbiochem, La Jolla, CA, U.S.A.) by

passing an aqueous solution of 2.0 mM DDMAU through the column at a flow rate of approx.  $1 \mu\text{L min}^{-1}$  for 3 h, before washing thoroughly with DI water for approx. 1.5 h at the same flow rate. Following conditioning the column coating remained stable for the entire period of this study, without signs of column bleed.

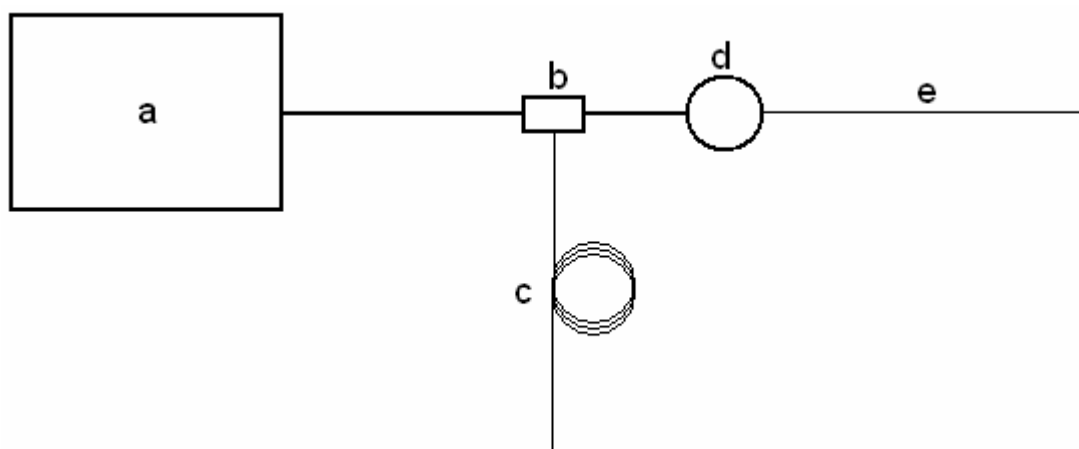


Figure 2.2: Schematic of flow system used to deliver  $\mu\text{L}$  flow rates to capillary monolith. (a) Conventional pump, (b) T-piece connector, (c) waste line, (d) injector (10 nL), and (e) column.

The detector used was a TraceDec Contactless Conductivity Detector (Innovative Sensor Technologies GmbH, Innsbruck, Austria). The detector was supplied with a detector cell, through which the above modified monolithic capillary column was directly fed, with the exact position of detection along the length of the capillary variable. With the column in a fixed position the detector cell could be moved along its length. Detector settings used were; frequency: 2XHIGH; voltage (amplifier):  $-18 \text{ dB}$ ; gain: 75% and offset: 0. Detector position: 13 cm from column inlet, unless otherwise stated. Processing of chromatograms was carried out using PeakNet 6.30 software (Dionex, Sunnyvale, CA, U.S.A.). Eluent pH was measured using an Orion Model 420 pH meter (Thermo Orion, Beverly, MA, U.S.A.) with a glass electrode.

### *2.2.2 Reagents.*

All chemicals used were of analytical reagent grade, and were supplied by Sigma–Aldrich (Tallaght, Dublin, Ireland). All eluents and standard solutions were prepared using deionised (DI) water from a Millipore Milli-Q water purification system (Bedford, MA, U.S.A.), and were twice filtered through a 0.45 µm filter and degassed by sonication.

### *2.2.3 Sample preparation.*

All samples were prepared from 1000 mg L<sup>-1</sup> stocks of the corresponding salt. Dilutions were made using DI water.

## **2.3 Results and discussion.**

### *2.3.1 Separation of inorganic anions on a capillary monolithic column.*

The reversed-phase monolithic silica based capillary column was dynamically modified with the amphoteric surfactant DDMAU, to impart anion-exchange properties to the monolithic silica phase. This coating has been characterised for its selectivity towards anions previously and has been shown to result in a stable coating on a similar reversed-phase monolithic silica phase (4.6 mm i.d. column) [14]. However, it should be noted that according to manufacturer's data on the Onyx monolithic C<sub>18</sub> capillary column, the capillary monolith has a higher carbon content of 18% mass, compared to the previously studied standard bore Chromolith Performance RP18e column, which has a 14% carbon mass. This should further increase the stability of the surface coating of DDMAU of the capillary monolithic column.

Figure 2.3 shows the overlaid chromatograms obtained on the DDMAU coated reversed-phase column for a series of mixed standards of iodate, nitrite, bromide and nitrate separated using a 0.5 mM phthalate eluent (pH 4.0). As can

be seen from the chromatograms shown, peak broadening for the higher concentration standards indicated that for future work the capacity of the monolith should ideally be increased. Comparing the peak areas for the analytes showed a good linear fit,  $R^2 > 0.99$  were obtained for all analytes (Figure 2.4).

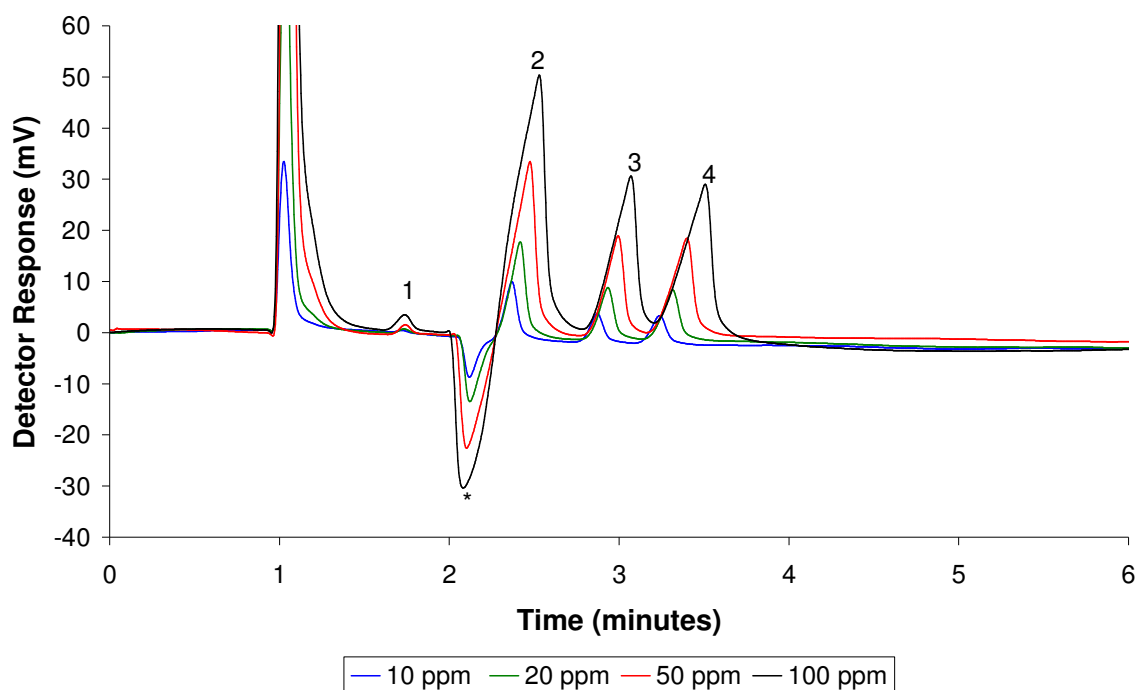


Figure 2.3: Overlaid chromatograms of mixed anion standards ranging from 10 to 100 mg L<sup>-1</sup> (100 pg to 1 ng injected mass) obtained using the DDMAU modified monolithic silica capillary column with a 0.5 mM phthalate eluent (pH 4.0) and on-column C<sup>4</sup>D detection. Detector position: 13 cm from column inlet. Flow rate = 1.0  $\mu\text{L min}^{-1}$ . Injection volume = 10 nL. Peak ID: 1= iodate, 2= nitrite, 3= bromide, 4= nitrate, \* = system peak.

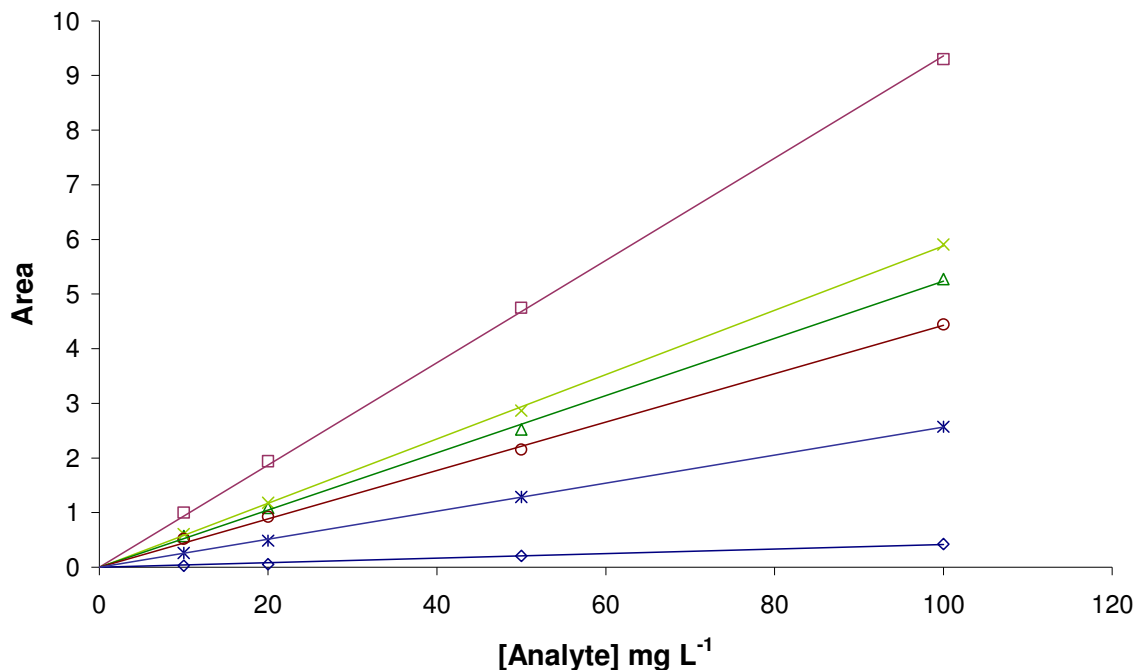


Figure 2.4: Linearity of inorganic anion separation on the DDMAU coated capillary monolith.  $\triangle$  = bromide,  $\square$  = nitrite,  $\diamond$  = iodate,  $\circ$  = sulphate,  $*$  = iodide,  $\times$  = nitrate. Conditions as per Figure 2.3.

### 2.3.2 Eluent variation and detector signal.

To evaluate the suitability of the C<sup>4</sup>D for use in capillary ion chromatography (Cap-IC) as an on-column detector it was important to evaluate detector performance, both directly across the modified monolithic silica column and also, for comparison purposes, across an open tubular fused silica capillary of similar dimensions (100  $\mu\text{m}$  i.d.). Initial linearity experiments were carried out with an unmodified monolith. The detector response across the monolith was recorded while pumping increasing concentrations of an acetate buffer through the column, over the range 1 to 50 mM (pH 4.0). An acceptably linear response over the range 1 to 20 mM was observed ( $R^2 = 0.9944$  for a linear regression, Figure 2.5), although above 20 mM detector linearity levelled off rapidly. A best fit was obtained using a 2<sup>nd</sup> order polynomial regression over the range 0 to 20 mM, giving  $R^2 = 0.9987$ . The detector response is shown graphically as Figure 2.6.

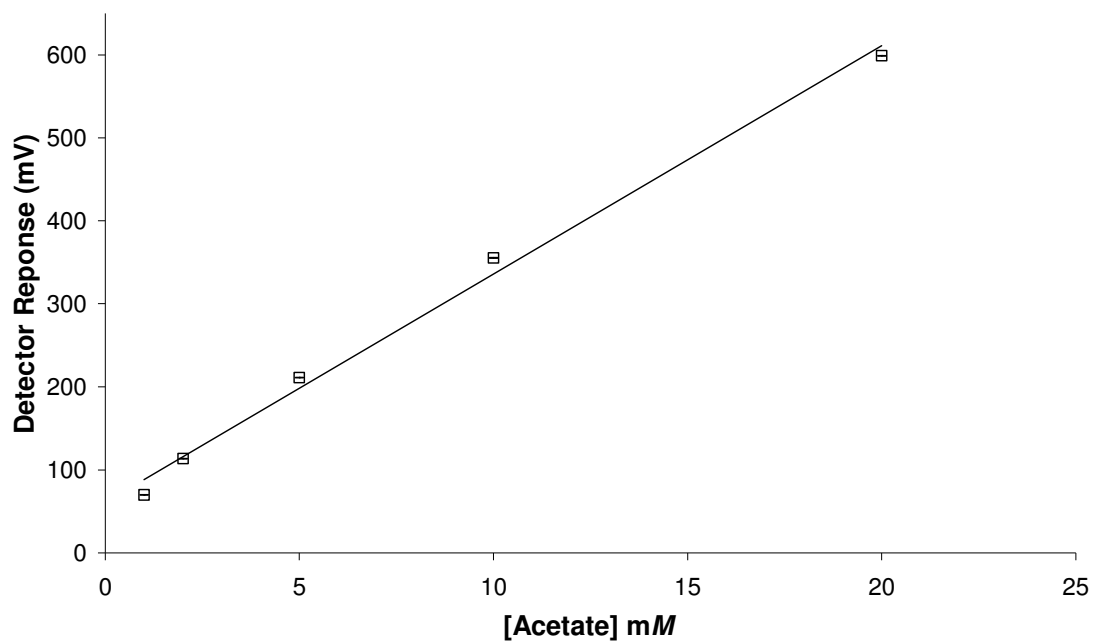


Figure 2.5:  $C^4D$  response across a silica reversed-phase monolithic column with acetate eluents of 1 to 20 mM (pH 4).

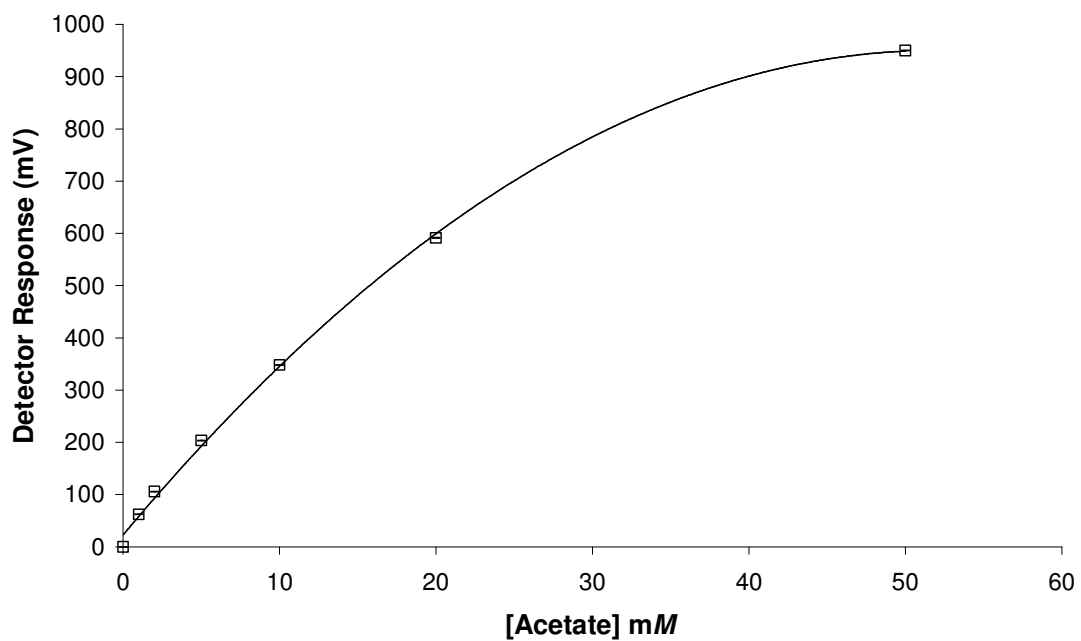


Figure 2.6:  $C^4D$  response across a silica reversed-phase monolithic column with acetate eluents of 1 to 50 mM (pH 4).

Taking the 1 mM acetate buffer solution as a model eluent, due to its low conductivity value (*ca.* 70 mV), the across column detector response to 10 nL injections of sodium chloride standards under simple flow injection analysis (FIA) conditions was then evaluated (10 to 250 mg/L, 0.28 to 7.05 mM). The same series of injections were made onto the open tubular fused silica capillary column, and again detected across column. In a third experiment, a short section of 100  $\mu\text{m}$  i.d. open tubular capillary was coupled to the end of the monolithic column with a zero dead volume capillary union. This short section of capillary was utilised as an open tubular ‘detector cell’ for  $\text{C}^4\text{D}$  detection. Figure 2.7 shows a schematic of the  $\text{C}^4\text{D}$  cell placed (a) directly on-column, (b) on open fused silica capillary and (c) on open fused silica capillary ‘detector cell’.

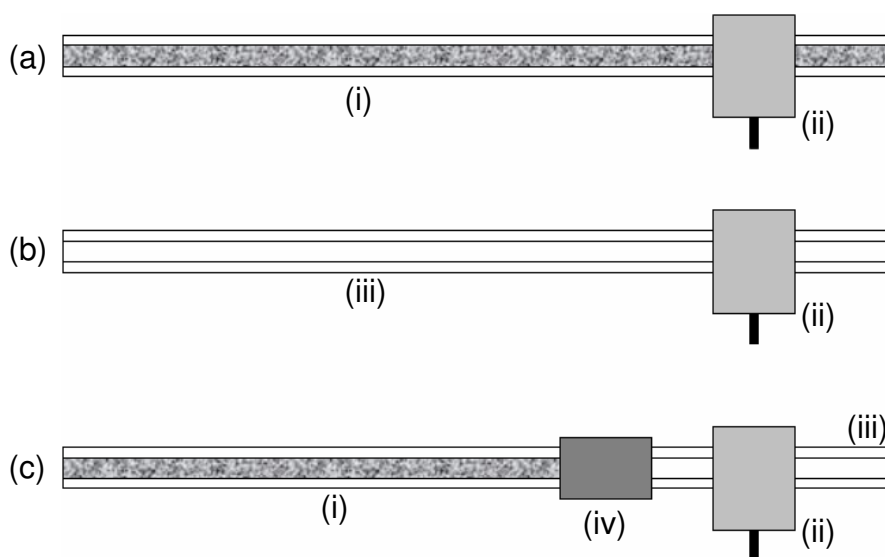


Figure 2.7: Schematic of the  $\text{C}^4\text{D}$  cell placed (a) directly on-column, (b) on open fused silica capillary and (c) on open fused silica capillary ‘detector cell’. (i) reversed-phase monolith, (ii)  $\text{C}^4\text{D}$  cell, (iii) open fused silica capillary and (iv) zero dead volume union.

For all experiments flow rate through each capillary was kept constant at  $0.96 \mu\text{L min}^{-1} \pm <5\%$ . The resultant calibration graphs for these FIA experiments are shown as Figure 2.8, here with data plotted as relative peak areas. Each data point shown is the average from three replicate injections. The recorded data are

plotted without background subtraction and clearly show different detector slopes for each experiment, with the open tubular capillary column showing the largest slope and greatest sensitivity. The use of the attached open tubular column coupled to the end of the monolithic column as a ‘detector cell’ improved detector sensitivity by approximately 40%, but for unknown reasons this was less than expected. Under all conditions linearity was greater than  $R^2 = 0.99$  over the investigated concentration range (Table 2.1).

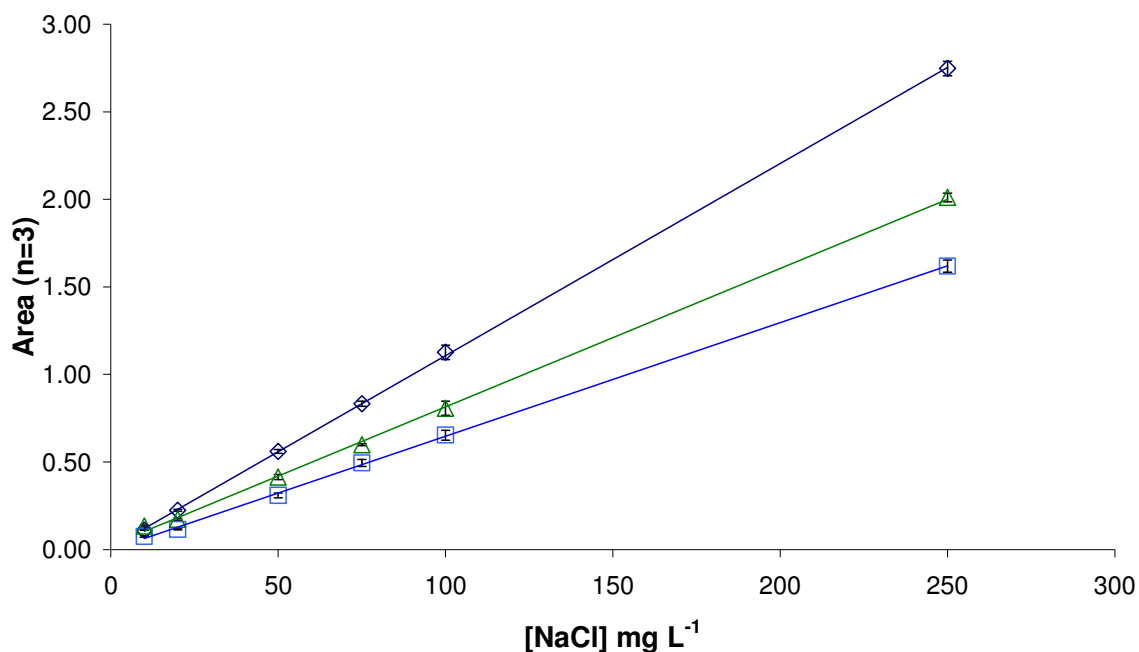


Figure 2.8: Peak areas of unretained chloride peaks recorded for the unmodified monolithic capillary column (□), a 100  $\mu\text{m}$  i.d. open capillary (◇) and a section of 100  $\mu\text{m}$  i.d. open capillary coupled to the end of the unmodified monolithic capillary column (△).

The greater sensitivity for the open tubular capillary column is as a result of the internal volume of the cell being larger for that of the monolithic column, referred to as the “virtual electrode” [19]. The cross-sectional area of the tube below the ring electrodes can be thought of as a circular plate electrode, similar to that in classical conductivity detection, separated by the distance between the two ring electrodes (Figure 2.9). Taking the cross sectional area of the 100  $\mu\text{m}$  i.d. open

tubular capillary column to be  $3.1 \times 10^{-8} \text{ m}^2$  and if the monolithic column has a porosity of 80%. Then the cross sectional area of the “virtual electrode” of the  $\text{C}^4\text{D}$  placed on the monolithic column is  $2.5 \times 10^{-8} \text{ m}^2$ . The reduction in signal observed for the monolith can also be attributed to the fact that the path between the two electrodes is not a linear one. The tortuous nature of monolithic material may result in the surface area of the two electrodes being of differing size and result in a less than expected signal.

Table 2.1: Linearity data for injection of KCl with 100  $\mu\text{m}$  i.d. FSC, silica monolith and silica monolith with 100  $\mu\text{m}$  i.d. fused silica capillary.

Detection	Slope	Intercept	$R^2$
Silica Monolith	0.0065	-0.0019	0.996
100 $\mu\text{m}$ i.d. FSC	0.011	0.0102	0.999
Silica Monolith + 100 $\mu\text{m}$ i.d. FSC	0.0079	0.0242	0.993

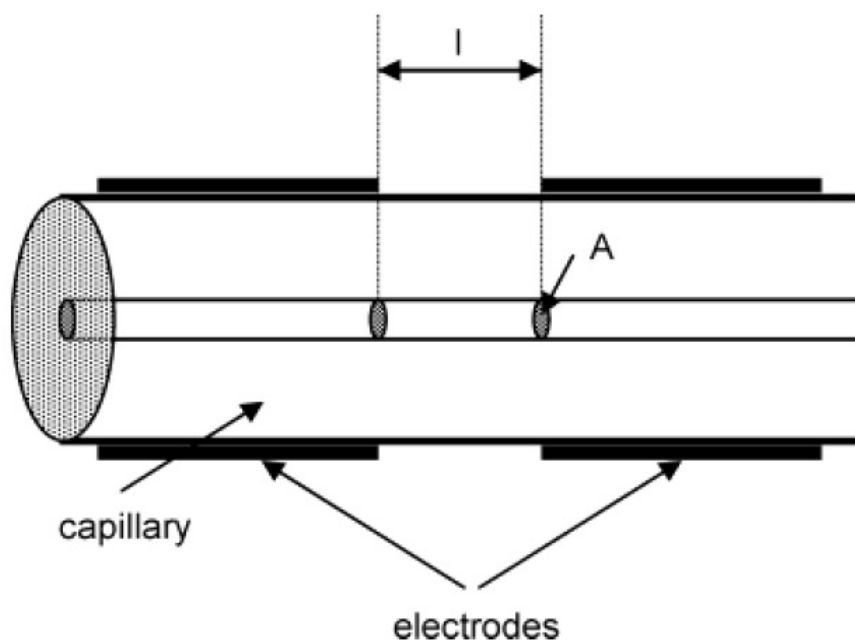


Figure 2.9: Sketch depicting the virtual electrode in a  $\text{C}^4\text{D}$  cell. A = cross sectional area below electrode, l = distance separating the electrodes [19].

The monolithic capillary column was then modified with the zwitterionic surfactant DDMAU, to convert the monolithic silica phase to an anion exchange phase. This coating has been characterised for its selectivity towards anions previously and has been shown to result in a stable coating on a similar reversed-phase monolithic silica phase [14]. A series of KCl eluents of increasing strength (1 to 50 mM, n=5) were passed through the modified monolithic capillary column and the across column detector response recorded. The same series of eluents were also pumped through the 100  $\mu$ m i.d. open tubular capillary. In addition, the detector response across each capillary was recorded with the capillary filled with de-ionised water only (blank/background value). The relative detector responses are shown as Figure 2.10. Once again the detector responses have been plotted without background correction and so the detector response across the modified monolith was greater than that seen across the open capillary. However, the detector responses recorded over this range of KCl concentration were clearly not linear using either capillary column, and an acceptable linear regression could only be obtained from a plot of the Log [KCl] against detector response, as shown in Figure 2.10. Comparison of the slopes obtained from the above plot showed the detector response across the open tubular column to be more sensitive, particularly at higher KCl concentrations.

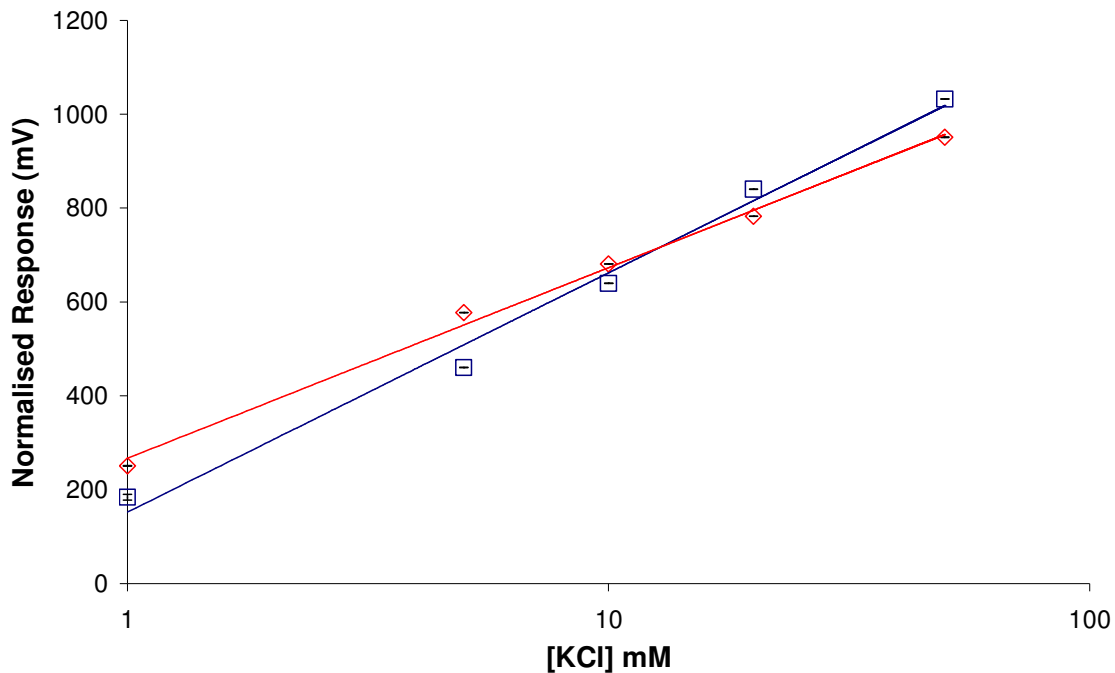


Figure 2.10:  $C^4D$  response across a DDMAU modified reversed-phase monolithic column (◇) and a 100  $\mu\text{m}$  i.d. fused silica capillary 'detector cell' (□) with KCl eluents (1 -50 mM).

When the blank detector response for the monolithic capillary column and the open tubular column (113 and 24 mV, respectively) were subtracted from the data shown in Figure 2.10, the relative response from the open tubular column exceeded that from the monolithic column for KCl concentrations above  $\sim 14$  mM. Therefore, over the KCl concentration range investigated, the background adjusted relative detector response ratio for the two capillary columns (detector response for open tubular column / detector response for monolithic capillary column) ranged from 0.73 for the 1 mM KCl to 1.09 for the 50 mM KCl eluent. Kuban *at al.* also reported a non-linear relationship for KCl eluents over the same concentration range [19]. However, no clear reason was given for the observation. Finally, detector linearity across the monolithic and open capillaries was evaluated with a low conductivity organic acid eluent, suitable for anion chromatography. The detector response was monitored over the concentration range 0 to 0.5 mM ( $n=3$ ) of phthalate (pH 4.0). The resultant calibration curves are shown as Figure

2.11. Once again, as expected, the background signal from the detector across the monolithic phase was greater than seen across the open tubular capillary, although both showed similar trends and both exhibited a clear curved detector response following that seen using KCl eluents.

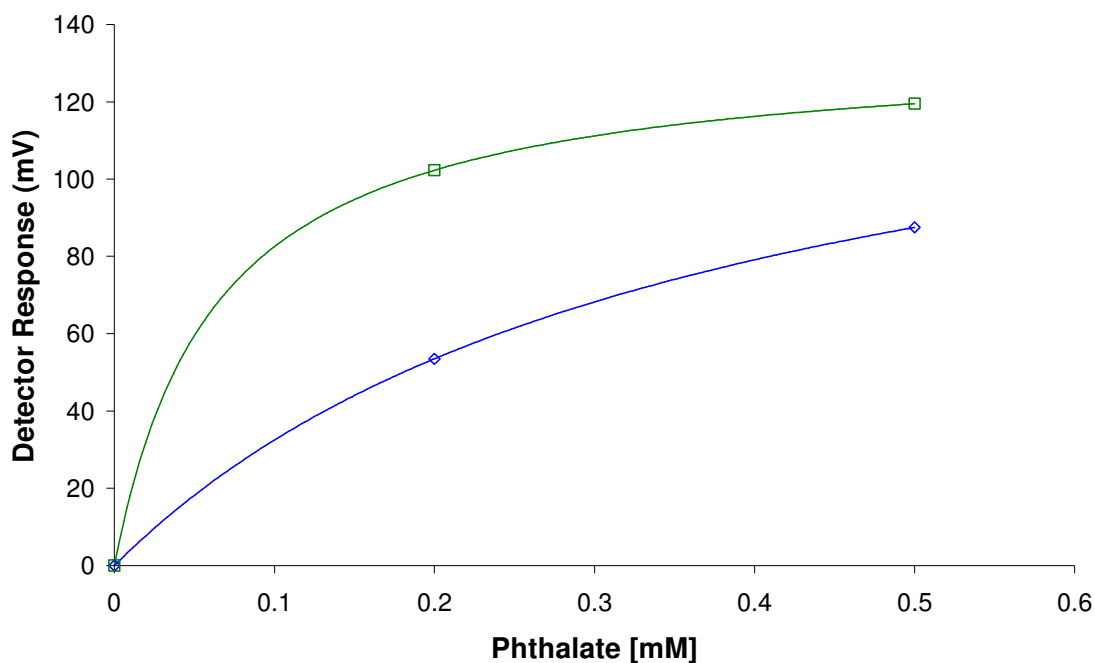


Figure 2.11: C<sup>4</sup>D response across a DDMAU modified reversed-phase monolithic column (□) and a 100 μm i.d. fused silica capillary 'detector cell' (◇) with phthalate eluents (0 -0.5 mM, pH 4.0).

### 2.3.3 On-column detection for separation of inorganic anions.

To compare the C<sup>4</sup>D response across the coated monolith and open fused silica capillary separations of the inorganic anions were performed in both modes. The porosity of the unmodified monolithic capillary column is about 80% of the total volume of corresponding empty capillary, so the lower conductivity response for each solution could be expected in this case, although the slope for the open capillary column was approximately two times higher than for the monolithic column. However, when comparing background signals for various eluents,

including water, within the open capillary and a DDMAU modified monolith, the modified monolith now exhibited a slightly higher background signal due to the contribution of the coating itself, which will obviously negatively affect signal-to-noise ratio when used as here for on-column detection in CapIC. Following the above study, a ~3 cm long section of the 100  $\mu\text{m}$  i.d. open tubular capillary was attached (with zero dead volume capillary connection) to the end of the modified 15 cm long monolithic capillary column and used as a 'detector cell' to compare peak width and height, to those seen with direct detection on the monolith. Figure 2.12 shows the resultant chromatograms. The effective column length ( $L_{\text{eff}}$ ) for the direct detection mode (Figure 2.12 (a)) was ~13 cm, whereas for the monolithic column with attached extension (Figure 2.12(b)) this was ~16 cm. As can be seen from the chromatograms shown, the addition of the open capillary tube as detector cell led to a clear peak broadening effect due to both increased retention (as a result of the extra stationary phase hidden by the detector when placed on-column and within the union), and more importantly the relatively large internal volume of the open capillary compared to the internal volume of the monolith. Figure 2.13 shows this effect most clearly with comparison of unretained injection peaks for the two configurations. Comparison of the baseline width and full width half maximum (FWHM) of the analyte peaks show an increase of *ca.* 10% in peak width for the open fused silica capillary compared to that of on-column detection. The peak height and area of the peaks was reduced when the 100  $\mu\text{m}$  i.d. detection window was placed after the column with a 16% and 34% reduction in peak area and height, respectively, for nitrite. This comparison indicated that despite the relative responses shown in Figure 2.7, the most suitable option for detection was direct detection on the monolithic capillary column itself.

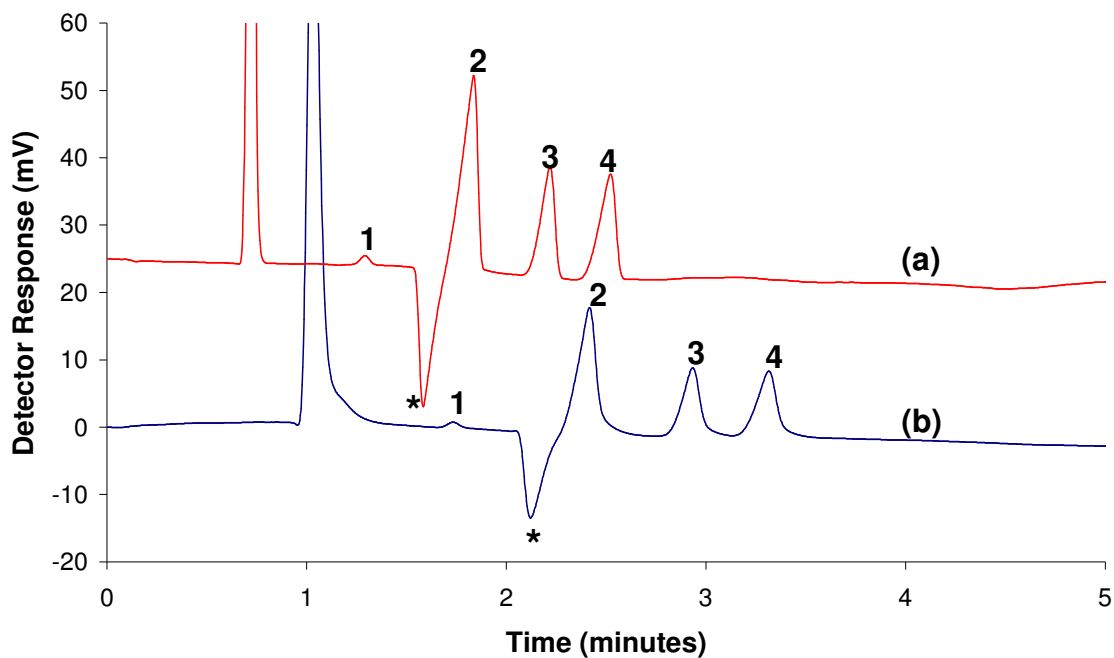


Figure 2.12: Separation of four anions on the modified monolithic silica capillary column recorded (a) directly on the monolithic capillary using  $C^4D$  at  $\sim 13$  cm column length, and (b) on an end-coupled  $100\ \mu\text{m}$  i.d. open capillary at  $\sim 16$  cm column length<sup>a</sup>. <sup>a</sup> Distance includes the length of open fused silica capillary, 1= iodate, 2= nitrate, 3= bromide, 4= nitrite, \* = system peak. All other conditions as Figure 2.3.

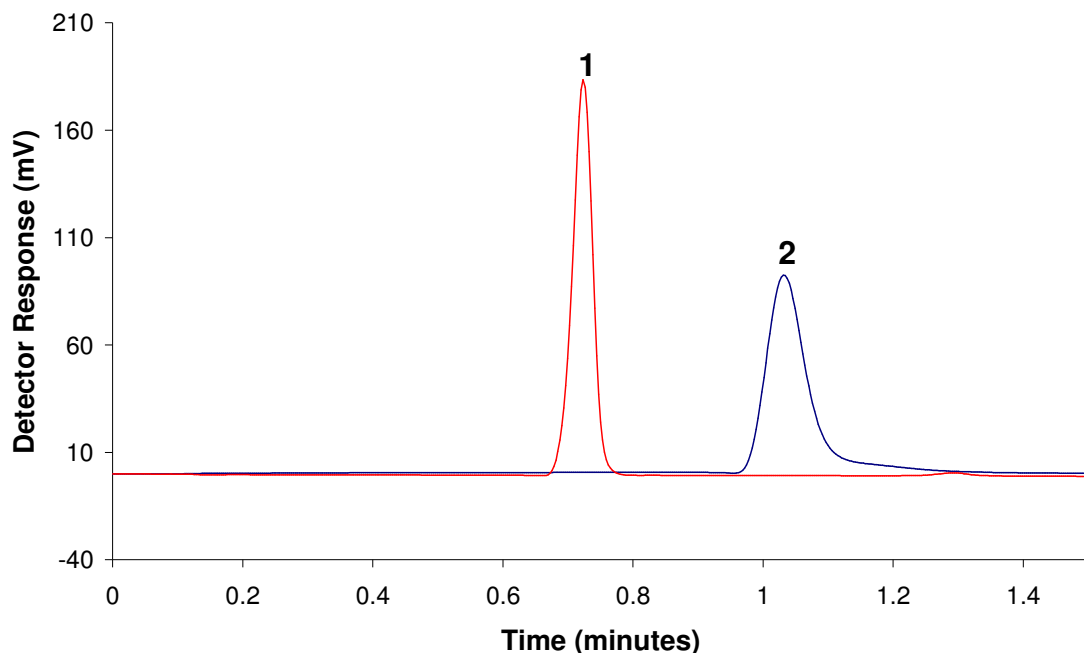


Figure 2.13: Comparison of unretained injection peaks recorded with the monolithic capillary column (1;  $t_0 = 0.72$  min) and with the coupled monolithic and open capillary columns (2;  $t_0 = 1.03$  min). All other conditions as per Figure 2.3.

## 2.4 Conclusions.

Capacitively coupled contactless conductivity detection ( $C^4D$ ) has been demonstrated as a viable detector for on-column Cap-IC, with surfactant coated monolithic capillary column. The comparison of on-column detection versus off-column showed that off-column detection gives a higher response for flow injection analysis; this follows the fact that the open fused silica capillary will have a larger volume of fluid between the two electrodes of the detector compared to that of the monolithic capillary column. When used as a detector for the separation of inorganic anions with a semi-permanently coated reversed-phase monolithic capillary column, the advantage of on-column detection overcomes the reduction in sensitivity resulting in higher efficiency. A loss of efficiency was seen between on and off-column due the extra-column band broadening introduced in to the system by the connections required to place open fused silica capillary after the

column as detection window. From this work it can be seen that C<sup>4</sup>D has great potential for use with capillary monoliths in ion chromatography, the very nature of the detection technique leads to minimal extra column band broadening, and its non-contact and non-invasive principle leads to the possibility of stationary phase characterisation.

## 2.5 References:

- [1] K.K. Unger, R. Skudas, M.M. Schulte, *J. Chromatogr. A.*, 2008, **1184**, 393.
- [2] R.M. Cassidy, S. Elchuk, *Anal. Chem.*, 1982, **54**, 1558.
- [3] D. Connolly, B. Paull, *J. Chromatogr. A*, 2002, **953**, 299.
- [4] D. Connolly, D. Victory and B. Paull, *J. Sep. Sci.*, 2004, **27**, 912.
- [5] S. Pelletier, C.A. Lucy, *J. Chromatogr. A.*, 2006, **1118**, 12.
- [6] K.M. Glenn, C.A. Lucy, P.R. Haddad, *J. Chromatogr. A.*, 2007, **1155**, 8
- [7] Q. Yu, M. Mori, K. Tanaka, M. Ikedo, W.Z. Hu, P.R. Haddad, *J. Chromatogr. A.*, 2004, **1041**, 95
- [8] W. Hu, P.R. Haddad, H. Cook, H. Yamamoto, K. Hasebe, K. Tanaka, J.S. Fritz, *J. Chromatogr. A.*, 2001, **920**, 95. TTA
- [9] W.Z. Hu, P.R. Haddad, K. Hasebe, H.A. Cook, J.S. Fritz, *Fresenius Journal of Anal. Chem.*, 200, **367**, 641.
- [10] Q. Xu, K. Tanaka, M. Mori, M.I. Helaleh, H. Toada, W. Hu, K. Hasebe, *Chromatographia*, 2003, **57**, 19.
- [11] J. Li, Y. Zhu, Y.Y. Guo, *J. Chromatogr. A.*, 2006, **1118**, 46.
- [12] W. Hu, T. Takeuchi, H. Haraguchi, *Anal. Chem.*, 1993, **85**, 2204. CHAPS
- [13] W. Hu, P.R. Haddad, K. Hasebe and K. Tanaka, *Anal. Commun.*, 1999, **36**, 309.
- [14] C. O'Riordian, L. Barron, E. Nesterenko, P.N. Nesterenko, B. Paull, *J. Chromatogr. A.*, 2006, **1109**, 111
- [15] W.Z. Hu, P.R. Haddad, K. Hasebe, K. Tanaka, *Anal. Comm.*, 1999, **36**, 97.
- [16] E.P. Nesterenko, P.N. Nesterenko and B. Paull, *J. Chromatogr. A.*, 2008, **1178**, 60.
- [17] Y. Salto, K. Jinno, T. Grelbrokk, *J. Sep. Sci.*, 2004, **27**, 1379.
- [18] T. Takeuchi, S. Tasumi, S. Masuka, K. Hirose, H. Uzu, J. Jin, C. Fujimoto, K. Ohta, J. Ryoo, S. Choi, *J. Chromatogr. A.*, 2003. **1021**, 55.
- [19] P. Kuban, P.C. Hauser, *Electrophoresis*, 2004, **25**, 3387.

---

**Chapter 3: Use of contactless conductivity detection for characterisation of capillary column surfactant coatings and subsequent ion chromatographic determination of cations and amino acids.**

---

“As an adolescent I aspired to lasting fame, I craved factual certainty, and I thirsted for a meaningful vision of human life - so I became a scientist. This is like becoming an archbishop so you can meet girls”

-M. Cartmill

### 3.1 Introduction.

From the previous Chapter it is apparent that  $C^4D$  can be a valuable detector in the field of Cap-IC. In the Sections pertaining to the comparison of detection on-column and on open fused silica capillary, it was mentioned that the act of coating a surfactant resulted in an increase of the background conductivity (Section 2.3.4). In this Chapter the processes of coating a capillary monolithic column with another surfactant, sodium dioctyl sulfosuccinate (DOSS) was investigated (Figure 3.1).

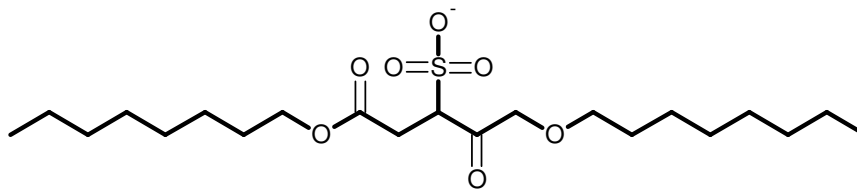


Figure 3.1: Structure of sodium dioctyl sulfosuccinate (DOSS).

#### 3.1.1 On-column detection for the evaluation of coating.

The modification of columns with surfactants involves the coating to excess with the surfactant and a comprehensive wash step to remove weakly unbound surfactant to yield a stable stationary phase coating [1-7]. However, the verification of the coating, in terms of longitudinal distribution (i.e. from the inlet to the outlet of the column) has not been known. To date the only methods used have been the monitoring of retention time of replicate injections [8,9]. The coating of the surfactant within the column may be stable, whereas the distribution may not be uniform. The ability to place the  $C^4D$  cell directly on-column permits the conductivity along its length to be monitored by systematic movement of the cell, thus creating a profile of the column. The non-contact, non-invasive and non-destructive nature of  $C^4D$  allows for replicate profiles of conductivity along the column length, i.e. both spatial and *temporal* studies into the coating behaviour. In Figure 3.2 the placement of a  $C^4D$  cell onto a monolithic capillary column can be seen.

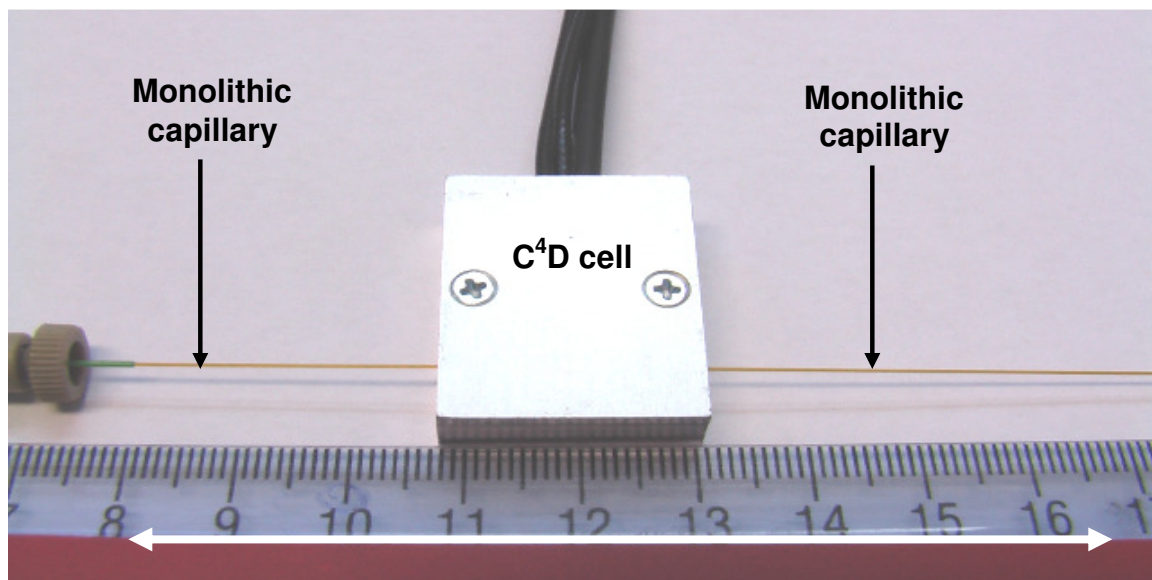


Figure 3.2: C<sup>4</sup>D cell placed directly on-column with a ruler as a guide to allow reproducible movement along the length of the column.

The use of guide (in this case a ruler) allows for the reproducible movement of the cell to any point on the column length accessible to the cell. In a recent review by Kuban *et al.* the authors say “*Capillary IC is an evolving field that is very much in the making. Whether it will finally emerge as a viable entity in the form of open, packed, or monolithic columns, in a capillary or a chip, will require a sharp enough vision to see inside a capillary*” [10]. Using C<sup>4</sup>D in a scanning mode along the length of the capillary column to investigate the stationary phase chemistry in both spatial and temporal terms gives the analyst a “*window*” inside the capillary in a way never before possible.

In this Chapter for the first time the ability of C<sup>4</sup>D to evaluate the processes involved in the coating of a reversed-phase column with surfactants was investigated in detail. The modification of the coating was also investigated in the form of solvent washing to form stationary phase gradients which were visualised by C<sup>4</sup>D and variation of the counter ion of the stationary phase to evaluate the detection process. Finally, the modified monolithic column was utilised for the

separation and quantitation of inorganic cations in water samples and for the preliminary separation of amino acids.

## 3.2 Experimental

### *3.2.1 Instrumentation.*

Conditions were as in Section 2.2.1, with the following exceptions; Eluent flow was measured with a nano flow sensor (Upchurch Scientific Inc., WA, USA) with a range of  $1.5 \text{ nL min}^{-1}$  to  $8 \text{ } \mu\text{L min}^{-1}$ . Settings for coating procedure and counter ion study: frequency, 3XHIGH; voltage, -12 dB; gain, 50% and offset, 0. Settings for cation separation and amino acid separation: frequency, 3XHIGH; voltage, -6 dB; gain, 50% and offset, 0. The capillary column used for this section of work was an Onyx monolithic reversed-phase  $\text{C}_{18}$  column ( $150 \text{ mm} \times 0.1 \text{ mm i.d.}$ ,  $0.365 \text{ mm O.D.}$ ) (Phenomenex, Cheshire, U.K.). The column was placed on an in-house mount. This in-house mount allowed for stable and reproducible movement of the detector cell along the length of the capillary and is depicted in Figure 3.3.

### *3.2.2 Reagents.*

Reagents used were as Section 2.2.2. Processing of chromatograms was carried out using a PeakNet 6.30 chromatography workstation (Dionex, Sunnyvale, CA, U.S.A.). Eluent pH was measured using an Orion 2 Star pH meter (Thermo Orion, Beverly, MA, U.S.A.) with an epoxy electrode. The eluent used for analysis of alkaline earth metals was  $0.5 \text{ mM}$  ethylenediamine adjusted to pH 4.5 with dilute  $\text{HNO}_3$ . The eluent used for amino acid analysis was  $10 \text{ mM}$  nitric acid, pH 3.0. The flow rate for both methods was  $1 \text{ } \mu\text{L min}^{-1}$ .

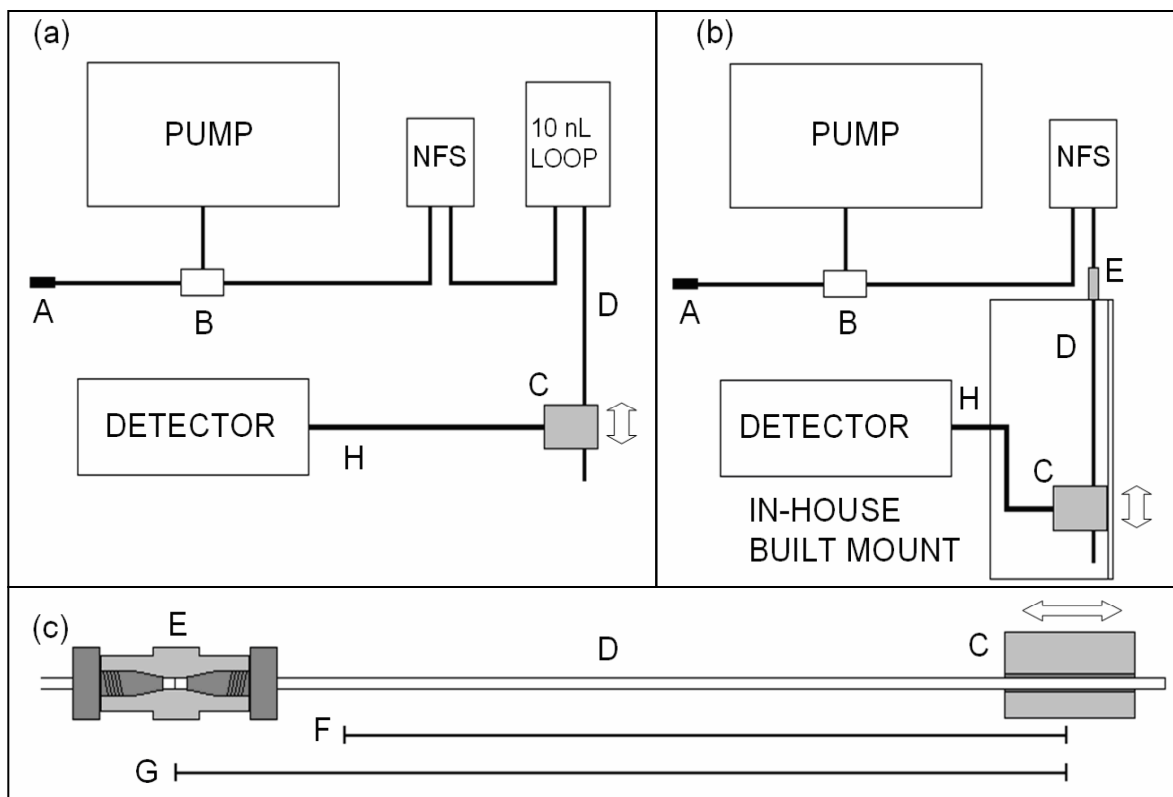


Figure 3.3: Chromatographic system used for separations (a), column coating/washing (b) and column set up used in coating/washing (c). A = back pressure regulator on waste line, B = T-piece connector as flow splitter, C = movable detector cell, D = capillary column, E = zero dead volume microtight union, F = range of positions available to measurement with C<sup>4</sup>D, G = effective column length, H =detector cell lead, NFS = nanoflow sensor. Note: (c) is not to scale.

### 3.2.3 Column coating and washing procedures.

There were three columns used in this study:

- Column # 1: Preliminary study.
  - Surfactant coating equilibration using C<sup>4</sup>D.
- Column # 2: Double coating comparison.
  - Separation of inorganic cations.
  - Separation of amino acids.

- Column # 3: Single coating comparison.
  - Stationary phase gradients.
  - Counter ion study.

#### *3.2.3.1 Coating and washing procedure for Column #1.*

The C<sup>4</sup>D response of the unmodified capillary column was first collected in triplicate and used as a reference value (Figure 3.6). A solution of 1 mM sodium dioctyl sulfosuccinate (DOSS) was then passed through the capillary at a flow rate of 1  $\mu\text{L min}^{-1}$  for 120 minutes and the response of the detector was monitored to achieve a breakthrough curve. Following initial coating the capillary was washed with water for 30 minutes and the response of the detector at each of the above ten positions then collected, whilst continuing to pump water through the modified capillary at 1  $\mu\text{L min}^{-1}$ . The capillary was placed on an in-house made mount to allow for stable and reproducible movement of the detector cell along the length of the capillary. The total length of the capillary was 15 cm (apparent length was reduced to 12.9 cm due to a section of the column within the union). A total of ten measuring positions were possible with this set-up, at 2.7, 3.7, 4.7, 5.7, 6.7, 7.7, 8.7, 9.7, 10.7 and 11.7 cm from the outlet of the capillary. The start position of 2.7 cm was due to a section of the column within the union and the size of the cell constricting the placement of the C<sup>4</sup>D cell. The final position of 11.7 cm was as a result of the dimensions of the C<sup>4</sup>D cell and a section of the column left unread to ensure that no eluent entered the C<sup>4</sup>D cell. Data was collected at each position for 30 seconds with a flow of 1  $\mu\text{L min}^{-1}$  of DI water. The column was then coated in the reverse direction (outlet to inlet) as before for 60 minutes and a second breakthrough collected and also a second C<sup>4</sup>D scan (Figure 3.6). The column was then returned to its original position (i.e. inlet fitted into the union) and the column washed with DI water at 1  $\mu\text{L min}^{-1}$  for a total of *ca.* 980 minutes. During this wash cycle profiles of the column were collected, as described above, every 30 minutes for 240 minutes. The column was then washed overnight and profiles collected the following day (*ca.* 980 minutes).

### *3.2.3.2 Coating and washing procedure for Column # 2.*

The C<sup>4</sup>D response of the unmodified capillary column was collected (in triplicate) at 1 cm intervals. The column was then coated for over 80 minutes with the DOSS solution at 1  $\mu\text{L min}^{-1}$  (flow from inlet to outlet). A DOSS breakthrough curve was collected by placing the C<sup>4</sup>D cell at the exit end of the column. Following this initial coating the capillary was then washed with water for 60 minutes at 1  $\mu\text{L min}^{-1}$ , to remove the unbound DOSS, and thereby allow measurement against a DI water background. Profiles of Column # 2 were collected as for Section 3.2.3.1, however, in this case, a micro-tight union (Upchurch Scientific Inc., WA, USA) was used to connect the capillary column to the flow path, allowing 12 measuring positions be used, at 2.6, 3.6, 4.6, 5.6, 6.6, 7.6, 8.6, 9.6, 10.6, 11.6, 12.6 and 13.6 cm from the inlet. The response at each of the twelve positions was collected, whilst continuing to pump water through the modified capillary at 1  $\mu\text{L min}^{-1}$ . The capillary column was then reversed and was coated for a further 80 minutes under the same coating conditions as the initial coating. A second DOSS breakthrough curve was collected. The capillary was washed with water (to remove unbound DOSS) for 30 minutes and the C<sup>4</sup>D response again collected at each of the twelve positions.

Finally, a very comprehensive washing procedure was instigated in order to achieve a stable column coating, whereby the capillary was returned to its original position and washed with water (i.e. from inlet to outlet) at 1  $\mu\text{L min}^{-1}$  while the C<sup>4</sup>D response of the modified capillary column was collected at each of the twelve positions every 30 minutes for 360 minutes. The capillary was then washed overnight. During the following day, the water washing procedure was continued, during which time the C<sup>4</sup>D response was collected at each detector position every 60 minutes for 600 minutes. At this point the cumulative water washing time had totalled 1,710 minutes. At the end of this second day the capillary column was again left washing for a second night. Finally, on the third day the washing procedure was continued and C<sup>4</sup>D responses collected every 60 minutes for 180

minutes. At this point the cumulative water washing time had totalled 2,700 minutes (i.e. 2,700  $\mu\text{L}$ ).

#### *3.2.3.3 Coating and washing procedure for Column # 3.*

Coating of capillary Column # 3 was carried out with a 1 mM DOSS solution at a flow rate of 1  $\mu\text{L min}^{-1}$  for 120 minutes. The coating of Column # 3 was carried out in one direction only (i.e. column inlet to column outlet), as opposed to coating the column in both a forward and reverse direction in Section 3.2.3.2. The column was subsequently washed with DI water at 1  $\mu\text{L min}^{-1}$  for ca. 8 hr to remove unbound DOSS and measured by C<sup>4</sup>D at 1 cm intervals along the column as in Section 3.2.3.1.

#### *3.2.4 Stationary phase gradients.*

To investigate the effect of organic solvents on the coating distribution on the modified capillary columns, Column # 3 was washed with differing concentrations of aqueous methanol. Column # 3 was washed for 30 minutes with 10, 20, 30, 40 and 50 % methanol. Following each methanol wash excess methanol was removed from the pores of the monolith with a flow of water at 1  $\mu\text{L min}^{-1}$  for 30 minutes and the profile of the column collected as per Section 3.2.3.1.

#### *3.2.5 Counter-ion study.*

Column # 3 was equilibrated with 2 mM solutions of nitric acid, sodium chloride and magnesium chloride for > 120 minutes. Once equilibrated the column was washed with DI water to remove any unbound counter-ions and profiles collected as per Section 3.2.3.1.

### 3.2.6 Separation of inorganic cations and amino acids.

Separations of inorganic cations and amino acids were performed using Column # 2. An eluent of 0.5 mM ethylenediamine (pH 4.5) was used for separations of inorganic cations. For the separation of amino acids a 10 mM nitric acid (pH 3.0) eluent was used. For all separation the flow rate was set at 1  $\mu\text{L min}^{-1}$  with an injection volume of 10 nL.

NOTE: Detection was via *indirect conductivity*; all chromatograms shown have been inverted to be presented in the conventional form.

### 3.2.7 Sample treatment.

All standards for the following work were prepared from 1000 mg L<sup>-1</sup> stock solutions of the analytes of interest. Real samples (i.e. bottled water and tap water) were first filtered through 0.2  $\mu\text{m}$  nylon membrane syringe filters (Supelco, Supelco Park, Bellefonte, PA, USA) and then diluted as required with DI water.

## 3.3 Results and discussion.

There are three constituents in the C<sup>4</sup>D response for capillary reversed-phase monoliths coated with ionogenic surfactants. The first is related to the inherent conductivity of the silica backbone, associated mainly with residual silanol groups at its surface. The second is due to the conductivity of the eluent used, and the final term is a contribution from the surfactant coating, consisting of the immobilised surfactant molecules and associated mobile counter ions. Obviously, all terms are interconnected with each other, respecting the principle of electroneutrality. However, the background contribution from the monolith itself can be regarded as a constant, and for these experiments all measurements were recorded using only DI water within the capillary. Therefore, one can conclude the

C<sup>4</sup>D response is directly related to the presence of the immobilised surfactant molecules and the nature of the ionic surfactant counter ion.

### *3.3.1 Preliminary use of C<sup>4</sup>D for stationary phase characterisation (Column #1).*

The response of the detector with an unmodified capillary was collected (in triplicate) at each of the above positions to yield a reference value. The column was then coated for over 120 minutes with the DOSS solution (flow from the inlet to the outlet of the capillary), and a breakthrough curve was seen at 26 minutes (*ca.* 26 nM DOSS), as is shown in Figure 3.4. Figure 3.5 shows the detector response for the unmodified (—\*—) and newly modified capillary (—◇—) at each of the measurement points along the length of the capillary. Clearly, this initial coating resulted in an uneven coating of the capillary, with the largest detector response being shown for the first half of the capillary column. This higher response at the inlet of the column may be due to preconcentration and self-retention of DOSS on the C<sub>18</sub> phase. The capillary was therefore reversed and was coated for a further 60 minutes with the same coating solution, resulting in a second breakthrough curve seen at 30 minutes (*ca.* 30 nM DOSS), as also shown in Figure 3.4. The capillary was then washed once more with water for 30 min and the response of the detector along the capillary at each position again collected. As is shown in Figure 3.5, this reversed second coating resulted in a much improved distribution of the DOSS surfactant along the length of the capillary (—□—).

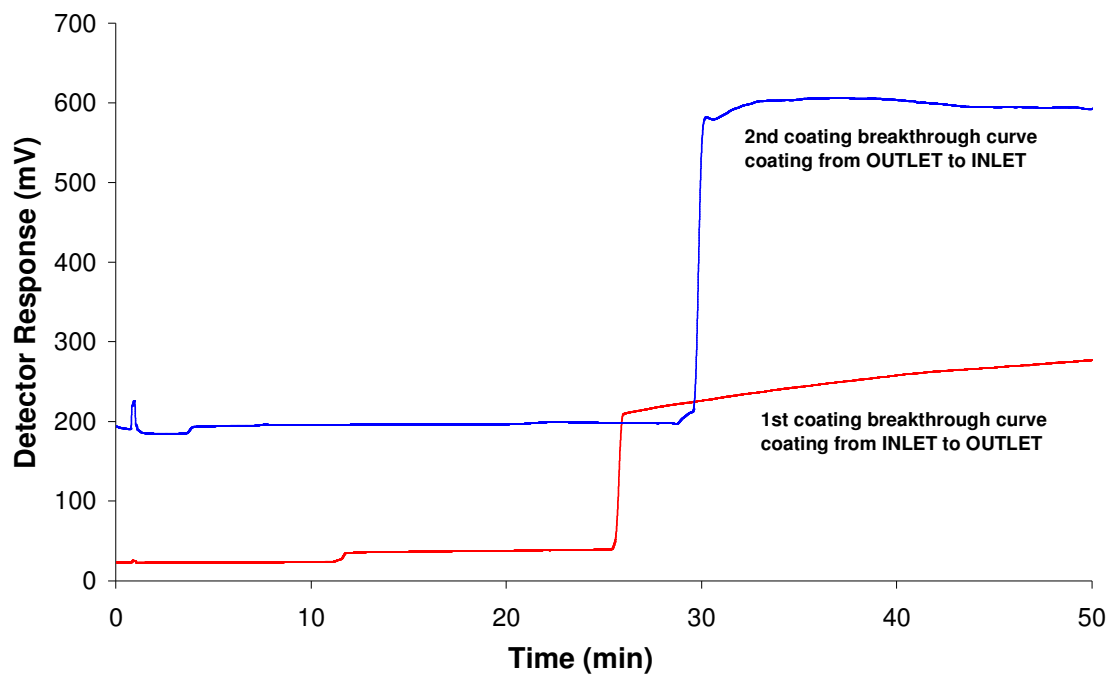


Figure 3.4: Breakthrough curves for a coating solution of 1 mM DOSS used to modify Column # 1, first coating from the capillary INLET to the OUTLET, followed by a second coating in the reverse direction.

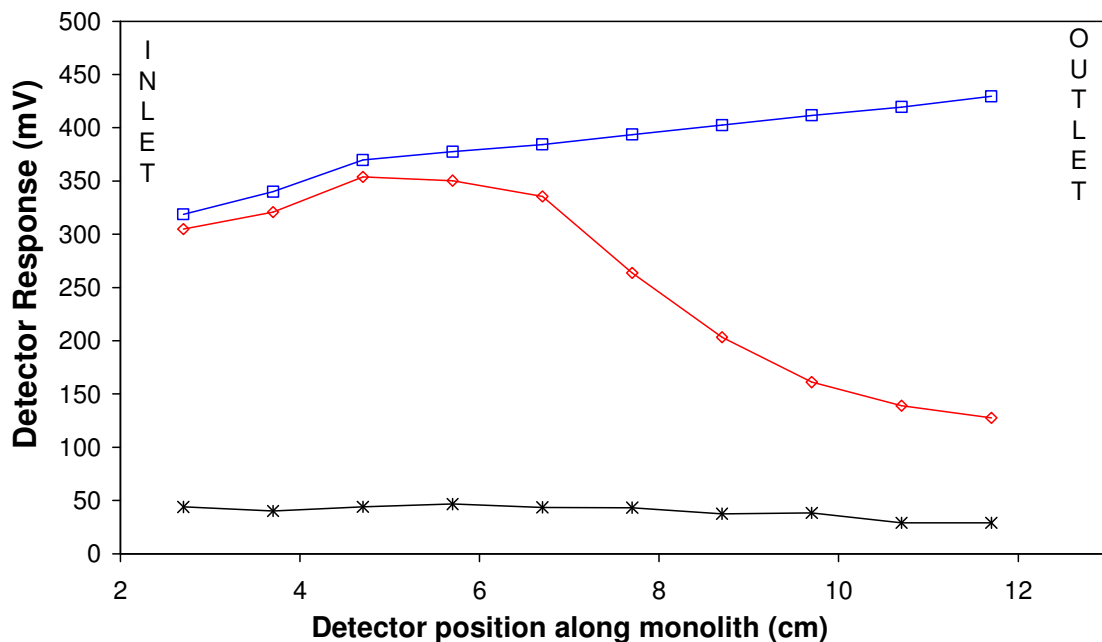


Figure 3.5: Detector response across an unmodified Column # 1 compared with responses across the same column modified once from INLET to the OUTLET, and a second time in the reverse direction. First coating inlet to outlet ( $\text{--}\diamond\text{--}$ ), second coating outlet to inlet ( $\text{--}\square\text{--}$ ) and unmodified ( $\text{--}\ast\text{--}$ ).

To test the stability of the coating with aqueous mobile phases, water was then passed through the capillary and the response monitored along the length of the capillary over time (ca. 30 minutes intervals for 240 minutes). Over this time the response of the detector at each point of the modified capillary was seen to decrease as a result of excess DOSS bleeding from the capillary (Figure 3.8, response curves A–I). Note that Curve A is the same as the second coating ( $\text{--}\square\text{--}$ ) in Figure 3.5. From the curves shown for this initial period of wash steps it is clear that an unstable portion of the coating was being removed in a way that exhibits similarities to frontal chromatography. The capillary was then washed with DI water overnight (ca. 980 minutes) at a flow of  $1 \mu\text{L min}^{-1}$ . Subsequent collection of the response along the capillary (ca. 30 minutes intervals for 90 minutes, response curves J–M) showed that the capillary coating had stabilised and yielded the desired uniform response along the length of the capillary, approximately four

times that of the unmodified capillary. The signal of *ca.* 200 mV for the washed column is similar to the signal at break through during the first coating step (Figure 3.4). This indicates that further coating of the column after breakthrough of the forward coating does not increase the capacity of the final equilibrated column and only results in the formation of multiple layers of unstable surfactant. The magnitude of the difference in response for the modified and unmodified capillaries also gives the analyst a useful visual indication of the degree of overall capacity of the final stable modified capillary column.

Such a well controlled and characterised stationary phase coating exhibiting longitudinal homogeneity could not be easily realised without the use of the radial capillary column contactless conductivity detector. This method presents the only simple, non-destructive characterisation of chromatographic capillary columns in regard to the density of ionic groups, their longitudinal distribution and temporal stability. Such characterisation not only increases the reliability and robustness of results generally but also opens new possibilities, such as for characterisation of capillary columns with a designed longitudinal gradient of stationary phase ion-exchange capacity for focusing methods or for sample preconcentration. Several papers have been published that deal with the modification of polymeric monolithic capillary columns via photografting techniques [11-15]. The ability to create a discrete zone of functionality within a column will allow C<sup>4</sup>D to spatially locate, optimise and investigate physiochemical properties of the modified stationary phase. To date, the only methods available for the characterisation have been either destructive [16] or indirect [8, 9]; however C<sup>4</sup>D allows for direct, non-contact and non-destructive characterisation of the stationary phase chemistry.

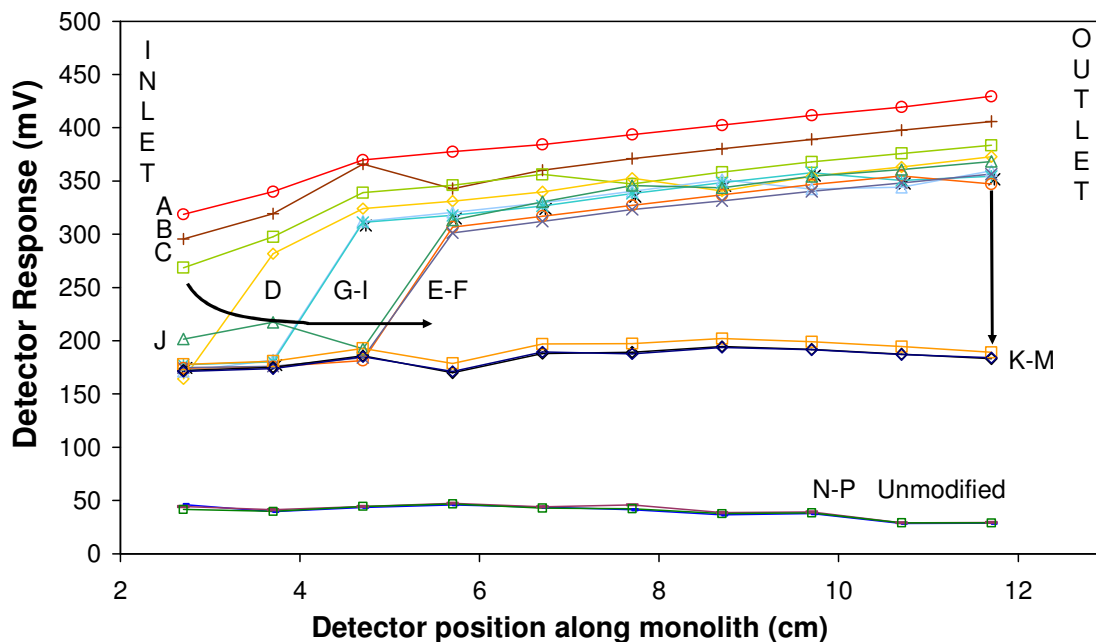


Figure 3.6: Detector responses recorded across Column # 1 following increasing periods of washing with deionised water (A–I show responses for subsequent 30 min intervals, J–M show stable response after washing for ~18 h). Note that curve A is the same as second coating outlet to inlet (—□—) in Figure 3.6.

### 3.3.2 Detailed investigation into the use of $C^4D$ in stationary phase characterisation (Column # 2).

The coating and washing procedure for Column # 1 was repeated for Column # 2 to investigate the repeatability of the coating process and to allow for a more detailed characterisation of the wash step using  $C^4D$ .

Therefore Column #2 was again coated both in a forward direction and a reverse direction, with breakthrough curves collected for each coating step (Figure 3.7). Immediately prior to the first “forward” coating, the response of the unmodified capillary at each of the measurement points along the length of the capillary was recorded and is illustrated in Figure 3.8. As expected, the measured response of the unmodified capillary was low; however, as mentioned above, this response

could be due to residual silanols. Such residual silanols provide quite a reasonable charge density as illustrated recently by Nie *et al.* who used a similar unmodified reversed-phase monolithic silica capillary column successfully as an on-chip electro-osmotic pump [17, 18]. Indeed the background conductivity of the capillary monolithic phase could in future be used to give some indication of residual silanol content.

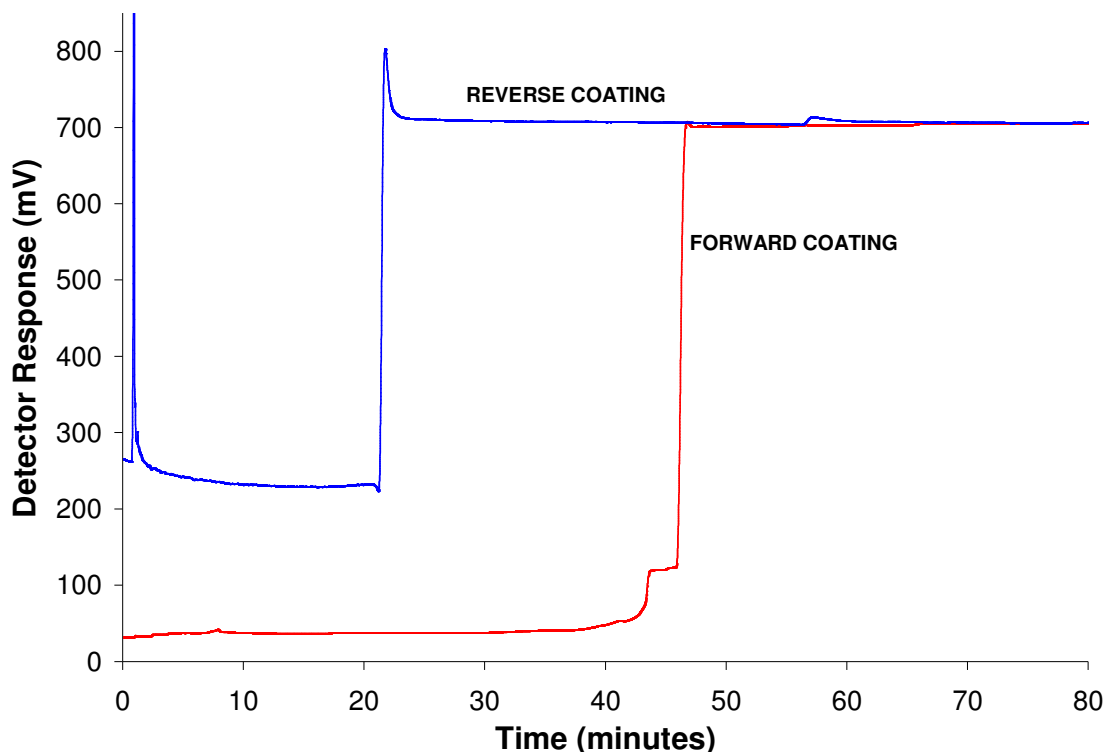


Figure 3.7: Breakthrough curves for Column # 2 for forward and reverse coating with 1 mM DOSS solution at  $1 \mu\text{L min}^{-1}$ .

The breakthrough curve for the first “forward coating” is shown in Figure 3.7. The “forward coating” curve demonstrates that breakthrough occurred at 46 minutes, resulting in approx 46 nM DOSS adsorbed on column.  $\text{C}^4\text{D}$  was then used to evaluate the longitudinal homogeneity of the first DOSS coating on capillary Column #2. The capillary was seen to have an uneven coating after the first coating with the largest detector response in the first (inlet) half of the capillary column (Figure 3.8), due to self retention of DOSS on this area of the column. This

corroborates the trend seen for Column # 1 (Figure 3.5). The capillary column was then reversed and was coated for a second time under the same coating conditions, resulting in a second breakthrough curve at 22 minutes (ca. 22 nM DOSS) as also shown in Figure 3.7. The reduction in breakthrough time is due to the fact that the previous coating step had reduced the adsorptive capacity of the C<sub>18</sub> column. Comparing the breakthrough times with those of Column # 1 (ca. 26 minutes, see Section 3.3.1), the forward coating breakthrough at ca. 46 minutes is almost twice that of Column # 1. The greater time required for breakthrough on Column # 2 may be due to this column having a higher capacity or greater self retention of DOSS than on Column # 1. The reverse coating of Column # 2 having a breakthrough of ca. 22 minutes is in closer agreement to that of Column # 1 at ca. 30 min. This indicates that the capacity of the column once coated in the forward direction is roughly the same for the reverse coating step.

Again the longitudinal homogeneity of the second coating was evaluated by measuring the C<sup>4</sup>D response at each detector cell position along the column. Unfortunately, the second coating did not immediately result in a significantly more uniform coating along the length of the capillary; however, the overall adsorbed capacity was clearly higher. As is shown in Figure 3.8, the coating of the capillary column in both directions showed a higher detector response for the section of capillary closest to the end of the column through which the coating solution was introduced (due to preconcentration). The different nature to that seen for coating of Column # 1 (Figure 3.5 (—□—)) may be due to different wash steps between forward and reverse coating (Column # 1 = 30 minutes, Column # 2 60 minutes) removing more DOSS before the collection of data. This resulted in more DOSS being removed from Column # 2 and thus a different shape compared to the curve for reverse coating of Column # 1. In order to achieve a uniform coating along the entire length of the column, the capillary was then returned to its original position and constantly washed with water (i.e. from inlet to outlet) at 1 μL min<sup>-1</sup> while the longitudinal homogeneity of the DOSS coating was monitored over time. The responses collected over time are shown in a 3D surface plot format in Figure 3.9. This surface plot can be subdivided into a number of regions to indicate the

chronology of data collection. Regions 1, 2 and 3 are the first, second and third days of data collection respectively, with a 12.5 hour overnight equilibration between days 1 and 2, and a 13.5 hour overnight equilibration between days 2 and 3.

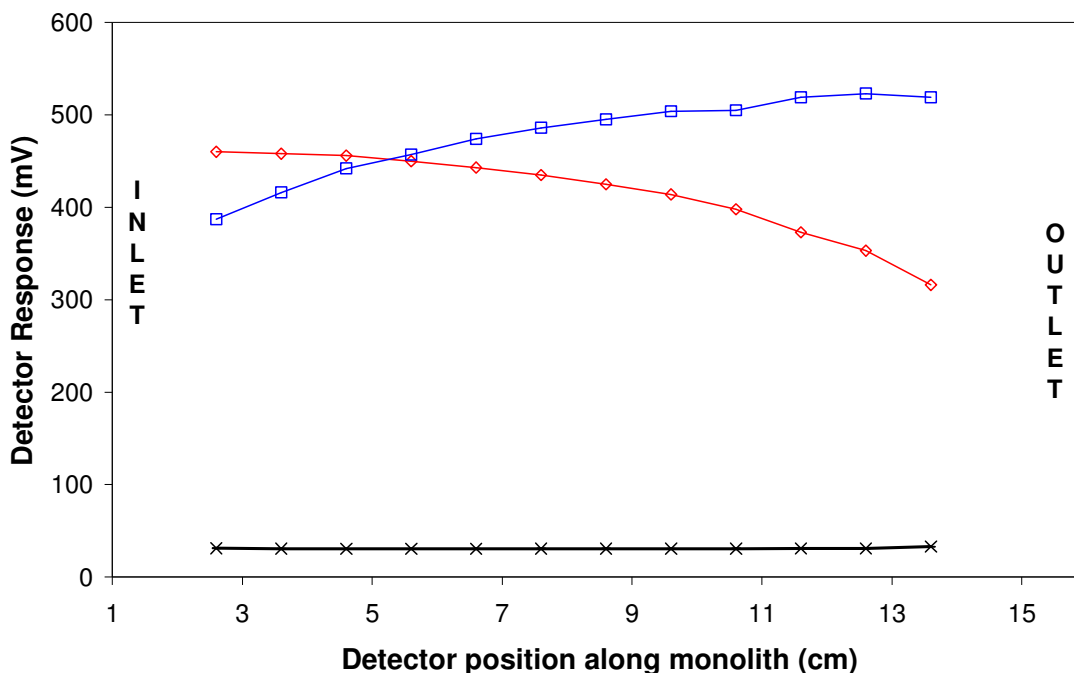


Figure 3.8: C<sup>4</sup>D response along the length of capillary Column #2 for the Unmodified monolith (—x—), coating from inlet to outlet (—◇—), and coating from outlet to inlet (—□—).

From the results obtained it can be seen that the coating firstly shows a decrease in response for the first 120 minutes, after which an increase in response is seen at the capillary inlet from 150 to 360 minutes, as indicated by Region A on the surface plot. It is proposed that this increase in C<sup>4</sup>D response is a front of unbound DOSS moving along the modified capillary column exhibiting frontal chromatography character. The overnight washing (360 minutes to 1110 minutes) resulted in a profile which follows this frontal chromatography behaviour, and can be seen clearly in the responses of 1110 to 1710 minutes (Region B on the surface plot). The profile collected during this time period shows the coating

response falling to a uniform level starting from the inlet. The second overnight washing results in a uniform profile, which corresponds to the levels seen at the inlet for the 1100 to 1710 minutes series of  $C^4D$  response values. The final three responses (i.e. 2580, 2640 & 2700 minutes) showed that the coating had reached a stable uniform level along the capillary length. At each measurement point along the column the standard deviation of the  $C^4D$  responses for the last three time points was calculated. The average of these standard deviation values was 0.89% as shown in Figure 3.6. The trend of frontal chromatography (Figure 3.9 (B)) corroborates the behaviour seen in the washing of Column # 1, as shown in Figure 3.6. This trend allows for monitoring and prediction of the wash step and its completion, until now only possible by indirect means [9].

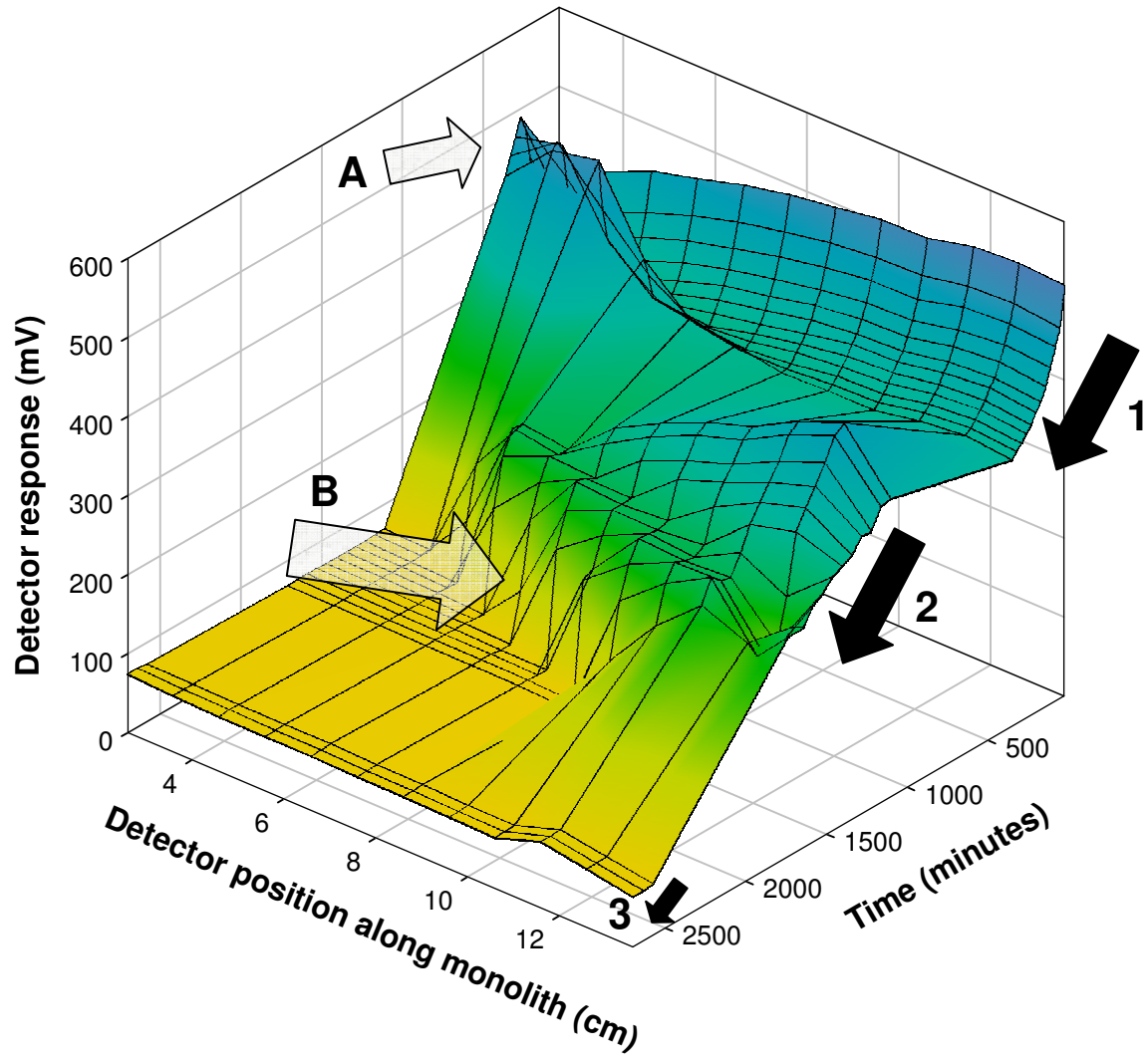


Figure 3.9: 3D representation of the concentration of charged groups, and their spatial distribution, along the length of Column # 2 as a function of equilibration time.

*3.3.3 Coating and washing of Column # 3.*

Column # 3 was coated in one direction only to allow for comparison with the final response of Column # 1 and Column # 2 (both of which were coated in two directions).

Column # 3 was coated in one direction as per Section 3.2.3.3 only, and breakthrough was observed at ca. 43 minutes. The column was then washed with

DI water for *ca.* 8 hr until stable baseline was achieved (Figure 3.10(—□—)). Column # 3 was then subjected to a series of methanol washes, as per Section 3.2.4, which resulted in the surfactant coating being removed from the C<sub>18</sub> phase.

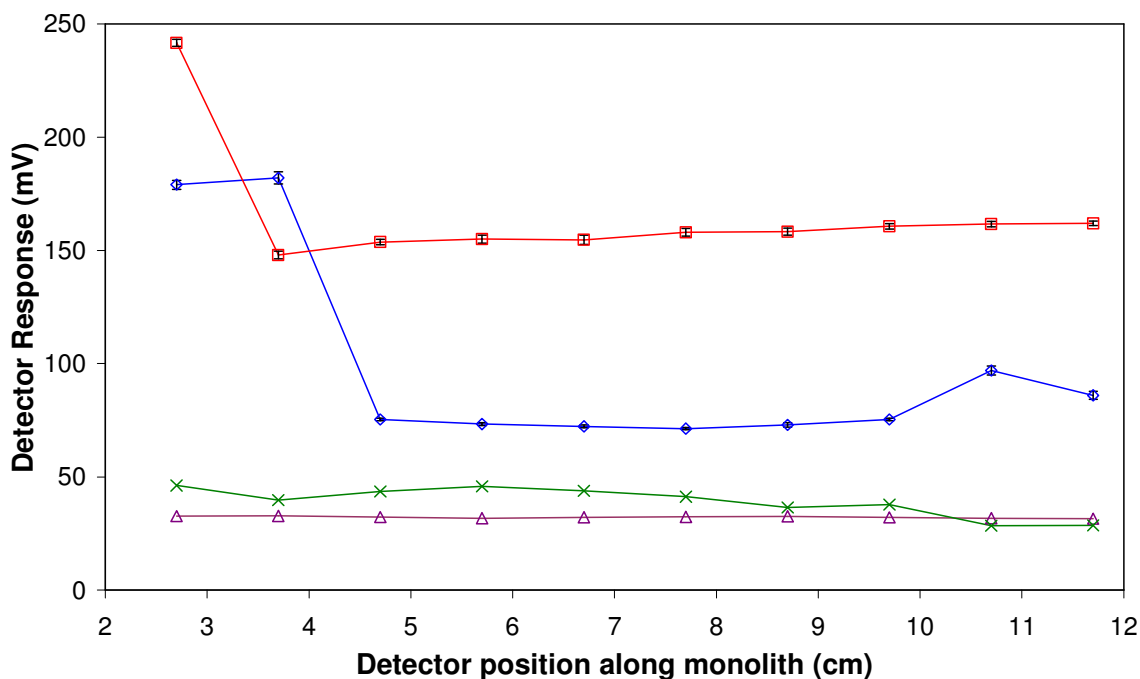


Figure 3.10: Comparison of Column # 3 under two separate coatings in one direction only. Unmodified Column # 3 prior to 1<sup>st</sup> coating (—×—), Column # 3 after 1<sup>st</sup> coating (—□—), unmodified Column # 3 prior to 2<sup>nd</sup> coating (—△—), Column # 3 after 2<sup>nd</sup> coating (—◇—) ( $n=3$ ).

Once the surfactant coating had been removed by the methanol washes Column # 3 was recoated, again in one direction only, for use in a counter ion study (as per Section 3.2.5). The column was then washed with DI water as in Section 3.2.3.3. The removal of the excess DOSS again followed a frontal chromatographic nature, however once the coating had stabilised it was found to have a lower response than for the first coating (Figure 3.10 (—◇—)).

From Figure 3.10 it can clearly be seen that there is marked difference in the both the response and the shape of the profile of Column # 3 after the two coatings. A drop in signal from *ca.* 150 to *ca.* 70 mV is observed. When the response for the

monolith prior to modification was compared for both coating steps, it was found that they had different responses (Figure 3.10). A possible explanation for the change observed is that the C<sub>18</sub> stationary phase itself has changed, possibly through the use of aqueous eluent and the washing with organic solvents. For both coatings a disturbance was seen at the column inlet, possibly due to inhomogeneity of the silica monolith at this point.

#### *3.3.4 Comparison of Column # 1, Column # 2 and Column # 3.*

The comparison of Column # 1 and Column # 2 shows a distinct difference in the response recorded for each column despite both columns being double coated and washed to completion. Figure 3.11 shows the profile of the two columns after coating in both directions and fully equilibrated (as per Sections 3.2.3.1 and 3.2.3.2). The difference in the response of the coatings is similar to that seen in Section 3.3.3, and the response of the unmodified monoliths prior to coating with surfactant also follows the same trend. This further corroborates the supposition that a difference in the monolith C<sub>18</sub> phase, through unknown factors, may be responsible for the differing coating responses.

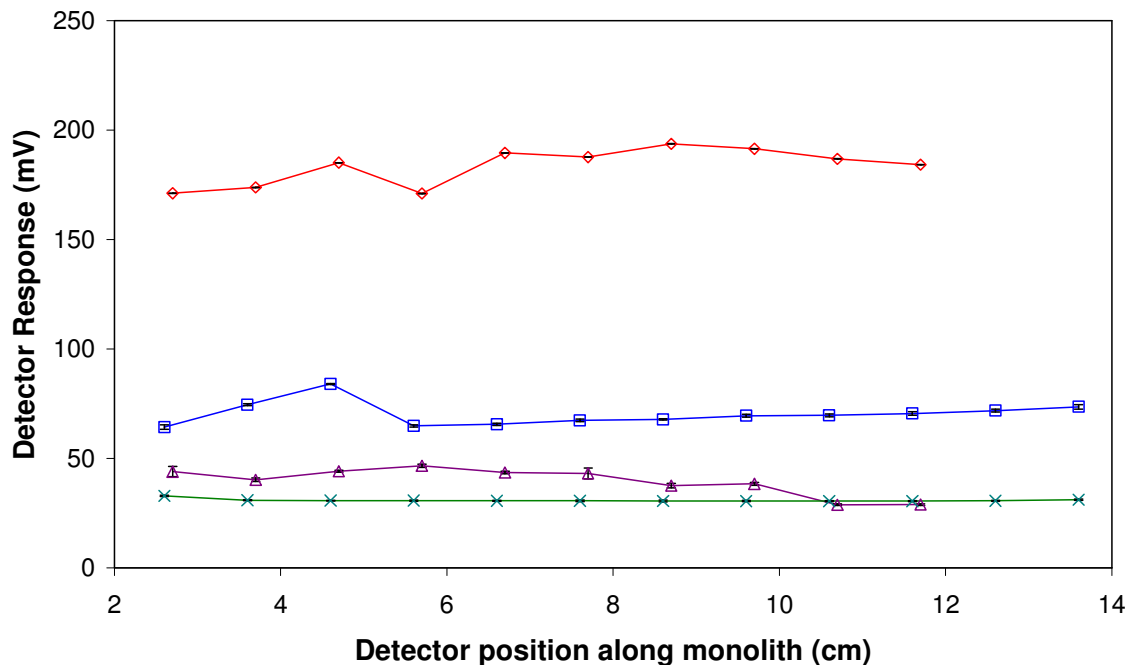


Figure 3.11: Comparison of Column # 1; unmodified ( $\triangle$ ) and coated ( $\diamond$ ) and Column # 2; unmodified ( $\times$ ) and coated ( $\square$ ) ( $n=3$ ).

The comparison of Column # 1 and Column # 3 (1<sup>st</sup> coating) showed a more similar response than with Column # 2. The values for the coatings of ca. 150 and 185 mV (Column # 1 and Column # 3 (1<sup>st</sup> coating), respectively), are in better agreement than Column # 1 compared to Column # 2. The responses of the unmodified column prior to coating also show good agreement compared to the comparison of unmodified Column # 1 and Column # 2 (Figure 3.12).

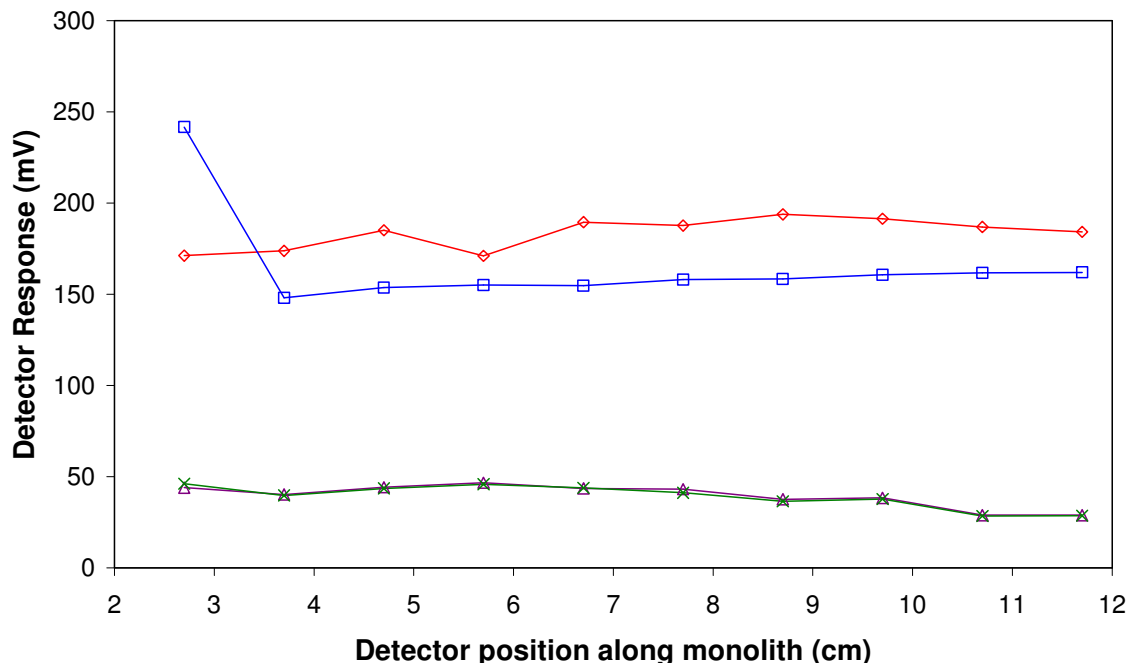


Figure 3.12: Comparison of Column # 1; unmodified (—△—) and coated (—◇—) and Column # 3 (1<sup>st</sup> coating); unmodified (—×—) and coated (—□—).

Figure 3.13 shows a comparison of the profiles of Column #3 (after 2<sup>nd</sup> coating, i.e. following stationary phase gradient study) and Column # 2. Taking the region of highest uniform coating for both columns, the responses were found to be similar to one another, with average responses of *ca.* 73 and *ca.* 69 mV for Column # 2 and 3, respectively. As with Column # 3 a disturbance in the conductivity response is seen at the inlet of the column (discussed in Section 3.3.3). This may be evidence that the functionalisation of the silica monolith with C<sub>18</sub> may not form a uniform distribution along the column length, but also that the extent of this differs from column to column. The response of the unmodified monolith prior to coating in both Column # 2 and 3 were found to in close agreement with each other, with responses of *ca.* 30-32 mV. Both coating and column equilibration procedures were compared (Column #2 versus Column #3), to evaluate the effect upon the final exchange capacity of both columns and coating homogeneity. This comparison of procedures revealed that both columns had roughly equivalent ion-exchange capacities after equilibration. Therefore,

there was clearly no real advantage in coating in two directions as opposed to one direction only. Indeed, results for Column #2 revealed that double coating a column requires a significantly longer equilibration time (ca. 45 hr for Column # 2 and ca. 8 hr for Column #3).

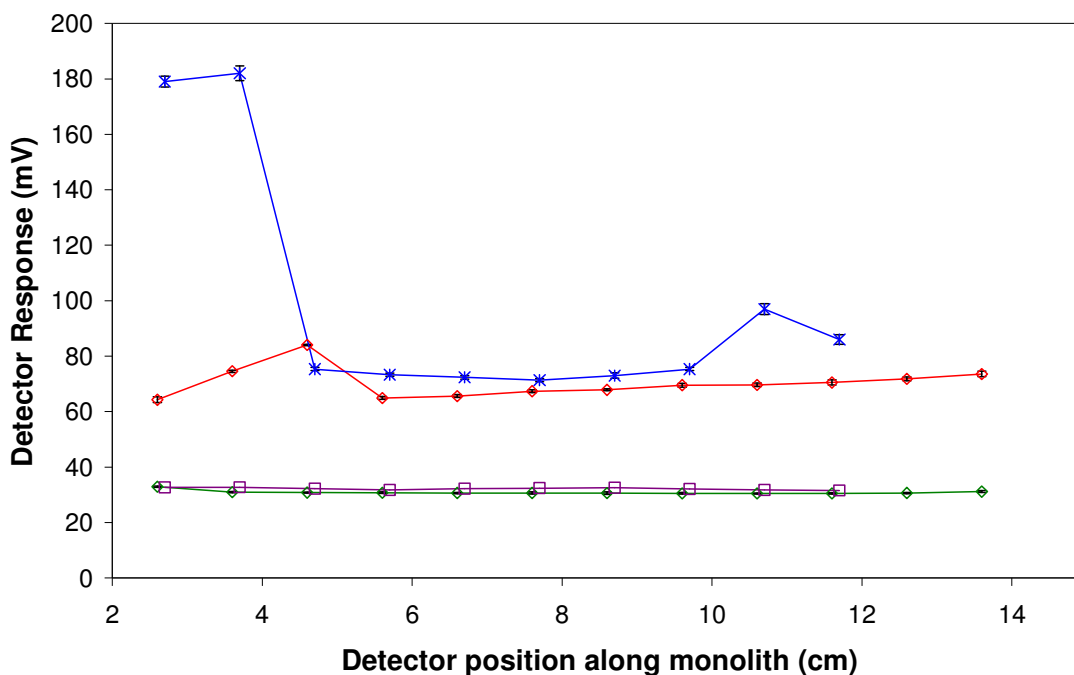


Figure 3.13: Comparison of Column # 2; unmodified (—◇—) and coated (—◇—) and Column # 3; unmodified (—□—) and coated (—\*—) ( $n=3$ ).

### 3.3.5 Controlled coating modification – stationary phase gradients.

Subsequent to the above observations, an investigation was carried out to evaluate if organic solvents could be utilised with C<sup>4</sup>D evaluation to control surfactant distribution and capillary monolith capacity. A column was coated and equilibrated with DI water using the procedure as for Column # 3. Five washing solutions of methanol:DI water were prepared, ranging from 10 % to 50 % methanol. The capillary monolithic column was washed with each solution in turn for a period of 30 minutes each. Between each of these organic washes the capillary was filled with DI water and the C<sup>4</sup>D response along the capillary taken. Figure 3.14 shows the responses obtained, including for comparison an

unmodified monolith. As can be seen from the figure shown, small changes were observed with a 10 % wash solution, but a shift in the stationary phase coating was observed at 20-30 %. However, it was the result of the 40 % wash which produced the most significant removal of the adsorbed surfactant, such that after the 30 minutes wash period, an almost perfect concave stationary phase gradient profile of coating was produced (expanded and shown as Figure 3.15). To the author's knowledge this is the first time such a coated stationary phase gradient has been produced in this way, (particularly on a capillary monolith) and visibly shown so clearly using non-invasive techniques. Washing the capillary monolith with the 50 % methanol solution resulted in complete removal of the DOSS coating within the 30 minute wash period. The use of C<sup>4</sup>D allowed verification of regeneration of the bare reversed-phase monolith, allowing for its use in further experimentation.

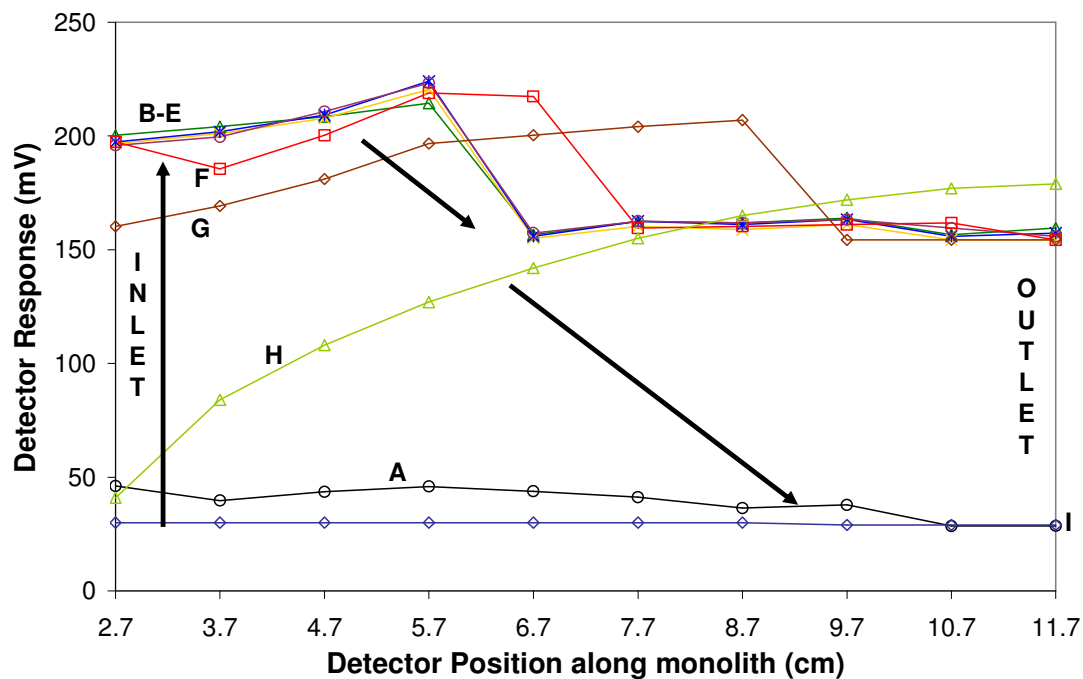


Figure 3.14: Effect upon coating distribution due to inclusion of increasing amount of methanol in DI washing solution passed through the Column # 3 at  $1 \mu\text{L min}^{-1}$  for 30 minutes. A= unmodified monolith, B = modified monolith following equilibration with water, C-E = following 10% methanol wash, F = 20 % methanol wash, G = 30 % methanol wash, H = 40 % methanol wash, I = 50 % methanol wash.

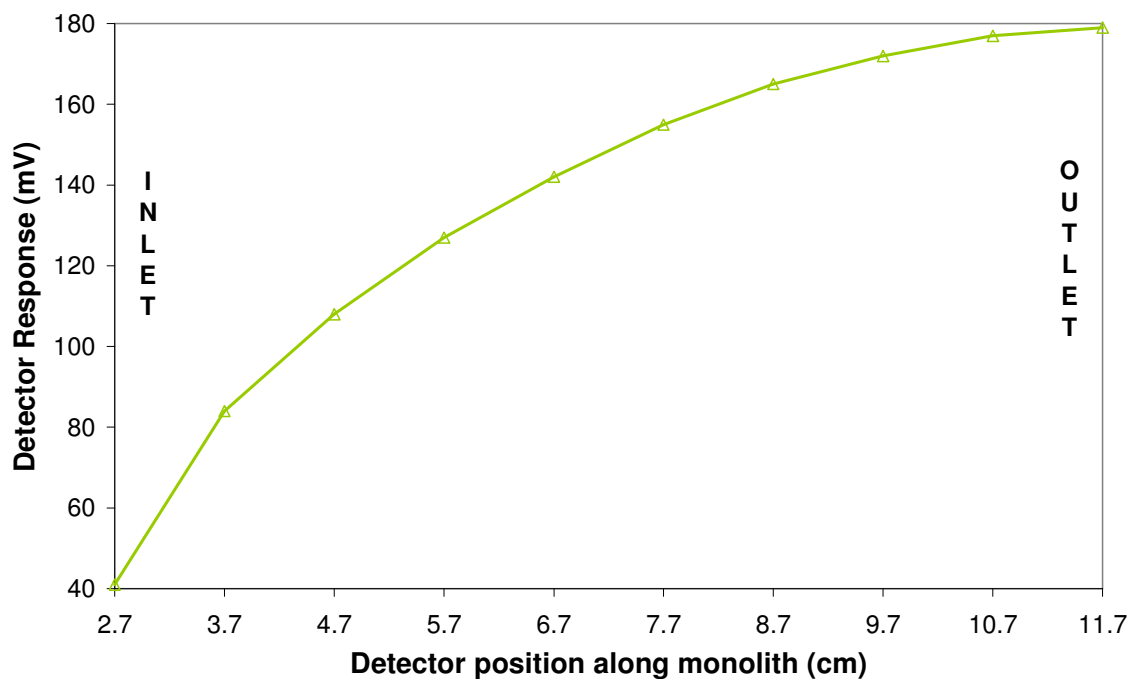


Figure 3.15: Expanded view of the effect of washing with 40 % methanol for 30 minutes. Column # 3.

This column once washed with 50 % methanol, and all the surfactant removed, was recoated in one direction only (inlet to outlet) and used for a counter ion study.

### 3.3.6 Counter ion study.

Once Column # 3 was washed fully with 50 % methanol in Section 3.3.5 was once again coated with DOSS as per Section 3.2.3.3. The DOSS coated monolith can be converted into any cation “form” by equilibrating the sulphonate ion exchange sites with a cation solution. A counter ion study was therefore performed for three different cations, whereby a solution of 2 mM nitric acid, sodium chloride or magnesium chloride was passed through Column # 3 at  $1 \mu\text{L min}^{-1}$ . The  $\text{C}^4\text{D}$  response was collected at the column exit. The equilibration of the column with this solution was judged to be complete when the detector response had stabilised (>120 minutes). Equilibrating the sulphonate groups on the column with these

cations essentially converts the column into hydronium form ( $\text{H}_3\text{O}^+$ ), sodium form ( $\text{Na}^+$ ) or magnesium form ( $\text{Mg}^{2+}$ ). The equilibrated column was then washed with water to remove all free cations in solution and the detector response again allowed to stabilise. Once all the excess counter ion solution had been removed from the column the  $\text{C}^4\text{D}$  response for the 10 positions along the column were collected (in triplicate). The resulting responses are shown as Figure 3.16. It was found that a different  $\text{C}^4\text{D}$  response was obtained for the column, depending upon whether the column was in the hydronium form, the sodium form or the magnesium form. As expected, the profiles closely mirror each other, since the distribution of sulphonate groups along the length of the column was the same in all three cases, with a slightly higher distribution of sulphonate groups at the column inlet. The counter ion profiles are offset relative to each other due to the difference in equivalent ionic conductance of each cation.

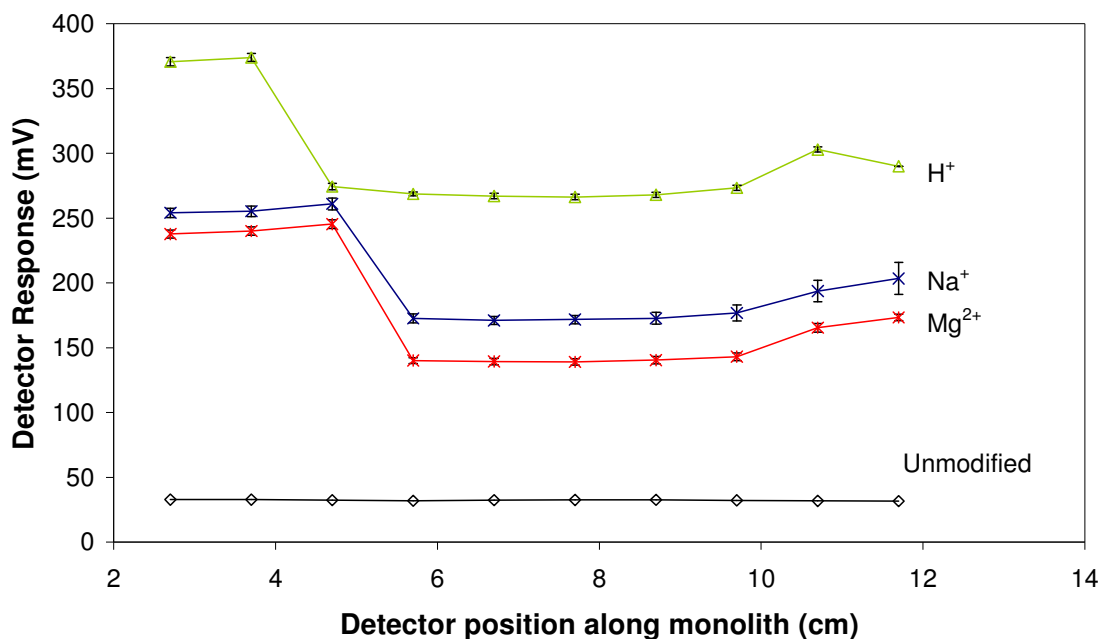


Figure 3.16: Response along column length for counter ion variation ( $n=3$ ). Column # 3.

Figure 3.16 also includes the C<sup>4</sup>D response of the “unmodified” silica based C<sub>18</sub> capillary column before coating with DOSS, for comparative purposes. The data points shown in Figure 3.16 are each based upon triplicate readings. The average %RSD for all profiles was > 2 %, showing stable and reproducible readings. Figure 3.17 shows the relative responses recorded for each counter ion plotted against their equivalent ionic conductances (EIC), with the EIC for magnesium divided by 2 to take into account the +2 cation charge. Figure 3.17 shows data for points at the inlet (top line), middle (bottom line) and outlet (middle line) of the capillary column, since different regions of the column have been shown to have different levels of DOSS coating. The background response from the unmodified monolith has been subtracted, so the data shown is the contribution from the absorbed ionic surfactant (constant) and the various counter cations only.

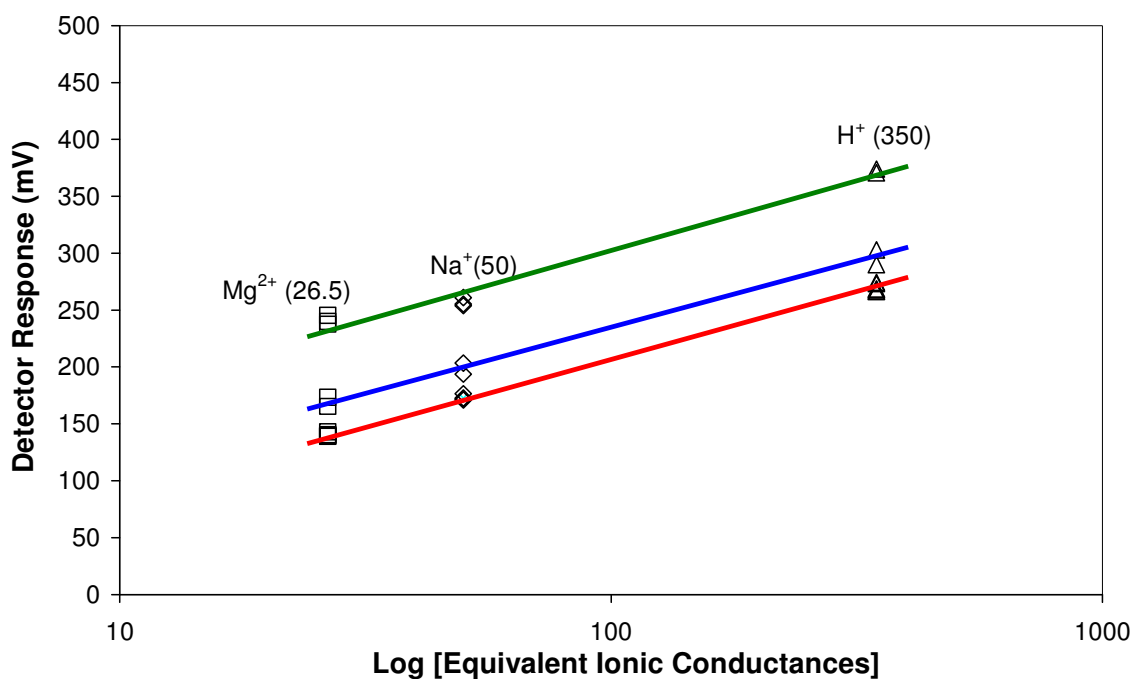


Figure 3.17: Logarithmic relationship between coating response and counter ion equivalent ionic conductance for Column # 3.

The measured electrical conductance, or conductivity detector response can be expressed as:

$$K = \frac{\Lambda_{DOSS} C_R + \Lambda_{CAT} C_{CAT}}{1000K} \quad (\text{Eq. 3.1})$$

where,  $\Lambda_{DOSS}$  and  $\Lambda_{Cat}$  represent the EIC of the immobilised DOSS and corresponding counter cation,  $C_{Cat}$  represents the concentration of ions in the phase of the cation-exchanger, which is ideally equal to the ion-exchange capacity,  $C_R$ , of the column, and  $K$  is the cell constant. The EIC for each counter ion was taken to be  $350 \text{ ohm}^{-1}\text{cm}^2\text{equiv}^{-1}$  for hydronium,  $50 \text{ ohm}^{-1}\text{cm}^2\text{equiv}^{-1}$  for sodium and  $53 \text{ ohm}^{-1}\text{cm}^2\text{equiv}^{-1}$  for magnesium [19]. However, the  $C^4D$  detector response for the ion-exchanger must include the distribution coefficients, as ion exchange columns exhibit different ion-exchange selectivity to different cations. In a general form the selectivity coefficient,  $K_{H^+}^{Cat}$ , can be expressed as:

$$K_{H^+}^{Cat} = \frac{[Cat^{n+}]_R [H^+]_S^n}{[H^+]_R^n [Cat^{n+}]_S} \quad (\text{Eq. 3.2})$$

After equilibration with relatively dilute, 2 mM, solutions of electrolytes the amount of adsorbed cation has to be proportional to the above distribution coefficients. For monovalent cations this distribution coefficient,  $K_D$ , is equal to:

$$\frac{[Cat^+]_R}{[Cat^+]_S} = K_D = K_{H^+}^{Cat+} \frac{[H^+]_R}{[H^+]_S} = K_{H^+}^{Cat+} \frac{C_R}{[H^+]_S} \quad (\text{Eq. 3.3})$$

And for divalent cations:

$$K_D = K_{H^+}^{Cat2+} \frac{[H^+]_R^2}{[H^+]_S^2} = K_{H^+}^{Cat2+} \frac{C_R^2}{[H^+]_S^2} \quad (\text{Eq. 3.4})$$

For hydronium selectivity  $C_{Cat} = C_R$  and formula (Eq. 3.1) is valid for the DOSS loaded reversed-phase capillary column in the  $H^+$  form. For other cations formula (Eq. 3.1) can be transformed as follows:

$$K = \frac{\Lambda_{DOSS} C_R + K_D \Lambda_{CAT} [Cat^+]_S}{1000K} \quad (\text{Eq. 3.5})$$

Therefore, as illustrated by the above formula, it is clear that the monitoring of the  $C^4D$  response for capillary ion-exchange columns in this way can provide unique possibilities for the accurate measurement of different physicochemical parameters within the ion-exchange equilibrium. As an example, Figure 3.17 clearly demonstrates the relationship between  $C^4D$  response and equivalent conductances of the prepared column equilibrated with 2 mM solutions of different electrolytes.

### 3.3.7 Analysis of cations.

To obtain optimum efficiency and reproducibility using surfactant coated ion exchangers, a homogeneous and uniform distribution of charged sites throughout the stationary phase is desirable. Using monolithic capillary columns, coated, equilibrated and evaluated using the above techniques (Column # 2), a number of Cap-IC separations were obtained and analytical performance data collected. The separations shown, using a stable homogenously modified DOSS monolithic capillary column, with on-column  $C^4D$  detection have not been previously achieved by other research groups. The use of on-column detection, as applied here, has the additional benefit of eliminating any extra column band broadening from connections, tubing and detector cells, which is often a major cause of loss of efficiency in capillary scale separation systems (shown previously in Chapter 2). Previously DOSS has been used for the separation of inorganic cations with an ethylenediamine and phthalate eluent and indirect conductivity detection [5]. In this work an eluent of 0.5 mM ethylenediamine eluent, adjusted to pH 4.5 with

dilute  $\text{HNO}_3$  was used for the separation of alkaline earth metal cations. A selectivity study was carried out to aid in the selection of the analytes for analysis; from Table 3.1 it can be seen that the cation exchange column showed good selectivity for alkaline earth metals. Of the analytes investigated four were chosen for analysis; calcium, magnesium, barium and strontium. All four cations were well resolved, eluting as efficient and symmetrical peaks (shown here as Figure 3.18). Column efficiency (N/m) was calculated (using data from 6 replicate injections) as  $42,700 \pm 2\%$  for magnesium,  $43,600 \pm 2\%$  for calcium,  $48,400 \pm 2\%$  for strontium and  $46,900 \pm 2\%$  for barium, representing some of the highest efficiencies achieved for capillary ion exchange separations of small ions, particularly on modified monolithic phases [20]. Peak asymmetry was also calculated from the above replicates and average values were 0.94 for magnesium, 1.01 for calcium, 0.96 for strontium and 1.04 for barium. Each linearity standard was run in triplicate and correlation coefficients exceeded  $R^2 = 0.99$  for all cations (see Table 3.2). Method precision was determined by performing six replicate separations of a mixed cation standard ( $5 \text{ mg L}^{-1}$  magnesium,  $10 \text{ mg L}^{-1}$  calcium,  $20 \text{ mg L}^{-1}$  strontium and  $40 \text{ mg L}^{-1}$  barium). The % RSD was  $< 1.5$  both for peak area and peak retention time. For the purposes of calculating limits of detection (LOD) for each analyte, the baseline noise was measured for three replicate blank injections using a least squares regression method in a two minute window centred around the retention time for each respective analyte. LODs were calculated using a signal to noise ratio of three, whereas limits of quantitation (LOQ) were taken over the same time frame with signal to noise ratio of ten. The concentration LODs were found to be in the sub  $\text{mg L}^{-1}$  range. The absolute detection limits of the 10 nL injection are in the pg range for all analytes (e.g. magnesium: 1.08 pg). The LODs achieved are in the order of 10 times lower than those previously reported in literature using a polymeric cation exchange capillary column with UV detection, which yielded detection limits of 1.38 and  $1.92 \text{ mg L}^{-1}$  for magnesium and calcium, respectively [20].

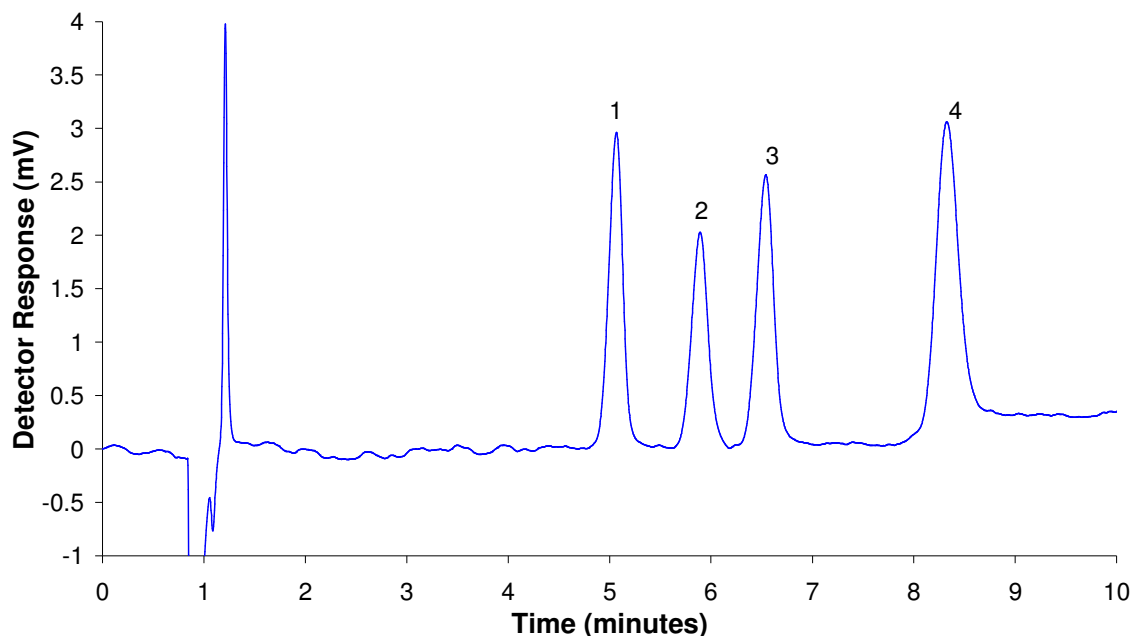


Figure 3.18: Separation of (1) magnesium ( $5 \text{ mg L}^{-1}$ ), (2) calcium ( $10 \text{ mg L}^{-1}$ ), (3) strontium ( $20 \text{ mg L}^{-1}$ ) and (4) barium ( $40 \text{ mg L}^{-1}$ ) on Column #2. Eluent:  $0.5 \text{ mM}$  ethylenediamine (pH 4.5), flow rate:  $1 \mu\text{L min}^{-1}$ , injection volume:  $10 \text{ nL}$ . Detection: Indirect  $\text{C}^4\text{D}$ . Column # 2.

Table 3.1: Selectivity of the DOSS coated column (Column #2) for selected alkali metals, alkaline earth metals and transition metals with an ethylenediamine eluent.

Cation	k	Cation	k
Potassium	0.34	Zinc	5.23
Sodium	0.34	Nickel	5.27
Lithium	0.34	Cadmium	5.36
Ammonium	0.34	Calcium	5.58
Magnesium	4.66	Strontium	6.30
Manganese	5.08	Barium	8.29
Cobalt	5.09	Copper	13.48

Table 3.2: Analytical performance data for separation of cations. Note: 0.25 mg L<sup>-1</sup> standard for strontium and barium was omitted since these levels are below their respective LOD's. Column # 2.

Analyte	Linearity		Precision %RSD (n=6)			
	Stds., Conc., mg L <sup>-1</sup>	R <sup>2</sup>	Retention Time	Peak Area	LOD (mg L <sup>-1</sup> )	LOQ (mg L <sup>-1</sup> )
Magnesium	0.25, 0.5, 1, 10, 20, 40	0.999	0.489	0.984	0.108	0.359
Calcium	0.25, 0.5, 1, 10, 20, 40	0.999	0.494	1.202	0.146	0.486
Strontium	0.5, 1, 10, 20, 40	0.998	0.501	1.151	0.359	1.197
Barium	0.5, 1, 10, 20, 40	0.999	0.477	1.243	0.898	2.992

### 3.3.8 Analysis of drinking water.

To demonstrate the applicability of the modified capillary column with radial across column detection to a common application, samples of drinking water were analysed. Two samples of commercial bottled drinking water and a sample from a source tap in the research laboratory were filtered (0.2 µm) and diluted with DI water as necessary. The samples were then injected in triplicate for the quantitation of magnesium and calcium using the linear regression curves discussed earlier.

Figure 3.19 shows a tap water sample and two bottled water samples overlaid with a standard and DI water blank. Calcium and magnesium are well resolved from strontium and barium, and there is no sign of interference from any late eluting peaks, despite the fact that the samples were ran consecutively and without delay. Table 3.3 summarises the results obtained for the analysis of the three samples.

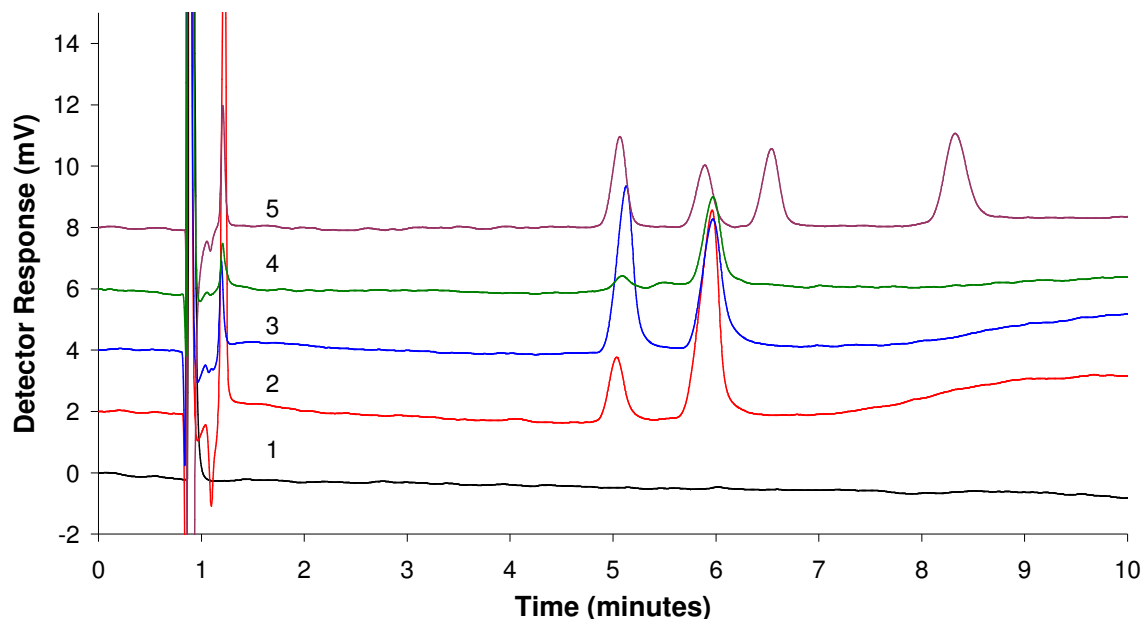


Figure 3.19: Chromatograms of real sample analysis, 1 = Blank, 2 = Bottled water sample #1 (1/2 dilution), 3 = Bottled water sample #2 (1/10 dilution), 4 = Tap water (1/10 dilution) and 5 = Standards Conditions as in Figure 3.20.

Table 3.3: Concentration of calcium and magnesium determined for thee samples.

	Calcium		Magnesium	
	mg L <sup>-1</sup>	%RSD*	mg L <sup>-1</sup>	%RSD*
Bottled water # 1	76.5	1.5	5.9	1.7
Bottled water # 2	298.2	4.1	115.6	4.4
Tap water	206.6	8.2	6.7	5.8

\*  $n=3$

### 3.3.9 Separation of selected amino acids.

Finally, as an alternative to inorganic cations, a separation of amino acids using a dilute nitric acid eluent was developed using the DOSS modified capillary monolith. The isocratic separation of up to twelve amino acids was possible in less than 15 minutes. A typical separation achieved is shown as Figure 3.20. The

mobile phase used was 10 mM nitric acid, once again with on-column C<sup>4</sup>D indirect detection. The efficiencies obtained for this separation are given in Table 3.4. Briefly the efficiencies ranged from *ca.* 20,000 to *ca.* 39,000 N/m for histidine and valine, respectively.

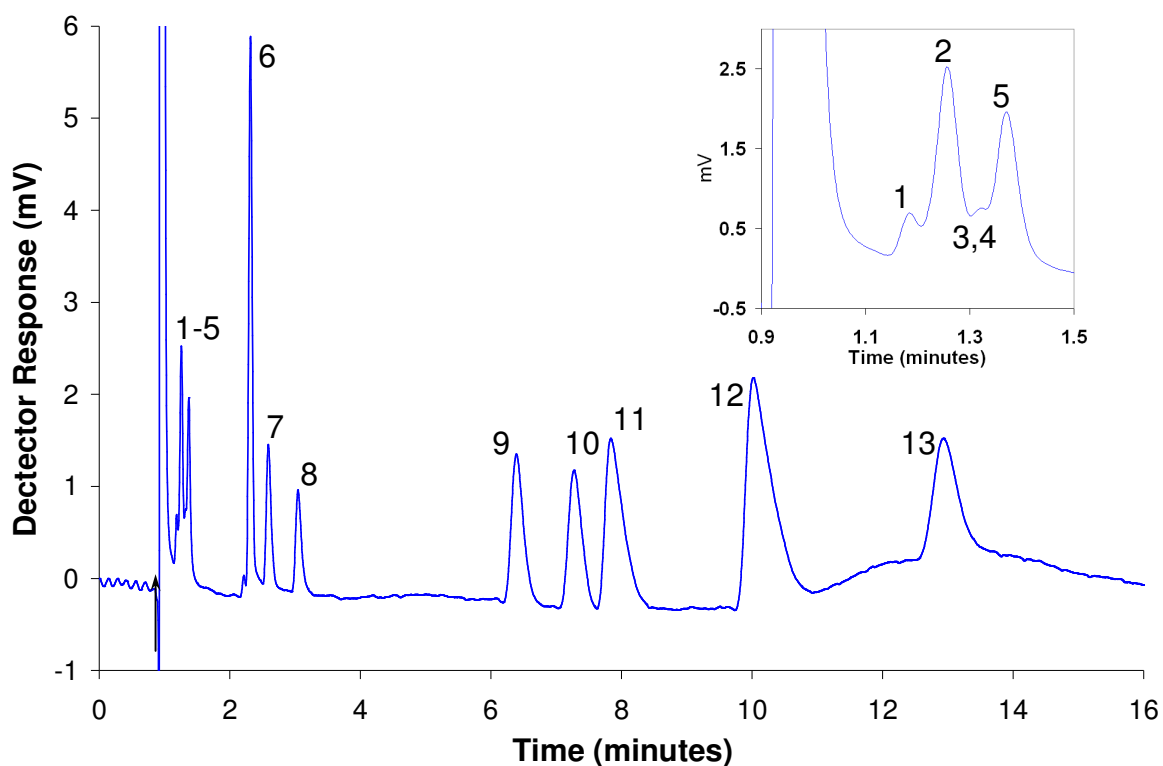


Figure 3.20: Separation of twelve amino acids on the DOSS coated capillary column (Column #2) (1= Asparagine, 2= Glycine, 3= Proline, 4= Glutamine, 5= Alanine, 6 =unknown, 7 =Valine, 8= Methionine, 9= Isolucine, 10 = Leucine, 11= Lysine, 12= Histidine, 13= Phenylalanine, 100 mg L<sup>-1</sup> each, 10 nL injection). Eluent: 10 mM nitric acid (pH 3.0), flow rate: 1 μL min<sup>-1</sup>, injection volume: 10 nL. Detection: Indirect C<sup>4</sup>D.

Table 3.4: Efficiency data for amino acid separation.

Analyte	N	N/m
Asparagine	n/a	n/a
Glycine	4,038	26,920
Proline	n/a	n/a
Glutamate	n/a	n/a
Alanine	4,602	30,680
Valine	5,873	39,153
Methionine	5,879	39,193
Isolucine	5,647	37,646
Leucine	5,612	37,413
Lysine	3,832	25,546
Histidine	3,127	20,846
Phenylalanine	5,586	37,240

### 3.4 Conclusions.

The results discussed in Chapter illustrate that the application of C<sup>4</sup>D detection to the examination of the longitudinal homogeneity of a surfactant coating on a capillary column is in the author's opinion, a significant advance in a number of ways.

Firstly, to the author's knowledge, C<sup>4</sup>D detection is the only methodology proposed to date, which can be used to compare the ion-exchange capacities (expressed as C<sup>4</sup>D response in millivolts) of a range of capillary ion chromatography columns immediately after column production, without the use of expensive liquid chromatography instrumentation. This method is a non-contact, non-invasive and non-destructive in-situ method to determine the levels of surfactant adsorbed on a stationary phase, since the columns are simply passed

through the cell of the C<sup>4</sup>D detector, without the need to cut the column, or in any way to compromise the stationary phase (for example by removing the phase for elemental analysis). Indeed C<sup>4</sup>D detection offers a complementary methodology to that of chromatographic techniques for determination of ion-exchange capacity, such that one methodology may be used to cross-validate the other.

Secondly, as discussed previously, C<sup>4</sup>D detection allows one to precisely map the spatial distribution of charge along the entire length of a column. The traditional way of reporting ion-exchange capacity of a column, expressed as milliequivalents per column, only gives a measure of the total exchange capacity. However, this measure obviously does not indicate whether the spatial distribution of the ion-exchange groups is longitudinally homogenous, or whether the local exchange capacity is higher or lower than in other regions along the length of the column. In Figure 3.21 the *theoretical* distribution of ion exchange sites, i.e. the capacity, for the three columns is the same (calculating area) but the only one column has a homogeneous distribution of capacity along the length of the column (Figure 3.21(a)), one column has a linear gradient of capacity (Figure 3.21(b)) and the third column has a decrease in capacity followed by a stable region and followed by an increase in capacity (Figure 3.21(c)). Using C<sup>4</sup>D with capillary monolithic columns the ability to spatially locate and also temporally map any changes in the signal, and therefore the capacity, adds invaluable information to the column characterisation.

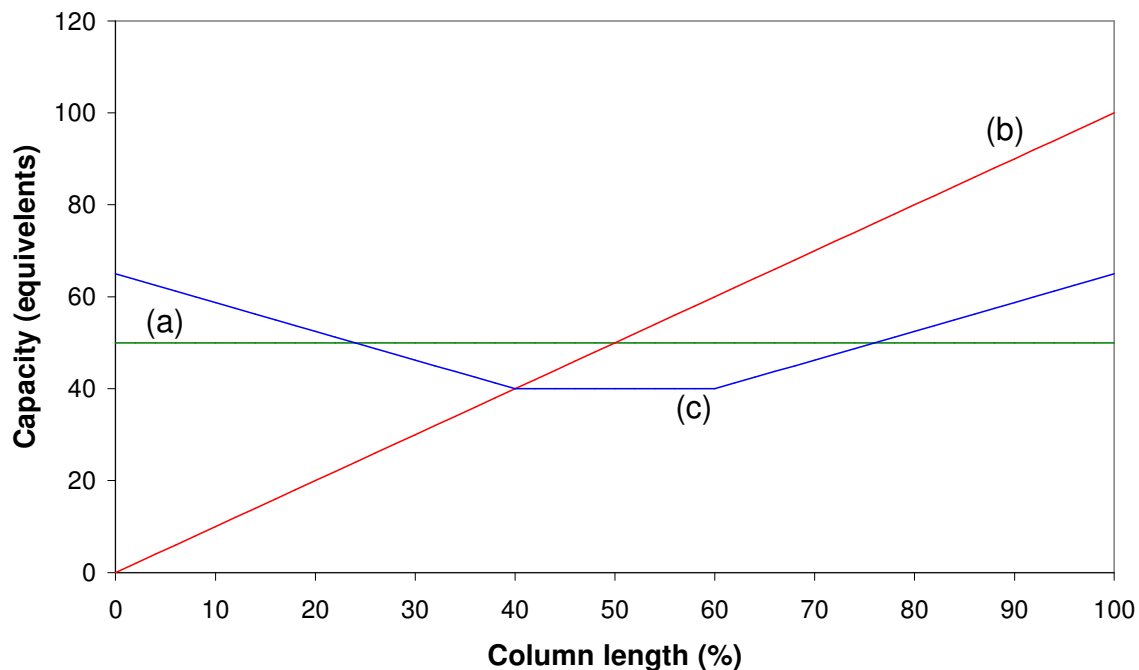


Figure 3.21: Theoretical comparison of columns with differing capacity distribution but with the same overall capacity. (a)= homogeneous distribution of capacity, (b) = linear gradient of capacity, (c) = non-linear distribution of capacity.

Thirdly,  $C^4D$  detection can not only be used to determine the point at which equilibration of a coated column is complete, but has also proven to be a useful method for monitoring the spatial distribution of charge on the column during a column washing procedure. This helps us to gain a much better understanding of the dynamics of column equilibration after coating with ionic surfactants. Finally, the combined advantages gained from the above measurements should allow more reproducible column production and ready evaluation of column aging over time, with the ability to produce longitudinally homogenous modified capillary monoliths for more efficient ion chromatographic separations. Before the use of  $C^4D$  in this application, it would have only been possible to place a fixed detector (such as UV or conductivity) at the end of the column during equilibration, and monitor the excess unbound surfactant bleed off the column. However, the use of  $C^4D$  with a moveable cell, allows the analyst to trace the exact longitudinal location of the frontal band of surfactant during equilibration.

### 3.5 References.

- [1] P. Hatsis and C. A. Lucy, *Anal. Chem.*, 2003, **75**, 995.
- [2] C. O Riordain, L. Barron, E. Nesterenko, P. N. Nesterenko and B. Paull, *J. Chromatogr., A*, 2006, **1109**, 111.
- [3] J. S. Fritz, Z. Yan and P. R. Haddad, *J. Chromatogr., A*, 2003, **997**, 21.
- [4] Z. Yan, P. R. Haddad and J. S. Fritz, *J. Chromatogr., A*, 2003, **985**, 359.
- [5] D. Connolly, D. Victory and B. Paull, *J. Sep. Sci.*, 2004, **27**, 912.
- [6] S. Pelletier and C. A. Lucy, *J. Chromatogr., A*, 2006, **1118**, 12.
- [7] K. Ito, Y. Takayama, N. Makabe, R. Mitsui and T. Hirokawa, *J. Chromatogr., A*, 2005, **1083**, 63.
- [8] C. O'Riordain, L. Barron, K. Nesterenko, P.N. Nesterenko, B.Paull, *J. Chrom. A.*, 2006, **1109**, 111.
- [9] K.M. Glenn, C.A. Lucy, *Analyst*, 2008, **133**, 1581
- [10] P. Kuban and P.K. Dasgupta, *J. Sep. Sci.*, 2004, **27**, 441.
- [11] T. Rohr, E.F. Hilder, J.J. Donovan, F. Svec, J.M.J. Frechet, *Macromolecules*, 2003, **36**, 1677.
- [12] V. Pucci, M.A. Raggi, F. Svec, J.M.J. Frechet, *J. Sep. Sci.*, 2004, **27**, 779.
- [13] S. Eeltink, E.F. Hilder, L. Geiser, F. Svec, J.M.J. Frechet, G.P. Rozing, P.J. Schoenmakers, W.T. Kok, *J. Sep. Sci.*, 2007, **30**, 407.
- [14] T.B. Stachowiak, F. Svec, J.M.J Frechet, *Chem. Mater.*, 2006, **18**, 5950.
- [15] D.S. Peterson, T. Rohr, F.Svec, J.M.J Frechet, *Anal. Chem.*, 2003, **75**, 5328.
- [16] E. Sugrue, P.Nesterenko, B. Paull, *J. Sep. Sci.*, 2004, **27**, 921.
- [17] F. Nie, M. Macka, L. Barron, D. Connolly, N. Kent, B. Paull, *Analyst*, 2007, **132**, 147.
- [18] F. Nie, M. Macka, B. Paull, *Lab-on-a-chip*, 2007. **11**, 1597.
- [19] J. Weiss. *Ion Chromatography. Second Edition.* VCH, Weinham, 1995, p.295.
- [20] Y. Ueki, T. Umemura, J.X. Li, T. Odake and K. Tsunoda, *Anal. Chem.*, 2004, **76**, 7007.

---

**Chapter 4: Characterisation of photografted polymeric  
monolithic ion exchangers using  
capacitively coupled contactless  
conductivity detection**

---

“What's the use of a good quotation if you can't change it?”  
-Dr. Who

## 4.1 Introduction.

One advantage of polymeric monolithic phases is the ability to modify their chemistries. There are three main methods of doing so, changing the starting monomer mixture [1], chemical reaction along the entire length of the monolith [2] and photografting (using UV transparent capillary) either in discrete zones [3, 4, 6] or along the entire length of the monolith [4]. These modifications can result in a differing chemistry ready for immediate use or can be used as intermediates for further modification [7, 8]. Photografting is used to functionalise monoliths to change the surface chemistry, without having to re-optimize the monomer mixture and it also allows for the use of chemistries of differing polarities, which if placed in the monolith solution may result in non-homogeneous mixture [9]. Photografting also allows for the creation of discrete bands of differing chemistries along the length of the monolith [3-6]. This advantage has been used to create monoliths with immobilised trypsin allowing for on-column digestion of proteins prior to solid phase extraction on the same monolith followed by mass spectrometric detection [4]. Also the ability to change the surface chemistry has been used to alter the hydrophobicity of the monolith surface for use with protein applications where non-specific interactions would be detrimental to the analysis [5]. Creation of differing ligand density is also possible with the use of gradient photografting. In this technique a substrate that has a variation in its UV transmission along the region to be photografted is used, thus varying the amount of UV energy initiating the photograft. These gradients can be of a linear nature or of a concave/convex nature depending on the method used [8].

The characterisation of surface modified monoliths poses some technical challenges, namely that the sample size is very small and is chemically bonded to the fused silica capillary. As a result most methods for the characterisation of the photografted monoliths are either indirect (EOF measurement [9], fluorescent microscopy [5]) or destructive in nature (SEM-EDX) [8, 9].

As shown in Chapter 2,  $C^{4}D$  affords rapid, non-contact, non-invasive and non-destructive characterisation of silica monoliths coated with ionic surfactants.

Connolly *et al.* further developed the use of C<sup>4</sup>D in the characterisation of stationary phase modification with the verification of photografting of AMPS and VAL. Discrete zones of AMPS were photografted and visualised by scanning C<sup>4</sup>D, and a protein was immobilised onto the surface of the monolith via photografted zones of VAL [3]. In this Chapter these advantages are applied to the characterisation of photografting processes. In the optimisation of photografting methods there are two main variables: (1) the concentration of the monomer used and (2) the amount of UV energy used to initiate the graft [8]. In recent years several ionic monomers have been photografted onto the surface of monoliths, the vast majority for use with capillary electrochromatography (CEC) [7-9]. These monomers have been both anionic, 2-acrylamido-2-methyl-1-propanesulfonic acid (AMPS), and cationic, [2-(methacryloyloxy) ethyl] trimethylammonium chloride (META) [9], or ionisable (boronic acids) [7]. However, the characterisation of these monoliths has relied heavily on their chromatographic performance. The homogeneity (location and amount of monomer photografted) of these photografting techniques is still an unknown parameter, especially when photo-patterning of a monolith is exploited. Sections 1.4.1, 1.4.2 and 1.4.3 detail some techniques currently used to evaluate photografting techniques.

In this Chapter, C<sup>4</sup>D is utilised to investigate the effect of energy used to initiate photografting of an anionic vinyl monomer, AMPS (Figure 4.1), onto the surface of a butyl-methacrylate monolith. The ability of C<sup>4</sup>D to detect differences in the amount of AMPS photografted (i.e. the capacity of each zone) is exploited to monitor wash steps and to create a calibration of AMPS capacity vs. UV energy used to initiate the photografting.

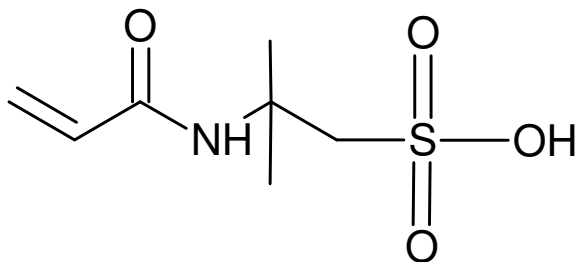


Figure 4.1: Structure of AMPS.

## 4.2 Experimental.

### 4.2.1 Instrumentation.

The pump used for washing monolithic capillary column was a quaternary gradient HP 1050 pump operated in isocratic mode at all times. The pump flow was split by the use of a T-piece connector with a section of 50  $\mu\text{m}$  i.d. fused silica capillary (Polymicro Technologies, Phoenix, AZ) on the waste side to create sufficient back pressure as to give the required split flow. The operational flow rate was 1  $\mu\text{L min}^{-1}$ . A pump was used to fill the pores of pre-formed monoliths with reactive monomers for photografting by placing a section of wide bore PEEK tubing as a reservoir between the pump and the monolith. This technique removes the need to pump monomer solutions through the pump, reducing problems of contamination of monomer mixture and/or damage to the pump. The detector used was a TraceDec capacitively coupled contactless conductivity detector (Innovative Sensor Technologies GmbH, Innsbruck, Austria). The exact position of the detection cell along the length of the monolithic column was varied by hand, using a ruler as a position indicator. The monolithic column itself was passed through the radial capillary detector cell, which was programmed with the following settings: frequency, 2X HIGH; voltage, -0 dB; gain, 50% and offset, 0. Wash steps required for vinylisation of fused silica capillary were carried out using Knauer pump (Model K120). A GFL water bath was used for capillary vinylisation, and the operational temperature was 60  $^{\circ}\text{C}$ . A Labnet Spectrafuge centrifuge was used to eliminate particulate matter during the preparation of monomer solutions.

Photopolymerisation and photografting was carried out using a Spectrolinker XL-1000 UV crosslinker (Spectronics Corp., Westbury, NY, USA). The operational wavelength of this lamp was 254 nm with an irradiation intensity of 0 to 1 J cm<sup>-2</sup> possible per dose incident on the capillary/monolith.

#### 4.2.2 Reagents.

Butyl methacrylate (99%, BuMA), ethylene dimethacrylate (98%, EDMA), benzophenone (99+%, BP), 3-(trimethoxysilyl) - propyl methacrylate (98%), 2, 2-dimethoxy-2-acetophenone (99%, DAP) 1, 4-butanediol, 1-propanol, *tert*-butyl alcohol (99.5%) and 2-acrylamido-2-methyl-1-propanesulfonic acid (99 %, AMPS) were purchased from Sigma-Aldrich (Tallaght, Dublin, Ireland). Methanol was purchased from Labscan (Stillorgan, Dublin, Ireland). All other reagents were of the highest available purity and used as received without additional purification or distillation before use. UV transparent Teflon coated fused silica capillary (360 µm o.d. and 100 µm i.d.) was obtained from Polymicro Technologies (Phoenix, AZ). DI water was produced with a Millipore Direct-Q™ 5 (Millipore, Bedford, MA, USA) water purification system, and eluents were vacuum filtered through a 0.2 µm filter (Supelco, Supelco Park, Bellefonte, PA, USA) and degassed by sonication.

#### 4.2.3 Vinylisation of fused silica capillaries for monolith production.

A suitable length of Teflon-coated fused silica capillary (100 µm i.d.), was rinsed with acetone using a pump at 10 µL min<sup>-1</sup>, and dried in a stream of nitrogen for 10 minutes at room temperature. The inner walls of the capillary were then activated with 0.2 M sodium hydroxide for 30 minutes by pumping at 10 µL min<sup>-1</sup>. The capillary was then washed in the following order at 10 µL min<sup>-1</sup>: water for 5 minutes, 0.2 M HCl for 30 minutes, water for 5 minutes and finally with acetone for 5 minutes. After drying the capillary again with nitrogen gas, a 50 wt % solution of 3-(trimethoxysilyl) propyl methacrylate in acetone was prepared. A length of PEEK tubing, of 435 µL volume, was then filled with the solution using a disposable

syringe. One end of the filled loop was attached to the empty capillary, and the other end to the outlet of a piston driven pump delivering methanol at  $10 \mu\text{L min}^{-1}$ . The reagent was pumped through the capillary at  $10 \mu\text{L min}^{-1}$  until all air was expelled from the capillary and the entire capillary length was full of reagent. The capillary was then end-capped with pieces of rubber septa, and immersed in a water bath at  $60 \text{ }^\circ\text{C}$  for 20 hr. Finally, the monolith end-plugs were removed, the monolith was flushed with acetone to remove excess 3-(trimethoxysilyl) propyl methacrylate, and the monolith was dried with a stream of nitrogen and stored until required.

#### *4.2.4 Preparation of methacrylate monolithic capillary columns.*

A polymerization mixture was prepared comprising 24 % BuMA, 16 % EDMA, 34 % 1-propanol, 26 % 1, 4-butanediol, and 0.4 % DAP as free radical initiator (all w/w) [10]. The solution was sonicated for 20 minutes to dissolve the DAP. The supernatant was degassed by allowing nitrogen gas to bubble through the solution for 10 minutes. The de-aerated monomer solution was introduced by capillary action, and each end of the capillary again sealed with rubber septa. Photoinitiated polymerisation in the UV transparent Teflon-coated capillaries required  $2 \text{ J cm}^{-2}$  using a Spectrolinker XL-1000 UV Crosslinker. After removing the seals, the monoliths were flushed with methanol at a flow rate of  $1 \mu\text{L min}^{-1}$  for 30 minutes to remove porogen and unreacted monomer using the HP 1050 pump with split flow.

#### *4.2.5 Photografting of porous methacrylate monoliths with 2-acrylamido-2-methyl-1-propanesulfonic acid (AMPS).*

A mixture comprising 15 wt % AMPS and 0.22 wt % benzophenone in a solvent mix comprising 75/25 t-butanol/water was prepared and vortexed vigorously to dissolve the benzophenone and AMPS [3]. After centrifuging at 13,000 r.p.m for 10 minutes, the supernatant was degassed with nitrogen for 10 minutes. The de-

aerated solution was pumped through the methacrylate monolith to completely fill the pores using the PEEK loop and pump as per Section 4.2.1. The photomask used for production of photografted monoliths was PEEK microtight sleeves (Upchurch Scientific, WA, USA) of 0.25" outer diameter and 0.0155" internal diameter. Sleeves were placed onto monoliths and secured with insulating tape to a black cardboard backing to allow placement of sleeves along the capillary monoliths and their subsequent movement within the UV oven, regions not to undergo photografting were covered with black cardboard to reduce the risk of unintended photografting. Figure 4.3 depicts the set-up used in photografting. The monolith was then end-capped with rubber septa and photo-grafting was achieved by irradiating the monolith through a number of precisely positioned PEEK photo-masks (of approximately 10 mm in length) at a wavelength of 254 nm for the required time to deliver the prescribed energy dose. In this study four monoliths were produced, the photografting of each monolith is detailed below in Table 4.1.

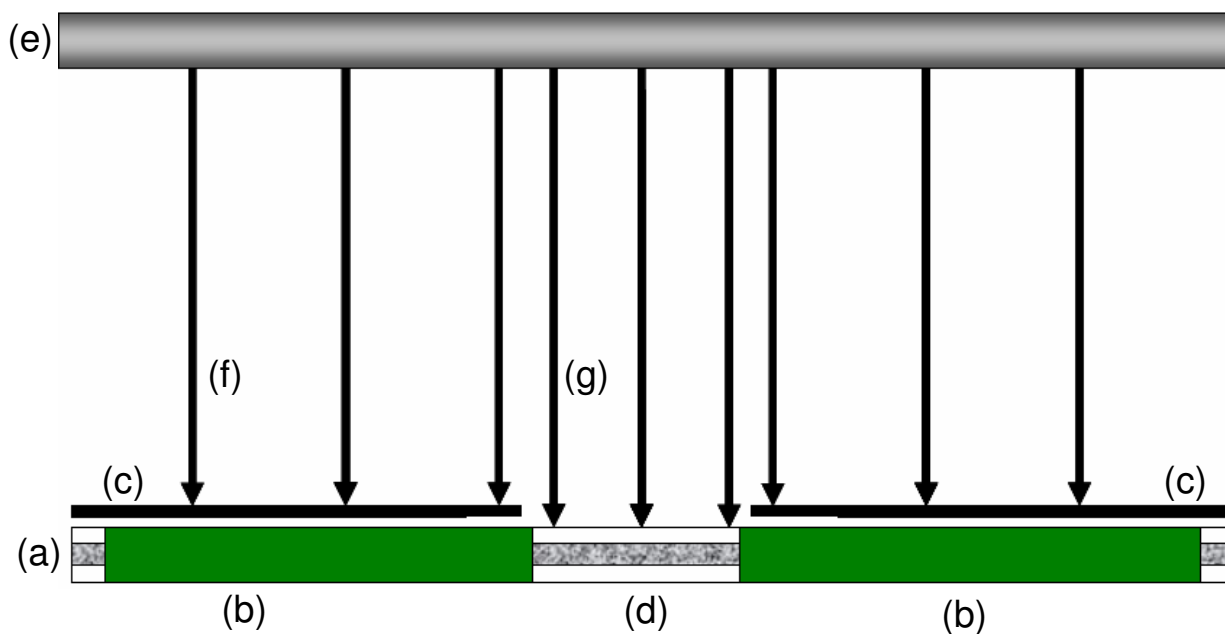


Figure 4.2: Set-up used for photografting of AMPS onto monolith surface, (a) monolith, (b) PEEK sleeves as masks, (c) cardboard covers, (d) area to be photografted (ca. 10 mm), (e) light source, (f) light blocked from initiating photografting, (g) light permitted to initiate photografting.

Table 4.1: The number of zones and the respective energy used to photograft each zone.

Monolith	Zones	Energy delivered ( $\text{J cm}^{-2}$ )	Holder
#1	3	1, 3, 5	A
#2	3	1, 3, 5	A
#3	5	1, 2, 3, 4, 7	B
#4	3	0.25, 0.5, 1	B

#### *4.2.6 Verification of the presence of charged groups on functionalised monoliths using C<sup>4</sup>D.*

While pumping water through the functionalised monolith at 1  $\mu\text{L min}^{-1}$ , the detection cell was physically scanned across the length of the monolith at 1 mm increments to allow the detection of localised regions of charge within the monolithic stationary phase. The conductivity value (reported as mV) at each mm location along the monolith was recorded. For each monolith prepared a baseline value was obtained before photografting with AMPS was carried out.

#### *4.2.7 Holder used for photografting.*

Photografting was carried out inside two in-house made holders, designed to reduce the amount of high angle incident UV light onto the capillary. As the UV oven does not operate with a collimator (as is commonly used for photografting of monoliths), light of high and low angle of incidence are created. UV transparent capillary can act as wave guide much the same way as a fibre optic cable, causing the UV light to move along the length of capillary and induce photografting beyond the un-masked region (Figure 4.3). This phenomenon has been reported for use in liquid core waveguide arrangements, with Teflon coated capillary being used in particular [11].

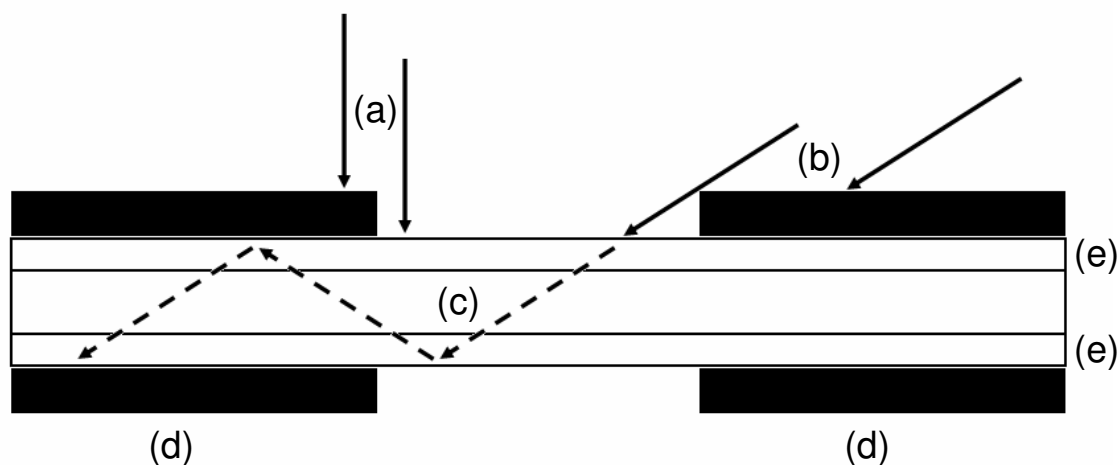


Figure 4.3: Wave-guide effect of FSC. Showing (a) perpendicular light, (b) high angle light, (c) high angle light undergoing total internal reflection and propagating along monolith, inducing photografting beyond mask, (d) PEEK sleeves, (e) capillary wall.

In an attempt to limit the high and low angle light incident on the monolith during photografting a holder was produced. This photografting holder consisted of a square tunnel “chimney” that reached almost to the UV light source. The chimney did not permit high or low angle UV light to reach the monolith within the holder, thus reducing the risk of photografting beyond the area intended. A schematic of the holder used is given in Figure 4.4. Monoliths # 1 and # 2 were prepared using an in house made holder with one chimney (A) allowing one zone to be photografted at a time, Monolith # 3 and # 4 were photografted using an in-house made holder with six chimneys (B) allowing for the photografting of multiple zones simultaneously.

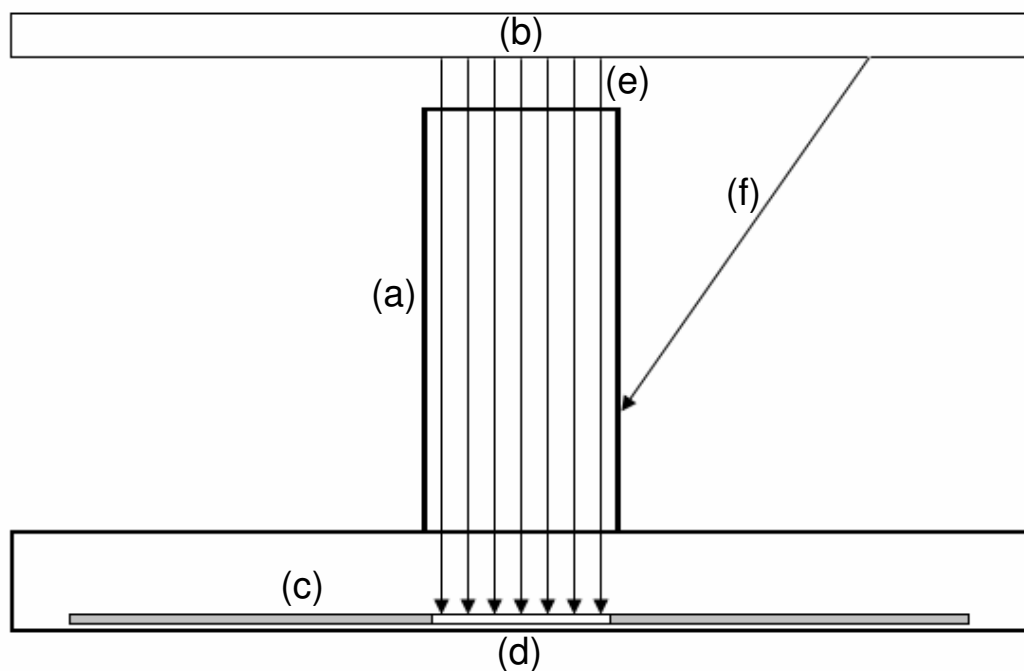


Figure 4.4: Schematic of in-house built photografting holder. (a) “Chimney” to allow only perpendicular and low angle light to enter, (b) UV lamp, (c) monolith to be photografted, (d) area to be photografted, (e) perpendicular UV light and (f) high angle UV light being blocked.

#### 4.2.8 Washing of photografted monoliths.

The monoliths produced were subjected to wash cycles to remove the excess ungrafted AMPS from the pores and the regions of photografting. The wash cycles are summarised in Table 4.2. All wash steps were carried out at flow rate of  $1 \mu\text{L min}^{-1}$ . After each column was washed with DI water, a second short methanol wash was performed to ensure the removal of AMPS from the photografted zones.

Table 4.2: Wash cycle of photografted monoliths.

Monolith	Methanol (hr)	DI Water (hr)	Methanol (hr)
# 1	3	24	1
# 2	14	24	1
# 3	3	72	1
# 4	3	72	1

### 4.3 Results and discussion.

Monoliths of BuMA/EDMA were chosen for use in this study as they have previously been used for the photografting of AMPS [1, 3, 8] and the production of BuMA/EDMA monoliths has also been well characterised in literature [10].

#### 4.3.1 Washing of photografted monoliths.

Monolith # 1 was photografted as per Table 4.1 and was subjected to a wash cycle that consisted of a short methanol wash followed by a long water wash (Table 4.2). Once the wash solvent was changed to water and scanning the C<sup>4</sup>D cell along the monolith, the methanol wash was found to have successfully removed the excess photografting solution from the pores of the monolith. However, the response of Zone 3 increased in value to the point where it was off scale for the detector setting used (Figure 4.5 (i)), after which it decreased in value. As Zone 3 of Monolith # 1 decreased it exhibited frontal chromatographic behaviour (Figure 4.5 (ii)), with the zone decreasing starting with the edge nearest the monolith inlet until Zone 3 reached stable readings (Figure 4.5 (iii)  $n=3$ ). Figure 4.6 shows an expanded view of this frontal chromatographic washing on Zone 3. Zones 1 and 2 were found to decrease slightly to stable readings ( $n=3$ ); however, no frontal chromatographic behaviour was observed.

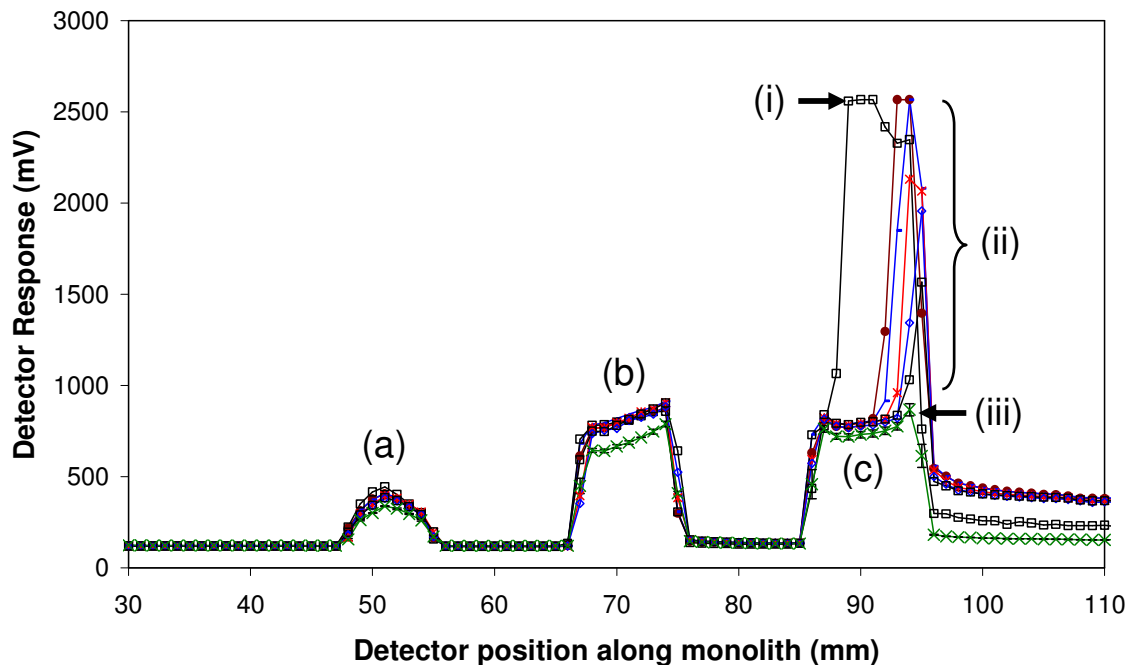


Figure 4.5:  $C^4D$  scan of Monolith # 1 showing the presence of three photografted zones of AMPS. (a) Zone 1, (b) Zone 2, (c) Zone 3, (i) starting position of Zone 3, (ii) excess AMPS washing from Zone 3, (iii) final reading of Zone 3 ( $n=3$ ) .

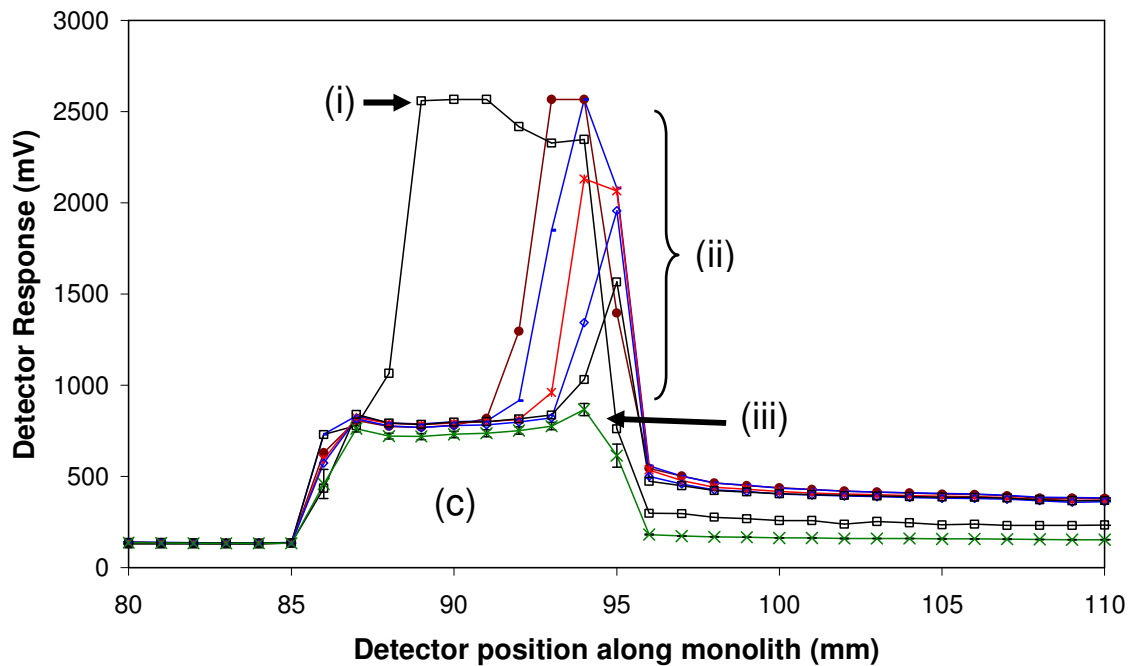


Figure 4.6: Expanded view of Figure 4.5, (c) Zone 3, (i) starting position of Zone 3, (ii) excess AMPS washing from Zone 3, (iii) final reading of Zone 3 ( $n=3$ ) .

Once Zone 3 stabilised, a second short methanol wash was carried out to investigate if any further AMPS could be removed, this resulted in a decrease of all three zones by approximately 10% for Zone 1, to stable readings (Figure 4.7 ( $\text{---}\triangle\text{---}$ )  $n=3$ ). This drop in signal after the methanol wash may have been due to collapse of the butylmethacrylate/AMPS phase in an aqueous environment resulting in free AMPS being trapped leading to a slightly higher signal (Figure 4.8). All subsequent monoliths were subjected to this additional methanol wash step, but data was not collected.

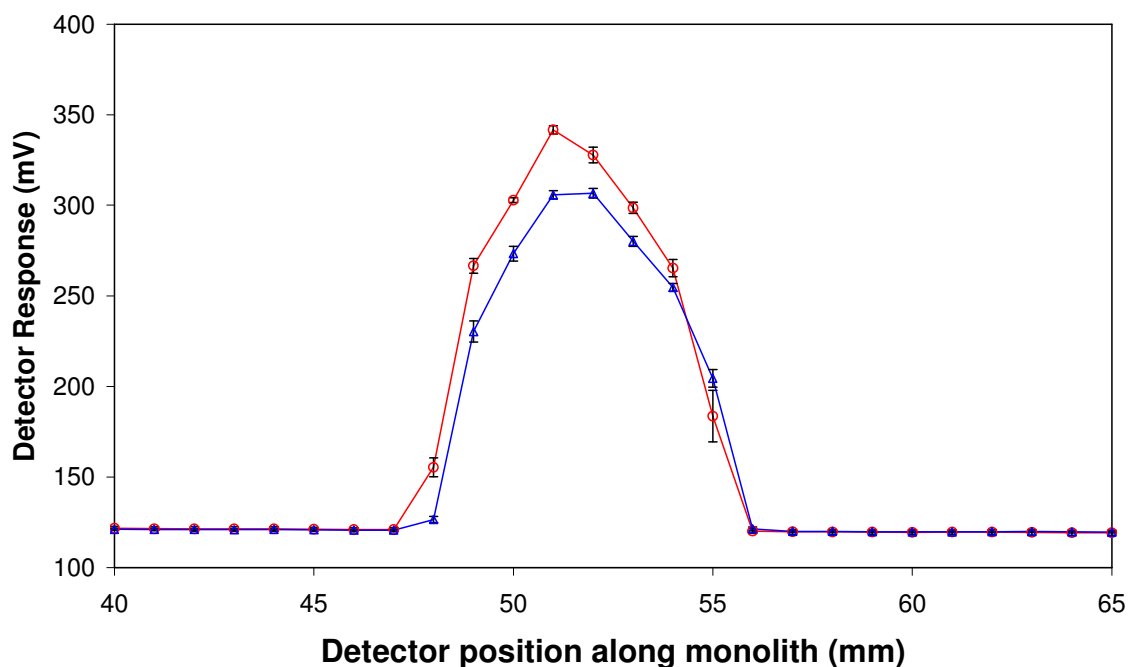


Figure 4.7: Effect of short methanol wash on Zone 1 of Monolith # 1, showing a ca. 10% decrease in signal from before short methanol wash ( $\text{---}\circ\text{---}$ ) and after short methanol wash ( $\text{---}\triangle\text{---}$ ),  $n=3$ .

To investigate the reproducibility of the photografting technique used, a second monolith (i.e. Monolith # 2) was photografted in an identical manner to Monolith # 1. During the wash step of Monolith # 2 the frontal chromatographic washing of excess AMPS from the column was more rigourously studied. Monolith # 2 was subjected to a long methanol wash followed by a long water wash (Table 4.2); the longer methanol wash (14 hr) failed to remove the excess AMPS from the photo-

grafted zones, but as before removed all excess AMPS from the pores of the unmodified zones. The water wash resulted in the increase in the signal for all zones, with frontal chromatographic behaviour on Zones 2 & 3. Figure 4.8 shows the washing of Monolith # 2 in a 3D-surface plot, clearly showing the frontal chromatographic nature of the washing of AMPS from the Zones 2 and 3.

The fact that an extended methanol wash did not result in a greatly reduced wash cycle is possibly as a result of the retention of free AMPS by hydrophilic or ionic interactions within the photografted AMPS zones.

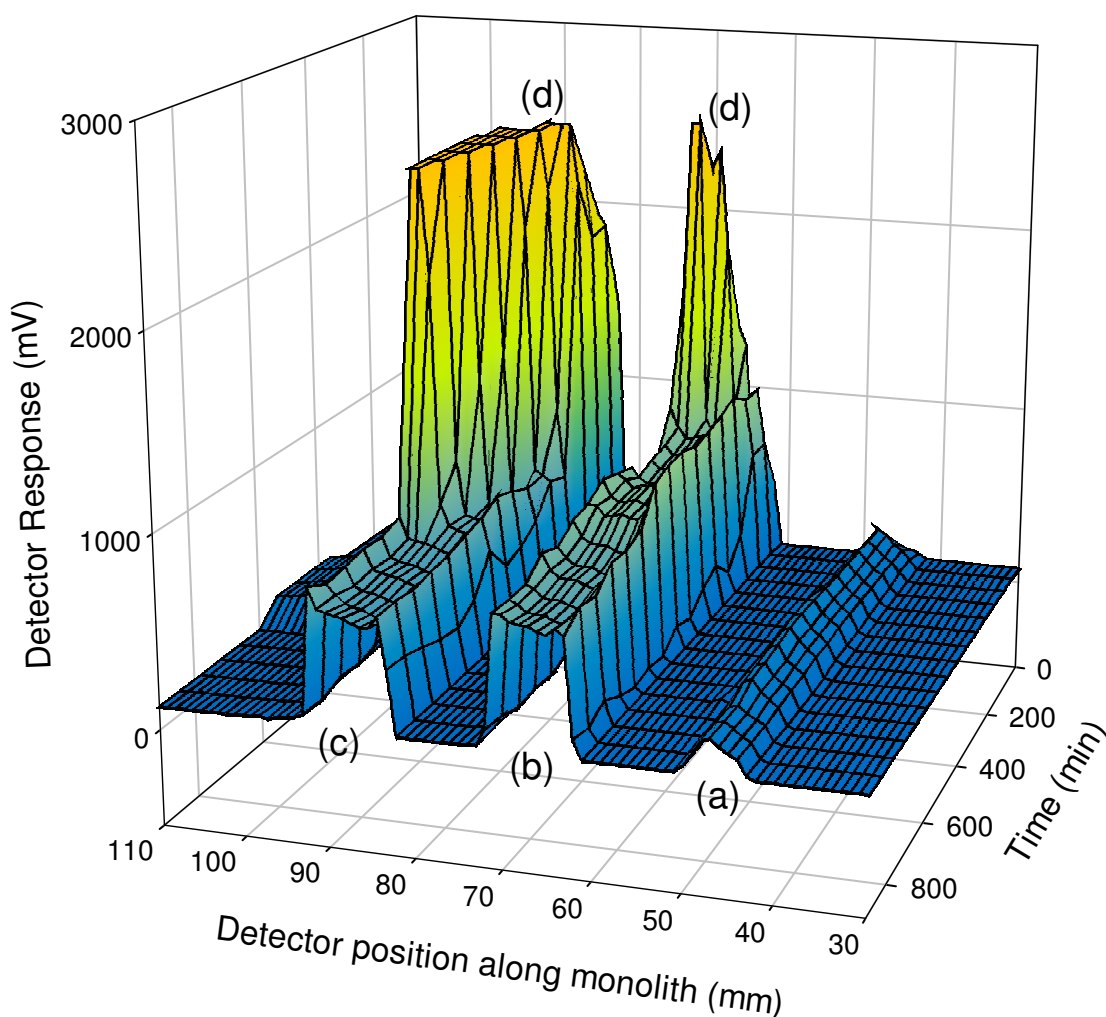


Figure 4.8: 3D-plot of washing of Monolith # 2. (a) Zone 1, (b) Zone 2, (c) Zone 3, (d) washing of excess AMPS in frontal chromatographic nature.

The water wash step for Monolith # 3 and 4 was not investigated based on the results of Monolith # 1 and 2 a short methanol wash followed by a extended water wash was used to remove AMPS from the pores of the monolith and the non-covalently bound AMPS associated with the photografted zones.

#### 4.3.2 Spatial location and accuracy of photografting procedure.

Taking Monolith # 1 and measuring the size of each zone the tolerances of the photografting procedure were investigated. The masks used for the photografting were placed in a manner such as to give three zones of 10 mm separated by 10 mm. Using the scan of Monolith # 1 the spatial locations of the AMPS zones was found to meet the expected results, with an average zone size of 10 mm ( $\pm 1$  mm) and the separation of the zones was 9.5 mm ( $\pm 0.7$  mm) see Figure 4.9. The close fit with the expected results show the advantage of C<sup>4</sup>D as a method for investigating the spatial location and the effectiveness of masks used in the grafting procedure.

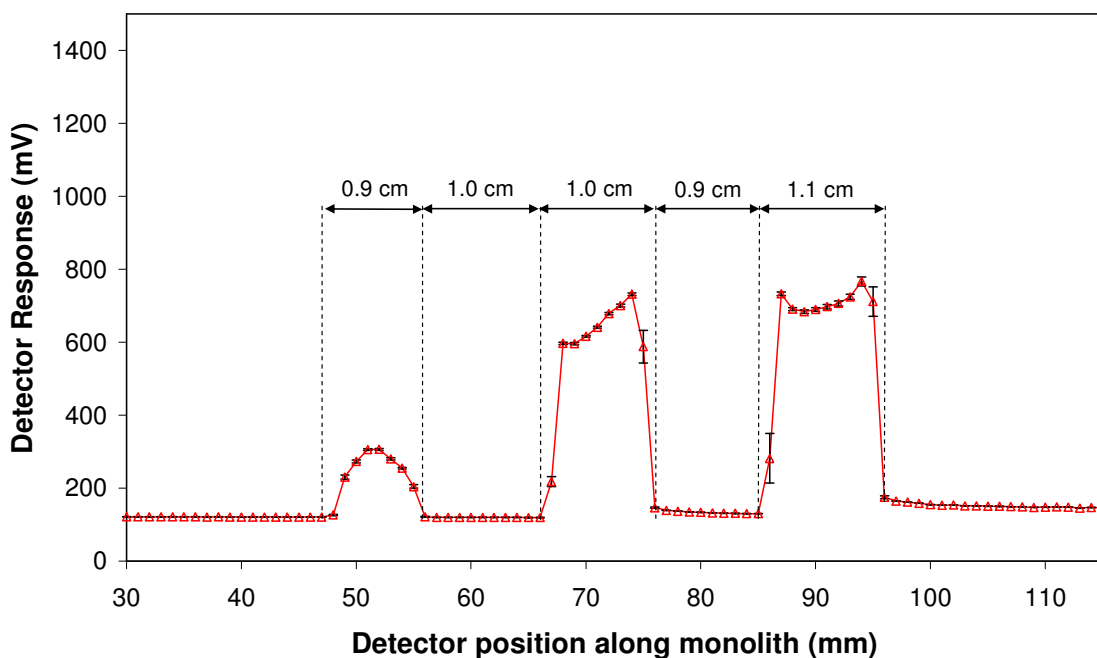


Figure 4.9: C<sup>4</sup>D profile showing the spatial tolerances obtained during photografting ( $n=3$ ) for Monolith # 1.

#### 4.3.3 Comparison of Monolith # 1 and Monolith # 2 using $C^4D$ response.

Once stable readings for the photo-grafted zones were obtained, the final responses of the zones could be compared (Figure 4.10). On both monoliths the same overall trend was observed, Zone 1 ( $1 \text{ J cm}^{-2}$ ) showed the lowest response and exhibited a bell shaped like profile, Zones 2 & 3 showed much higher response than Zone 1. Rohr *et al.* observed similar results using fluorescence microscopy of Rhodamine 6G immobilised via VAL, where under low irradiation conditions the intensity of the graft dissipated towards the edges of the mask [6]. However, with higher irradiation conditions clear edges perpendicular to the capillary axis were found. The responses of Zone 2 & 3 were similar in magnitude, showing much less difference than between both zones and Zone 1.

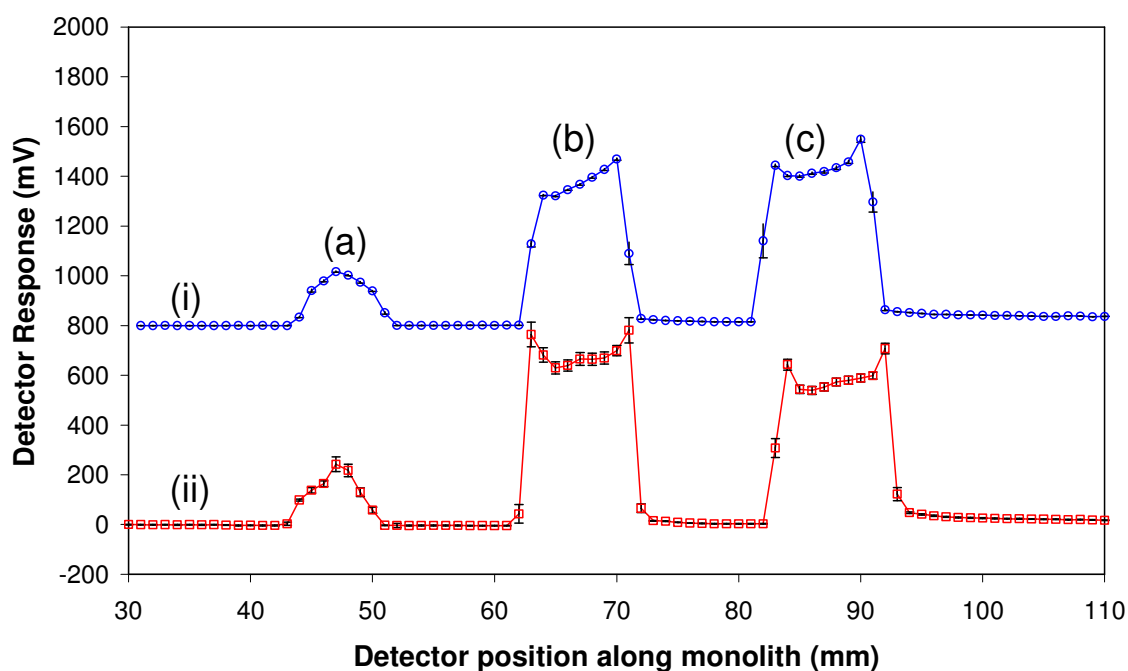


Figure 4.10: Comparison of Monolith # 1 (i) & # 2 (ii) after wash cycles, (a) Zone 1 ( $1 \text{ J cm}^{-2}$ ), (b) Zone 2 ( $3 \text{ J cm}^{-2}$ ) and (c) Zone 3 ( $5 \text{ J cm}^{-2}$ ). Each scan is an average of triplicate reading (errors bars equal to standard deviation).

#### *4.3.4 Calibration of photografted zones (Monolith # 3 and 4).*

It can clearly be seen from Section 4.4.2 and 4.4.3 that C<sup>4</sup>D allows for not only the spatial location of the zones to be investigated but also the extent of photografting. To further investigate this advantage two more columns were fabricated with zones of photografted AMPS receiving different UV energies. From these columns it was possible to construct a calibration curve of photografting using their C<sup>4</sup>D response with respect to the UV energy used to initiate the graft.

Zones of AMPS were photografted onto Monolith # 3 with UV doses of 1, 2, 3, 4 and 7 J cm<sup>-2</sup> (Zones 1, 2, 3, 4 and 5 respectively, see Table 4.1). Washing was carried out as previously described in Table 4.2. The resulting monolith was found to have five discrete zones of AMPS photografted onto it. The zones with AMPS photografted onto them showed a similar trend to that seen in Monoliths # 1 and 2, i.e. zone 1 (1 J cm<sup>-2</sup>) showed the lowest response and exhibited a bell shaped like profile, Zones 2 to 5 showed much higher responses than Zone 1. However, the difference in signal for Zone 2 to 5 was much less than for Zone 1 to 2. Figure 4.11 shows the profile of Monolith # 3 which is an average of three replicate readings.

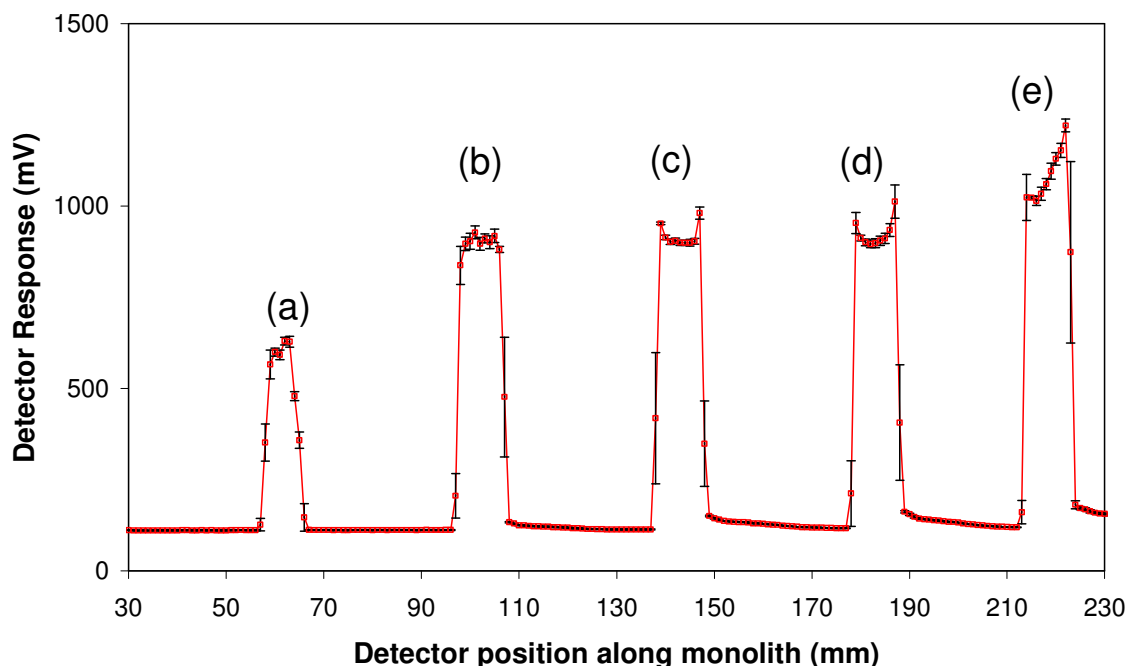


Figure 4.11: Monolith # 3, showing five zones of photografted AMPS. (a) Zone 1 ( $1 \text{ J cm}^{-2}$ ), (b) Zone 2 ( $2 \text{ J cm}^{-2}$ ), (c) Zone 3 ( $3 \text{ J cm}^{-2}$ ), (d) Zone 4 ( $4 \text{ J cm}^{-2}$ ) and (e) Zone 5 ( $7 \text{ J cm}^{-2}$ ).

Monolith # 4 was photografted with three zones of  $0.25$ ,  $0.5$ , and  $1 \text{ J cm}^{-2}$  of UV energy. The zones that received  $0.25$  and  $0.5 \text{ J cm}^{-2}$  of UV showed no evidence of photografting having occurred whereas the zone receiving  $1 \text{ J cm}^{-2}$  of UV energy resulted in photografting, see Figure 4.12. The regions of Monolith # 4 where the grafting of  $0.25$  and  $0.5 \text{ J cm}^{-2}$  was expected are highlighted in Figure 4.12, at  $50$  to  $60 \text{ mm}$  ( $0.25 \text{ J cm}^{-2}$ ) and  $80$  to  $90 \text{ mm}$  ( $0.5 \text{ J cm}^{-2}$ ), and it can be clearly seen that no photografting measurable by  $\text{C}^4\text{D}$  was observed. The response for Zone 3 of Monolith # 4 was to be  $106\%$  of that of Monolith # 3 receiving the same  $\text{J cm}^{-2}$  (Zone 1), when calculating the area below the photografted zones (Figure 4.13; Monolith #3 =  $3500 \text{ mm.mV}$ , Monolith # 4 =  $3720 \text{ mm.mV}$ ) showing good column-to-column reproducibility.

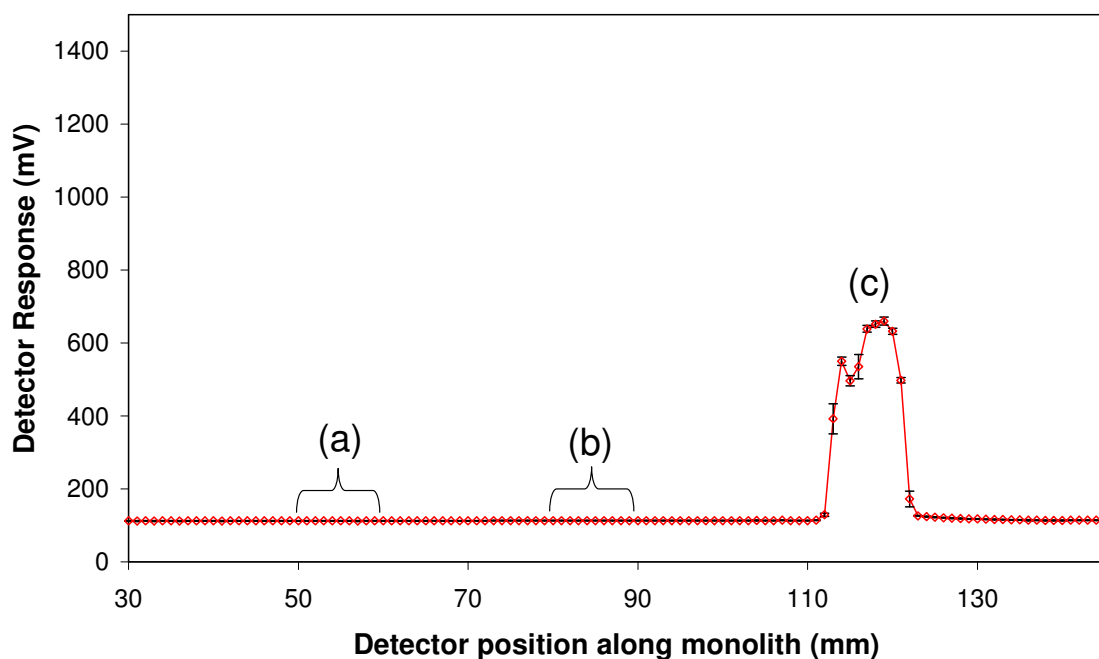


Figure 4.12: Monolith # 4, showing one zone of photografted AMPS ( $n=3$ ). (a) Zone 1 ( $0.25 \text{ J cm}^{-2}$ ), (b) Zone 2 ( $0.5 \text{ J cm}^{-2}$ ) and (c) Zone 3 ( $1 \text{ J cm}^{-2}$ ).

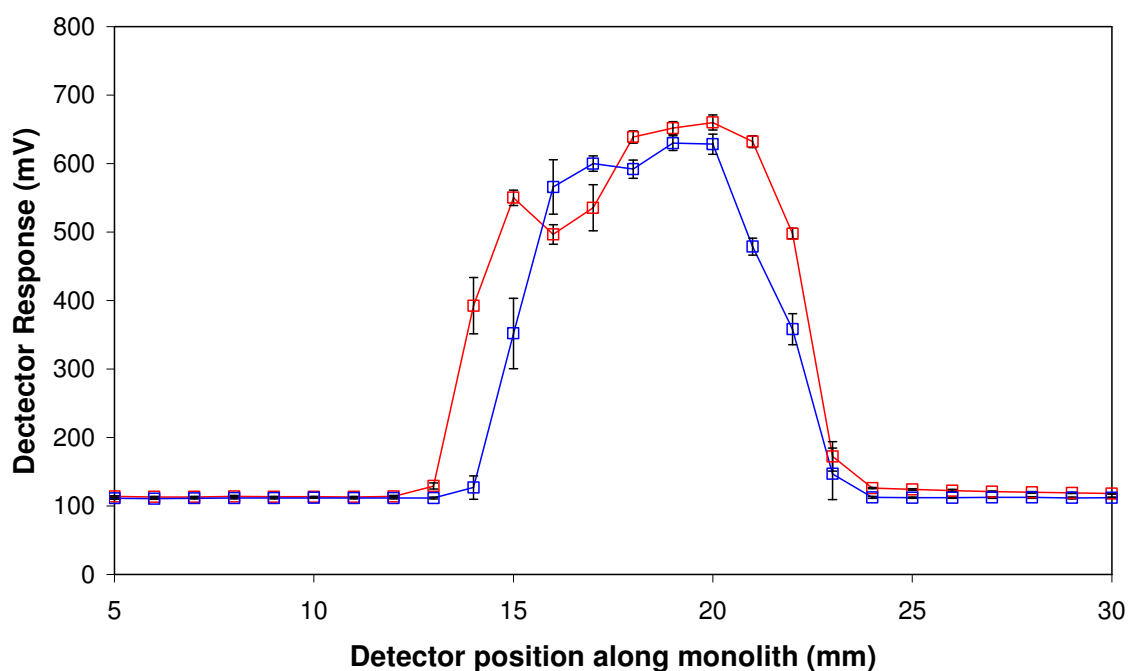


Figure 4.13: Comparison of Zone 1 (receiving  $1 \text{ J cm}^{-2}$  of UV energy) for Monolith # 3 ( $\square$ ) and Monolith # 4 ( $\square$ ) ( $n=3$ ).

(it should be noted that the difference in the height of the AMPS zones between Monolith # 1 and # 2 with Monolith # 3 and # 4 is due to the difference in the geometry of the in-house made photographing holders used for these monoliths allowing more incident UV light and therefore affecting the amount of photografted AMPS).

Using the maximum zone height for each zone (Figure 4.11 and 4.12) the area of the zone a calibration curve of the amount of AMPS photografted per amount of UV energy incident on the capillary can be constructed. From Figure 4.14 it can be seen that there is a minimum amount of UV energy required to initiate the graft, 0.5 to 1 J cm<sup>-2</sup>, after which the amount of AMPS grafted increases dramatically until 2 J cm<sup>-2</sup>, after which the increase per amount of UV energy levels off. From 4 to 7 J cm<sup>-2</sup> of UV energy the increase is only 10-20%. The trend observed in the Figure 4.14 is similar to that seen in Eeltink *et al.* using the measurement of electroosmotic mobility as an indirect means of evaluating graft density [5].

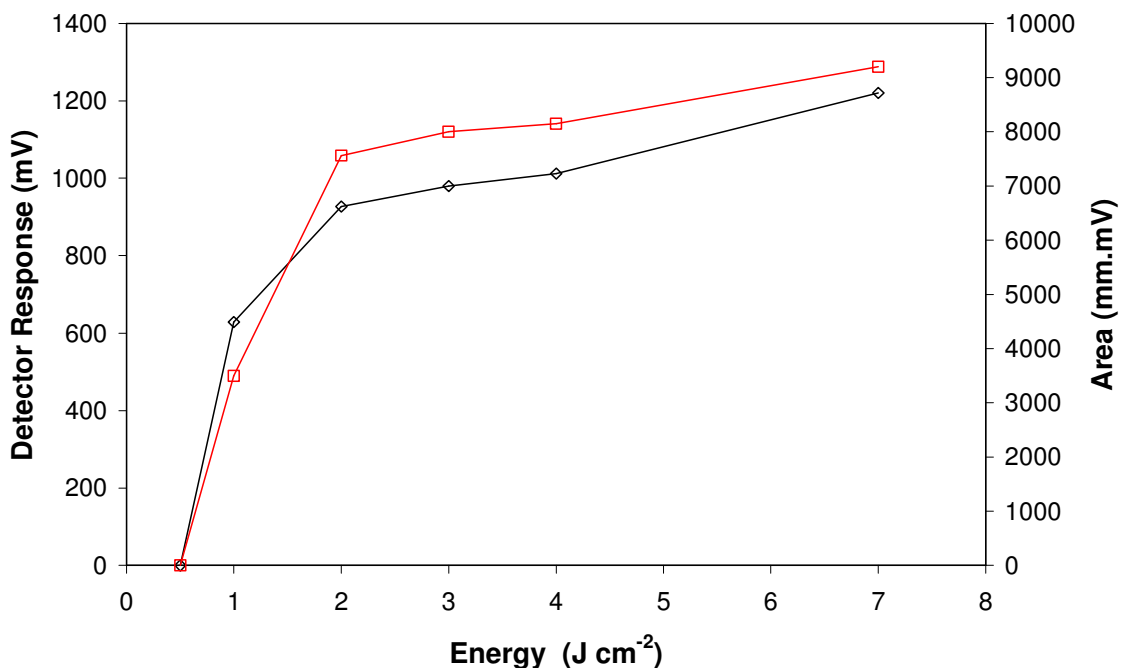


Figure 4.14: Effect on UV energy used to photograft on (—◇—) zone height and (—□—) area of zone.

#### 4.4 Conclusion.

The investigation of the effect of photografting on  $C^4D$  response has been clearly shown. The non-contact and non-invasive manner of  $C^4D$  permitted repeated scans of the modified columns, allowing for the wash cycle to be characterised. It was found that the methanol wash to remove free AMPS from the monolith after photografting was only successful in removing AMPS from the pores of the unphotografted regions of the monolith. However, once the monolith was washed with water excess AMPS was seen to wash from the photografted zones only, possibly due to ionic or hydrophilic interactions.

The response of the photografted zones was found to show a dependence on the amount of UV energy used to initiate the graft. From the trend it was possible to construct a semi-quantitative calibration curve of  $C^4D$  response (and therefore capacity) as a function of UV energy. The calibration curve indicates that a minimum energy is required to initiate the photograft, having a value between 0.5 and 1 J cm<sup>-2</sup>.

The ability not only to visualise the presence and location of photografted zones, but also to semi-quantitatively characterise the capacity, opens up the possibility to use  $C^4D$  to characterise other characteristics of photografted zones (e.g. physio-chemical properties such as  $pK_a$ ) directly on-column.

#### 4.5 References.

- [1] E.F. Hilder, F. Svec, J.M.J. Frechet, J. Chromatogr. A, 2004, **1053**, 101.
- [2] Y. Ueki, T. Umemura, J. Li, T. Odake and K. Tsunoda, Anal. Chem., 2004, **76**, 7007.
- [3] D. Connolly, V. O'Shea, P. Clark, B. O'Connor and B. Paull, J. Sep. Sci., 2001, **30**, 3060.
- [4] D.S. Peterson, T. Rohr, F. Svec and J.M.J Frechet, Anal. Chem., 2003, **75**, 5328.
- [5] T.B. Stachowiak, F. Svec and J.M.J Frechet, Chem. Mater., 2006, **18**, 5950.
- [6] T. Rohr, E.F. Hilder, J.J. Donovan, F. Svec, J.M.J. Frechet, Macromolecules, 2003, **36**, 1677.
- [7] O.G. Potter, M.C. Breadmore and E.F. Hilder, Analyst, 2006, **131**, 1094.
- [8] V. Pucci, M.A. raggi, F. Svec and J.M.J. Frechet, J. Sep. Sci., 2004, **27**, 779.
- [9] S. Eeltink, E.F. Hilder, L. Geiser, F. Svec, J.M.J. Frechet, G.P. Rozing, P.J. Schoenmakers, W. T. Kok, J. Sep. Sci., 2007, **30**, 407.
- [10] L. Geiser, S. Eeltink, F. Svec, J.M.J Frechet, J. Chromatogr. A, 2007, **1140**, 140.
- [11] P.K. Dasgupta, Z. Genfa, S.K. Poruthoor, S. Caldwell, S. Dong, S.Y. Liu, Anal. Chem., 1998, **70**, 4661.

---

**Chapter 5: Accurate non-invasive determination of  $pK_a$  of immobilised functional groups on polymeric monoliths using capacitively coupled contactless conductivity detection.**

---

“Mistakes are the portals of discovery”

James Joyce

## 5.1 Introduction.

As previously discussed, the production of new monolithic stationary phases in capillary formats has generated considerable interest over the past decade, with the production of a variety of phases ranging from ion exchange [1-8] to affinity-based monoliths [9]. However, once the column has been produced, characterisation of the stationary phase within the column can pose a significant challenge [10], often requiring invasive and destructive methods for chemical and physical characterisation [10, 11].

As the previous Chapters have shown, C<sup>4</sup>D is a technique that affords the rapid and non-invasive profiling of the spatial and temporal distribution of semi-permanently coated ionic surfactants along the length of a single C<sub>18</sub> silica capillary monolith for CapIC (see Chapter 3). Later, the same procedure was further developed to allow for the evaluation of photografted ionic species and proteins within polymeric capillary columns (Chapter 4) [12]. These studies have clearly demonstrated that C<sup>4</sup>D is a useful tool for the non-invasive, non-destructive and non-contact characterisation of capillary columns, whether they are semi-permanently or covalently modified.

The previous examples of semi-permanently or covalently modified monolithic columns (Chapter 3 & 4) have involved the use of species that are ionised to the same extent across the entire pH range, i.e. strong acids (DOSS and AMPS). The ability to characterise ionisable species immobilised onto the surface of polymer monoliths is another avenue that C<sup>4</sup>D can be applied to. Weak acid/base character stationary phases have strong pH dependant selectivity, due to a change in their ionisation state. Two stationary phase chemistries that have such ionisation character are boronic acids and aminopolycarboxylates.

The ability to modify the surface chemistry of polymeric monoliths has been discussed previously (Chapter 1) and among the possible functional groups that can be utilised for such modification is vinyl azlactone (VAL). VAL is a vinyl monomer that can easily be photografted onto the surface of a polymer monolith,

and will then react to covalently bond amine containing species to the surface (Figure 5.1 (a)). In the work presented here, VAL is exploited to immobilise three functionalities onto the surface of a methacrylate-based monolith; a boronic acid and two aminopolycarboxylates.

The ability of boronic acids to form complexes with 1, 2 and 1, 3-*cis*-vicinal-diol functionalities at high pH, with the subsequent dissociation of the complex at low pH, has been utilised for the preferential capture of glycoprotein over non-glycosylated protein [13], the separation of nucleosides [9] and for extraction of sugars [14]. The primary mechanism involves shifting the pH above 8.5, which promotes the conformational change of the boronic acid group from the planar to the tetrahedral form. In this form the boronic acid anion is well known to selectively retain molecules with 1, 2- and 1, 3-*cis*-vicinal diol moieties via the reversible formation of cyclic anionic esters [9, 13, 14]. 1, 2- and 1, 3-*cis*-vicinal diol moieties are present on carbohydrates and subsequently the glycan region of glycoproteins giving the selectivity of boronic acids for glycoproteins. As illustrated in Figure 5.1 (b), the transition from the planar to the tetrahedral form is accompanied by a change in charge on the boronic acid functional group.

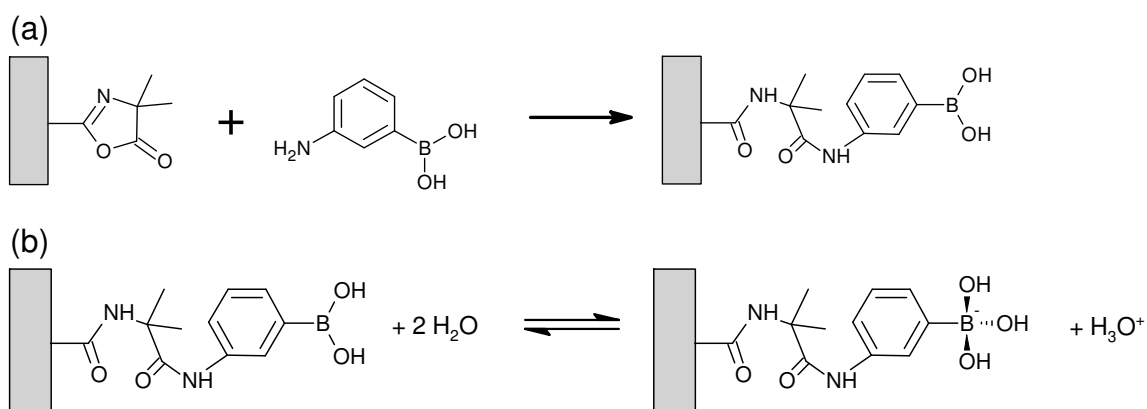


Figure 5.1: Schematic representation of (a) the reaction of azlactone and *m*-aminophenylboronic and (b) the transition of planar boronic acid to a tetrahedral boronic acid anion under high pH conditions.

Aminopolycarboxylates are compounds such as iminodiacetic acid (IDA) and ethylenediaminetetraacetic acid (EDTA). The main functional group of these molecules is an amine with two or more carboxylate groups attached. Iminodiacetic acid stationary phases have previously been used for the separation of transition metals [15-22] and are used in immobilised metal affinity chromatography (IMAC) [23-25]. IDA is a tridentate ligand with the diacetic acid group along with the lone pair on the amine allowing for the complexation of transition metals (e.g. copper). Separations of transition metals on IDA phases are typically carried out at acidic pH in high ionic strength buffers. Salts (e.g. KCl and  $\text{KNO}_3$ ) are included in the mobile phase to suppress ion exchange equilibrium such that chelation is the predominant retention mechanism.

As shown in Chapter 4, the spatial location of photografted zones can be easily evaluated by  $\text{C}^4\text{D}$ . The  $\text{C}^4\text{D}$  response is due to several contributions. These contributions are the silica capillary itself, the monolith and the eluent. The same contributions are present in regions of photografting, with the added contribution of the photografted functional groups (Figure 5.2 (a)). The  $\text{C}^4\text{D}$  response of a strong acid functional group will be fixed for all conditions used. However, if the functional group is ionisable, the conductivity response of the photografted zone will change with a variation of pH (Figure 5.2 (b)). By comparing the  $\text{C}^4\text{D}$  response of the photografted zone with that of the un-photografted monolith, the extent of ionisation can be investigated (Figure 5.2 (c)). Through monitoring of the  $\text{C}^4\text{D}$  response (i.e. the conductivity and therefore the ionisation) of photografted zones, the  $\text{p}K_{\text{a}}$  of the immobilised functional group can therefore be determined directly on-column.

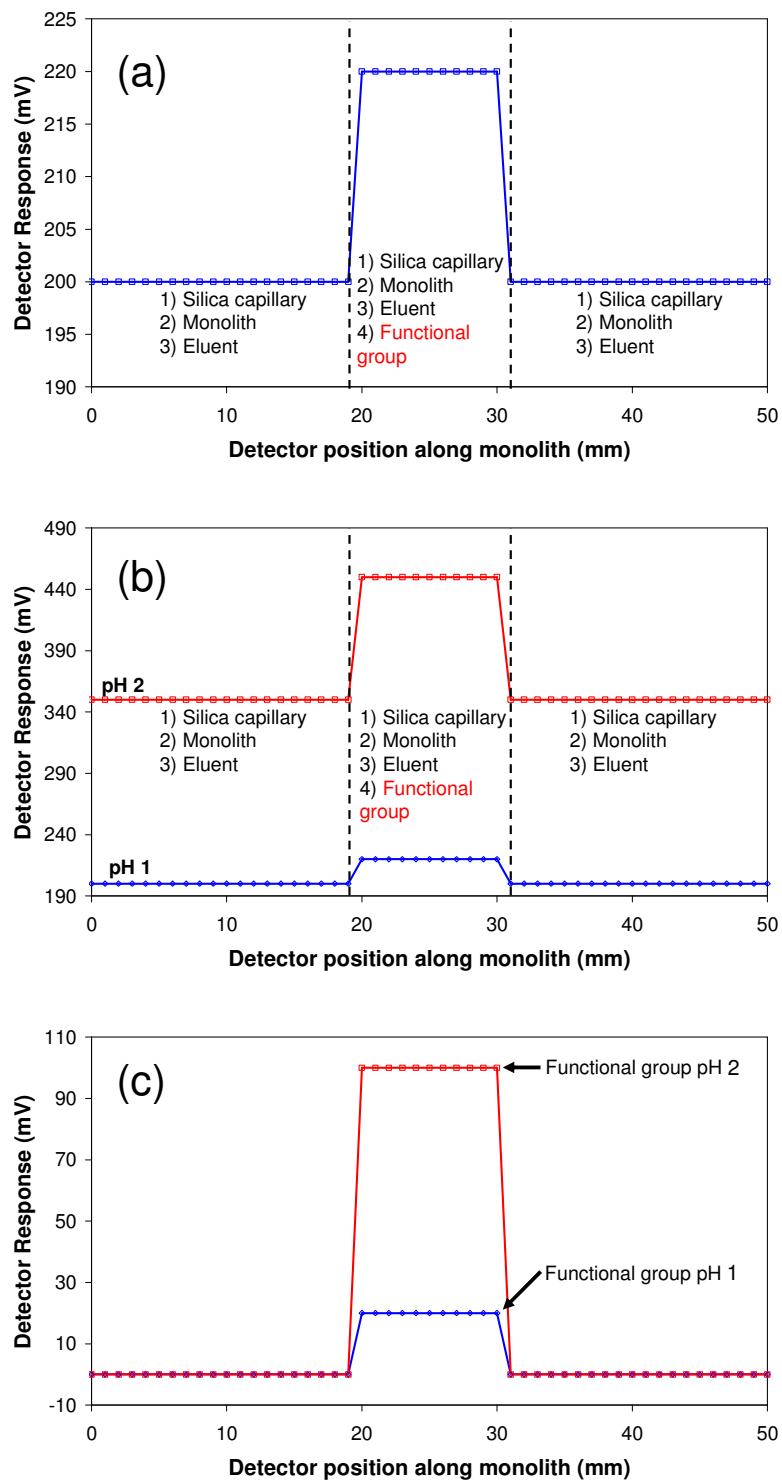


Figure 5.2: (a) Contributions of C<sup>4</sup>D signal of a photografted zone at two pH values, (b) contributions to C<sup>4</sup>D signal of a photografted zones and (c) background subtracted signal for a photografted zone at two pH values.

In this Chapter, for the first time C<sup>4</sup>D is utilised to characterise a novel immobilisation strategy for *m*-aminophenylboronic acid and two aminopolycarboxylates onto the surface of pre-formed polymeric monolith phases within capillary columns. Using the height of the immobilised zones(s) over a pH range, the pH dependant behaviour of the immobilised species is investigated. The ability to non-invasively characterise the pH dependence of immobilised boronic acid and aminopolycarboxylate functionalities allows for a better understanding of the processes involved in their use as stationary phases. The study also has implications for the characterisation of any capillary monolithic column containing weakly acidic or basic functional groups resulting in a strongly pH-dependant ion-exchange capacity of the stationary phase.

## 5.2 Experimental.

### 5.2.1 Instrumentation.

As per Section 4.2.1. The detector used was a TraceDec capacitively coupled contactless conductivity detector (Innovative Sensor Technologies GmbH, Innsbruck, Austria). The monolithic column itself was passed through the radial capillary detector cell, which was programmed with the following settings: frequency, 2X HIGH; voltage, 0 dB; gain, 50% and offset, 0. Regression analyses of the results obtained were carried out using Sigma Plot v8.1.

### 5.2.2 Reagents.

Butyl methacrylate (99%, BuMA), ethylene dimethacrylate (98%, EDMA), benzophenone (99+%, BP), poly(ethylene glycol) methacrylate (M<sub>n</sub> 360, 99%, PEGMA), 3-(trimethoxysilyl)- propyl methacrylate (98%), *m*-aminophenylboronic acid hemisulfate salt (> 97.0 %, APBA), 2,2-dimethoxy-2-acetophenone (99%, DAP) 1,4-butanediol, *tert*-butyl alcohol (99.5%), iminodiacetic acid (> 98%, IDA) and N-(2-acetamido)iminodiacetic acid (> 98%, ADA) were purchased from

Sigma-Aldrich (Tallaght, Dublin, Ireland). 2-vinyl-4,4-dimethylazlactone (vinyl azlactone, VAL) was purchased from TCI Europe (Boerenveldseweg, Belgium). Methanol was purchased from Labscan (Stillorgan, Dublin, Ireland). All other reagents were of the highest available purity and used as received without additional purification or distillation before use. UV transparent Teflon coated fused silica capillary (100  $\mu\text{m}$  i.d.) was obtained from Polymicro Technologies (Phoenix, AZ). DI water was produced with a Millipore Direct-Q™ 5 (Millipore, Bedford, MA, USA) water purification system, and eluents were vacuum filtered through a 0.2  $\mu\text{m}$  filter (Supelco, Supelco Park, Bellefonte, PA, USA) and degassed by sonication.

### *5.2.3 Fabrication of methacrylate monoliths.*

As per Section 4.2.3 and 4.2.4.

### *5.2.4 Photografting of polyethylene glycol methacrylate.*

Prior to the photografting of VAL, the column was rendered hydrophilic by the photografting of polyethylene glycol methacrylate onto the surface of the monolith using the two-step photografting procedure described by Stachowiak *et al.* [25]. Rendering the column hydrophilic was performed with the view to using the column in combination with proteins, where a bare BuMA monolith would result in non-specific interactions. Briefly, benzophenone (50 mg mL<sup>-1</sup> in methanol) was grafted onto the entire length of the monolith without the use of a photomask using a total UV dose of 3 J cm<sup>-2</sup>. The excess benzophenone was washed from the column with methanol for 30 minutes at 1  $\mu\text{L min}^{-1}$ . A solution of 36  $\mu\text{L mL}^{-1}$  PEGMA in water was pumped into the column and photografted using a total UV dose of 3 J cm<sup>-2</sup>. Excess PEGMA was washed from the column with water at 1  $\mu\text{L min}^{-1}$  for 30 minutes. This two step approach results in the PEGMA being photografted onto the surface on the monolith and not in the pores, which would result in the blocking of the through pores.

### *5.2.5 Photografting of vinyl azlactone.*

For the immobilisation of functional groups onto the monolith surface azlactone chemistry was utilised. In this procedure vinyl azlactone (VAL) was photografted onto two discrete zones within the polymeric monolith. A solution of 0.14 mL VAL in 75:25 *t*-butanol:water with 2.2 mg benzophenone (BP) was pumped into the base monolith prior to photografting. Photografting was carried out by delivery of 3 J cm<sup>-2</sup> of energy from a Spectrolinker XL-1000. Once the photografting was complete the excess VAL was removed by washing with methanol (1 hr) followed by water (1 hr).

### *5.2.6 Immobilisation of *m*-aminophenylboronic acid via azlactone chemistry.*

VAL was photografted onto the monolith as per Section 5.2.7 and a solution of 1 mg mL<sup>-1</sup> *m*-aminophenylboronic acid was then pumped through the column at a flow of 1 μL min<sup>-1</sup> for 3 hr. After washing with DI water any unreacted VAL groups were blocked using 1 M ethanolamine at 1 μL min<sup>-1</sup> for 1 hr, to prevent any unwanted reaction with amine containing buffers.

### *5.2.7 Immobilisation of ADA and IDA via azlactone chemistry.*

ADA and IDA were immobilised as per Section 5.2.6 with the exception of using 1 mg mL<sup>-1</sup> ADA and IDA as the immobilisation solutions, respectively.

### *5.2.8 Immobilisation of ethanolamine via azlactone chemistry.*

VAL was photografted onto the monolith as per Section 5.2.5 and was then reacted with 1 M ethanolamine at 1 μL min<sup>-1</sup> for 1 hr.

### 5.2.9 Verification of immobilised zones.

As per Section 4.2.8.

### 5.2.10 Titration of free *m*-aminophenylboronic acid.

Batch titrations of free *m*-aminophenylboronic acid (APBA) were performed using a 1 mg mL<sup>-1</sup> APBA solution with 0.2 M NaOH. Titrations were carried out using an Orion 2 Star (Thermo) pH meter with a glass electrode.

### 5.2.11 On-column titration of immobilised APBA.

The conductivity value at each millimetre location along the column was recorded. The titration buffers used were chosen, where possible, to have low conductivity and compatibility with bio-molecules for future work. The buffers ranging from pH 4 to 10.2 are given in Table 5.1.

Table 5.1: Buffers used for on-column titration of APBA.

pH	Buffer
4	5 mM acetate
4.9	5 mM acetate
6.1	5 mM MES/Histidine
6.8	10 mM TES/MES
8.1	5 mM TES/4 mM ethanolamine
9	2.5 mM TES/3 mM ethanolamine
10.2	1 mM ethanolamine

Each buffer was passed through the column and allowed to equilibrate for 1 hr before any readings were taken. Calculation of  $\Delta$  Response was carried out by using the average of 3 baseline points immediately before and after the respective zone ( $n=6$ ), followed by subtraction of this baseline conductivity reading from that

recorded at the maximum zone height. In this way background conductivity from the base monolith and the various buffer solutions was subtracted from the conductivity resulting from the immobilised boronic acid.

#### *5.2.12 On-column titration of immobilised IDA, ADA and ethanolamine.*

As per Section 5.2.11, with extra buffers of 10 mM nitric acid (pH 3), 1 mM histidine/5 mM MES and 5 mM MES/10 mM histidine (pH 6.3).

#### *5.2.13 On-column titration of ADA in the presence of metals.*

The buffers in Table 5.1 containing solutions of 0.1 mM of each metal (as chloride salt) were passed over the column for 1 hr before profiles were collected. Between each metal containing buffer the column was washed with nitric acid (pH 3) to remove any electrostatically or chelated metal from the monolith before the next was applied.

### **5.3 Results and discussion.**

#### *5.3.1 Immobilisation of APBA via VAL.*

From Figure 5.3 the successful immobilisation of APBA on the surface of the monolith via VAL can be seen. Covalent bonding of APBA to poly(glycidyl methacrylate-co-ethylene glycol dimethacrylate) monolithic capillary columns has previously been reported by Potter *et al.* [9] using nucleophilic attack of the epoxide with *p*-hydroxyphenylboronic acid. In an effort to increase the surface coverage of boronic acid groups on the monolith, Potter *et al.* also grafted chains of glycidyl methacrylate groups onto the surface of the monolith prior to reaction with the *p*-hydroxyphenylboronic acid. In this Chapter, however, the approach of using VAL chemistry to covalently bond the APBA to the monolith surface was exploited. VAL chemistry has previously been utilised for the immobilisation of

proteins [12]. In this work VAL is used to immobilise APBA onto a monolithic stationary phase via the free amine group on the APBA molecule. The immobilisation strategy of Potter *et al.* is quite lengthy, taking 20 hours at 60 °C, whereas the VAL method takes only 3 hours at room temperature. In addition, Potter *et al.* used triethylamine as a base in the reaction (the reaction required alkaline conditions to occur), but found that a positive surface charge was obtained since the monolith exhibited an anodic EOF [9]. Potter *et al.* postulated that the triethylamine had also acted as a nucleophile and had attacked the epoxy groups resulting in immobilised charged ammonium groups on the monolith in addition to the boronic acid groups [9]. The strategy proposed herein results in no such unwanted immobilisation of other functional groups, since the APBA is presented to the VAL grafts in water alone.

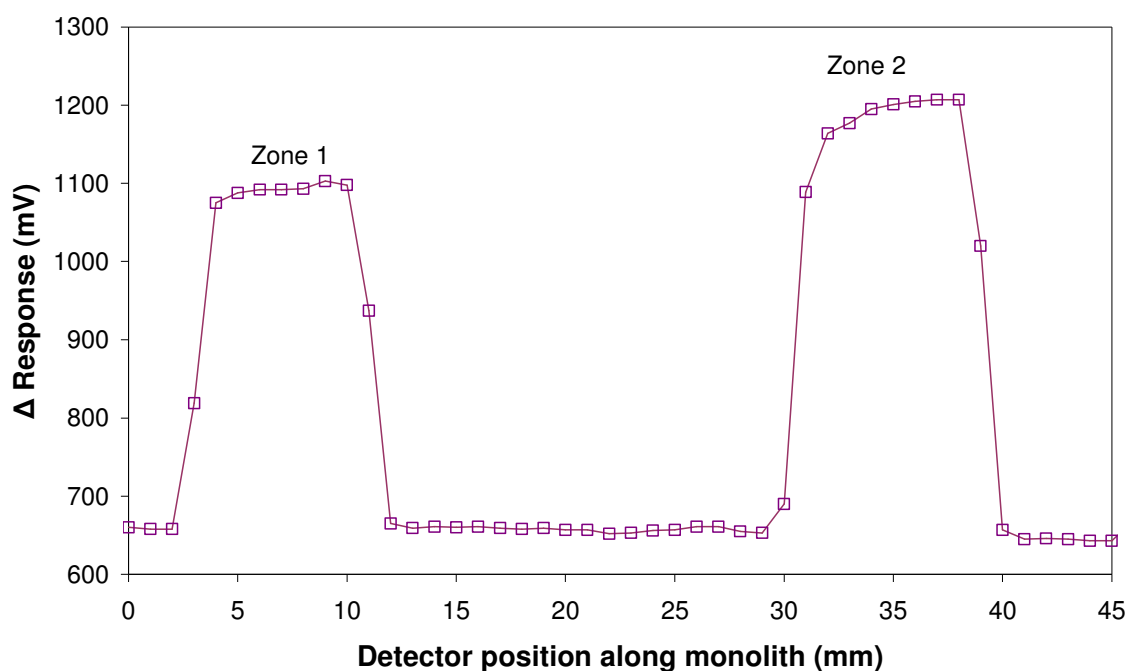


Figure 5.3: Uncorrected C<sup>4</sup>D scan of two VAL-APBA modified zones on a monolithic capillary column with pH 10.2 buffer.

### 5.3.2 On-column titration of APBA.

The monolith with VAL-APBA immobilised on its surface was equilibrated (1 hr) with a series of buffers (Table 5.1) and the profile of the column at each pH collected. The profiles collected showed a difference between the two zones of APBA covalently bound to the column, with Zone 2 having a higher response than Zone 1 (Figure 5.3). This may have been due to subtle differences in the photografting of VAL onto the monolith. Over the pH range it was found that the  $\Delta$  Response of the APBA zones changed from *ca.* 40 to 430 and *ca.* 50 to 550, for Zone 1 and 2, respectively, as was expected. In Figure 5.4 it can be seen that the low pH buffers resulted in a low response for the APBA zones ((~~—\*~~) pH 4.0), but as the pH was increased (> 8.5) the response from of the zones increased dramatically ((~~—□~~) pH 10.2). As previously reported in Chapter 3, the “form” of the monolith surface functionalities can be determined via C<sup>4</sup>D; here the change in response is due to the change in the confirmation of the boronic acid groups from the planar form to the tetrahedral form, and thus an increase in charge. The increase in zone height with pH can be clearly seen to be independent of eluent conductivity, which shows no discernable trend (see Figure 5.5). When the  $\Delta$  Response was plotted against pH, the immobilised boronic acid zones displayed the expected S-shape titration curves (see Figure 5.6). The difference in the peak height was reflected throughout the titration curve (Figure 5.6).

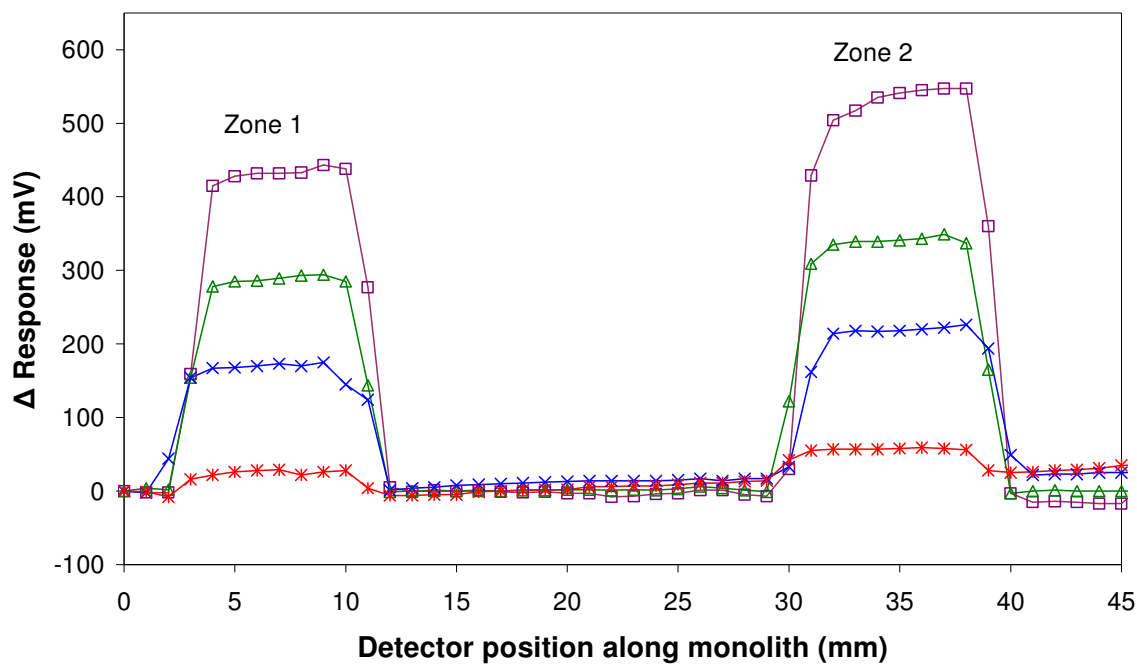


Figure 5.4: C<sup>4</sup>D scan of VAL-APBA modified zones on a monolithic capillary column at (—\*) pH 4.0, (—x) pH 6.1, (—Δ) pH 6.8 and (—□) pH 10.2 (normalised to first reading of each column).

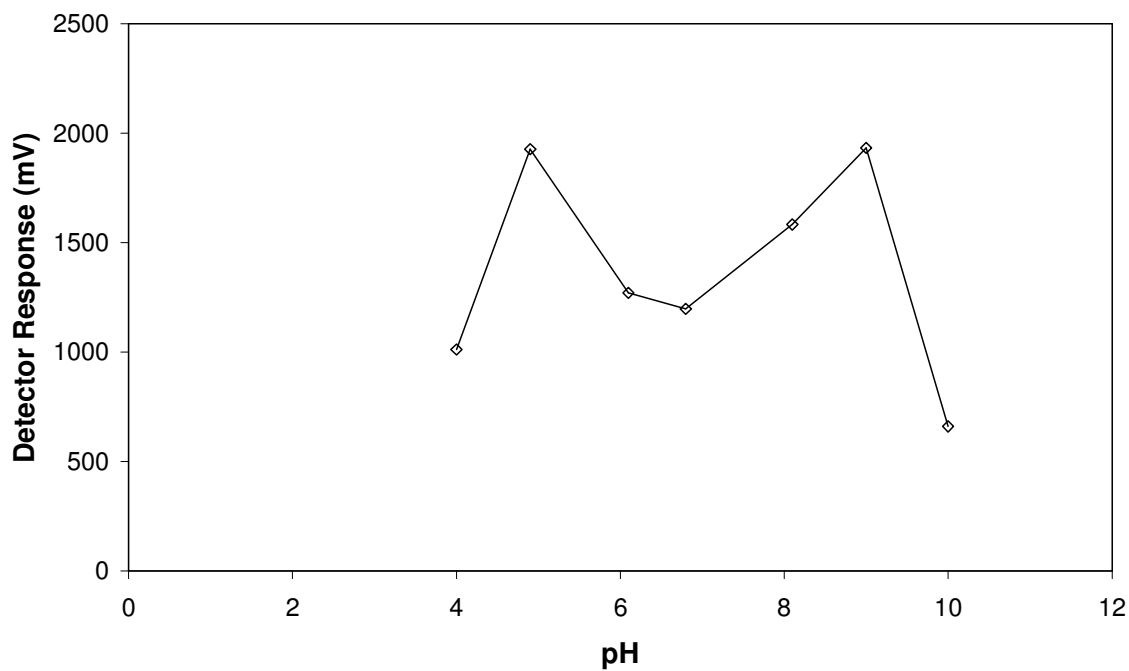


Figure 5.5: Baseline response of unmodified monolithic capillary column for each buffer used in on-column titration of VAL-APBA.

When a sigmoidal regression was carried out on the data collected for the two APBA zones the  $R^2$  values returned were 0.999. The classical pH ranges used with boronic acids (covalently bound to agarose gel) has been  $> 8.5$  for the tetrahedral form and pH 4.5 for the planar form [27]. The results obtained here show that the maximum response obtained for the APBA region was reached at *ca.* pH 9.0 (with little change between this and pH 10.2), indicating that the groups have fully converted to the tetrahedral form (and thus fully ionised). The minimum response was obtained at pH below 4.9 with little change between pH 4.9 and 4, indicating that the APBA groups are in the neutral planar form. The pH characteristic of the covalently bound APBA groups has shown good agreement with those used in classical boronic acid affinity chromatography for the purification of glycoprotein [13, 26, 29].

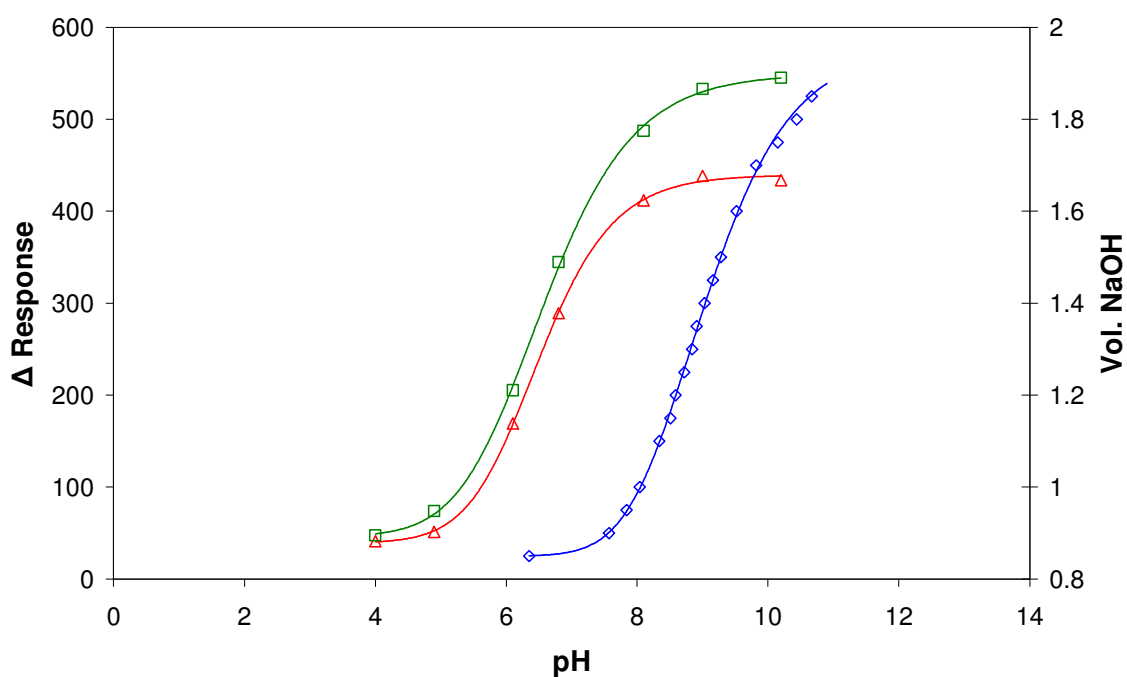


Figure 5.6: Comparison of on-column titration of a polymer monolith capillary column modified with two zones of VAL-ADA over pH a range of 4 to 10 with titration of APBA in solution. Zone 1 ( $\square$ ) and Zone 2 ( $\triangle$ ) and free APBA in solution ( $\diamond$ ).

From Figure 5.7 it is possible to accurately determine the  $pK_a$  of the immobilised boronic acid. Using first derivative analysis of the regression obtained the  $pK_a$  of the two APBA zones was found to be 6.4 (Figure 5.7). The difference in the height of Zone 1 and 2 (Figure 5.3) was found not to have any affect on the 1<sup>st</sup> derivatives, yielding the same  $pK_a$ . Previous studies have calculated the  $pK_a$  of APBA-based molecules immobilised onto microspheres consisting of styrene, butyl acrylate, and *m*-acrylamidophenylboronic acid (synthesised from APBA), where the phenylboronic acid phase was found to have a  $pK_a$  of 7.0 (by bulk titration of modified microspheres). The deviation from the reference  $pK_a$  of 8.77 was attributed to a disturbance of the dissociation behaviour of the phenylboronic acid due to being immobilised onto a polymer surface [27]. As a molecule is immobilised it may experience interactions (e.g. hydrogen bonding) with other molecules or the substrate itself. The act of immobilisation may result in a change of electron density on the molecules, via these interactions, and thus change its physio-chemical properties (such as  $pK_a$ ). Here the titration of APBA in free solution resulted in a  $pK_a$  of 8.9 (Figure 5.7), which is in good agreement with literature values (i.e. 8.9) [28]. In this work it follows that as the phenylboronic acid is immobilised onto the monolithic stationary phase, the  $pK_a$  of the acid has been similarly perturbed and reduced from 8.9 to 6.4. To investigate the reproducibility of the data collected, triplicate profiles for pH 9 were collected, and the average %RSD was found to be < 1%. A second column was produced to investigate the reproducibility of (1) the immobilisation procedure and (2) the  $pK_a$  of the immobilised APBA. Figure 5.8 shows the 1<sup>st</sup> derivative analysis of the two columns both with two zones of APBA. The  $pK_a$  determined was found to be  $6.45 \pm 0.06$  ( $n=4$ ) (Figure 5.8), showing good agreement between the four zones of the immobilised APBA.

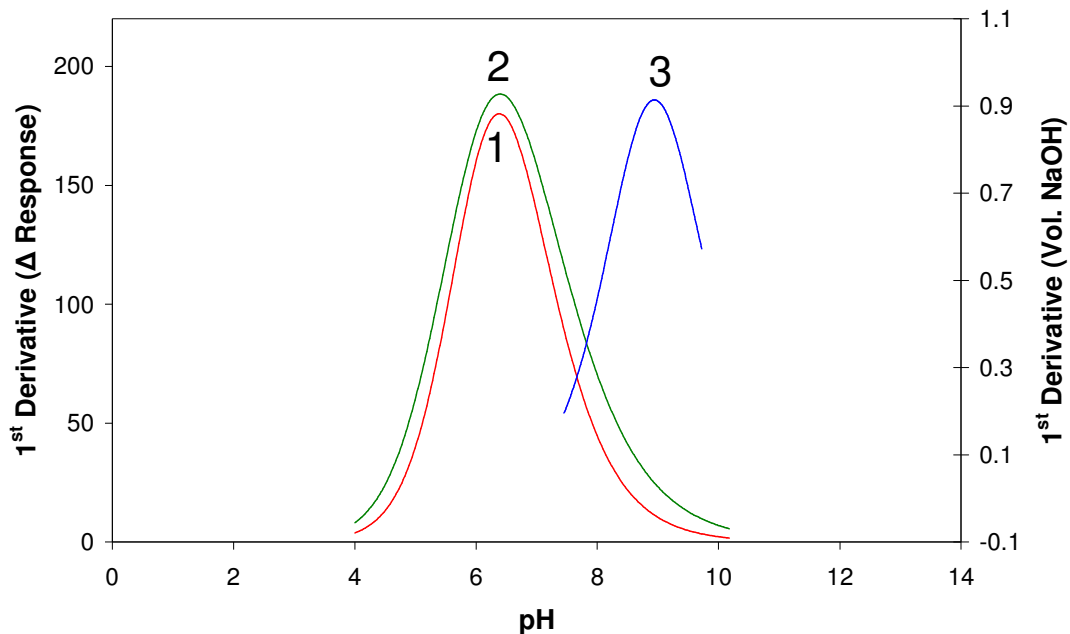


Figure 5.7: 1<sup>st</sup> derivative analysis of two zones of VAL-APBA on modified monolithic capillary columns (1) Zone 1 & (2) Zone 2 on column and (3) titration of APBA in solution.

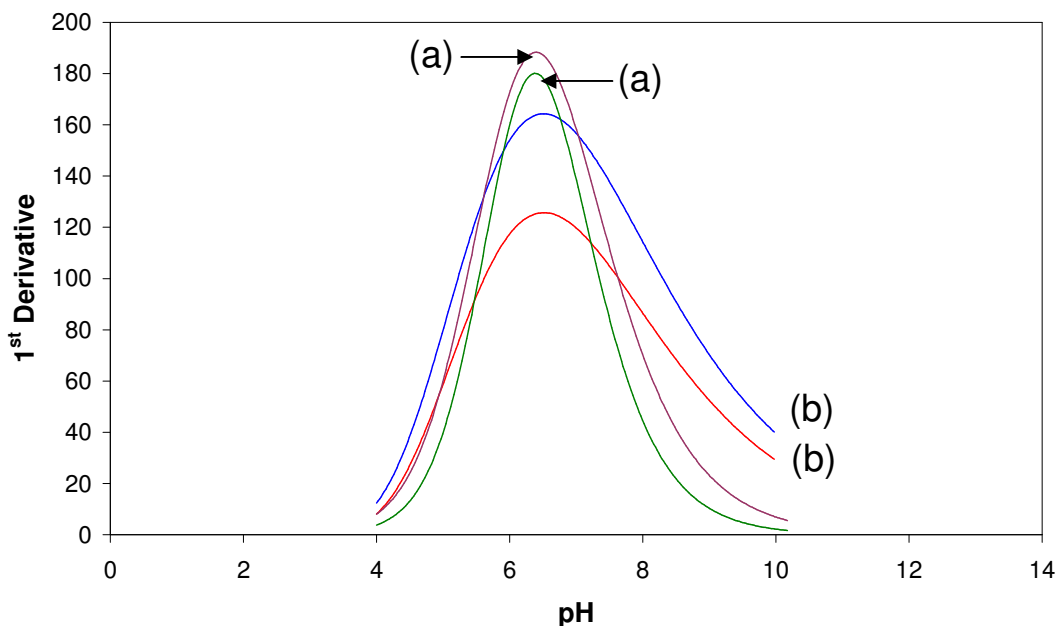


Figure 5.8: 1<sup>st</sup> derivative analysis of four zones of VAL-APBA on modified monolithic capillary columns, ( $n=4$ , two columns each with two zones) with an average  $pK_a$  of  $6.45 \pm 0.06$ , (a) Column #1 and (b) Column # 2.

The ability to investigate the changes in conductivity of photografted zones as the eluent pH is varied has allowed for the determination of the  $pK_a$  of APBA on-column. To the authors knowledge no other method exists that allows for the non-contact and non-destructive determination of such physio-chemical properties. The on-column determination of  $pK_a$  has important impacts on the production and characterisation of novel stationary phases, as it was found here that the  $pK_a$  of APBA changed from 8.9 to 6.4 once immobilised. Such changes in  $pK_a$  will undoubtedly have an impact on the selectivity and efficiency of novel stationary phases.

### *5.3.3 Immobilisation of ADA via VAL.*

To investigate the effect on the pH dependant behaviour of a polyprotic species, ADA (an aminopolycarboxylate) was immobilised via VAL onto the surface of the monolith (as per Section 5.2.7). Once ADA was immobilised onto the VAL activated monolith the  $C^4D$  cell was scanned along the length of the column and a profile collected. The resultant profile revealed two discrete zones of VAL-ADA each of *ca.* 10 mm (as was expected). Figure 5.9 is a profile of VAL-ADA monolith at pH 9.

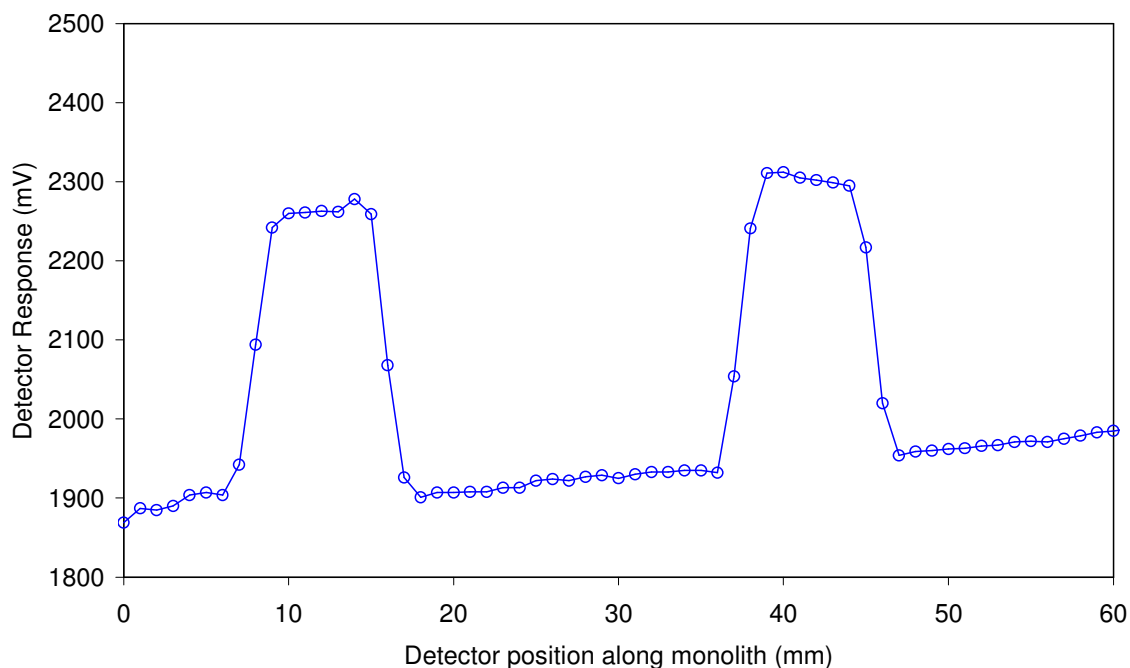


Figure 5.9: Uncorrected  $C^4D$  scan of VAL-ADA modified zones on a monolith capillary column with pH 10.2 buffer.

#### 5.3.4 On-column titration of ADA.

ADA was chosen as the molecule to be immobilised via VAL as the iminodiacetic acid group would be separated from the reaction with VAL. This would reduce the effect of the immobilisation strategy on the amine group (immobilisation via VAL convert amines to amides). The on-column titration of ADA immobilised via azlactone chemistry was found to give a trend following that for a diprotic species (Figure 5.10). Using 1<sup>st</sup> derivative analysis of the sigmoidal regressions the inflection points of the titration curve, and thus the  $pK_a$  values were found to be 5.2 and 6.9 (Figure 5.11). It is clear from these values that the  $pK_a$ 's have been perturbed from the literature  $pK_a$  values for ADA (2.3 and 6.6) [30].

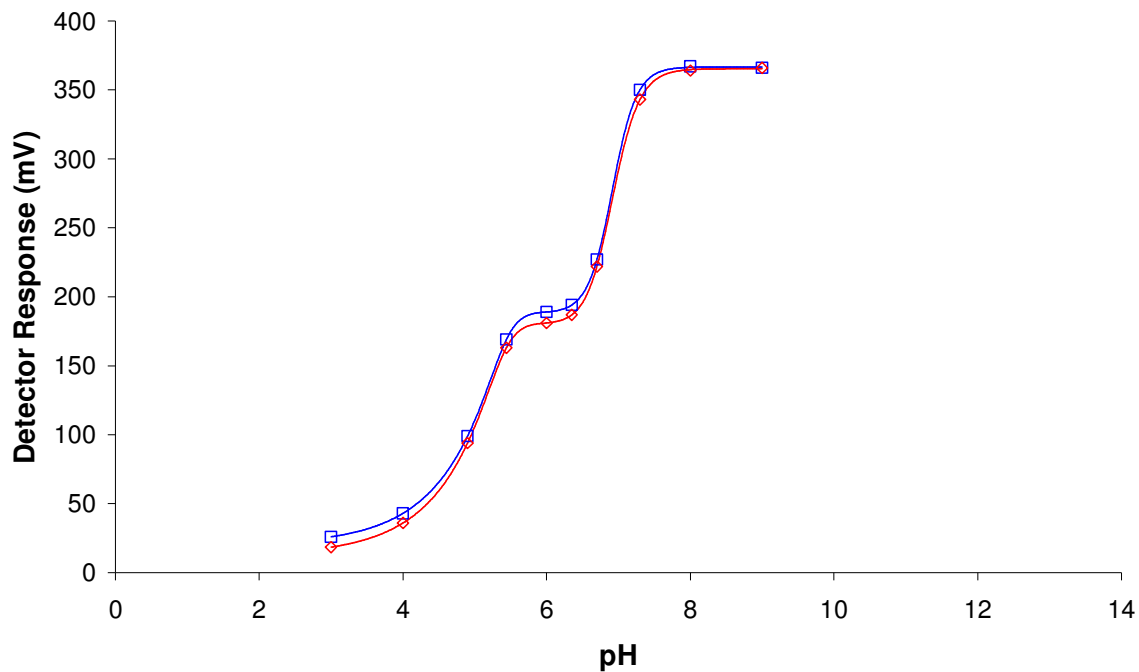


Figure 5.10: On-column titration of a polymer monolith capillary column modified with two zones of VAL-ADA over a pH range of 3 to 10.

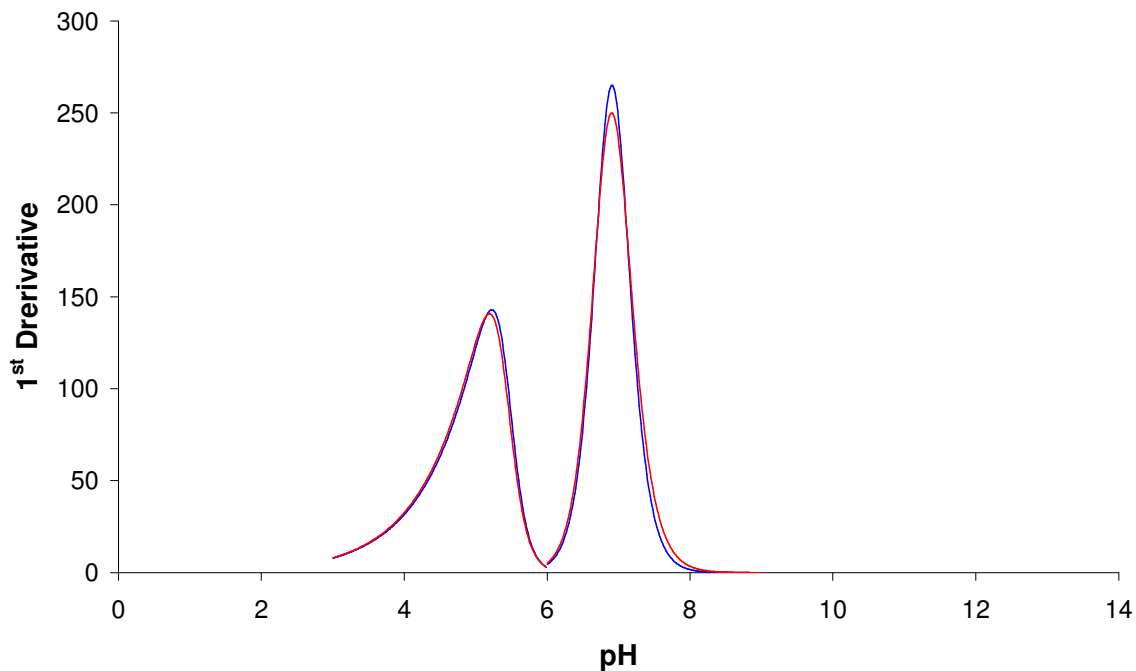


Figure 5.11: 1<sup>st</sup> derivative of on-column titration of a polymer monolith capillary column modified with two zones of VAL-ADA over a pH range of 3 to 10.

To assign the  $pK_a$  values from the on-column titration of VAL-IDA, it is important to understand the structure of the molecule once immobilised on the monolith surface. The structure of the immobilised ADA molecule (Figure 5.12) shows that there are three groups that have an acid/base character, namely an amine group and two carboxylate groups. From Figure 5.12 it can be seen that the linkage contains an imide group (-CONHCO-). Imide groups are reactive under basic conditions, whereby the -NH- forms an anion. The reaction of the anionic imide with alkyl halides results in the synthesis of a primary amine. The linkage used here may afford stabilisation of the acidic imide proton (Figure 5.12 (a)). The formation of hydrogen bonds with adjacent VAL-ADA groups, and also the polymeric substrate, may also stabilise the imide group present in the linker. This stabilisation may result in the imide group having no acid base character under the conditions used in this study.

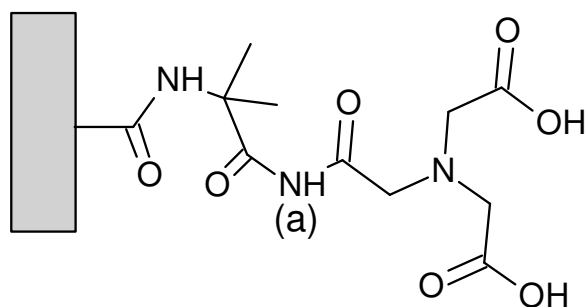


Figure 5.12: Structure of VAL-ADA.

The immobilisation of ADA onto the surface of the monolith via azlactone chemistry will result in the ADA functional groups being in close proximity to each other and to the base monolith. Interactions with other ADA molecules and base monolith may result in the formation of short-strong hydrogen bonding (SSHB). Haggmann *et al.* studied the effect of such bonding on the pH dependent nature of alkyl IDA molecules [31]. When the alkyl chain was short (i.e. methyl-, *n*-hexyl-*N*-iminodiacetic acid) the molecules existed as monomers in solution and the  $pK_a$ 's determined were within the expected range (e.g. 1.82, 2.22 and 9.59 for methyl-iminodiacetic acid). However, long alkyl chains derivatives (i.e. *n*-dodecyl-*N*-

iminodiacetic acid, C<sub>18</sub>-IDA) existed as aggregates in solution, and the pK<sub>a</sub>'s were found to shift from the expected values. One carboxylate group became more acidic and the other became much weaker than expected, with a pK<sub>a</sub> of 5.6 to 7.1 for the weakened carboxylate group. It was also found that the ionic strength the C<sub>18</sub>-IDA molecules experienced affected the recorded pK<sub>a</sub>, ranging from 5.6 for high ionic strength, to 7.61 for low ionic strength mediums. In comparison to the work reported by Haggmann *et al.*, where only alkyl-aminopolycarboxylate molecules were present, here ADA is placed into a much more complex environment. The polymer backbone of the monolith contains both hydrogen and oxygen atoms which may form SSHB with the carboxylate groups of the ADA. Under the conditions used by Haggmann *et al.* the effect on the amine group was found to be minimal for all conditions. The effect of the formation of aggregates on the pK<sub>a</sub> of C<sub>18</sub>-IDA can also be applied to the effect of chemically bonding molecules onto the surface of large polymeric scaffolds (such as a polymer or monolith).

Chen *et al.* determined two pK<sub>a</sub> values for a glycidylmethacrylate-IDA (GMA-IDA) polymer. The pK<sub>a</sub> values for GMA-IDA were 3.06 and 8.5 [32]. The values obtained by Chen *et al.* correspond to the carboxylic acid group (3.06) and the amine group (8.5) present in the polymer. Upon using different monomer mixtures and repeating units (i.e. PGMA-IDA-co-methylacrylate, and PGMA-IDA-co-acrylamide) the pK<sub>a</sub>'s were found to change with a maximum pK<sub>a</sub> of 3.86 and 9.54 for the carboxylate and amine group, respectively. Another publication by Chen *et al.* documents a similar effect of IDA functionalised latex polymers, with the pK<sub>a</sub> values ranging from 4.48 to 4.68 for the weakened acidic proton (i.e. weaker than for PGMA-IDA-co-methylacrylate, and PGMA-IDA-co-acrylamide) [33]. The changes in the pK<sub>a</sub> values for the aminopolycarboxylate functionalised polymers were attributed to the stereo structure of the polymer. This structure would result in the carboxylate groups being in close proximity to each other, and electrostatic attraction of neighbouring carboxylate groups impeding the removal of protons, i.e. a similar process to that of SSHB postulated by Haggmann *et al.*

The effects on the  $pK_a$  values of aminopolycarboxylate functional groups reported for aggregated surfactants and on polymeric substrates, supports the shift in  $pK_a$  observed here for aminopolycarboxylate groups on the surface of a polymer monolith. The structural and chemical environment in which the aminopolycarboxylate group is placed will have a direct effect on the ionisation characteristics of the molecule. The presence of electrostatic interactions with adjacent aminopolycarboxylate groups and the polymer substrate, results in a deviation from the  $pK_a$  of aminopolycarboxylates in solution. Here the immobilised ADA ( $pK_a$  in solution: 2.3 and 6.6) has had its  $pK_a$ 's changed to 5.2 and 6.9.

### 5.3.5 Immobilisation of IDA via VAL.

The presence of the immobilised zones of VAL-IDA was verified by scanning the  $C^4D$  cell along the length of the column. Figure 5.13 shows the resultant scan, with two discrete zones of VAL-IDA located on the monolith.

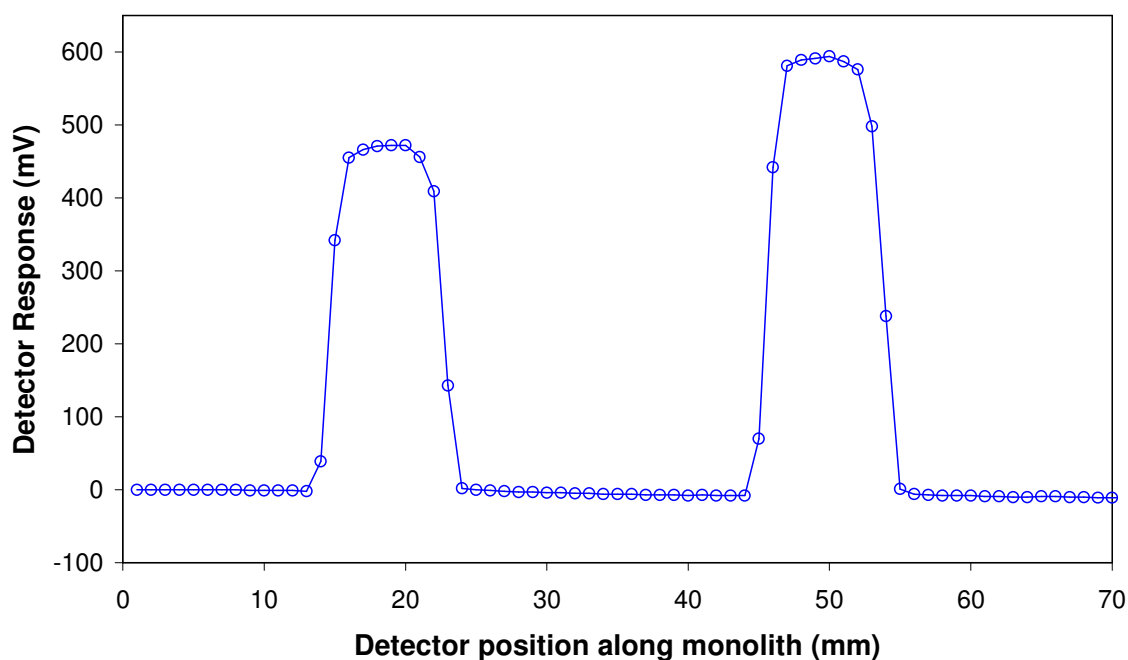


Figure 5.13:  $C^4D$  scan of VAL-IDA modified zones on a monolith capillary column with pH 10.2 buffer.

### 5.3.6 On-column titration of IDA.

The immobilisation of IDA via VAL was expected to yield a titration curve showing diprotic behaviour. From Figure 5.14 it can be seen that the amine group has reacted with VAL and has been converted to amide group, which has no acid/base character (due to stabilisation of the amide by delocalisation of the lone pair of the nitrogen through orbital overlap with the carbonyl group adjacent to it). The two acetic acid groups of IDA are the only functional groups within the immobilised molecule that can undergo acid/base transformations.

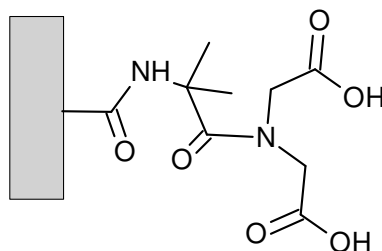


Figure 5.14: Structure of IDA linked to monolith surface via azlactone (note the amide group).

As with the immobilised ADA the IDA will similarly be affected by SSHB's. This may result in the weakening of one of the carboxylate  $pK_a$ 's. The titration curve for VAL-IDA shows what appears to have a diprotic behaviour. The data obtained for the on-column titration of VAL-IDA resulted in regressions with  $R^2 > 0.99$  (Figure 5.15). The 1<sup>st</sup> derivative analysis of the regressions yielded  $pK_a$  values of 5.1 and 6.9. These  $pK_a$ 's have been perturbed from the literature values for IDA  $pK_a$ 's of 1.76 and 2.70 (for the carboxylate groups) and 9.73 for the amine group [15] (Figure 5.16). The diprotic behaviour of the on-column titration may be due to both of the carboxylate groups having their respective  $pK_a$ 's weakened through SSHB's, or due to effects of changing ionic strength as seen by Haggmann *et al.* The lack of any inflection point in the region of 8 to 10 is evidence of the formation of the amide group in the reaction of IDA with VAL. The same trend may also have been present for the VAL-ADA monolith, but the amino group ionisation may have

dominated the second weak carboxylate  $pK_a$ , and thus was not observed. The  $pK_a$  value of 5.1 is similar to the  $pK_a$  of 5.2 determined for VAL-ADA, corresponding to a weakened carboxylate group.

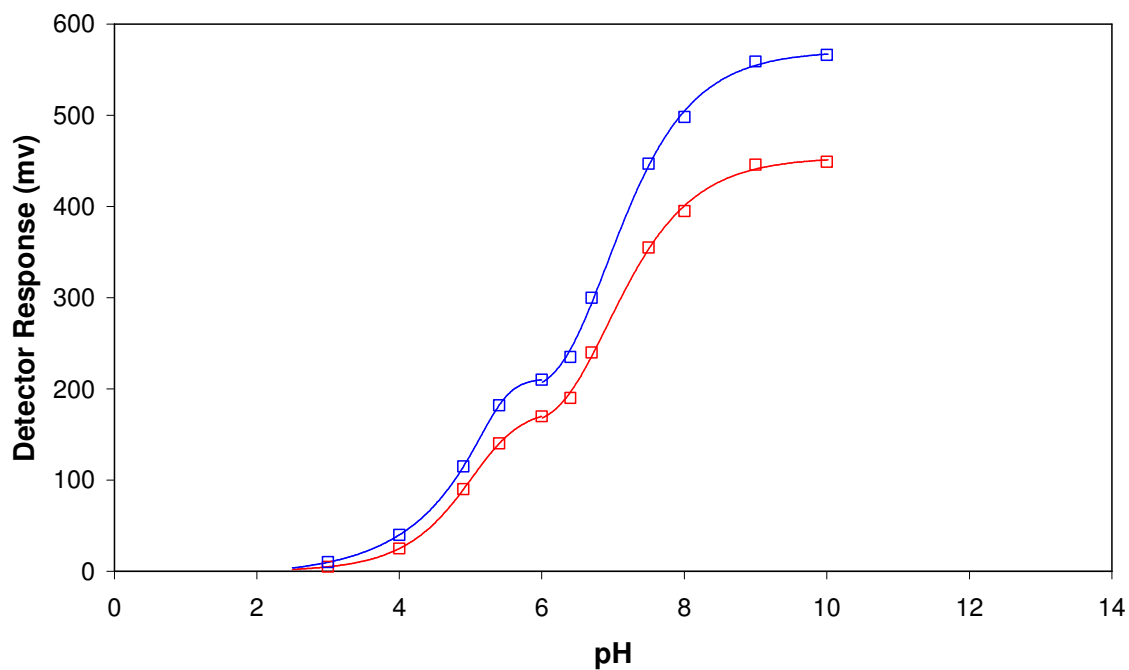


Figure 5.15: On-column titration of a polymer monolith capillary column modified with two zones of VAL-IDA over a pH range of 3 to 10.

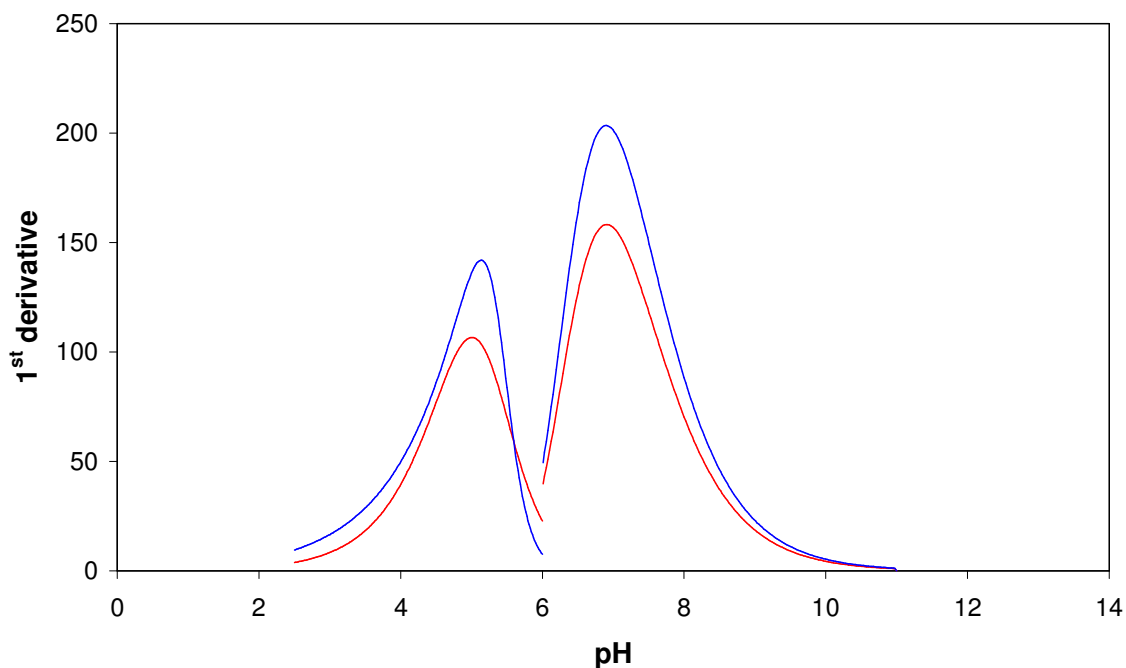


Figure 5.16: 1<sup>st</sup> derivative of on-column titration of a polymer monolith capillary column modified with two zones of VAL-IDA over a pH range of 3 to 10.

### 5.3.7 On-column titration of ethanolamine.

The reaction of VAL was used with the previous monoliths to ensure any unreacted VAL groups were blocked and therefore could not react with the buffers used. The structure of ethanolamine once reacted with VAL is shown in Figure 5.17. As with the other immobilised molecules, the reaction forms an amide bond, which has no acid/base character. The other functional group present is a hydroxyl group, which under the pH range used for the on-column titration has no acid/base character. Therefore using ethanolamine as the blocking agent should not readily contribute to the response of the zones.

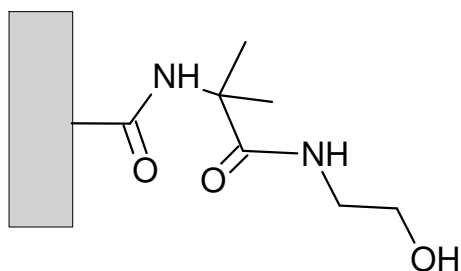


Figure 5.17: Ethanolamine linked to the monolith surface via VAL.

The resultant on-column titration curve for ethanolamine immobilised onto the monolith surface via VAL, although showing an increase in signal over the pH range, shows that the contribution from the blocking step can be considered to be negligible for all columns heretofore titrated (Figure 5.18). The zone height for the VAL zone once reacted with 1 *M* ethanolamine was found to be much less than for the monoliths reacted with boronic acid or aminopolycarboxylates. Assuming that in this column all available VAL sites have reacted with ethanolamine the contribution to the responses of the boronic acid and aminopolycarboxylate columns would be much less. If boronic acid and aminopolycarboxylate react with 90 % of the available VAL sites, the signal contribution of the blocking step would be only 10 % of that observed for the ethanolamine column. Therefore the contribution of ethanolamine-VAL to the signal of boronic acid and aminopolycarboxylate zones can be taken to be minimal.

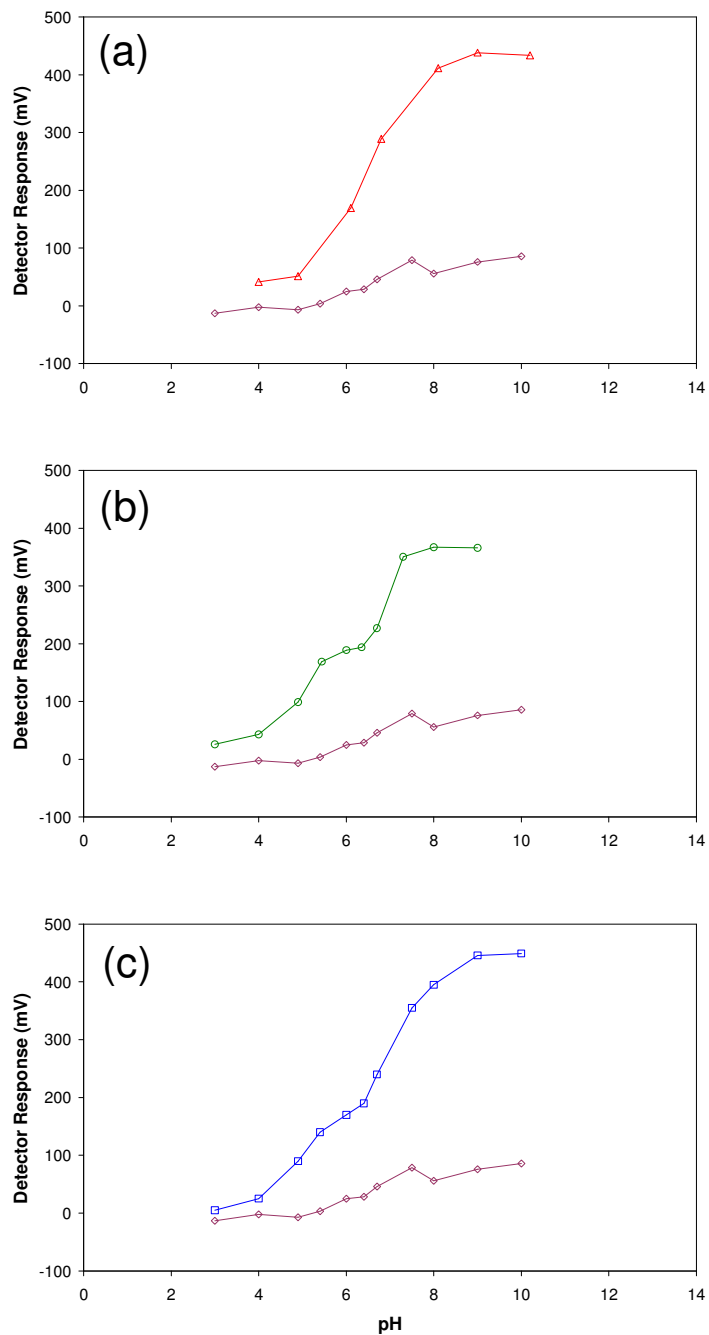


Figure 5.18: Comparison of the on-column titrations of VAL zones reacted with (a) APBA ( $\blacktriangle$ ), (b) ADA ( $\ominus$ ) and (c) IDA ( $\blacksquare$ ) and then blocked with ethanolamine, with the on-column titration of VAL zones reacted with ethanolamine only ( $\blacklozenge$ ).

### 5.3.8 Investigation of VAL-ADA complexation with metals using $C^4D$ .

As the structure of the IDA molecule once linked with VAL has no free lone pair on the nitrogen to undergo complexation, the ADA functionalised monolith was chosen to investigate the effect of including metals in the buffers. Inclusion of copper in the buffer solutions over the pH range studied showed a large deviation from the previous on-column titration for ADA (Figure 5.19), with a suppression of the signal below and above pH 6.7. It is suggested that the change in signal below pH 6.7 is due to electrostatic interactions of copper with the ADA. Above pH 6.7 the interactions change to chelation as the amine group is deprotonated, thus allowing for the lone pair on the nitrogen to form the co-ordinating bond. Tsukagoshi *et al.* in the preparation of IDA modified capillaries for use in CEC found that the EOF was reduced for the IDA modified capillary and the formation of an IDA-Cu (II) complex reduced the EOF further. The reason given for this change in EOF behaviour from the free IDA to IDA-Cu(II) was attributed to the formation of the complex reducing the charge on the capillary wall by the blocking of the carboxylate groups in the complex [29]. In the results obtained from the on-column titration of VAL-ADA in the presence of Cu(II) a similar behaviour is observed. The charge of the VAL-ADA functionalised monolith reduces upon the formation of the complex.

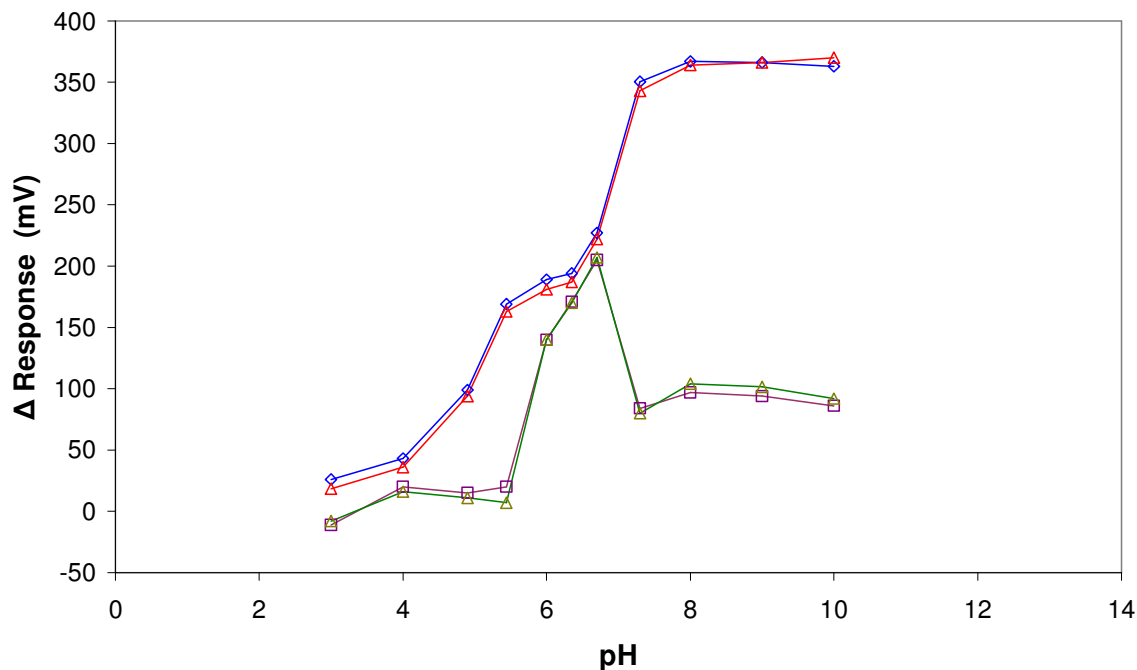


Figure 5.19: Effect of the inclusion of copper on the on-column titration of VAL-ADA over pH 3 to 9. Zone 1 titration ( $\text{---}\diamond\text{---}$ ), Zone 2 titration ( $\text{---}\triangle\text{---}$ ), Zone 1 titration with copper ( $\text{---}\triangle\text{---}$ ) and Zone 2 titration with copper ( $\text{---}\square\text{---}$ ).

Following on from this, a series of metals (potassium, copper, nickel and cobalt) were included in the pH 9 buffer and the change in the zone heights monitored. Transition metals resulted in the reduction in the responses of the zones, whereas the inclusion of an alkali metal (potassium) was found to have little effect (Figure 5.20). The reduction in the signal of the zones when transition metals were included in the buffer may be evidence of complexation of the metal into the ADA functional group. Comparing the responses of the metals to their known formation constants with a structurally similar IDA molecule (N-(hydroxymethyl)-iminodiacetic acid) [34], there was a clear distinction between the alkali metal and transition metals. The transition metals reduced the zone height by greater than 50 % whereas the alkali metal had little effect on the zone height. In the presence of potassium cations the carboxylic groups will form potassium salts, with no noticeable change in the conductivity of the zone. Conversely, in the presence of a transition metal, a complex is formed reducing the overall charge of the ADA

functional group. The response for calcium, nickel and cobalt were approximately the same, with copper giving the lowest response for the four transition metals studied. The extent to which the signal is reduced may be an indication as to the stability (i.e. formation constant) of the complex with differing metals. Copper, here giving the lowest response, is reported as the most stable complex formed with IDA type ligands of the metals studied here [34].

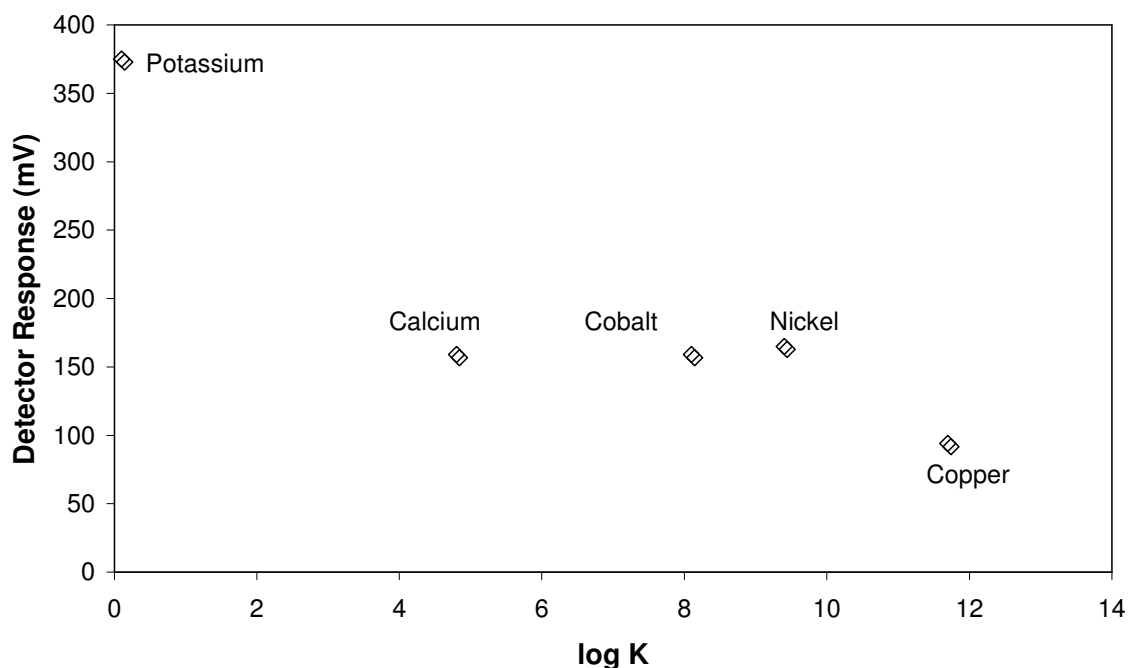


Figure 5.20: Comparison of the response for VAL-ADA modified monolithic capillary monolith with a series of metals, at pH 9, compared to the known formation constant of these metals with N-(hydroxymethyl)-iminodiacetic acid.

The ability to visualise the formation of a complex's on-column may be applicable to use with other chelating or inclusion complex functionalities (e.g. cyclodextrins, crown ethers etc.).

## 5.4 Conclusion.

This Chapter shows how the physio-chemical properties of polymeric monolithic stationary phases modified with acidic or basic functional groups can be characterised using  $C^4D$ . The ability to rapidly and non-invasively study the pH behaviour of covalently bound groups, together with the visualisation of the magnitude the functionalised zone, leads to a better understanding of how such phases work and opens up the possibility of using  $C^4D$  for investigation into other significant physio-chemical properties (e.g.  $pI$  and binding co-efficient for immobilised proteins).

The on-column titration of a boronic acid functionality showed a deviation from the pH dependant character of the molecule in solution. The  $pK_a$  once immobilised onto the surface of the monolith was found to drop 2.5 pH units. The on-column titrations obtained for ADA and IDA show a more complex nature, as expected due to their polyprotic nature. The assignment of the functional group  $pK_a$  is difficult due to the complex nature of the immobilised molecules and their interaction with the base monolith (e.g. short strong hydrogen bonds). Further, more detailed investigations into the effect of different buffer compositions to further clarify the pH dependence of polyprotic molecules on the surface of a monolith are required. The inclusion of metals into the buffers with the ADA stationary phase resulted in a dramatic change in the zones responses. The event of complexation is posited as the cause for the change. This may lead to the use of  $C^4D$  as a method of investigating complex formation within the stationary phase and the ability to determine physical constants (e.g. formation constants, stability constants) for other complex forming compounds.

## 5.5 References:

- [1] Y. Ueki, T. Umemura, J. Li, T. Odake, K. Tsunoda, *Anal. Chem.*, 2004, **76**, 7007.
- [2] E.F. Hilder, F. Svec, J.M.J. Frechet, *J. Chromator. A.*, 2004, **1053**, 101.
- [3] P. Zakaria, J.P. Hutchinson, N. Avdalovic, Y. Liu, P.R. Haddad, *Anal. Chem.*, 2005, **77**, 417.
- [4] J.P. Hutchinson, E.F. Hilder, R.A. Shellie, J.A. Smith, P.R. Haddad, *Analyst*, 2006, **131**, 215.
- [5] T. Ikegami, J. Ichimaru, W. Kajiwara, N. Nagasawa, K. Hosoya, N. Tanaka, *Anal. Sci.*, 2007, **23**, 109.
- [6] J. Jaafar, Y. Wanatabe, T. Ikegami, K. Migamoto, N. Tanaka, *Anal. Bioanal. Chem.*, 2008, **391**, 2551.
- [7] A. Suzuki, L.W. Lim, T. Hiroi, T. Takeuchi, *Talanta*, 2006, **70**, 190.
- [8] A.Y. Katyanyeva, E.N. Viktorova, A.A. Korolev, A.A. Kurganov, 2007, **30**, 2836.
- [9] O. G. Potter, M. C. Breadmore and E. F. Hilder, *Analyst*, 2006, **131**, 1094.
- [10] T. Rohr, E. F. Hilder, J.J. Donovan, F. Svec and J. M. J. Frechet, *Macromolecules*, 2006, **36**, 1677
- [11] E. Sugrue, P.N. Nesterenko and B. Paull, *J. Sep. Sci.*, 2004, **27**, 921.
- [12] D. Connolly, V. O'Shea, P. Clark, B. O'Connor and B. Paull, *J. Sep. Sci.*, 2007, **30**, 3060.
- [13] Y. Chi, E.L. Larsson, H. Junguid, I.Y. Galaev and B. Mattiasson, *J. Chromator. A.*, 2001, **909**, 137.
- [14] M. Matsumoto, K. Ueba and K. Kondo, *Sep & Pur. Tech.*, 2005, **43**, 269.
- [15] M.G. Kolpachnikova, N.A. Penner, P.N. Nesterenko, *J. Chromator. A.*, 1998, **826**, 15.
- [16] P.N. Nesterenko, P. Jones, *J. Chromator. A.*, 1998, **804**, 223.
- [17] W. Bashir, B. Paull, *J. Chromator. A.*, 2002, **942**, 73.
- [18] E. Sugure, P. Nesterenko, B. Paull, *Analyst*, 2003, **128**, 417.
- [19] P.N. Nesterenko, O.A. Shpigun, *Russian Journal of Coordination Chemistry.*, 2002, **28**, 726.

- [20] P.N. Nesterenko, P. Jones, J. Chromator. A., 1997, **770**, 129.
- [21] J. Tria, P.R. Haddad, P.N. Nesterenko, J. Sep. Sci., 2008, **31**, 2231.
- [22] C.M. Bo, B.L. Gong, W.L. Hu, Chinese Journal of Chemistry, 2008, **26**, 886.
- [23] C.L. Chiang, C.Y. Chen, L.W. Chang, J. Chromator. B., 2008, **864**, 116.
- [24] L.H. Tan, D.S. kim, I.K. Yoo, W.S. Choe, Chemical Engineering Science, 2007, **62**, 5809.
- [25] T.B. Stachowiak, F. Svec and J.M.J. Frechet, Chem. Mater., 2006, **18**, 5950.
- [26] Y. Chi, U. Pfuller, E.L. Larsson, H. Junguid, I.Y. Galaev and B. Mattiasson, J. Chromator. A., 2001, **925**, 115.
- [27] Y. Chi, J.O. Jeppsson, M. Jornten-Karlsson, E.L. Larsson, H. Junguid, I.Y. Galaev and B. Mattiasson, J. Chromator. B., 2002, **776**, 149.
- [28] J. Yan, G. Springsteen, S. Deeter and B. Wang, Tetrahedron, 2004, **60**, 11205.
- [29] K. Tsukagoshi, R. Kawasaki, M. Maeda and M. Takagi, Anal. Sci., 1996, **12**, 721.
- [30] R. Williams, pKa compilation ,[http://research.chem.psu.edu/brpgroup/pKa\\_compilation.pdf](http://research.chem.psu.edu/brpgroup/pKa_compilation.pdf), 26-11-08, 13:00.
- [31] L. Haggmann, C. Lindbald, H. Oskarsson, A.S. Ullstrom, I. Persson, J. Amer. Chem. Soc., 2003, **125**, 3631.
- [32] C.Y. Chen, C.Y. Chen, Journal of Applied Polymer Science, 2002, **86**, 1986.
- [33] C.Y. Chen, C.Y. Chen, European Polymer Journal, 2003, **39**, 991.
- [34] J. C. Janson, L. Ryden, Protein Purification: Principles, High Resolution Methods and Applications (2<sup>nd</sup> Ed.) Wiley Blackwell, 1998, ISBN: 978-8471186267.

---

**Chapter 6: Development of a contactless conductivity detector cell for 1.6 mm O.D. ( $1/16^{\text{th}}$  inch) HPLC tubing micro-bore columns with on-column detection.**

---

“I love deadlines. I like the whooshing sound they make as they fly by”  
-Douglas Adams

## 6.1. Introduction.

Over the last decade  $C^4D$  has exclusively been applied to separation methods utilising capillary scale formats, the cell dimensions generally being 365  $\mu\text{m}$  o.d., and 10 to 150  $\mu\text{m}$  i.d.  $C^4D$  has also begun to be incorporated into micro-fluidic systems due to its inherent non-contact and zero dead volume advantage [1-12]. Applications of  $C^4D$  in other modes and scales of chromatography have been limited due to the restricted dimensions of the detector cells available with commercial instruments.

However, early versions of  $C^4D$  technology were actually of a much greater scale, prior to considerable efforts into the miniaturisation of the technique for use as an analytical CE detector. For example, as early as 1989 a patent was lodged for the use of  $C^4D$  for the evaluation of milk bottle production [13], in a set-up whereby the measured capacitance was directly proportional to the thickness of the glass walls of each bottle. A larger scale early version of  $C^4D$  has also been used in flow injection analysis (FIA) [14] and HPLC [15,16], based upon Teflon coated electrodes and a post-column flow through detector cell design.  $C^4D$  has also previously found an application in high frequency titrations [17].

Therefore, the redesign of the currently available  $C^4D$  cell geometry for use with larger dimensioned chromatographic columns, particularly as an 'on-column' detector option, (micro-scale and upwards) seems overdue. This Chapter describes the optimisation and evaluation of a  $C^4D$  detector cell designed to house 1.59 mm o.d. (1/16") standard LC tubing and micro-bore columns, allowing for non-invasive and zero dead volume 'on-column' detection. The clear advantage of a  $C^4D$  detector cell of these dimensions for non-invasive evaluation of stationary phase packing homogeneity and for mid-run adjustment of column effective length is also discussed in detail, together with a performance comparison with a commercial capillary format  $C^4D$  system.

## 6.2. Experimental.

### 6.2.1 Instrumentation.

#### 6.2.1.1 Chromatographic instrumentation.

The pump used for packing PEEK columns with stationary phase, washing and equilibration of the packed column, acquisition of Bode plots for detector optimisation, and chromatographic evaluation of the detector, was a quaternary gradient HP 1050 pump operated at all times in isocratic mode. The pump was operated in direct flow mode (i.e. no split was used) with an operational flow rate of  $20 \mu\text{L min}^{-1}$  (pressure  $>1500$  psi). A HP 1050 autosampler was used to make  $1 \mu\text{L}$  injections onto the column, with the exception of the intra-run detector movement study, for which a  $10 \mu\text{L}$  injection volume was used.

#### 6.2.1.2 Preparation of packed capillary columns.

All columns were packed using a Nanobaume SP 400 column packer (Western Analytical Products, CA, USA). All columns were packed in polyether ether ketone (PEEK) tubing of  $380 \mu\text{m}$  i.d. and with a  $1.59 \text{ mm}$  ( $1/16''$ ) o.d. (Upchurch Scientific Inc., WA, USA). The end of the column was fitted with a  $0.15 \text{ mm}$  bore stainless steel union which had a sweep volume of  $0.63 \mu\text{L}$  and with a  $0.5 \mu\text{m}$  steel frit installed. Packing was performed by pumping a packing solvent into the Nanobaume packing bomb, where the only exit for the solvent was through the empty column via the vial containing the phase, this causes the phase to be swept into the empty column and packed against the frit (Figure 6.1). A length of  $100 \mu\text{m}$  i.d. fused silica capillary was fitted to this union as a column outlet to allow connection of a commercial  $\text{C}^4\text{D}$  detector for comparative analysis (Figure 6.2). Acetonitrile was used as the packing solvent and was delivered at a flow rate of  $20 \mu\text{L min}^{-1}$  such that a packing pressure of  $200 \text{ bar}$  was achieved. Packing was considered to be complete after the column pressure had been held stable at  $200$

bar for 8 hours. The column was subsequently gradually depressurized overnight to ensure that the integrity of the packed bed (particularly at the column head) was not compromised. An equivalent stainless steel union and 0.5  $\mu\text{m}$  frit (as above) was fitted to the head of the column. The column used for detector optimisation studies, and signal to noise studies, was a 190 mm  $\times$  380  $\mu\text{m}$  i.d. PEEK column packed with Dionex OmniPac 8.5  $\mu\text{m}$  PAX-100 anion exchange resin. The column used for comparative analysis of the new detector cell with a commercially available detector was a 400 mm  $\times$  380  $\mu\text{m}$  i.d. PEEK column packed with the same resin as above. For intra-run moving detector studies, a 250 mm  $\times$  380  $\mu\text{m}$  i.d. PEEK column was used, packed with 10  $\mu\text{m}$  Hamilton PRP-X100 phase as described.

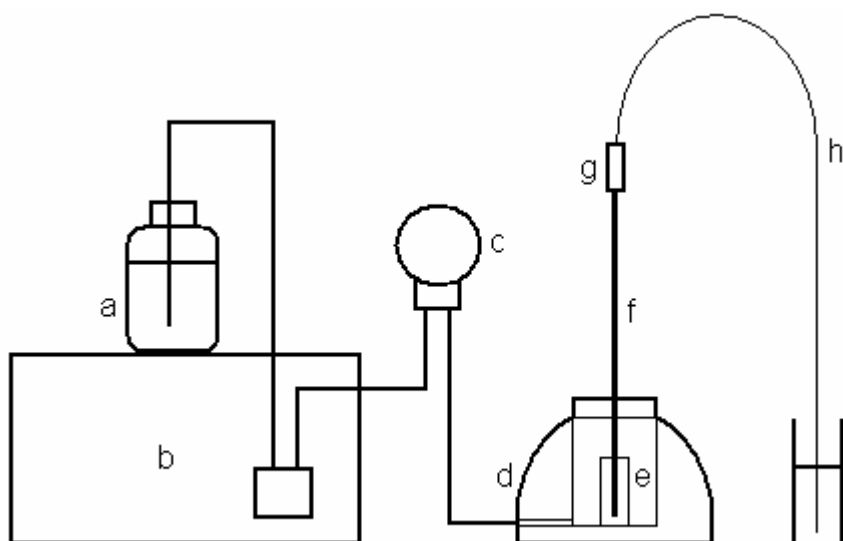


Figure 6.1: Set-up used to pack PEEK columns. (a) Packing solvent, (b) HPLC pump, (c) pressure gauge, (d) high pressure packing bomb, (e) vial with phase, (f) column, (g) union with frit, (h) waste line, (i) waste packing solvent.

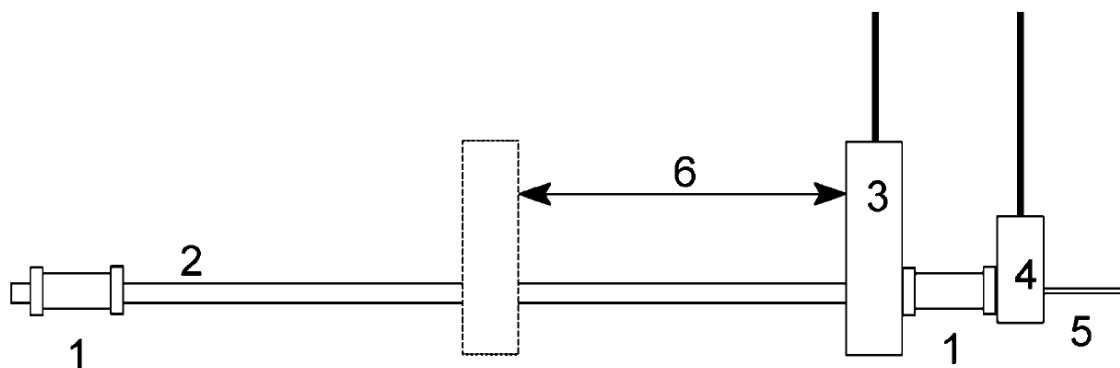


Figure 6.2: Schematic of dual C<sup>4</sup>D set-up. 1 = Union with frit, 2 = 1.59 mm o.d. (1/16") packed PEEK column (381 μm i.d.), 3 = C<sup>4</sup>D cell under investigation (suitable for 1.59 mm (1/16") PEEK tubing), 4 = commercial C<sup>4</sup>D cell, 5 = 360 μm o.d. 100 μm i.d. fused silica capillary, 6 = Movement of the test C<sup>4</sup>D cell along the column length.

### 6.2.1.3 Contactless conductivity 1.59 mm (1/16") detector cell.

The detector cell comprised of an electrically grounded die-cast metal box (38 mm x 92 mm) containing the cell electrodes, Faraday shield, pick-up amplifier and a feedback resistor, and is shown in Figure 6.3. The feedback resistor was positioned such that it could easily be exchanged for higher or lower rated resistors by soldering. A length of 2 mm x 55 mm Teflon tubing passed through the centre of the cell, with two 2 mm copper electrodes (excitation and pick-up) wrapped around this tubing and positioned 2 mm apart from each other. An internal metallic shield (Faraday shield) completely enclosed the excitation electrode, (except for a small hole through which the Teflon tubing was passed), in order to minimise direct capacitive coupling between the electrodes.

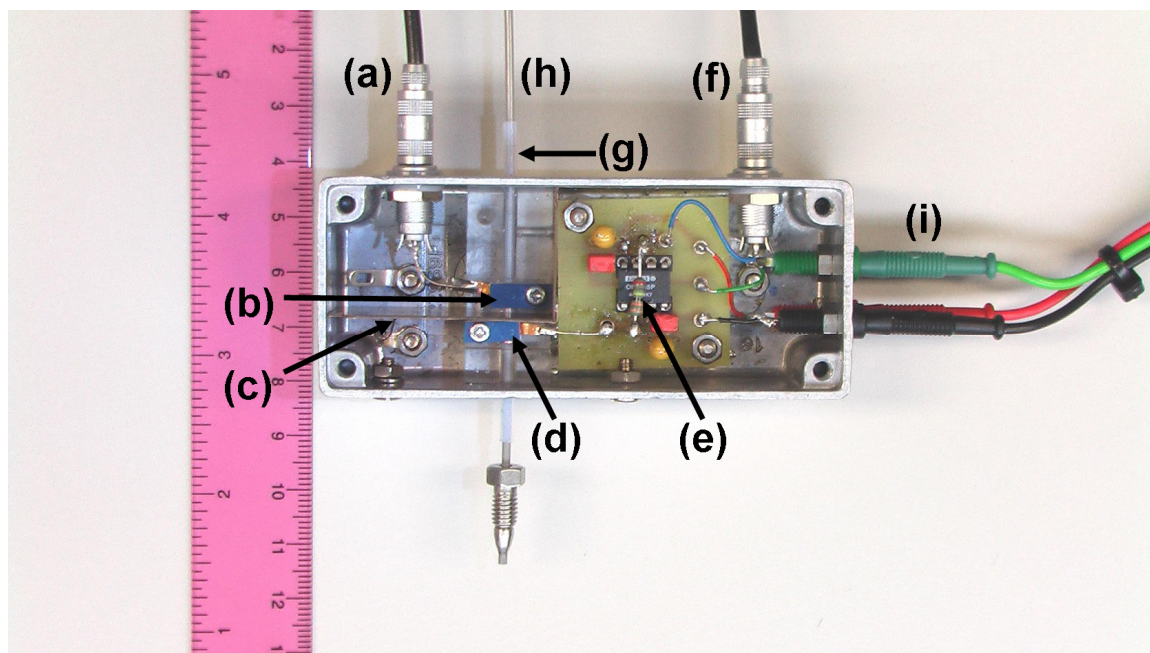


Figure 6.3: Layout of C<sup>4</sup>D detector cell for use with 1.59 mm o.d. (1/16<sup>th</sup>) PEEK tubing; (a): cell input (excitation) lead, (b): copper excitation electrode, (c): Faraday shield. (d): copper signal pick-up electrode, (e): feedback resistor, (f): signal output lead, (g): Teflon sleeve, (h): column, (i): cell power leads.

The Teflon tubing acted as a sleeve through which the packed analytical column or empty PEEK tubing could be passed. The detector cell was placed directly on-column for all measurements. The position of the column was fixed, and the exact position of the mobile detection cell along the length of the column was varied manually with a graduated position guide (i.e. a ruler). The detector was controlled by a function generator (Model GFG-8216A, Goodwill Instruments, Taiwan) which was operated at different sinusoidal wave input frequencies ranging from 100 Hz to 1 MHz. Peak-to-peak input voltage ( $V_{(p-p)}$ ) of 20–25 V was used throughout the experiment. All input (excitation) and output (signal) frequencies and voltages were measured using an oscilloscope (Model TDS-1001, Tektronix), with the output signal monitored from the coaxial cable (Figure 6.3(a)). The output signal was rectified and processed as described in J. Tanyanyiwa *et al.* [18]. Data acquisition and processing was carried out using PowerChrom version 2.5.4 (eDAQ, NSW, Australia). Figure 6.4 depicts the instrumentation used.

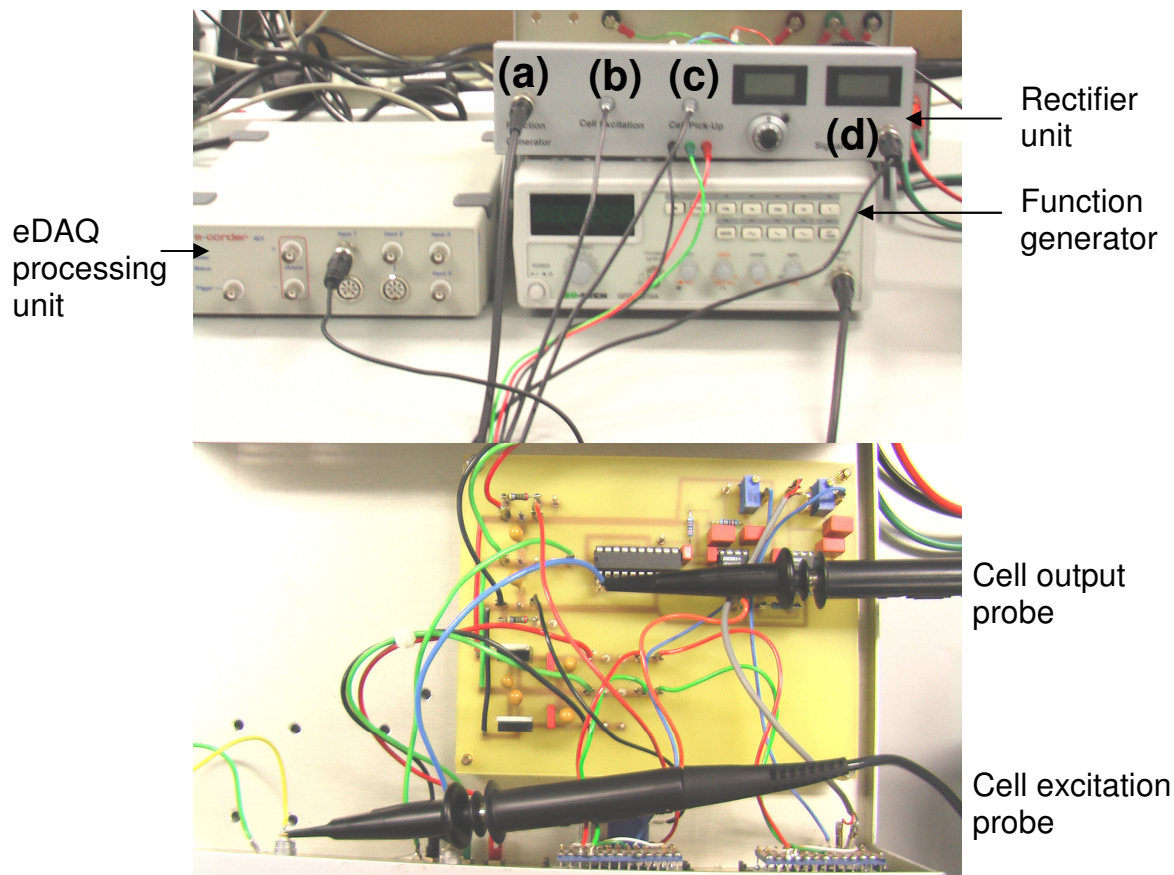


Figure 6.4: Pictures of signal generation, pick-up and processing., a= in-pu from function generator to rectifier unit, b = input signal from rectifier unit to cell, c = output signal from cell to rectifier unit, d = signal out from rectifier to eDAQ

#### 6.2.1.4 Comparative studies.

The commercial detector used for comparative analysis was a TraceDec capacitively coupled contactless conductivity detector (Innovative Sensor Technologies GmbH, Innsbruck, Austria). This detector was used off-column by passing the column outlet tubing (100  $\mu\text{m}$  i.d. fused silica capillary) through the radial capillary detector cell immediately after the column end fitting (see Figure 6.2). Detector settings used were: frequency, 2XHIGH; voltage, 0 dB; gain, 50% and offset, 50. Data acquisition and processing was carried out using TraceMon v.0.08c software (Innovative Sensor Technologies GmbH, Innsbruck, Austria) and Chromeleon v. 6.70 (Dionex Corporation, Sunnyvale, CA, USA).

### *6.2.2 Reagents.*

Methanol and acetonitrile were purchased from Labscan (Stillorgan, Dublin, Ireland). Sodium benzoate, potassium hydrogen phthalate, sodium nitrate, sodium nitrite and sodium sulfate were purchased from Sigma–Aldrich (Tallaght, Dublin, Ireland). Stock solutions of analyte anions ( $1 \text{ g L}^{-1}$ ) were prepared in DI water and working standards were prepared fresh daily from these stocks. Polyimide coated fused silica capillary ( $100 \text{ }\mu\text{m}$  i.d. was obtained from Polymicro Technologies (Phoenix, AZ). DI water was produced with a Millipore Direct-Q™ 5 (Millipore, Bedford, MA, USA) water purification system, and eluents were vacuum filtered through a  $0.2 \text{ }\mu\text{m}$  filter (Supelco, Supelco Park, Bellefonte, PA, USA) and degassed by sonication. The eluent used for generation of Bode plots was  $0.5 \text{ mM}$  sodium benzoate containing 2% methanol. Evaluation of the homogeneity of stationary phase packings, chromatographic evaluation of the detector and comparative analysis was done using an eluent of  $2.5 \text{ mM}$  sodium benzoate containing 2% methanol. The eluent used for intra-run detector movement studies was  $1 \text{ mM}$  phthalate (pH 4.0) containing 2% methanol. In all cases, the flow rate applied was  $20 \text{ }\mu\text{L min}^{-1}$ . Acetonitrile was used as packing solvent for preparation of packed anion-exchange columns.

### *6.2.3 Noise calculation.*

An appropriate section of blank baseline was plotted and a line of best fit obtained using the method of least squares. Fitting each original timepoint to the equation of the line yielded a subset of “expected results”. Finally, the range of the residuals (obtained by subtraction of the expected result from the actual result) was determined and used as the signal noise for calculations.

### 6.3. Results and discussion.

#### 6.3.1 Detector design and optimisation: Bode plots.

A 190 mm × 380 μm i.d. PEEK column packed with Dionex OmniPac 8.5 μm PAX-100 anion exchange resin was positioned within the cell as described above with a mobile phase of 0.5 mM sodium benzoate containing 2% methanol delivered at a flow rate of 20 μL min<sup>-1</sup>. Optimisation of the detector cell involved incremental changes in the input frequency and recording the resulting output voltage  $V_{(p-p)}$ . Ideally, the optimised detector operating conditions would result in the majority of the measured output voltage being due to capacitive coupling through the solution between both electrodes, whereas *direct coupling* between the electrodes (stray capacitance) would be minimised. The optimum input frequency and also the extent of stray capacitance was evaluated by constructing a “Bode plot” of the log of the input frequency ( $x$  axis) *versus* the output voltage ( $y$  axis). The frequency range chosen for acquisition of Bode plots was 100 Hz to 1 MHz. At the low end of the range (<100 Hz), it was anticipated that no measurable signal would be observed at the output of the pick up amplifier since the capacitances are too small to allow capacitive coupling at these frequencies. Bode plots were constructed by manually controlling the input frequency (applied to the excitation electrode) from the function generator, with the oscilloscope being used to ensure that the input waveform was a clean sine wave. Subsequently, each output voltage (from the pickup electrode *via* the amplifier and feedback resistor) was recorded, with its peak-to-peak amplitude,  $V_{(p-p)}$ , being displayed numerically by the (dual channel) oscilloscope. An additional factor which increased the output signal was the size of the feedback resistor (Figure 6.3(e)), with higher value resistors resulting in higher signal amplitude. A maximised output voltage is expected to result in a better signal to noise ratio (and hence better detection limits). With the circuitry employed in this work, output voltages are limited to 7.5 V. Therefore resistors higher than 5 MΩ were avoided, and three different metal

film resistors of 1.0, 3.3 and 4.7 M $\Omega$  were alternately fitted to the cell by soldering, with three separate Bode plots constructed as described.

The resulting overlaid Bode plots obtained for each feedback resistor are shown in Figure 6.5(a) and were collected with the 380  $\mu\text{m}$  i.d. anion exchange column positioned between the electrodes. The signal obtained is due to capacitive coupling of the input voltage through the mobile phase between the electrodes and also due to the charged stationary phase. In order to measure the signal due to stray capacitance alone (at each frequency and for each resistor), the column was removed from the cell and replaced with dry, empty PEEK tubing with the same dimensions as that of the column, *i.e.* 1.59 mm o.d. and 380  $\mu\text{m}$  i.d. Bode plots were again collected for each resistor and are shown in Figure 6.5(b).

Figure 6.5(a) clearly demonstrates that the 1 M $\Omega$  resistor failed to yield the classic Bode plot plateau at any frequency (see Section 1.7.2.3), however, the 3.3 and 4.7 M $\Omega$  resistors resulted in a plateau above 100 kHz. The maximum  $V_{(p-p)}$  obviously increased with increasing resistance (1 to 4.7 M $\Omega$ ), with the 3.3 M $\Omega$  resistor resulting in the best Bode plot, since the 4.7 M $\Omega$  resistor showed a drop in the plateau over 250 kHz, pointing to a significant contribution from stray capacitance (direct coupling between the electrodes). The effect of the stray capacitance evident in Figure 6.5 (b) for these two resistors was found to level out above 250 kHz with the 4.7 M $\Omega$  resistor giving the highest  $V_{(p-p)}$  for stray capacitance (0.56 V). The maximum values for the stray capacitance corresponds exactly to the drop in signal observed in the Bode plots in Figure 6.5 (a). Based on these results, a resistor of 3.3 M $\Omega$  with an input frequency of 200 kHz was initially chosen as the optimum detector settings conditions.

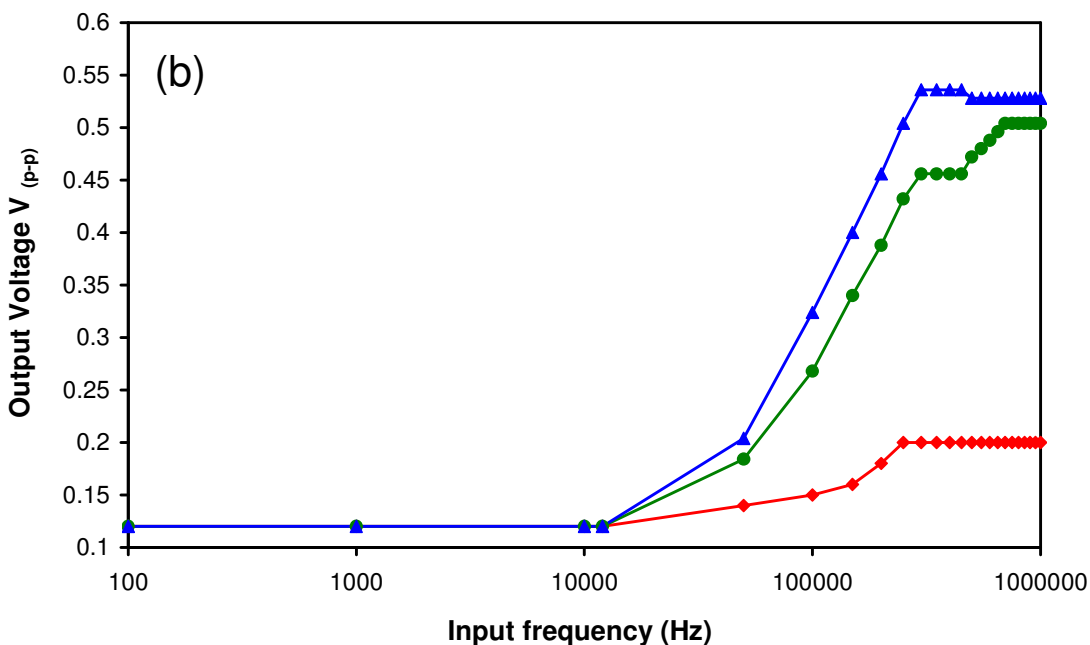
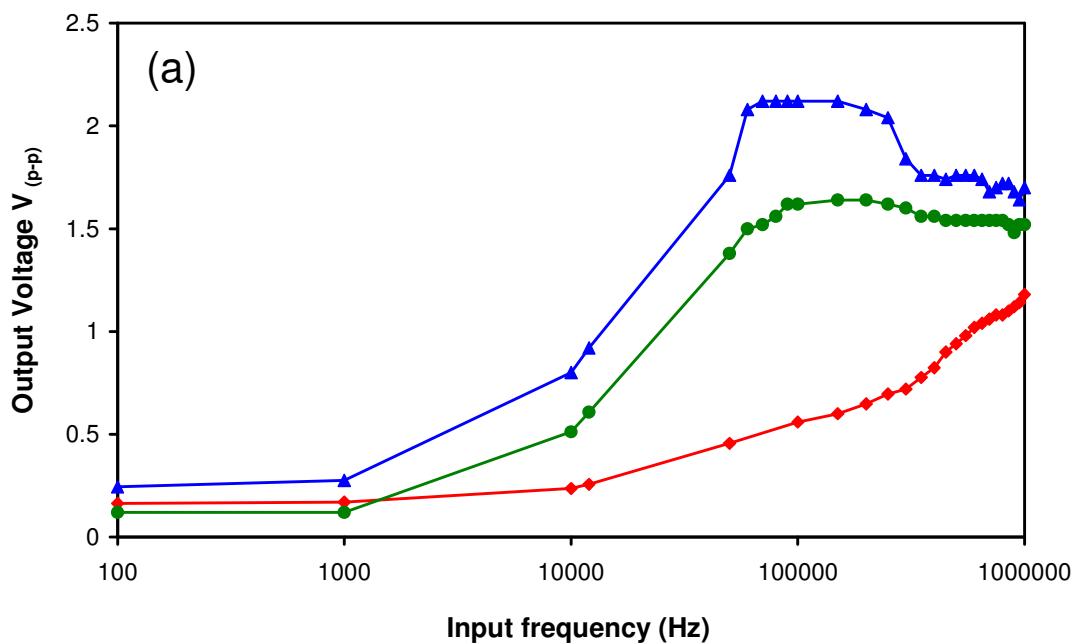


Figure 6.5 (a) Bode plots with column and mobile phase positioned within the cell. *Column*: 190 mm × 380 μm i.d. PEEK column packed with Dionex OmniPac 8.5 μm PAX-100 anion exchange resin. *Mobile phase*: 0.5 mM sodium benzoate containing 2% methanol. *Flow rate*: 20 μL min<sup>-1</sup>. (b) Bode plots illustrating stray capacitance with dry empty PEEK tubing (1.59 mm × 380 μm) positioned within the cell. *Legend*: 4.7 MΩ (—▲—), 3.3 MΩ (—●—) and 1.0 MΩ (—◆—).

### 6.3.2 Detector optimisation: response, signal to noise and peak shape.

As described above, the optimum detector conditions were derived using a constant flow of mobile phase through a packed anion exchange column placed between both electrodes, but without the injection of analyte onto the column. In order to study the effect of the input detector frequency upon signal to noise ratio and peak shape, 1  $\mu\text{L}$  injections of a 10  $\text{mg L}^{-1}$  nitrite standard were made at a range of input frequencies from 10 kHz to 1 MHz (using a cell fitted alternately with a 1.0, 3.3 and 4.7  $\text{M}\Omega$  resistor). Plots of both peak height and signal to noise ratio *versus* input frequency (see Figure 6.6 (a) and (b)) clearly illustrates that the maximum sensitivity was obtained in the frequency range of 150–200 kHz for all resistors, with peak height (Figure 6.6 (a)) and signal to noise ratio (Figure 6.6 (b)) significantly reduced at frequencies outside of this range. Figure 6.6 confirms the results shown in Figure 6.5, with an input frequency of 200 kHz (3.3  $\text{M}\Omega$  resistor) therefore being chosen as the optimum detector settings for all subsequent work.

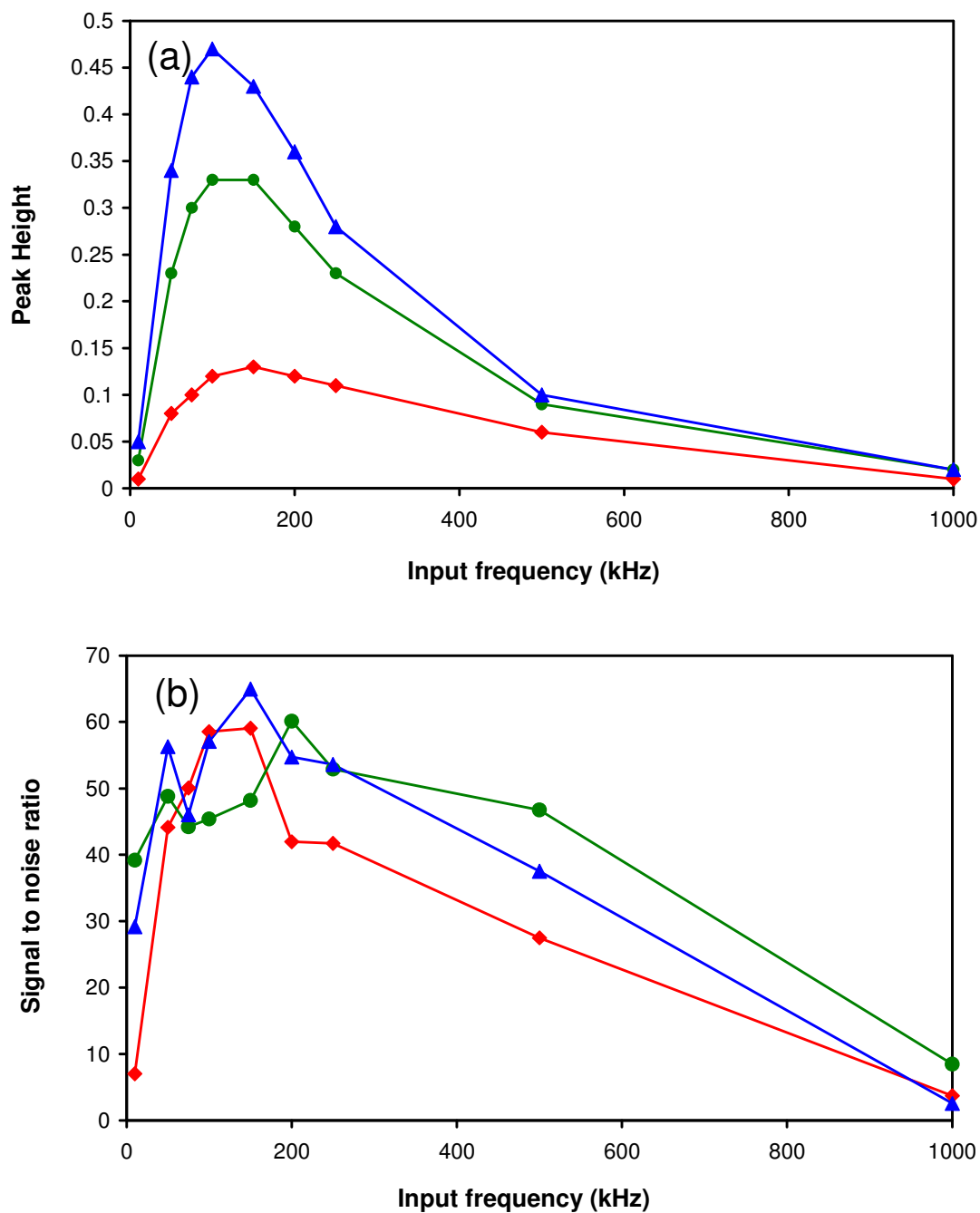


Figure 6.6: Effect of input frequency upon (a) peak height and (b) signal to noise ratio for three different resistors. Conditions as in Figure 6.5. Other conditions: *Injection volume*: 1  $\mu\text{L}$ , *Sample*: 10  $\text{mg L}^{-1}$  nitrite. *Noise calculation*: noise was measured from 2.5 minutes to 4.5 minutes in each blank chromatogram. *Legend*: 4.7 M $\Omega$  ( $\blacktriangle$ ), 3.3 M $\Omega$  ( $\bullet$ ) and 1.0 M $\Omega$  ( $\blacklozenge$ ).

The effect of input frequency upon peak shape was investigated by injecting 10 mg L<sup>-1</sup> nitrite standards onto the column at three different extremes of input frequency and overlaying the resulting chromatograms. Figure 6.7 illustrates “peak overshooting”, a phenomenon discussed in previously published work on C<sup>4</sup>D optimisation (due to an inappropriate input frequency and results in misshapen non-Gaussian peaks, with a baseline dip at the leading edge and/or the tailing edge of a peak) [14]. This is particularly noticeable in Figure 6.7(c). The optimised input frequency of 200 kHz (Figure 6.7(a)) clearly shows a marked improvement over 10 and 1000 kHz frequencies, both in peak height and peak shape with no evidence of peak overshooting.

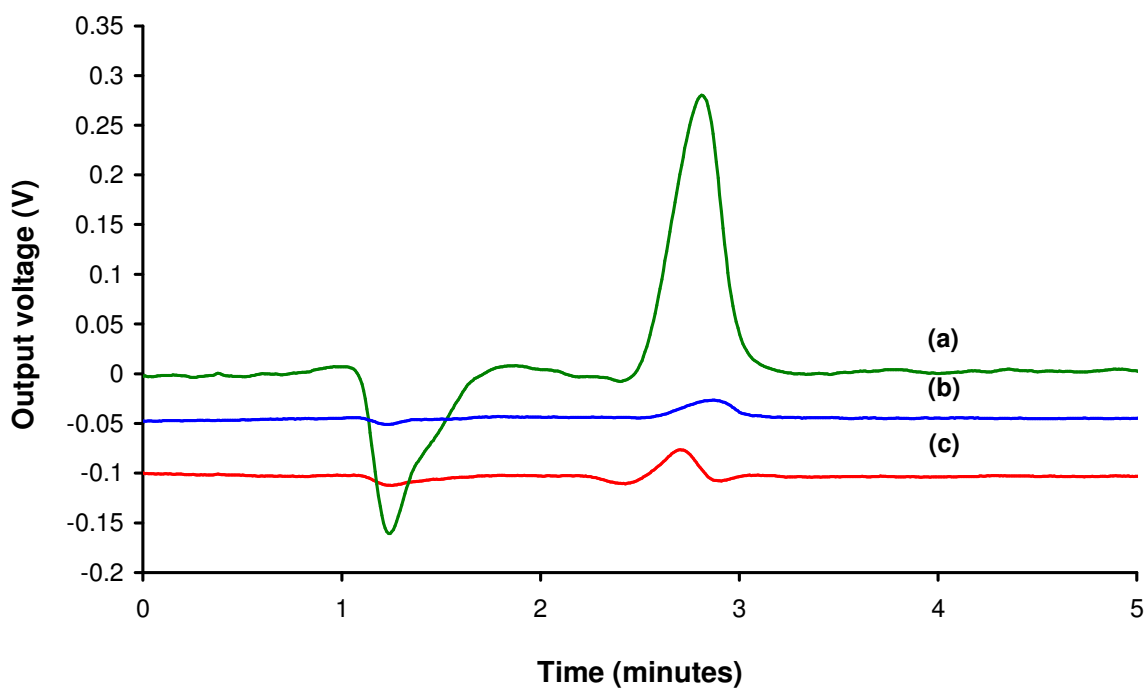


Figure 6.7 Chromatogram of 10 mg L<sup>-1</sup> nitrite at (a): 200 kHz (b): 1000 kHz and (c): 10 kHz showing the effect of frequency on peak height and shape. Conditions as in Figure 6.6.

### 6.3.3 Performance evaluation compared with commercial C<sup>4</sup>D detector.

A longer 400 mm × 380 μm i.d. column was packed with Dionex PAX-100 resin to allow determination of standard analytical performance criteria such as linearity,

precision and sensitivity on actual anion separations. The chromatographic setup is illustrated in Figure 6.2., showing the TraceDec capillary detector cell placed on a piece of 100  $\mu\text{m}$  i.d. fused silica capillary fitted to a union immediately after the column, as described in Section 6.2.1.2. Data collection was simultaneous for both detectors during a single injection. With an eluent of 2.5 mM sodium benzoate containing 2% methanol, linearity standards ranging from 5 to 100  $\text{mg L}^{-1}$  for nitrite and 2 to 100  $\text{mg L}^{-1}$  for nitrate were injected in triplicate to construct four point calibration curves of each analyte. The data presented in Table 6.1 shows the response of each detector to be comparable, with all correlation coefficients  $>0.99$ . Precision was determined for six injections of each analyte with both detectors, and again the performance of each detector was well matched. The absolute noise for each detector was measured in a blank injection over a three minute time window bracketing the retention time of each analyte, as described in Section 6.2.3. The difference in absolute noise measurements between both detectors was found not to be significant (with a difference of 0.00062 V,  $< 10\%$ ). Signal to noise values were compared for each detector using a 2  $\text{mg L}^{-1}$  nitrite standard and a 5  $\text{mg L}^{-1}$  nitrate standard. Finally, the limit of detection (LOD) of the detector under evaluation was not found to be markedly different from the sensitivity of the commercial TraceDec C<sup>4</sup>D.

Table 6.1: Comparison of the analytical performance criteria for the 1.59 mm C<sup>4</sup>D and commercial C<sup>4</sup>D.

	1.59 mm detector		TraceDec C <sup>4</sup> D	
	Nitrate	Nitrite	Nitrate	Nitrite
% RSD peak area (n=6)	3.53	1.85	3.88	2.34
% RSD peak height (n=6)	2.77	2.22	2.04	2.07
R <sup>2</sup> for linearity (peak area)	0.9998	0.9997	0.9992	0.9999
R <sup>2</sup> for linearity (peak height)	0.9938	0.9986	0.9932	0.999
Absolute noise /V	0.00677		0.00615	
Signal to noise ratio*	2.9	3.01	4.64	3.35
LOD/mg L <sup>-1</sup> *	5.17	2	3.23	1.79
N/m	2268	2014	2178	2141

\* 2 mg L<sup>-1</sup> nitrite standard and a 5 mg L<sup>-1</sup> nitrate standard

The overlaid chromatograms in Figure 6.8 clearly demonstrate that the C<sup>4</sup>D detector under investigation performs on a par with the commercially available TraceDec detector. It should be noted that the chromatograms appear to be offset along the retention time axis, because the lower chromatogram (TraceDec) was run with an effective column length of 400 mm whereas the upper chromatogram (test detector) had an effective column length of 342 mm.

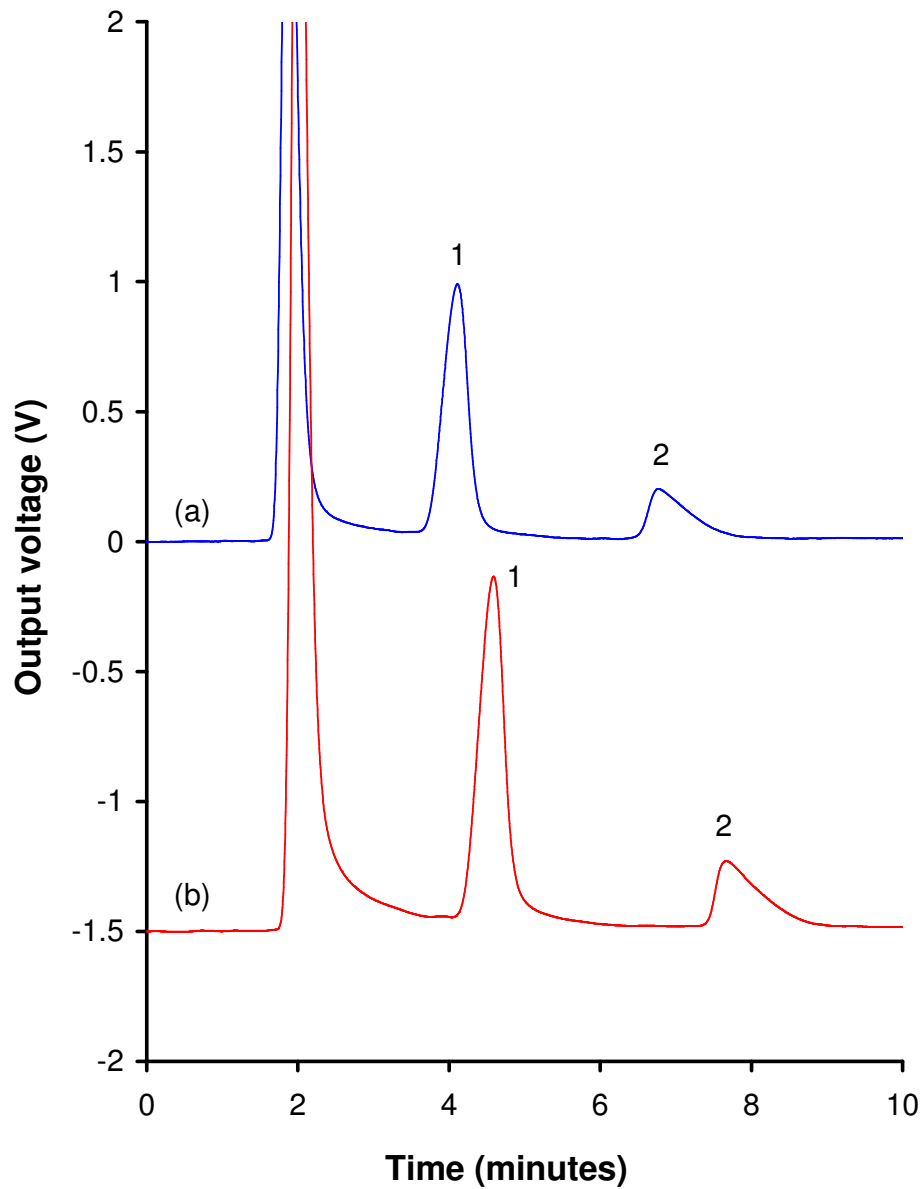


Figure 6.8: Comparison of chromatograms obtained with (a) 1.59 mm C<sup>4</sup>D on-column detector and (b) off-column commercial detector for 20 mg L<sup>-1</sup> nitrite (1) and 10 mg L<sup>-1</sup> nitrate (2). Eluent: 2.5 mM sodium benzoate (2% methanol), flow rate: 20  $\mu\text{L min}^{-1}$ , injection volume: 10  $\mu\text{L min}^{-1}$ .

#### 6.3.4 Intra-run detector movement.

The ability to physically move a detection cell to any point along a HPLC column during or between chromatographic runs has a number of clear and potential advantages. This has previously been shown in capillary electrophoresis by Macka *et al.* [19], but has heretofore not been shown in an LC separation. Placing the contactless conductivity detection cell halfway along a 400 mm column essentially reduces the effective length ( $L_{\text{eff}}$ ) of that column to 200 mm. The simple use of a sliding detector cell would allow the analyst to increase or decrease the effective length of a column to suit a particular application, which would facilitate more rapid method development. The analyst need no longer settle for the conventional column lengths offered by most column manufacturers (5 cm, 10 cm, 15 cm, 25 cm and 30 cm) but could instead define their own optimum column length.

A further significant advantage of the movable detector cell is that the effective length of a column can be changed mid-run, to speed the elution of strongly retained species in a sample once the early eluters have been detected. Indeed changing the effective column length during a run could also result in improved peak shape and peak height for a strongly retained species, thus improving sensitivity. This effect is similar to that achieved by running a mobile phase gradient, but can be carried out using a conventional inexpensive isocratic pump.

The effect of adjusting the effective column length during a chromatographic run upon a typical separation was demonstrated using a 250 mm  $\times$  380  $\mu\text{m}$  i.d. capillary column that was packed with Hamilton PRP-X100 (10  $\mu\text{m}$ ) phase. Using a 1 mM phthalate eluent (pH 4.0) containing 2% methanol, a simple separation of nitrite, nitrate and sulfate was achieved. Relatively fast eluting species such as nitrite and nitrate were baseline resolved ( $R = 1.52$ ) within 5 minutes, whereas the broad doubly charged sulfate peak eluted at 18 minutes when the detector was placed at  $L_{\text{eff}}$  230 mm, as shown in Figure 6.9 (a). Moving the detector to an  $L_{\text{eff}}$  of 60 mm reduced the retention time of sulfate to 8 minutes but resulted in a near co-

elution of nitrite and nitrate (see Figure 6.9 (b)). Finally, the same detector cell was placed at two separate positions on the column during a single injection in order to achieve both baseline resolution of relatively fast eluting species nitrite and nitrate, and shorter retention of the sulfate. The detector was initially placed at  $L_{\text{eff}}$  230 mm and after nitrate and nitrite were eluted (baseline resolved  $R = 1.54$ ), the detector was rapidly moved to an  $L_{\text{eff}}$  of 60 mm. This shortened column length facilitated the rapid elution of sulfate within 8 minutes (from the point of injection) as shown in Figure 6.9(c) The negative baseline dip at four minutes is due to the disturbance caused by physically moving the cell. The apparent lower overall conductivity of the stationary phase after four minutes, relative to the first four minutes is possibly due to the slight upwards electronic drift (from left to right) at the time of the study, although this may also be due an aberration in the electronics due to the movement of the detector.

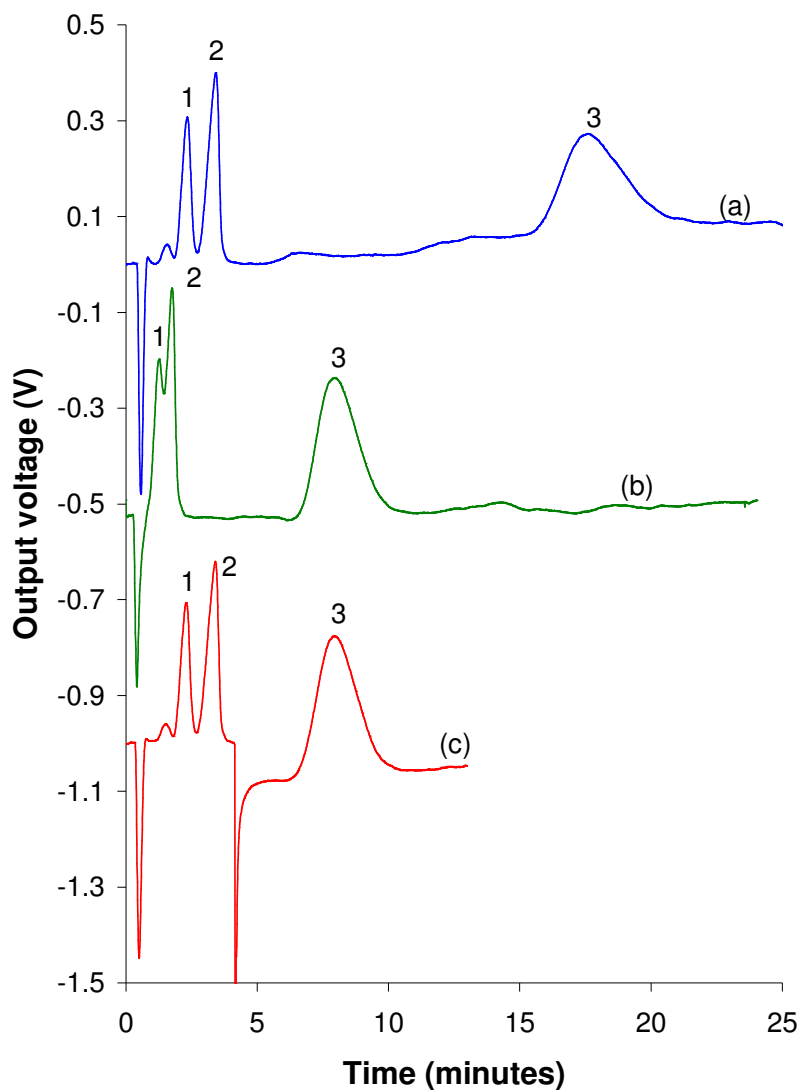


Figure 6.9: Separation of nitrite, nitrate and sulfate at (a)  $L_{\text{eff}}$  230 mm, (b)  $L_{\text{eff}}$  60 mm, and (c) initial  $L_{\text{eff}}$  230 mm with detector moved to 60 mm after 4 minutes. *Column:* 250 mm  $\times$  380  $\mu\text{m}$  i.d. PRP-X100 phase. *Eluent:* 1 mM phthalate eluent (pH 4.0) containing 2% methanol. *Flow:* 20  $\mu\text{L min}^{-1}$ , *injection volume:* 10  $\mu\text{L}$ . *Peaks:* (1) 10  $\text{mg L}^{-1}$  nitrite, (2) 10  $\text{mg L}^{-1}$  nitrate, (3) 20  $\text{mg L}^{-1}$  sulfate.

### 6.3.5 Evaluating the homogeneity of stationary phase packing.

An additional benefit of on-column detection is its application to the rapid non-invasive evaluation of the homogeneity of a particulate stationary phase packing

along the entire length of a column. In order to demonstrate the use of the 1.59 mm contactless conductivity detector for this purpose, a second longer column was packed with the same stationary phase as before (Dionex PAX-100) to allow more measurement points to be taken along the column length. Firstly, the effect of the presence of a stationary phase bed within a column was investigated.

A short length of empty 380  $\mu\text{m}$  i.d. PEEK tubing was placed within the cell and filled with 2.5 mM sodium benzoate and 2% methanol. The measured output signal was then recorded at discrete intervals along the length of the tubing by physically moving the detector at 15 mm increments by hand. The tubing was then replaced with a PEEK column of identical dimensions (400 mm  $\times$  380  $\mu\text{m}$ ), this time packed with stationary phase as previously described. While pumping the same eluent as before, the signal measurements were then taken again at the same equivalent locations along the length of the packed column and the overlay of both signal outputs are shown in Figure 6.10.

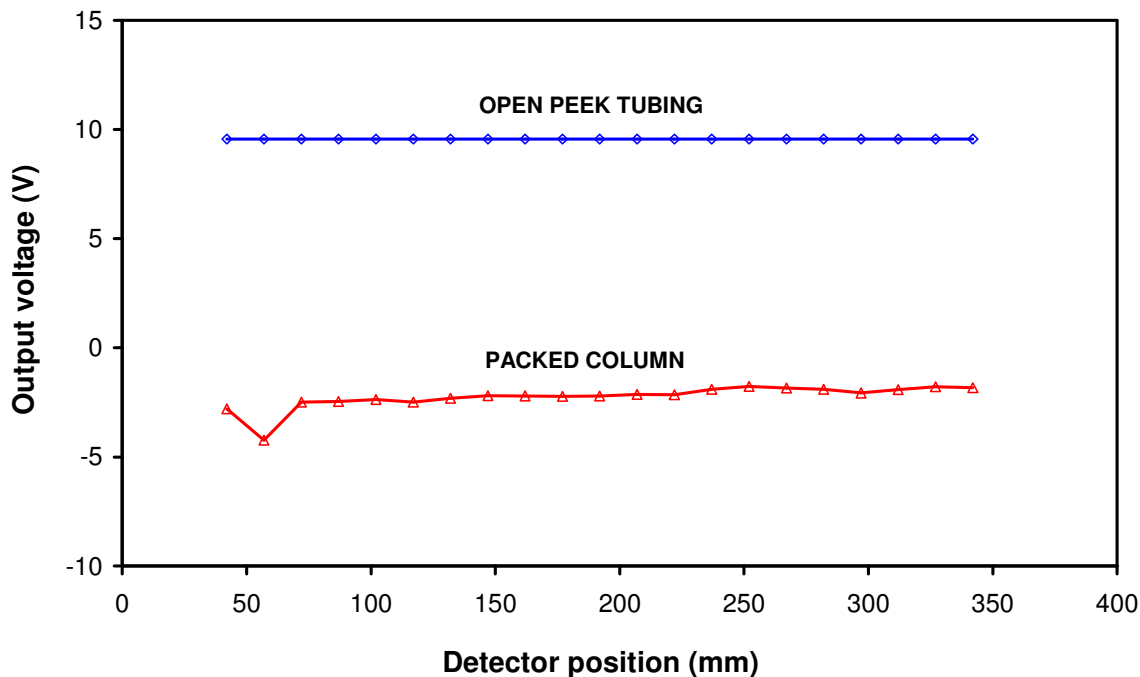


Figure 6.10: Evaluating the homogeneity of the stationary phase packing of a 1.59 mm o.d. column using contactless conductivity. Each point along both horizontal lines represents a location on the column at which the cell (measured from the exact position of the electrodes within the die-cast metal casing) was placed and an output voltage reading was recorded.

The presence of a stationary phase bed resulted in a lower signal than that obtained in the empty PEEK tubing filled with the same eluent. The actual cell volume can be viewed as the product of the cell length (the distance between the electrodes, which remains constant) and the cross-sectional area of the capillary tubing. Kubáň *et al.*, have likened this cross-sectional area to two parallel “virtual electrodes” [20]. Therefore, a possible explanation for the change in signal is that when the PEEK tubing is filled with stationary phase, only the inter-particle spaces are filled with mobile phase (electrolyte), which results in much smaller virtual electrodes and therefore reduced signal, compared with an unpacked column with virtual electrodes of 380  $\mu\text{m}$  in diameter. Physically moving or “scanning” the detector cell along the length of the column allows examination of the physical homogeneity of the column packing at different locations on the column. For

example, if a void or disturbance exists within the stationary phase due to compression of the bed or poor packing technique, the virtual electrode at that location on the column would be larger, resulting in a larger signal.

The profile of the packed PEEK column illustrated in Figure 6.10 shows that the column had a largely homogeneous profile with a small deviation from the normal value ( $-2.12 \pm 0.24$  V) at  $L_{\text{eff}}$  57 mm of  $-4.2$  V. It should be noted that a negative signal was obtained for the packed column because an offset was applied to the data acquisition system in order to prevent the signal for the open PEEK tubing from going off scale, such that both signals could be measured with identical settings.

#### **6.4. Conclusion.**

A 1.59 mm contactless conductivity detector cell suitable for use with standard HPLC 1.59 mm o.d. (1/16") tubing and packed micro-bore columns has been developed and evaluated. The Bode plots generated during detector optimisation are in close agreement with those obtained by other workers, and clearly illustrate that the new larger cell geometry behaves predictably, with the same mode of operation as smaller diameter cells. Previously, smaller diameter cells have been placed off-column in LC applications. However in this work, the detector cell has been shown to detect directly across a 381  $\mu\text{m}$  i.d. charged anion exchange stationary phase bed.

The test detector cell has been found to be at least as sensitive, linear and reproducible as a commercially available alternative cell (albeit a smaller i.d. cell), which, when moved along the column length, could increase or decrease the effective length of a HPLC column before or during a chromatographic run.

Finally, as the new  $\text{C}^4\text{D}$  cell was able to detect minor changes in bed homogeneity, its application as a new tool for the evaluation of micro-bore column packing techniques was also demonstrated.

## 6.5 References.

- [1] M. Pumera, J. Wang, F. Opekar, I. Jelinek, J. Feldman, H. Lowe and S. Hardt, *Anal. Chem.*, 2002, **74**, 1968.
- [2] Q. Lu, P. Wu and G. E. Collins, *Electrophoresis*, 2007, **28**, 3485.
- [3] J. Chen, Y. Lin and G. Chen, *Electrophoresis*, 2007, **28**, 2897.
- [4] M. Pumera, *Electrophoresis*, 2007, **28**, 2113.
- [5] P. Tuma, E. Samcová, F. Opekar, V. Jurka and K. Stulík, *Electrophoresis*, 2007, **28**, 2174.
- [6] Z. G. Chen, O. W. Li, Q. L. Li, X. Zhou, Y. Lan, Y. F. Wei and J. Y. Mo, *Talanta*, 2007, **71**, 1944.
- [7] A. Escarpa, M. C. Gonzalez, A. G. Crevillen and A. J. Blasco, *Electrophoresis*, 2007, **28**, 1002.
- [8] S. Qu, X. H. Chen, D. Chen, P. Y. Yang and G. Chen, *Electrophoresis*, 2006, **27**, 4910.
- [9] J. Tanyanyiwa and P. C. Hauser, *Anal. Chem.*, 2002, **74**, 6378.
- [10] J. Tanyanyiwa, E. M. Abad-Villar, M. T. Fernández-Abedul, A. Costa-García, W. Hoffmann, A. E. Guber, D. Herrmann, A. Gerlach, N. Gottschlich and P. C. Hauser, *Analyst*, 2003, **128**, 1019.
- [11] W. S. Law, P. Kubáň, J. H. Zhao, S. F. Y. Li and P. C. Hauser, *Electrophoresis*, 2005, **26**, 4648.
- [12] P. Kubáň and P. C. Hauser, *Electrophoresis*, 2005, **26**, 3169.
- [13] Andersen et al., Glass container wall thickness inspection machine, US Pat., 4 888 824, 1989.
- [14] E. Pungor, F. Pal and K. Toth, *Anal. Chem.*, 1983, **55**, 1728.
- [15] J. F. Alder, P. R. Fielden and A. J. Clark, *Anal. Chem.*, 1984, **56**, 985.
- [16] F. Pal, E. Pungor and E. Kovats, *Anal. Chem.*, 1988, **60**, 2254.
- [17] T. S. Burkhalter, *High Frequency Conductometric (Impedimetric) Titrations*, Elsevier, Amsterdam, 1964, 215.
- [18] J. Tanyanyiwa, B. Galliker, M. A. Schwarz and P. C. Hauser, *Analyst*, 2002, **127**, 214.

- [19] M. Macka, J. Hutchinson, A. Zemmann, S. S. Zhang and P. R. Haddad, *Electrophoresis*, 2003, **24**, 2144.
- [20] P. Kubáň and P. C. Hauser, *Electrophoresis*, 2004, **25**, 3387.

---

## **Chapter 7: Final conclusions and summation**

---

“Molōn labe!”  
-King Leonidas (480 BC)

From the work presented herein the application of C<sup>4</sup>D not only as a viable detection technique in Cap-IC, but also as a tool for the characterisation of modified monolithic stationary phases has been shown. The use of C<sup>4</sup>D as an on-column detector for use in Cap-IC provides not only a sensitive detection option, but also provides a successful approach to limit extra column band broadening. Extra column band broadening introduced by the connecting of the analytical column to the detector is of great importance when working at  $\mu$ L and nL flow rates, and the on-column nature of C<sup>4</sup>D has been shown to reduce this effect by approximately 10 % in the separation of inorganic anions, compared with off-column detection.

The ability to place the C<sup>4</sup>D cell directly onto the monolithic capillary columns has the added advantage of then being able to vary the position along such columns. In the application of this variable detector position to the monitoring of the surfactant modified silica C<sub>18</sub> capillary monoliths, the actual real time coating and subsequent removal of weakly coated surfactant could be probed in detail (both in spatial and temporal terms). This on-column characterisation of surfactant coated ion exchange phases has never before been reported. The potential to monitor the modified stationary phase also allows for the characterisation of further modifications of the stationary phase in the tailoring of the distribution of the surfactant to form gradient phases. In the use of organic solvent wash steps, the change in the distribution of the surfactant longitudinally within the column could be monitored and the stationary phase capacity tailored to form a concave gradient from the column inlet to outlet. The ability to characterise these changes in stationary phase distribution, and therefore capacity, gives the chromatographer added possibilities in the formation and control of novel stationary phases. The non-contact and non-invasive character of C<sup>4</sup>D permits the repeated characterisation of the stationary phase under varying conditions, such as a variation of the counter ion associated with the ion exchange moieties (i.e. physico-chemical properties of a stationary phase). The C<sup>4</sup>D signal was found to reflect the equivalent ionic conductance of the counter ion associated with the ion exchange

phase. The ability to interrogate the stationary phase in such a manner has never before been documented, and opens up further possibilities for the characterisation and optimisation of stationary phase chemistries and therefore the separations obtained. In the application of the modified stationary phase to the separation of inorganic cations, efficiencies of over 40,000 N/m were achieved, showing some of the most efficient separations of such analytes at the capillary scale.

From the study of C<sub>18</sub> silica capillary monoliths modified with surfactants, the advantages of C<sup>4</sup>D were also applied to the characterisation of the modification of polymeric monoliths. The characterisation of photografting methods has until now relied either on destructive methods (e.g. SEM) or indirect methods (e.g. chromatographic performance, EOF). The non-contact and non-destructive nature of C<sup>4</sup>D allows for both the spatial and temporal characterisation of polymeric monoliths modified using photografting methods. Indeed the optimisation of photografting techniques benefits greatly from C<sup>4</sup>D as the equilibration of the photografted zones can be directly monitored and the response recorded can be directly related to amount of energy used to initiate the photograft. C<sup>4</sup>D therefore leads to the ability to control the capacity and also optimise the photografting process in a non-contact and non-destructive manner, which also allows for repeated interrogation of the same column under varying conditions.

The on-column characterisation of photografted polymer monoliths by C<sup>4</sup>D opens up the possibility to investigate the effect of immobilisation of functional groups onto such macromolecular scaffolds. The change in chemical environment (i.e. from solution to covalently bound to a polymer) results in perturbation in the physio-chemical properties of immobilised functional groups, such as their pK<sub>a</sub>. Using C<sup>4</sup>D, on-column titrations of modified stationary phases was possible, allowing for a greater understanding of the physio-chemical character of the stationary phase. The immobilisation of three functional groups via VAL chemistry resulted in a change in the pK<sub>a</sub> of the groups, which would affect their behaviour

as a stationary phase. The immobilisation of *m*-aminophenylboronic acid resulted in a change in  $pK_a$  from 8.9 to 6.4. This clearly shows that novel stationary phases based on known ligands may not have the same physio-chemical properties as those ligands in solution. The ability to investigate these changes in physio-chemical properties allows for a deeper understanding of the conditions within the column. The benefit of such information allows for the construction of more finely controlled stationary phase chemistries, ultimately leading to more specific and efficient separations.

The non-contact nature of  $C^4D$  lends itself to application in any scale. The investigation of the application of  $C^4D$  to detection using microbore packed ion exchange columns, showed that  $C^4D$  at larger scales behaves equivalent to those in the capillary scale. Analytical performance of the in-house fabricated large scale detector compared satisfactorily with a commercial capillary  $C^4D$ . The limits of detection for both the on-column large scale detector and the off-column capillary scale detector were determined to be in the low ppm range. The ability to characterise the packing within the microbore column indicated that  $C^4D$  on larger scale columns will be as versatile as has been found with capillary columns. The ability to fit a  $C^4D$  cell onto a standard column (4.6 mm i.d.) may prove to be a useful tool for the investigation of fundamental chromatography principles.

In conclusion,  $C^4D$  has been shown to be an invaluable in the characterisation of modified capillary monolithic stationary phases. The non-contact, non-destructive and non-invasive character inherent to this detection technique affords itself to the characterisation of modified stationary phases, whether they are of surfactant coated or chemically modified. The direct visualisation of the chemical environment within the column without the requirement of destructive or indirect methods will only further the understanding of the production of more efficient stationary phases. The use of  $C^4D$  in the interrogation of stationary phase chemistries will open new avenues for the optimisation and control of novel stationary phase chemistries and permits repeated measurements on the same

column under varying conditions. All these factors lead to C<sup>4</sup>D as described in this thesis as a powerful analytical method for the characterisation of modified stationary phases for use in separation science.